J. App. Em. Sc
Vol 3, Issue 1, July 2012
ISSN 1814-070X

Quality & Excellence in Education

BUITEMS

JOURNAL OF APPLIED & EMERGING SCIENCES

Balochistan University of Information Technology
Engineering and Management Sciences

J. App. Em. Sc
Vol 3, Issue 1, July 2012
ISSN 1814-070X

JOURNAL OF APPLIED AND EMERGING SCIENCES

Balochistan University of Information Technology Engineering and Management Sciences, Quetta

Acknowledgement: Financial Support of BUITEMS through the forum of Directorate of Research is gratefully acknowledged.

Preface

This is the issue number 1 of the third volume of the Journal of Applied and Emerging Sciences published and distributed by the Balochistan University of Information Technology, Engineering and Management Sciences BUITEMS, a leading university of Balochistan and Pakistan with vision and mission statements as follows:-

Vision

To be among the leading universities of the world – accessible to all, imparting quality education and promoting cutting edge research.

Mission

We are committed to providing quality education with focus on research and to equip students with the art of living as productive members of society, contributing to the socio-economic uplift of Pakistan in general, and Balochistan in particular.

The original work of researchers published here in this issue is yet another effort of the university to meet its mandate expressed in the vision and mission statements for the promotion of research despite all odds. The editorial committee selects quality papers with continuous effort to improve the criteria for evaluation of papers with help of referees and subject experts. Present issue publishes 15 papers, but the editorial committee has recommended many more which will appear in following issues for the reason of time constraints in the processing.

The editors wish to express their sincere gratitude to Engr. Ahmed Farooq Bazai, Vice Chancellor for his personal involvement and participation in BUITEMS publications including Research Journal.

The editors also wish to express thanks to all those who helped and provided their services in publishing this issue.

Editor

Jamil Ahmad, PhD

Director ORIC

Email: jamil.ahmad@buitms.edu.pk

INSTRUCTIONS TO AUTHORS

Authors are requested to send the manuscripts typed in MS WORD and on CD-ROM, only those articles will be considered in which the work reported is original and the results are solely contributed to this journal. Screening of the articles will be done by the referees. In case they do not consider an article suitable for publishing, they can reject the article or send it back to the author for revision. The comments of referees are considered as the final decision.

Typescript

Articles must be typed on one side of the paper. It should be double-spaced and with a 30mm margin on all sides on white bond paper. This also applies to the abstract, tables, figure captions and the list of references each of which should be typed on separate sheets.

Title Page

Title should be brief and informative, typed in 14 pts. First alphabet of each word except prepositions should be capital and the rest in small letters. Names of authors should be followed by address of Institutions. The address for communication (along with e-mail address and telephone, telex and fax numbers), should also be given.

Abstract

The abstract should indicate the objective of the study, method, principal findings and should be typed in double space. It should not be more than 150 words.

Key words

Four to six key words must be provided which could assist in indexing.

Text Heading

All headings should be left aligned and BOLD. The main sections headings should be typed in 14 pts. Capital letters and the sub-headings should be typed similarly in lower case (12 pts.) bold letters.

Introduction

The paper must start with ‘Introduction’ which should not be more than 200 words. Text of the paper must be typed in 12 pts.

Materials and Methods

The Materials and Methods section should include sufficient technical information to allow the experiments to be repeated. Give enough information about the maker and model of instrument, operating conditions and other details of the experimental procedures. For commonly used materials and methods simple reference is sufficient.

Results and Discussion

Results followed by discussion can be included under the same heading of Results and Discussion or as separate.

Acknowledgement

Few lines of any desired acknowledgement of research support or other credit should be added if required.

Tables and Graphs

All tables must be numbered consecutively in Arabic numerals in the order of appearance in the text. Tables and graphs representing the same set of data should be avoided. All tables, figures, illustrations should be self-contained and have a descriptive title or creatively prepared so that their size can be adjusted as desired. Details of experiments (not mentioned in the text) may be indicated in brief below the table as a legend.

Figures and Photographs

Figures and photographs can be included as jpg, bmp or pdf attachments. Photographs should be numbered consecutively along with the figures in Arabic numerals in the order of appearance in the text. Photographs should be sharp, with an indication of the scale. Do not include line drawings and photographs in the same plate.

References

References should be cited in the text by author and year, not by number. If there are more than two authors, reference should be made to the first author followed by *et al* in the text. References at the end of the paper should be listed alphabetically by authors' names, followed by initials, year of publication, full title of the paper, name of the journal volume number, initial and final page numbers. References to books should include: name(s) of author(s), initials, year of publication, title of the book, edition if not the first, initials and name(s) of editor(s) if any, preceded by ed(s), place of publication, publisher, and pages referred to.

Examples

Reference pattern_ journal

Marazita ML, Ploughman LM, Rawlings B, Remington E, Arnos KS, and Nance WE. (1993) Genetic Epidemiological studies of early onset deafness in U.S school-age population. Am J Med Genet 46:486-491.

Reference pattern_book

Karathwohl DR. (1988) How to prepare a research proposal. Guidelines for funding and dissertations in the social and behavioural sciences. 3rd Ed. New York, Syracuse University Press.

OR

Blumenfeld H (2001) Neuroanatomy through Clinical Cases. Yale University School of Medicine, New York.

Reference pattern_conference

Asmussen LE, Hicks DW, Leonard RA, Knisel WG, and Perkins HF. "Potential Pesticide Contamination in Groundwater Recharge Areas: A model Simulation". Proceedings of the Georgia Water Resource Conference, University of Georgia. 161-164, Georgia, May, 1989.

Authors are requested to prepare the manuscript carefully before submitting it for publication so as to minimize the corrections. Proofs of articles will not be provided. lf there is any Editorial revision, it must be made while your article is still in manuscript form.

CONTENTS

The Schema as the Predictor of Depression among the Adolescents

Ayesha Manzoor[1,*] Sundus Sial[2], Faiza Manzoor[3] and Anwar-ul-Haq[4]

[1] Department of Social Sciences, Balochistan University of Information Tecnology, Engineering & Management Sciences, Quetta,[2] International Islamic University, Islamabad,
[3]Department of Sociology, University of Balochistan, Quetta,[4]Department of Psychiatry, Capital Hospital Islamabad

Abstract

The paper focuses on the role of individual's schema in generating the depression among the adolescents. A purposive sample of 100 adolescents male and female with age range of 10 to 25 years was taken from non-clinical population. The Beck Depression Inventory II and Young Schema Questionnaire (Short Form) were administered on the subjects to determine the level of depression stimulated by schema. The Readiness Ruler was also administered to determine how much the subject was ready or how much daily life events make him to alter his schemas. In addition to these measures the Demographic Information sheet was also provided to subjects to get the background information from them. Data was analyzed by applying Pearson Product Moment Correlation and Regression analysis. The results clearly supported the hypotheses that the disorganized or false schemas and beliefs lead to depression. Results are discussed in relation to latest schema theories and cognitive therapy which can be used to rationalize the beliefs in maintaining the good mental health of an individual.

Key Words: Schema, Depression, Adolescents, Cognitive Therapy, Mental Health

[*]Corresponding Author's email:- ayesha.manzoor@buitms.edu.pk

INTRODUCTION

The psychosocial factors play a major role in the development of depression, aggression, anxiety and other psychological disorders. This study aims to find out whether the core beliefs, negative thoughts and prejudiced attitudes lead to depressive symptoms and other maladaptive behaviors or not. Also how these depressive thoughts and beliefs effect our decisions, daily living, our relations and so on. According to Beck (1976), depressive information processing stems from the activation of pathological cognitive structures or schemas that develop early in life and become activated in adulthood in response to stressful experiences. These schemas lead to the development of beliefs which in future restrain or catalyze living a healthy sociable life, making constructive decisions and maintaining relationships.

Once activated, such schemas are thought to offer access to a host of negative themes, and guide a pattern of negative self-reference information that precipitates depression (Beck et al., 1979; Segal & Shaw, 1988). Cognitive products may take the form of negative attributions, pessimistic or hopeless expectations for the future, or perceptions of inferiority (Rector et al., 1998). The studies by Segal et al (1988) and Segal & Vella (1990) suggest that depressive information processing is driven by the activation of negative elements within a self-structure, rather than the activation of an enduring depressive self-schema. The schemas lead to the development of beliefs about our various related events, issues, things and people; also that these beliefs not solely depend upon our relative experiences but also strengthened by the cultural perspectives of everyday living. Ellis and Harper in 1961 (Rahman & Ahmed, 2005) outlined a number of dysfunctional cognitive processes and irrational beliefs that lead to

depression which include: Demand for approval, high self expectations, blame proneness, frustration reaction, emotional irresponsibility, anxious over concern, problem avoidance, helplessness for change, and perfectionism.

Adolescence is considered as transitory phase, which Erickson (Rahman & Ahmed, 2005) called identity versus role diffusion; as going through transitions these young minds may avoid problems rather than solving them. In addition, frustration reaction was found to be a predictor of depressive symptoms both in males and females (Rahman & Ahmed, 2005). Gotlib proposed that interpersonal cognitive schemas, i.e., how the individual perceives him/herself in relation to interpersonal relationships, should be emphasized in research on interpersonal pathways to depression. In line with these integrative interpersonal models of depression, Schmidt and Young (1999) noted that schema-based formulations of interpersonal relationships can be useful in understanding the role of interpersonal factors in the course of depression. Beck theorized that early parenting style and early negative life experiences may result in the development of maladaptive, negative core beliefs or schemas about oneself and how the world functions. When early maladaptive schemas are activated by related interpersonal or stressful events later in life, the individual is likely to develop a negative view of self and the event, and cognitively distort relevant information, which may lead him/her to experience depression. Hence, Beck proposed maladaptive schemas and dysfunctional cognitive styles as vulnerability factors to depression that potentially exacerbate the effects of stressors on depression. In general, research with children as well as adults on the role of cognitions in depression provided support for Beck's theory of depression (Schmidt and Young, 1999 Cankaya, 2002). The question of which cognitive schemas as measured by Young's Schema Questionnaire (Young, 1994) were related to depression was examined in several studies. Schmidt et al., (1995) reported that 'dependency' and 'defectiveness' predicted depression in an undergraduate student sample. 'Mistrust/abuse', 'abandonment', and 'social isolation' predicted depression in college students in Harris, Curtin, and Vicente's study (1999). 'Defectiveness/shame', 'self-sacrifice', and 'insufficient self-control' in a clinical sample and 'vulnerability to harm' in a nonclinical sample predicted depression in Shah and Waller's study (2000). Further, Shah and Waller showed that the EMSs; 'vulnerability to harm' in the nonclinical sample, and 'vulnerability to harm', 'dependence/ incompetence', 'emotional inhibition', 'failure to achieve', and 'unrelenting standards' in the clinical sample were the subscales of the Yaung that acted as mediators in the relationship between early parental experiences and depressive symptomatology. Taken together, while inconsistent across studies, the seven cognitive schemas directly related to depression in previous research afforded the highest likelihood of establishing connections to depression (Cankaya, 2002).

Rationale

So far little work has been done on the schema, cognition and irrational beliefs as the predictors of psychological problems in the Pakistani population. Particularly the schema has not been among the most of interest of the Pakistani researchers. However, these are the basic structures that organize our knowledge and assumptions about something and are used for interpreting and processing information. This study mainly aims to find out the basic distortions in our cognitions and thoughts that lead us to maladaptive behaviors. This research based on the adolescents of the society will help and guide the professionals in the society who are working as the social mediators and also the psychologists and psychiatrists to look more clearly into the process and help people to alter their beliefs and live a healthy mental life.

MATERIALS AND METHODS

Sample collection

Adolescents aged 10-25 years were selected by purposive sampling. Among them there were 54 males and 46 females chosen from educational institutes, hospitals, and

organizations. The reason being the language of measuring instruments must be properly comprehended by the subjects i.e. English.

Measurements

Demographic Information Sheet

Demographic information sheet was given to the subjects to get their information regarding age, gender, birth order, education and marital status.

Young Schema Questionnaire (Short Form)

The measure of schemas was the Young Schema Questionnaire that consists of 75 items. Each item is scored on a 6 point scale i.e. from completely or almost completely untrue of me (1) to describe me perfectly or almost perfectly (6). It covers 15 major hypothetical dimensions of schema (Stopa, L., & Waters, A. 2005). The SQ has been found to have adequate test-retest reliability - the stability scores for subscales range from 0.50 to 0.82 (Schmidt et al., 1995).

Beck Depression Inventory-II

Depressive symptoms were measured through Beck Depression Inventory II. BDI-II is a self report inventory that comprised of 21 items and used to measure levels of depression. Each item is scored on a 4 point scale i.e. from minimal depression (1) to severe depression (4). The test retest reliability of BDI-II is reported to be 0.93 (Steer and Brown, 1996).

Readiness Ruler

The Readiness to Change Scale was also used to assess how the individual's core beliefs create hindrance or catalyze the treatment process.

Procedure

A pilot study was conducted on 10 students (5 males and 5 females) at the university, with their consent and the purpose of the study was explained to them. The objective of the pilot study was to find and make clear that the mode of instructions, language of the scales is easily understandable by the subjects; also to check the total time taken by the individuals for the completion of two questionnaires.

The Research design employed was Repeated Measure Design. The participants were given the demographic data sheet for knowing their background information. The participants were presented the Young Schema Questionnaire to know their schemas. Then the time break of 20 minutes was given before presenting them the BDI-II for measuring their level of depression. The participants rated themselves on the 10 point scale of readiness ruler to find out how much they had an insight into their cognitions and how much they feel themselves to bring a change in their thoughts and imaginations

RESULTS AND DISCUSSION

The Table I shows the results of total score, and for men and women separately (Stopa and Waters, 2005). The results are computed by using SPSS.16 (Statistical Software).

	Male		Female	
Scales	M	S.D	M	S.D
ED	11.59	4.19	11.04	4.53
AB	12.87	5.22	12.46	5.72
MA	12.43	4.60	12.13	3.64
SCI	12.57	5.17	12.67	5.23
DEF	11.09	5.24	10.70	5.55
FAIL	12.20	6.17	11.26	5.23
DI	11.87	5.86	10.15	5.21
VUL	12.35	6.38	10.61	4.91
EMN	12.43	5.37	12.04	6.14
SJ	12.14	4.84	11.59	4.43
SS	15.78	6.87	16.86	6.47
EI	14.00	4.74	13.50	4.76
US	17.03	5.37	17.39	5.68
ENT	15.22	5.55	13.96	4.97
ISC	14.63	5.78	13.11	4.73
Total YSQ Score	198.22	58.30	189.48	51.71
Total BDI Score	16.06	8.87	15.63	9.57
Total RR	5.48	2.44	5.83	2.10

ED= Emotional Deprivation, AB=Abandonment, MA=Mistrust and Abuse, SCI=Social Isolation, DI=Defectiveness and Social Undesirability, FAIL=Failure, DI= Dependence/ incompetence VUL= Vulnerability to Harm and Illness, EMN=Enmeshment, SJ=Subjugation, SS= Self Sacrifice, EI=Emotional Inhibition, US=Unrelenting Standard, ENT= Entitlement, ISC=Insufficient Self Control

Table 1

Means and Standard Deviations of the total and subscale scores of YSQ, total of BDI and total of Readiness ruler for male and female Adolescent participants (M=54, F=46) . The level of depression i.e. Total BDI score for male (M=16.06, SD=8.87) and female (M=15.63, SD=9.57) is moderately low and

also the total score on YSQ for male (M=198.22, SD=58.30) and female (M=189.48, SD=51.71) is quite low. The Total RR score for male (M=5.48, SD=2.44) and female (M=5.83, SD=2.10) is also moderately low. To determine the relationship between the schema and depression the Pearson Product Moment Correlation was applied.

Table 2

Pearson Product Moment Correlation Coefficient between total score of BDI -II With the total was used and subscales of YSQ and Readiness to change Ruler for 100 adolescents (N=100)

Scales	Total	Males	Females
ED	.321**	.420**	.220
AB	.319**	.345*	.292*
MA	.314**	.339*	.286
SCI	.287**	.304*	.270
DEF	.265**	.201	.329*
FAIL	.159	.209	.094
DI	.180	.165	.199
VUL	.243*	.310*	.154
EMN	.189	.297*	.084
SJ	.028	.026	.027
SS	.292**	.267	.328*
EI	.210*	.207	.211
US	.294**	.361**	.228
ENT	.255*	.256	.255
ISC	.282**	.342*	.207
Total YSQ Score	.349**	.375**	.320*
Total RR	.036	.024	.055

ED= Emotional Deprivation, AB=Abandonment, MA=Mistrust and Abuse, SCI=Social Isolation, DI=Dependence/incompetence, DEF= Defectiveness, social undesirability, FAIL=failure, VUL= Vulnerability to Harm and Illness, EMN= Enmeshment, SJ=Subjugation, SS= Self Sacrifice, EI=Emotional Inhibition, US=Unrelenting Standard, ENT= Entitlement, ISC=Insufficient Self Control.

Note:*=p< 0.05, **=p< 0.01

The schema and depression are significantly correlated, $r = 0.349$, $p < 0.01$.

Among the hypothetical schemas Emotional Deprivation, Abandonment, Mistrust and Abuse, Social Isolation, Defectiveness, Social Undesirability, Self Sacrifice, Unrelenting Standard, Insufficient Self Control are the most highly correlated with depression. The results also demonstrating the negative correlation between the depression and readiness to change, though not quite significantly. To predict the relation between schema and depression the Regression Analysis was applied.

Table 3

Relationship between total score of BDI-II with the total and sub-scale scores of YSQ and Readiness Ruler using Multiple Regression Analysis for the total sample (N=100).

Scales	B	SEB	β
ED	.89	.27	.42**
AB	.36	.28	.21
MA	.12	.31	.05
SCI	.37	.38	.21
DEF	-.45	.35	-.26
FAIL	-.43	.29	-.27
DI	1.19	.32	.73**
VUL	.13	.26	.08
EMN	-.24	.27	-.15
SJ	-1.39	.31	-.70**
SS	.67	.21	.49**
EI	-.74	.36	-.38
US	.18	.30	.11
ENT	.16	.31	.09
ISC	.24	.35	.14
Total YSQ Score	.06	.016	.352**
Total RR	-.08	.39	-.02

ED= Emotional Deprivation, AB=Abandonment, MA=Mistrust and Abuse, SCI=Social Isolation, DEF= Defectiveness and Social Undesirability, FAIL=Failure, DI=Dependence/incompetence, VUL= Vulnerability to Harm and Illness, EMN= Enmeshment, SJ=Subjugation, SS= Self Sacrifice, EI=Emotional Inhibition, US=Unrelenting Standard, ENT= Entitlement, ISC=Insufficient Self Control

Note: R^2= .103, ΔR^2=.103, B= Unstandardized Coefficient, SE B= Standard Error of Unstandardized Coefficient, β=Standardized Coefficient Beta, **=p< 0.01

The results reveal the overall weak prediction of depression. However the hypothetical schemas including Emotional Deprivation, Dependence/ incompetence, Subjugation and self sacrifice are the strongest predictors of depression of the overall group of individuals.

The overall analysis also indicates that the subjects' depressive thoughts make changes in expected direction as hypothesized.

DISCUSSION

The aim of this paper was to investigate the role of individual's schema in generating the depression among the adolescents. The results indicate that emotional deprivation, dependence/ incompetence, subjugation and self sacrifice are the strongest predictors of depression among the adolescents. The results also demonstrate the negative correlation between the depression and readiness to change, though not quite significantly. However, these results must be interpreted cautiously as the sample was small and the schemas are pre-conceived ideas that vary from time to time and from individual to individual following different as well as adverse circumstances. The study shows that even very modest shifts in mood can influence the way in which participants respond to some questions on the YSQ. Changes in mood may alter a person's view of self in a negative direction (Stopa and Waters, 2005). As adolescents is a transitory phase, which Erickson (Rahman and Ahmed, 2006) called identity versus role diffusion; as going through transitions these young minds may avoid problems rather than solving them. It highly advocates our results of reluctance to change their current schemas as they consider themselves well inclined to their life issues and changes. Young (1999) proposed that schemas can be grouped into domains, which represent the hypothesized developmental origins of the schemas. He described five domains: disconnection and rejection, impaired autonomy and performance, impaired limits, other-directedness, and over-vigilance and inhibition. Each domain represents a grouping of developmental needs. There is no evidence at this stage to indicate whether the developmental stage at which the schema emerged influences when and how that schema is retrieved. However, it is interesting to note that both of the schemas which were raised in the depressed mood condition belong to the earliest domain, that is, disconnection and rejection. On the other hand, entitlement which is raised in the happy condition belongs to the later developmental domain of impaired limits (Stopa and Waters, 2005).

In the whole study we found the low score on the Entitlement; we have found that this schema can be problematic for clinical patients, both when it is high and also when it is low. For example, people with very low entitlement scores may be unable to appropriately assert themselves, may feel that their needs are unimportant, and may tolerate unacceptable behavior from others. It is possible that moderate levels of entitlement are both healthy and have a protective function for the individual. Again, these points must be interpreted with caution, as we do not have data on the 'healthy' range of entitlement scores (Stopa and Waters, 2005). A basic premise of Jeffrey Young's approach is that individuals with more complex problems have one or more early maladaptive schemas, which makes them vulnerable to emotional disorders.

Most of our hypotheses have been approved as per our results indicated. The question of which cognitive schemas as measured by Young's Schema Questionnaire (Young, 1994) were related to depression has been examined in several studies. Schmidt et al. (1995) reported that 'dependency' and 'defectiveness' predicted depression in an undergraduate student sample. 'Mistrust/abuse', 'abandonment', and 'social isolation' predicted depression in college students in Harris, Curtin, and Vicente's study (1999). ('Defectiveness/shame', 'self-sacrifice', and 'insufficient self-control' in a clinical sample and 'vulnerability to harm' in a nonclinical sample predicted depression in Shah and Waller's study, 2000). Taken together, while inconsistent across studies, the seven cognitive schemas directly related to depression in previous research afforded the highest likelihood of establishing connections to depression (Cankaya, 2002). The present design and time duration did not allow us to examine why some schemas should be affected whereas others were not. One of the main weakness was that individuals were currently in varied circumstances and those affected significantly in their responses to the questionnaires. As the Young Schema Questionnaire was adapted, for this study mainly due to the reason as it measures

specifically negative schemas, the population used was non clinical and this is the most important reason probably for non significant results. However, the implication of this research may help the professionals by keeping in view the vulnerability of the individuals that may adapt to some maladaptive or negative schemas which they carry on in their lives without changing them. The reason being their current situation, their interpersonal relations, social desirability, parental attitudes, etc. As particularly in our Pakistani culture the adolescents are at the most sensitive stage where they have to cope many entangled problems of the society and family conflicts as well as cultural varsities; they may form the schemas that drastically lead them to depression and many other cognitive dysfunction. So keeping in view all this we could formulate more constructive strategies and chalk out future plans to lower the rapidly increasing psychological problems in our country.

REFERENCES

Ÿ Beck AT, Rush AJ, Shaw BF and Emery G. (1979). Cognitive therapy of depression. New York: Guilford Press.

Ÿ Beck AT, Steer RA and Brown GK. (1996). *Beck depression inventory-II* (2nd ed.). USA: The Psychological Corporation.

Ÿ Beck AT. (1976). Cognitive therapy and the emotional disorders. New York: International University Press.

Ÿ Cnakaya B. (2002). Psychosocial Factors, Maladaptive Cognitive Schemas, and Depression in Young Adults: Virginia Polytechnic Institute and State University.

Ÿ Rahman NK and Ahmed MM. (2006). Irrational Beliefs as Predictors of Depressive Symptoms among Urban Adolescents of Lahore, Pakistan. *Pakistan Journal of Professional Psychology, Research and Practice*, 1: 25-33.

Ÿ Rector NA, Segal ZV, Gemar and Michael. (1998). Schema research in depression: a Canadian perspective. *Canadian Journal of Behavioural Science*.

• Rector NA. (1998). Schema research in depression: a Canadian perspective. *Canadian Journal of Behavioural Science.*

• Schmidt NB, Joiner TE, Young J E and Telch MJ. (1995). The Schema Questionnaire: Investigation of psychometric properties and the hierarchical structure of a measure of maladaptive schemas. *Cognitive Therapy and Research.*

Ÿ Schmidt NB, Schmidt KL and Young JE. (1999). Schematic and interpersonal conceptualizations of depression: An integration. In T. Joiner, & J. C.Coyne (Eds.), Advances in interpersonal approaches: The interactional nature of depression pp. 127-148. Washington, DC: American Psychological Association USA.

Ÿ Schmidt NB, Joiner TE, Young JE and Telch MJ. (1995). The Schema Questionnaire: Investigation of Psychometric properties and the hierarchical structure of a measure of maladaptive schemas. *Cognitive Therapy and Research,* 19(3): 295-321.

Ÿ Segal ZV and Vella DD. (1990). Self-schema in major depression: replication and extension of a priming methodology. *Cognitive Therapy and Research,* 14(2): 161-176.

Ÿ Segal ZV, Hood JE, Shaw BF and Higgins, ET. (1988). A structural analysis of the self-schema construct in major depression. *Cognitive Therapy and Research,* 12: 471-485.

Ÿ Stopa L and Waters A. (2005). Psychology and Psychotherapy: Theory, Research and Practice, *The British Psychological Society. 7*8: 45–57.

Ÿ Young JE. (1994). *Cognitive therapy for personality disorders* (2nd ed.). Sarasota, FL: Professional Resource Exchange.

Optimization of Energy Consumption during Natural Gas Dehydration

Abdul Qadeer[1*], Adnan Aftab[2], Imran Nazir[3]

[1] Department of Chemical Engineering, [2] Department of Petroleum and Gas Engineering, Balochistan University of Information Technology Engineering & Management Sciences Quetta, [3] Department of Chemical Engineering, Mehran University of Engineering and Technology, Jamshoro, Pakistan.

Abstract

The aim of this work is to design an efficient Natural gas dehydration plant (using TEG as desiccant) in both terms i.e., optimized desiccants flow rate as well as optimized energy requirements. For this purpose the Natural Gas Plant of Hassan Gas Field, Shikarpur was selected as case model and the basic design study was carried out for the said plant. Natural gas is one of the important fossil fuels, used after treatment. Treatment includes removal of acid gases and dehydration. The major methods of dehydration are Direct Cooling, Absorption and Adsorption. The present work is the study of efficient design for Dehydration using absorption column by Triethylene Glycol (TEG) as desiccant. Efficiency of the Natural Gas Dehydration Column can be measured through optimized flow rates of desiccant or optimized energy requirements.

Keywords: Energy Consumption, Natural Gas, Optimal Energy

INTRODUCTION

Pakistan is one of Natural gas dependent economies of the world. Pakistan has 27.89527 TCFT proven reservoirs of gas. This include 34.78 MMCF of associated reservoirs (Pakistan Energy Yearbook, 2010). During the financial year 2009-10 Pakistan produced 1482846 MMCFT (Pakistan Statistical Year Book, 2011).

The pressure and temperature of natural gas are reduced, when the gas is produced from the reservior during flow from subsurface to wellhead; hence the gas yields liquid water condensate. Due to presence of water vapors in gas may cause gas hydrates in sale gas transmission lines which could stop gas transportation or supply (Donald and Robert, 1990; Boyun and AIi 2005, Vincente *et al*, 1992). Natural gas some time may contain H_2S, which itself is a poisoning gas (Gas Processors Suppliers Association, 1987). It is necessary to remove H_2S gas (gas sweetening) prior to the dehydration of NG because it may corrode transportation and processing facilities, which may create many health, safety and environment issues (Meyers, 2003).

Natural gas dehydration may be achieved by four techniques i.e. direct cooling, compression followed by cooling, absorption and adsorption. In Absorber the hydrates are removed by hygroscopic liquid, i.e. ethylene glycol (EG), diethylene glycol (DEG), triethylene glycol (TEG), and tetraethylene glycol (T_4EG) (Saeid *et al.*, 2006; Lurance, 1978). Pipeline specification for water content in NG is 7lb_m/MMSCF (Donald and Robert, 1990).

TEG flow rate in absorption column is dependent on water content in the NG, commonly flow rate of 2 to 6 gallon of TEG/ lb_m of water with concentration of 99.0% to 99.9% is used (Landreau *et al.,* 1999; Kohl, and Riesenfeld, 1985).

Process Description

Sweet gas / wet gas delivered to the bottom of gas absorber tower and lean TEG is showered from top of the tower. Both gas and TEG solution counter affect each other during this phenomena.

Glycol achieves solubility with water phase

because of H-O bond and very low water vapor pressure. Water rich glycol passe through filter. Separation of water from TEG is achieved in surge tank. Separated lean glycol is again ready to be reused in absorber tower (Mohamadbeigy, 2008; Jou. *et al.,* 1987). A process flow diagram (PFD) is shown in figure 1.

MATERIALS AND METHODS

Design Standards for NG dehydration unit

Optimum flow rate of TEG for dehydration of gas may be calculated by using standard models containing associated graphs and tables. The availability of following parameters is necessary.

- Flow rate of Gas in MMSCFD
- Gas Specific gravity
- Gas Operating pressure in psig
- Gas inlet temperature in ^{0}F
- Gas Water content required at Outlet in lb_m / MMSCF

Natural gas water content was found by using McKetta and Wehe Chart (McKetta and Wehe Chart, 1958; Chorng *et al.,* 2005) in lb_m H_2O/MMSCF at operating conditions of 60°F, 14.7 psia.

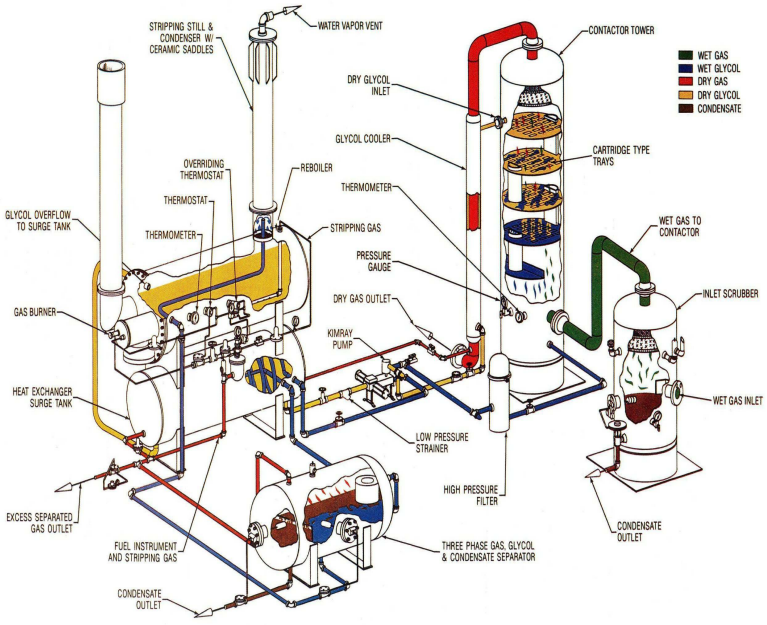

Figure 1. Process Flow Diagram (PFD) of Natural Gas Dehydration Unit

The absorbing capacity of gas was corrected on operating temperature and sp: gravity by using Sivalls Correction Factors and equation 1.

$$G_s = \frac{G_o}{(C_t)(C_g)} \quad (1)$$

Dew point depression was calculated from Equation 2. It remained constant for the optimized flow rate of TEG

Dew point Depression= Inlet Gas Temp: – Outlet Dew point Temp: (2)

Quantity of water removed was calculated by using Equation.

$$W_r = \frac{(W_i - W_o)(G)}{24} \quad (3)$$

Flow rate of TEG in Absorber column was calculated by using Equation.

$$L = \frac{L_w (W_i)(G)}{24} \quad (4)$$

Heat consumption for TEG as sensible heat in reboiler was calculated by utilizing equation.

$$Q_s = L(r_L)(C)(T_2 - T_1) \quad (5)$$

Required energy for vaporization of water was calculated from Equation

$$Q_w = \frac{970.3(W_i - W_o)(G)}{24} \quad (6)$$

Energy consumed inside the reflux for vaporizing the water was calculated from equation

$$Q_r = 0.25(Q_w) \quad (7)$$

TEG losses during regeneration process was calculated by using the equation

$$\text{Loss of TEG} = (0.04)L(r_L) \quad (8)$$

Case Study of Dehydration unit, Hassan Gas Filed Shikarpur

Hassan Gas Field is situated in gas block F-22 near Shikarpur, Sindh. Gas field is operated by the Pakistan Exploration Limited (PEL). The gas capacity of field is 20 MMSCFD and currently it is processing 14 MMSCFD.

Gas composition prior to the dehydration is shown in Table.1 Operating parameters

of Hassan Gas field dehydration unit used in this analysis are shown in Table. 2 Regeneration of TEG consumes a high amount of energy. Number of iterations was made by forming the sets of TEG flow rate and concentration, from flow rate 3.5 to 3.0 gal/lb_m of water and concentration from 99.0 to 99.9%, a constant variation of 0.1 gal. / lb_m of water and 0.1% was made in flow rate and concentration respectively.

Table 1. Gas composition prior to the dehydration.

Compound	Mole%
C_1	63.5240
C_2	1.5217
C_3	0.3800
i-C_4	0.0897
n-C_4	0.1252
i-C_5	0.0505
n-C_5	0.0313
C_6	0.1240
N_2	32.4560
CO_2	1.7007
H_2S 100/Scf	1 grain
H_2O	120 lb_m H_2O/ MMSCF

Table 2. Available data of Hassan Gas Filed dehydration unit

Gas flow rate	14 MMSCFD
Specific gravity of gas	0.721
Operation pressure	825 psig
Gas inlet temperature:	120 °F
Outlet gas water content	7lb_m H_2O / MMSCF
Glycol to water circulation rate	3.5 Gallon TEG / lb_m of H_2O
Lean TEG concentration	99.0%

Table 3. Calculated parameters and Operating conditions of the dehydration unit, Hassan gas field

TEG- Gas Contactor	
Outlet temperature	34°F
Dew point depression	86°F
Water Removed	68.1 lb_m/ hr
TEG Concentration in Rich Solution	96.01%
TEG Concentrator	
Circulation Rate	238.42 gal/ hr
TEG sensible heat	281.960 BTU/ hr
Heat of vaporization for Water	66,097 BTU/ hr
Heat vaporized the water reflux	16,925.25BTU/ hr
Heat Losses of Reboiler	10,000 BTU/ hr
Total Heat in Reboiler	374573.2 BTU/ hr
TEG losses	7.153 gal/ hr

RESULTS AND DISCUSSION

It was observed that when the Glycol (TEG) to water ratio is decreased from 3.5 to 3.0 Gallon TEG / lb_m of H_2O, simultaneously the Lean TEG flow rate at the top of the absorption column is also decreased from 238.42 to 204.36 gal/hr. as shown in Figure 2.

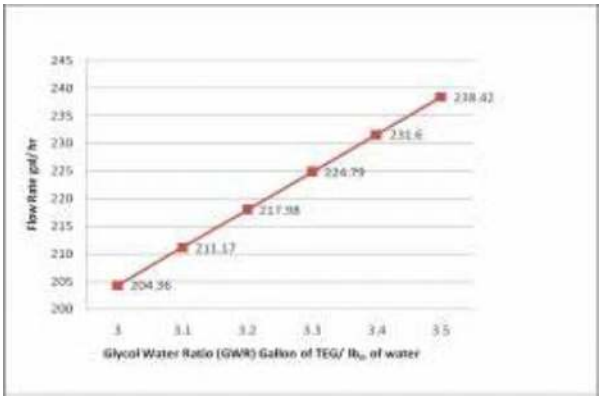

Figure 2. Relation of flow rate and glycol water ratio.

Figure 3 indicates the Rich TEG concentration when lean TEG concentration flowed on the top of the absorption column at different flow rates ranging from 3.0 to 3.5 Gallon TEG / lb_m of H_2O. This shows that as the Lean TEG concentration and GWR increased, the concentration of Rich TEG also increases. This supports the proposed energy saving plan parameters for Hassan

Gas Field Dehydration Column with the same concentration of the rich TEG.

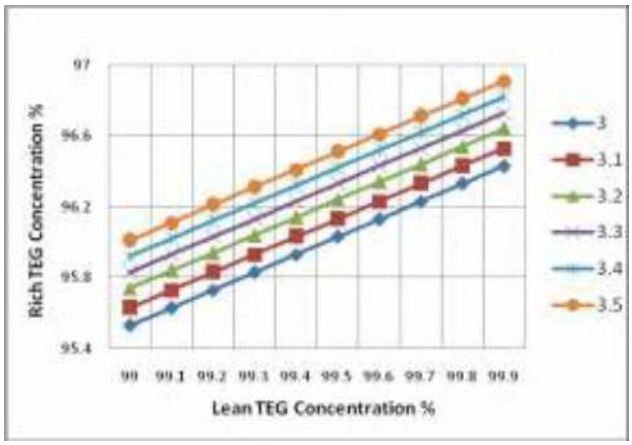

Figure 3. Rich TEG concentration on various Lean TEG

Sensible heat is consumed by Glycol during the regeneration of the TEG; this indicates that as the GWR decreased from operating condition of 3.5 to 3.0 Gallon TEG / lb_m of H_2O, the sensible heat also decreased from 281.952 to 242.8936 K BTU/ hr by optimum selection of GWR and Lean TEG concentration, as shown in figure 4.

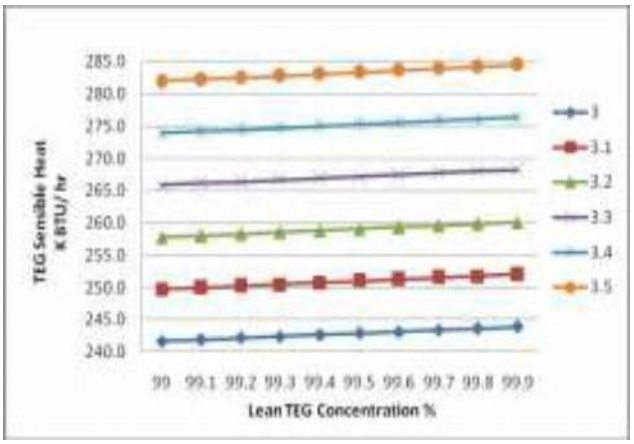

Figure 4. Consumption of Sensible Heat on different flow rates of GWR and Lean TEG concentration

Total load on the reboiler was calculated through the sum of sensible heat of TEG, energy for vaporization of water and energy consumed inside the reflux for vaporizing the water. This resulted in decrease on the Load of reboiler as the flow rate of TEG decreased with the varing concentration of lean TEG, shown in figure 5.

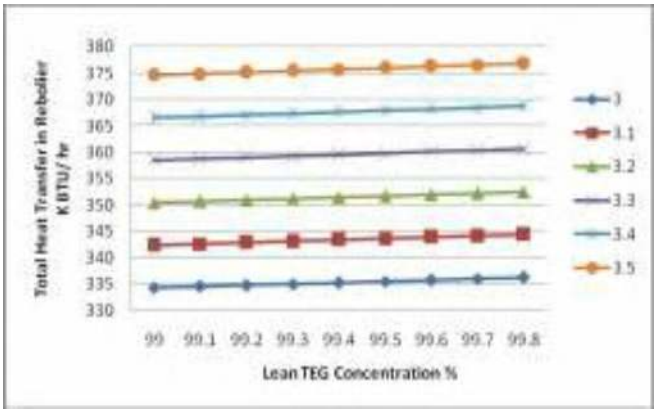

Figure 5. Total Heat Transfer inside the Reboiler on Different flow rates of GWR and Lean TEG concentration

Loses of TEG on different flow rates are calculated by using the Eq. 8. Figure 6 shows that as the GWR increased the losses of TEG increased at the same rate.

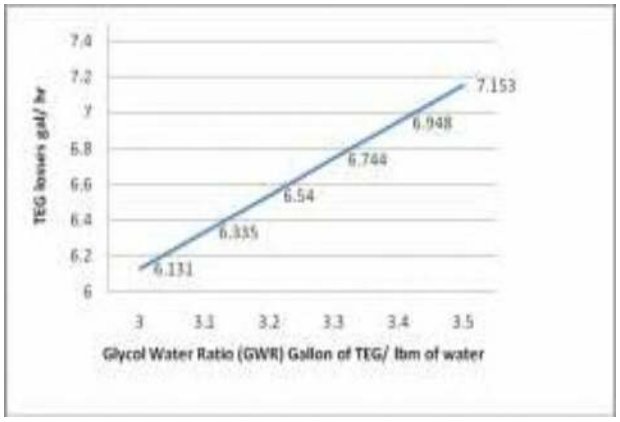

Figure 6. TEG loses at different flow rates of GWR

CONCLUSION

After the detailed designing of the dehydration column it was observed that the design of the column had the satisfactorily matching with the present design and did not require any fabrication. By changing the operating conditions a handsome amount of energy was saved during the process. By changing the GWR and concentration of the Triethylene Glycol (TEG) improved the dehydration of the natural gas on the same number of the plates inside the dehydration column. Comparison of existing parameters and proposed parameters showed the following facts.

With increase of the concentration from 99.0 to 99.5 % Lean TEG reduced GWR from 3.5 to 3.0 gal of TEG / lb of H_2O. Concentration of the TEG in rich solution was maintained as the optimized condition on 96.0%, so that the regeneration of the TEG was done on the same temperature of 350°F. Glycol circulation rate reduced from the 238.42 to 204.36 gal/hr. This shows that the duty of the TEG pump reduced up to 14.5%. Total heat load on reboiler reduced from the 374573.2 to 335514.9 BTU/hr, an amount 39058 BTU/hr saved during the operation which was about 10.5% of the regeneration energy consumption.

ACKNOWLEDGEMENT

The authors would like to acknowledge the support of Hassan Gas Field and Pakistan Exploration (Pvt.) Limited.

REFERENCES

Ÿ Boyun G and Ali G. (2005). *Natural Gas Engineering Hand Book*, Gulf Publishing Company, Houston, P. 126

Ÿ Donald LK and Robert LL. (1990). *Natural Gas Engineering Production and Storage*, McGraw Hill International, P.617-619

Ÿ Gas Processors Suppliers Association, Engineering Data Book, 1987.

Ÿ Mohamadbeigy K. (2008). Studying of the effectiveness parameters on gas dehydration plant. *International Journal for Petroleum Processing, Petro-chemistry and Coal Processing.* 50(2): 47-51.

Ÿ Kohl A and Riesenfeld F (1985). Gas Purification. Gulf Publishing Co., Houston.

Ÿ Landreau B, Amande J, Doerler N and Bojey A. (1999). Gas drying process using glycol, including purification of discharged. US patent documents.

Ÿ Lurance SR. (1978). Method of removing water from glycol solutions, US patent documents.

Ÿ Meyers RA. (2003). Handbook of Petroleum Refining Processes, McGraw-Hill Professional, third edition, 2003.

Ÿ Pakistan Energy Yearbook. (2010). Hydrocarbon Development Institute of Pakistan,

Ÿ Pakistan Statistical Year Book. (2011). P .159, 2011.

Ÿ Saied M, William A, Poe and James GS. (2006). Handbook of Natural Gas Transmission and Processing. *Elsevier*. 323.

Ÿ Takahashi S and Kobayashi R. (1982). The Water Content and the Solubility of CO2 in Equilibrium with DEG-Water and TEG-Water Solutions at Feasible Absorption Conditions. Technical Publication TP-9, GPA, 1982.

Ÿ Vincente N, Hernandez-V, Michael WH. , Jerry AB. (1992). Design Glycol Units for Maximum Efficiency. Proceedings of the 71st GPA Annual Convention. Tulsa, OK: Gas Processors Association. 310-317.

To Study the Basic Concepts of Monte Carlo Simulation by Calculating the Value of π

Hamdullah Khan[1*], Anees ur Rahman[2], Fazli Manan[3]

[1]Department of Physics, Balochistan University of Information Technology Engineering & Management Sciences Quetta, [2]Centre for Nuclear Medicine and Radiotherapy, Quetta, [3]Department of Electronics, Quaid-i-Azam University, Islamabad.

Abstract

The Monte Carlo Simulation is a basic tool in computational and theoretical physics by which complicated and difficult physical, statistical and mathematical problems are solved which cannot be solved by usual analytical means. In this paper the basic concepts of Monte Carlo techniques are discussed and used by calculating the value of π by Monte Carlo simulation and generating random numbers with the help of a computer program (Mathematics).

Key words: Monte Carlo Method, Simulation, Random numbers, Probability, C++.

[*]Corresponding Author's email: hamdullah.khan@buitms.edu.pk

INTRODUCTION

The Monte Carlo method was discovered in 1940 by John Von Neumann, Stains Law Ulam and Nicholas Metropolis during their research on the nuclear weapon project (Manhattan project) in the Los Alamos National Laboratory. Its name relates to the Monte Carlo Casino, a well know Casino of which where Ulam's Uncle was a member.

Monte Carlo is a technique which involves using random numbers and probability statistics to solve problems (Wittwer J). Monte Carlo methods are computer algorithm depending upon the repeated random sampling to compute their results for the physical, statistical and mathematical problems. These methods are used when complicated problems cannot be solved by conventionally analytical methods (Harvill and pipes, 1970, Vose, 2008).

Monte Carlo Method has applications equally in physical sciences, nuclear physics, space physics, fluid mechanics, telecommunication, engineering, computation biology, applied statistics, games, finance and business etc. They are widely used as well in mathematics to calculate multidimensional definite integrals with complicated boundary conditions. There is difference between a simulation, Monte Carlo method and Monte Carol simulation. A simulation is a fictitious representation of reality, a Monte Carlo method is a technique which is used to solve a mathematical and statistical problem and a Monte Carlo simulation uses repeated sampling to determine the properties of some action (Wikipedia). For example if we toss a coin once, head or tail outcome can be used to simulate the tossing of coin. This can be done by drawing one pseudo random uniform variable from the interval [0, 1] is simulated the toss of coin. If the value is less than or equal to 0.5, designate the outcome as head, but if the value is greater than 0.5 the outcome as tails. This is simulation but not Monte Carlo simulation. The area of an irregular shape inside in a unit area of square and computing the ratio of hits within the irregular figure to the total number of darts thrown. This is a Monte carol method but not a simulation. If we select to draw a large number of pseudo random uniform variable from the internal [0, 1] and assigning values less than or equal to 0.5 as heads and greater than 0.5 as tails is a Monte Carlo simulation of the behavior of tossing a coin (Woller, 1996).

MATERIALS AND METHODS

Monte Carlo (MC) methods stochastic technique which based on the use of random numbers and probability statistics to

investigate problems. It has applications in many fields.
The methodology to calculate the value of π by using this technique is discussed as below by considering the square and an inscribed circle in it as below.

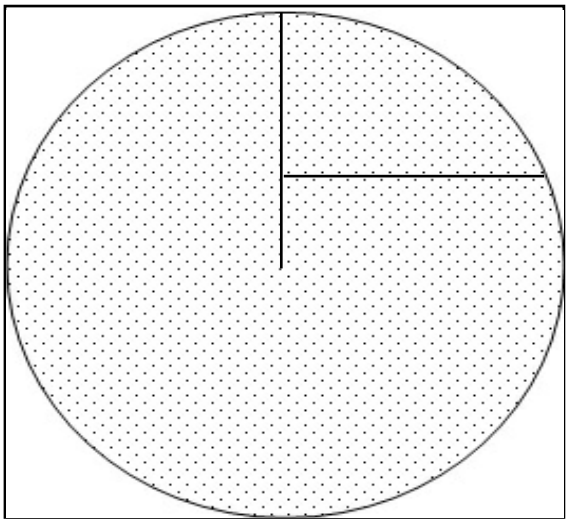

2r
Figure:1 The circle of radius r is inscribed in the square of side 2r . Let us consider a circle inscribed in a square of having side 2r and radius of circle is r. The ratio of area of a circle to the square is

$$\frac{\pi(r)^2}{(2r)^2} = \frac{\pi}{4}$$

If we imagine the player of dart who hits the darts to a square and counts that of hits and missing. It is obvious that area of the square and circle is proportional to the No. of hits.
In other words

$$\frac{\text{Number of darts hitting shaded area of circle}}{\text{Number of darts hitting entire square}} = \frac{\pi r^2}{4 r^2} = \pi/4$$

$$\pi = \frac{4 * \text{Number of darts hitting shaded area of circle}}{\text{Number of darts hitting Entire Square}}$$

If each dart thrown hits somewhere inside the square, the ratio of hits in the shaded area to throws will be one fourth the value of π. If we do this experiment it takes a very large number of throws to get a proper value of π. To perform this procedure a computer program has been written in C++ language. The algorithm of this program is as under,

```
#include<iostream.h>
#include<stdio.h>
#include<conio.h>
#include<stdlib.h>
#include<iomanip.h>
#include<math.h>
void main(void)
{
clrscr();
FILE*stream;
float r,s,x,y,dist,z;
int i,k,n,range,min,max;
cout<<"enter min and max,try"<<"\n\n";

cin>>min>>max>>n;
cout<<"# of Iteration"<<setw(12)<<"# of hits"<<setw(16)<<"value of pi";
cout<<"\n\n";

stream=fopen("MCData.txt","w+");
fprintf(stream,"# of iteration # of hits value of pi");

fprintf(stream,"\n\n");

range=(max*100)-(min*100);
k=0;
for(i=1;i<=n;i++)
{r=rand()/10%(range+min);
s=rand()/10%(range+min);
x=r/100;
y=s/100;
dist=sqrt(x*x+y*y);
if(dist<=1&&dist>=0)
 k=k+1;
z=4.0*k/i;
cout<<i<<setw(18)<<k<<setw(16)<<z;

fprintf(stream," %d %d %f",i,k,z);
fprintf(stream,"\n\n");
cout<<"\n\n";
}
fclose(stream);
getch();
}
```

In this program random numbers are generated. If we suppose our circle has radius 1.0unit, then for each throw we can generate two random numbers as x and y coordinates which are used to calculate the distance from the origin (0,0) using the pythagora's theorem $x^2 + y^2 = 1$. If the distance from the origin is less than or equal to 1.0 then it means that value lies within the shaded area and counts as hit. Repeat

this process thousands of times and we get an estimated value of π. The accuracy of this value depends on number of iterations and the quality of random numbers generated (Woller, 1996).

RESULTS AND DISCUSSION

For the scientific program execution, three inputs are entered, one is minimum, second maximum value and third is number of iterations (4). From minimum and maximum values the range is determined and the computer codes generates random number between 0 and 1. In the first iteration these random numbers are checked the condition $x^2 + y^2 <= 1$, if this condition satisfied it means our first throw hit is within circle otherwise it is outside from circle and count as a missing (5). Then we try second, third and repeatedly try to get hits and miss of throws. Finally by calculating the probability of hits and multiplying it by 4 we get estimated value of π i.e. 3.142. By giving the inputs min =0,max=1 and number of attempts 1000 the outputs of some values are illustrated as below.

# of iteration	# of hits	value of pi
1	1	4.000000
2	2	4.000000
3	3	4.000000
4	4	4.000000
5	5	4.000000
6	6	4.000000
7	6	3.428571
8	7	3.500000
9	8	3.555556
10	9	3.600000
11	10	3.636364
12	11	3.666667
13	12	3.692308
14	13	3.714286
15	13	3.466667
16	14	3.500000
17	14	3.294118
18	15	3.333333
19	15	3.157895
20	16	3.200000
636	499	3.138365
637	500	3.139717
638	501	3.141066
639	502	3.142410
640	503	3.143750
641	503	3.138845

Thus there are two main reasons which compel to use Monte Carlo method because of their anti aliasing properties and their ability to approximate quickly an answer that would be very time-consuming to find out the answer too if we were using methods to determine the exact answer. The second point refers to the fact that Monte Carlo method is used to simulate problems that are too difficult and time-consuming to use other methods for.

CONCLUSION

By the Monte Carlo method and simulation, different types of complicated physical, mathematical and statistical problems can be solved. This technique has been used for the calculations of value of π successfully by using computer scientific program. Monte Carlo simulation can be improved by powerful computer, proper computer codes, random numbers and number of iterations.

ACKNOWLEDGEMENT

We are thankful to Syed Zaheer Abbas Gilani Assistant professor Physics department BUITEMS for his help in using C++ computer language.

REFERENCES

· Harvill LR and Pipes LA. (1970).Applied Mathematics for Engineers And Physicists. 3rd Edition,New York, Mc Graw. Hill Inc.

· Monte Carlo method –Wikipedia, the free encyclopedia

· Woller T. 1996).The Basics of Monte Carlo Simulation, http://www.chem.unl.edu/zeng/joy/mclab/mcintro.html

· Wittwer J. Monte Carlo Simulation Basics,http//www.vertex42.com/ ExcelArticles/mc/monteCarlo simulation.html.

Ÿ Vose D. (2008). Risk Analysis, A Quantitative Guide (3rd. Ed). John Wiley & Sons.

Statistical Analysis of the Macro-economic Variables Affecting the Profitability of Commercial Banks of Pakistan

Muhammad Zubair Khan[1], Muhammad Iqbal[2]

[1]Faculty of Arts and Basic Sciences, Balochistan University of Information Technology Engineering & Management Sciences Quetta,
[2]Department of Statistics, University of Peshawar

Abstract

This paper aims to examine the level of influence of some external factors (macro-economic variables) have on the profitability of commercial banks in Pakistan. The study covers the period from 2005 to 2009. The period under analysis (2005-2009) was selected mainly because during the said period, the world banking industry showed a huge declining trend in profitability due to global economic recession with many renowned banks filing for liquidation and this affected the Pakistani banking scenario as well, and the local banks both public and private showed a declining trend. The data used in the study is panel data. Panel data refers to pooling of observations on a cross-section of firms (say banks) over several time periods. Four variables including interest rate, exports, imports and inflation rate are used as independent variables (external factors). All the analysis of this study is carried out using the statistical package "Eviews". The stationarity of data is tested by applying the individual unit root test. To test the multicollinearity in the data the correlation matrix is made. Durbin-Watson statistic is used to detect auto correlation. To measure the individual impact of each of these independent variables on ROA as well as their pair wise impact on ROA and further joint impact of three variables on ROA, the technique of "all possible regression" is used to reach the best panel regression model. The results obtained from the regression models show that interest rate and imports have significant affect on the bank's profitability. The best regression model is consisting of the macro-economic variables, imports, inflation rate and interest rate.

Keywords: Macro-economic variables, Commercial Banks of Pakistan

Corresponding Author's email: iwu2005@yahoo.com

INTRODUCTION

Banks play an important role in the operation of an economics. This is particularly true in the case of Pakistan, where banks are the major providers of funds and their stability is very important to the financial system. An understanding of determinants of banks profitability is essential and crucial to the stability of the economy. External factors used by contemporary researchers as determinants of bank's profitability include interest rate (intr), inflation rate (ir), exports and imports (imp), etc. There are a number of studies on determinants of profitability in the banking sector (Indranarain 2009, Valentina et al. 2009, Panayiotis 2005, Kyriaki et al., 2002, Krunakar et al. 2008), there is hardly any such study in the context of Pakistan.State Bank of Pakistan is the governing body of the banking sector in Pakistan. Banking sector of Pakistan comprises of banking and non-banking financial institutions. The banking institutions mainly comprises commercial banks which may be further classified as domestic and foreign commercial banks. Domestic commercial banks are further classified as; public sector and private sector commercial banks.

This study examines the contribution of macro-economic (external) factors to the variation in profitability across domestic commercial banks in Pakistan. The quarterly data of macro-economic variables for 5 years for the period 2005-2009, is used to determine the important factors in achieving high profitability.

The study used Return on Assets (ROA) as a measure of profitability in line with

Indranarain 2009, Valentina et al., 2009, Panayiotis 2005, Kyriaki et al., 2002 and Krunakar et al., 2008. ROA, defined as net income divided by total assets, reflects how well a bank's management is using the bank's real investment resources to generate profits. The banking sector in Pakistan has been going through a comprehensive but complex and painful process of restructuring since 1997. It is aimed at making these institutions financially sound and forging their links firmly with the real sector for promotion of savings, investment and growth. Although a complete turnaround in banking sector performance is not expected till the completion of reforms, signs of improvement are visible. The almost simultaneous nature of various factors makes it difficult to disentangle signs of improvement and deterioration.

Today's commercial banks are more diverse than ever. We can find a tremendous range of opportunities in commercial banking like starting at the branch level where you might start out as a teller to a wide variety of other services such as leasing, credit card banking, international finance and trade credit. Public banks are those which are operated by government. A public bank is that in which there are numerous partners or shareholders, and they elect from their own body a certain number, who are interested with its management. There are four public banks in Pakistan. Limited Bank that is limited by charter or by regulation to offering only certain services to the public. Limited service banks have narrow product lines, such as credit cards or auto loans, and may offer other services on an irregular basis.

MATERIALS AND METHODS

As there are 29 domestic (4 public + 25 private) commercial banks in Pakistan so a sample of 15 banks is drawn by simple random sampling using Goldfish bowl method. Sample size of n=15 banks out of N=29 is a moderate size (n/N > 50%), and the sample results can better depict the target population. For a sample that consists of 15 banks and each bank requires data for six variables. Data for the four external variables (interest rate, exports, imports and inflation rate) is retrieved from the web site of IMF through State Bank of Pakistan.

Data Analysis

Since this study involves panel data, so the technique of "all possible regression" is applied to panel data to reach the best model. The best model is selected on highest R^2. A panel data regression differs from a regular time-series regression or cross-section regression in that way that it has a double subscript on its variables, i.e.

$$\mathbf{y_{it} = A + BX_{it} + \varepsilon_{it}}$$

where, $i = 1, \ldots, N; \quad t = 1, \ldots T$

"i" denotes the bank and "t" denotes the period or the time. In other words "i" denotes the cross-section and "t" denotes the time series. "A" is the intercept; "B" is K x 1 vector and "X_{it}" is the ith bank on kth independent variable at time "t".

Where $\mathbf{\varepsilon_{it} = u_i + v_{it}}$

"u_i" is called unobserved effect and "v_{it}" is the remainder disturbance. For example in an equation measuring the profitability of bank, "y_{it}" measures the profit of the ith bank, whereas X_{it} contains the set of independent variables like bank size, deposits, interest rate etc. "u_i" is time-invariant and accounts for individual banks that is not included in the regression. In our study "u_i" is banks unobserved ability and "v_{it}" varies with banks and time and therefore called as usual disturbance term in the regression. Alternatively in profitability equation y_{it} measures the output and X_{it} measures the inputs. The unobserved bank specific effect is measured by "u_i" and we can think of this as unobserved managerial skills (Baltagi, 2005).

This study used cross-section weights for every observed bank *i* at time *t*, and the true variance components, in order to produce a matrix-weighted average of the within and the between (which is obtained by regressing the cross section averages across time) estimators (Baltagi, 2001). More over all the panel regression models are run using fixed effect (FE), because of the reason that null hypothesis under Hausman test is; there is no substantial difference between FE and random effect (RE) models. If the null hypothesis is re-

jected, FE model is better than RE model (Gujarati, 2004).

Before running the panel regression models some preliminary tests are performed which include unit root test for checking stationarity of data, correlation matrix for checking multicollinearity and Durbin-Watson Statistic is used as a check for autocorrelation. The study is already using the least square method to fixed effects models, where the standard errors are calculated by using White's (1980) transformation to control for cross-section heteroscedasticity.

Preliminary Tests

The correlation matrix (Table-1) showed that the variables exports and imports have high correlation (coefficient of correlation greater or equal to 0.90). The variable 'import' is removed from the regression models but its individual significance is measured on ROA before its removal and proved insignificant. Table (2) shows the results of individual unit root test for the four external variables. P-values of all the four variables are suggesting stationarity of data at 10% level of significance. Durbin-Watson statistic is given in each table of regression model suggesting no autocorrelation problem at all for all the variables.

Table1: The Correlation Matrix

	EXPORTS	IMP	INTR	IR
EXPORTS	1	0.935587	0.820249	0.664447
IMP	0.935587	1	0.761665	0.734661
INTR	0.820249	0.761665	1	0.318169
IR	0.664447	0.734661	0.318169	1

Note:- "*" indicates high correlation.

Table2: Panel Unit Root Test for Bank Specific variables

S/No	Variable	ADF Fisher Chi-Square	Im, Pesaran & Shin W-Statistic	Hadri Z-statistic	Brietung t-statistic	Stationary/ Non-Stationary
1	Interest Rate **(intr)**	44.5669* (0.0423)	-1.2588* (0.1040)	2.7523* (0.0030)	-2.8050* (0.0025)	Stationary
2	Exports	64.0095* (0.0003)	-3.9498* (0.0000)	4.4255* (0.0000)	0.0353* (0.5141)	Stationary
3	Imports **(imp)**	35.0277* (0.2416)	-1.2898* (0.0986)	1.8245* (0.0340)	-2.6812* (0.0037)	Stationary
4	Inflation Rate **(ir)**	62.2420* (0.0005)	-3.8039* (0.0001)	5.6123* (0.0000)	-10.2067* (0.0000)	Stationary

Note:
1. '*' shows the value of the statistic used.
2. In the parenthesis p-values are given.
3. Exports and imports are considered stationary as three out of four tests suggest stationarity.

RESULTS AND DISCUSSION

Using the technique of "all possible regression" four models are run each of which is for one external variable to test its individual significance. Table (4) suggests that only 'interest rate' is significantly affecting the profitability on individual basis. All the four external variables are affecting the ROA negatively. The best significant regression model on the basis of highest R^2 is,

ROA = 0.279227 - 0.006347 (interest rate).

Table 3: Individual Impact of Variables on ROA

Variable	Coefficient	Std. Error	t-Statistic	Prob.	R-Squared	Durbin-Watson statistic
IMP	-9.45E-08	7.63E-08	-1.238346	0.2166	0.422556	1.316936
INTR*	-0.006347	0.005253	-1.813746	0.0708	0.363542	1.309016
IR	-0.003671	0.005463	-0.672068	0.5021	0.431942	1.311532
EXPORTS	-1.54E-07	1.20E-07	-1.285783	0.1996	0.420487	1.856716

Note:- '*' shows the significant variables at 10% level of significance.

Table (5) shows pair wise results. All the three models (pairs) are significantly affecting ROA as all the p-values are zero. Individually no variable is significant. The best significant regression model on the basis of highest R^2 is,

ROA = 0.269160 + 0.000904 (exports) - 2.06E-07 (inflation rate).

Predictors	F-Stat	individually Significant variable	P-Value	R-Squared	Durbin-Watson statistic
Exports, intr	8.861908	NIL	0	0.351149	1.838200
Exports, ir *	11.65659	NIL	0	0.415838	1.685123
Intr, ir	9.342024	NIL	0	0.363262	1.702156

Note:- "*" shows best model among all.

Table (6) shows result for full fledge model. The model is significantly affecting ROA but individually no variable is significant. The variable 'exports' is positively affecting the ROA while the others negatively affect the ROA. The model is,

ROA = 0.280647 + 2.92E-11 (exports) - 0.002613 (inflation rate) – 0.006846 (interest rate).

Table 6: Full panel regression model with three predictor Variables

Dependent Variable: ROA
Method: Panel EGLS (Cross-section weights)
Date: 09/09/12 Time: 15:40
Sample: 2005Q1 2009Q4
Cross-sections included: 15
Total panel (unbalanced) observations: 279
Linear estimation after one-step weighting matrix

Variable	Coefficient	Std. Error	t-Statistic	Prob.
C	0.280647	0.050912	5.512385	0.0000
IR	-0.002613	0.006956	-0.375675	0.7075
EXPORTS	3.89E-08	3.95E-07	0.098300	0.9218
INTR	-0.006846	0.008074	-0.847971	0.3972

Effects Specification

Cross-section fixed (dummy variables)

Weighted Statistics

R-squared	0.349328	Mean dependent var	0.281991
Adjusted R-squared	0.306947	S.D. dependent var	0.325361
S.E. of regression	0.270863	Sum squared resid	19.14869
F-statistic	8.242587	Durbin-Watson stat	1.827651
Prob(F-statistic)	0.000000		

Unweighted Statistics

R-squared	0.334879	Mean dependent var	0.210329
Sum squared resid	21.62282	Durbin-Watson stat	1.669186

In all the regression models Durbin-Watson statistic is suggesting no autocorrelation problem. All the external variables are negatively affecting the profitability (ROA) of domestic commercial banks of Pakistan.

CONCLUSION

This study is all about analyzing the important and significant external factors, affecting the profitability of domestic commercial banks of Pakistan. “All possible regressions” technique is used to estimate the impact of each individual predictor variable, pair wise predictor variables and three predictor variables on ROA. Only one variable out of four predictor variables was found individually significantly affecting the profitability of commercial bank of Pakistan; the variable is interest rate. All the four co-efficient are negatively affecting the bank’s profitability.

All the three panel regression models of pair wise bank specific variables are significantly affecting the ROA. Co-efficients of all variables are negative in all the three regressions. The full fledge panel regression model is also significantly affecting the ROA. Co-efficients of inflation rate and interest rate are negative while co-efficient of exports is negative in this model.

REFERENCES

- Baltagi BH. (2001). Econometric Analysis of Panel Data (second edition). John Wiley & Sons, Chichester. P, 93-113.
- Baltagi BH. (2005). Econometric Analysis of Panel Data (third edition). John Wiley & Sons, Chichester.
- Gujarati D. (2004). Basic Econometrics (4th edition). New York: McGraw-Hill.
- Indranarain R. (2009). Bank-Specific, Industry-Specific and Macroeconomic Determinants of Profitability in Taiwanese Banking System: Under Panel Data Estimation, *International Research Journal of Finance and Economics.* 34: 160-167.
- Karunakar M, Vasuki K and Saravanan S. (2008). Are Non - Performing Assets Gloomy Or Greedy From Indian Perspective?, *Research Journal of Social Sciences*, 3: 4-12.
- Kyriaki K, Sailesh T, Fotios P. (2005). Determinants of Profitability of Domestic UK Commercial Banks: Panel Evidence from the Period 1995-2002, Money Macro and Finance Research Group, 37th conference. 1-27
.
- Panayiotis PA, Sophocles NB and Matthaios DD. (2005). Bank-Specific, Industry-Specific and Macroeconomic Determinants of Bank Profitability, working paper No.25, Bank of Greece 5-35.
- Valentina F, Calvin M and Liliana S. (2009). The Determinants of Commercial Bank Profitability in Sub-Saharan Africa, IMF working Paper, WP/09/15, 2-32.

Comparative Genome/Proteome Analysis of Four Serotypes of Dengue Virus Using Bioinformatics Tools

Ayesha Arsha[1], Muhammad Naeem Shahwani,[1] Asma Yousufzai[1], Fazal-ur-Rehman,[2] Muhammad Asif,[1] Nazeer Ahmed[1]*
[1]Department of Biotechnology and Informatics, Balochistan University of Information Technology, Engineering and Management Sciences, Quetta,[2]Department of Microbiology, University of Balochistan, Quetta

Abstract

Dengue viral infections pose threat to almost half of the world's population health. The recent outbreak of dengue fever in Pakistan has invited attention of the scientific community to attempt devising ways and means and initiating programs controlling this menace. This work is also a step forward in the same direction. Utilizing different in-silico approaches like CLC Bio workbench, Protparam and Virus mploc comparative analysis of the full length genome and proteome of dengue virus serotypes was performed. All the four serotypes exhibited high level of similarities both at genome and proteome level. However, variations still existed though insignificant. Concerning prediction of sub-cellular localization of viral capsid, envelop and membrane glycoprotein in the host cell, all three proteins in four serotypes were shown to target endoplasmic reticulum. Endoplasmic reticulum hosting the viral structural proteins emerges as the pivot of the future studies aiming controlling dengue infections.

Key words: Dengue serotypes – in-silico-subcellular localization- Genome-Bioinformatics-Proteome

Corresponding author's email: (nazirdurrani@yahoo.com)

INTRODUCTION

The mysterious viruses are small, infectious, obligate intracellular parasites solely relying on host cells for their existence as they lack the fundamental biochemical machinery (Koonin et al. 2006). Although Viruses are one of the most important biological entities on the earth, still very limited understanding is there of both the number of virus species and the diversity of viral genes and genomes. It is however, beyond doubt that they infect almost all forms of life, including bacteria, archaea and eukaryotes from plants to humans to fungi (Prangishvili et al. 2006).

Among various viral infections, Dengue infection has been observed to cause havoc every now and then putting approximately, 40% of the world population at risk. The estimated figure of dengue infections is 50-100 million people worldwide (WHO 2012). Dengue virus (DENV), which is a mosquito-borne flavivirus causes a wide range of diseases in humans, from a self-limited Dengue fever, to a life-threatening syndrome called Dengue Hemorrhagic Fever (DHF). There are four antigenically different serotypes of the virus: DENV-1, DENV-2, DENV-3 and DENV-4. within the *Flavivirus* genus of the family *Flaviviridae (van der Most et al. 1996)* All four serotypes cause dengue fever (DF), and occasionally the potentially fatal dengue hemorrhagic fever (DHF) and dengue shock syndrome (DSS)(Melo et al. 2007). Despite many ongoing vaccine development programs, no prophylactic vaccine is currently available to prevent infection of DENV and the most effective protective measures are those that avoid mosquito bites. Precedents for successful vaccines exist against Flaviviruses (FV) like the one against yellow fever but vaccine design for other FV seems more complicated (Adams and Boots 2006; Seligman and Gould 2004; Thomas et al. 2006). For example, a primary infection with one strain of DV may predispose an individual to Dengue Hemorrhagic Fever, a more severe disease, if infected subsequently with a different DV strain. It is thus critically important to distinguish the common features of these viruses, as well as differences that may be associated with lethality.

This work aims at comparative analysis of the genomes and proteomes of all four serotypes of dengue virus with the purpose of finding the similarities and differences among all four serotypes. Similarities/differences at both DNA and amino acid level along with

predicting localization of viral proteins in the host cell will hopefully help the future work aiming at controlling the complications linked with the Dengue virus and even in vaccine/drug development.

MATERIALS AND METHODS

Sequences Retrieval

Complete genome and amino acid sequences of DENV 1-4 were retrieved from the National Center for Biotechnology Information (NCBI) resource (http://www.ncbi.nlm.nih.gov)

Nucleotide Sequence Analysis

CLC Sequence Viewer creates a software environment enabling users to make a large number of bioinformatics analyses. In this study CLC sequence viewer 6.5.4 version has been used to find out the nucleotide sequence statistics of all four serotypes of dengue virus. http://www.clcbio.com/products/clc-sequence-viewer/ .

Amino acid sequence Analysis

Protpsaram, a web based bioinformatics tool was used to calculate molecular weight, isoelectric point, sequence length and number of negatively and positively charged amino acids of all dengue serotypes (http://web.expasy.org/protparam/).

Predicting Subcellular Localization of Viral<Proteins in Host

Virus mPloc which is freely available on web was used to putatively predict localization of viral structural proteins in the host cell. The capsid, envelop and membrane proteins of four dengue serotypes were predicted for their subcellular localization**.**

RESULTS AND DISCUSSION

Nucleotide Sequence Statistics of all four serotypes of Dengue virus.

The comparative nucleotide sequence statistics of different serotypes of Dengue represents that all four serotypes possesses RNA genome. Among all serotypes, DENV-1 possesses the largest genome with a length of 10,735bp hence, bearing highest molecular weight of 3,471.58kDa. Furthermore highest GC contents were observed in DENV-4 i.e. 47.1% and lowest in DENV-2 i.e. 45.8%. DENV-1 and DENV-3 contains an equal amount of GC content i.e. 46.7%. Complete details of nucleotide sequence statistics of all serotypes is shown in table 1.

Table 1 Nucleotide Sequence Statistics of all Serotypes

Serotype	Sequence Type	Length	Count	C+G A+U	Frequency
DENV-1	RNA	10,735bp	3426,2240, 2770, 2299	5010 and 5,725	C+G=0.467 A+U=0.533
DENV-2	RNA	10,723,bp	3553, 2200, 2713, 2257	4913 and 5814	C+G=0.458 A+U=0.542
DENV-3	RNA	10,707bp	3425, 2218, 2783, 2281	5,001 and 5,706	C+G=0.467 A+U=0.533
DENV-4	RNA	10,649bp	3298, 2214, 2804, 2333	5,018 and 5631	C+G=O.471 A+U=0.529

Isoelectric point, molecular weight and nature of amino acids in Dengue serotypes

ProtParam is a web based tool which is widely used to compute different physical and chemical parameters for a query protein (http://www.expasy.ch/tools/protparam.html). The parameters, among others, include the molecular weight, theoretical pI and amino acid composition Isoelectric point (PI) refers to a pH at which a molecule carries no electrical charge. The theoretical Pi of the four Dengue serotypes ranged from 8, 63 to 8, 77. DENV3 was observed with the lowest PI while DENV2 manifested the highest.

The protein molecular weight of the four serotypes revealed that the DENV3 has the minimum while the DENV2 has the maximum molecular weight (377923,2 & 379803 respectively). The number of amino acids for the four serotypes, however, showed the difference of five amino acids between the largest (DENV1 with 3392 aa) and smallest (DENV4 with 3387 aa). The PI, Molecular weight and Number of amino acids for dengue serotypes are shown in table

Table 2: **Molecular weight, theoretical pI and Amino Acid sequence length of Dengue serotypes**

	DENV1	DENV2	DENV3	DENV4
Number of amino acids	3392	3391	3390	3387
Molecular weight	378755	379803	377923,2	378371,4
Theoretical pI	8,71	8,77	8,63	8,76

Positively charged and negatively charged amino acid residues were also calculated for dengue virus and comparison was made among the four serotypes. DENV2 contained the highest number of both positively and negatively charged residues followed by DENV4. Figure1 shows the detailed results.

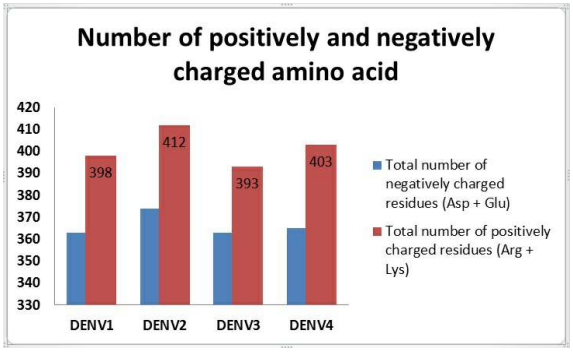

Fig 1. Comparative analysis of Dengue Serotypes in respect of variation in number of negatively and positively charged amino acids

Dengue protein subcellular localization in the host cell

Virus-mPLoc: is a freely available on line tool and is extensively used to predict the subcellular localization of viral proteins within host and virus-infected cells (Shen and Chou 2010). The same tool was used to putatively know the sub cellular localization of capsid, envelop and membrane glycoproteins of all four serotypes of dengue virus. Results are summarized in the following table.

Table 3: Putative location of Dengue structural proteins in the host

Protein	gi number	Amino acid length	Predicted location in host
Capsid protein Dengue virus 1	gi|158348409	100	Endoplasmic reticulun
Capsid protein Dengue virus 2	gi|159024809	100	Endoplasmic reticulun
Capsid protein Dengue virus 3	gi|164654862	100	Endoplasmic reticulun
Capsid protein Dengue virus 4	gi|282765486	115	Endoplasmic reticulun
Envelope (E) protein [Dengue virus 1	gi|158828123	495	Endoplasmic reticulun
Envelope (E) protein [Dengue virus 2	gi|159024812	495	Endoplasmic reticulun
Envelope (E) protein [Dengue virus 3	gi|164654853	493	Endoplasmic reticulun
Envelope (E) protein [Dengue virus 4	gi|73671171	495	Endoplasmic reticulun
Membrane glycoprotein Dengue virus 1	gi|158828122	75	Endoplasmic reticulun
Membrane glycoprotein Dengue virus 2	gi|159024811	75	Endoplasmic reticulun
Membrane glycoprotein Dengue virus 3	gi|158828127	75	Endoplasmic reticulun
Membrane glycoprotein Dengue virus 4	gi|73671170	75	Endoplasmic reticulun

All structural proteins of all serotypes of dengue virus are predicted to be localized in the Endoplasmic reticulum of the host. As far as amino acid length of these proteins is concerned, no difference was recorded for each of the three protein types among the serotypes except for capsid protein of DENV4 which was 115 amino acid long as compared to 100 for the rest of three dengue types.

DISCUSSION

The main focus of this work was to predict with the help of bioinformatics tools the sub-cellular localization of different dengue proteins in the host. Not only the prediction was made for all three structural proteins but also a comparative analysis was made among Dengue serotypes. Surprisingly all structural proteins belonging to all four serotypes were predicted to be localized in the Endoplasmic reticulum of the host cell. In a previous such work these proteins were predicted to be localized in the host plasma membrane(Somvanshi and Seth 2009). The discrepancy probably is due to usage of different versions of the same tool that is Virus ploc and its improved Virus mploc version. As the later was used in this study, we expect more sensitivity. As far as physical and chemical parameters of the amino acid sequences is concerned, DENV2 manifested the highest molecular weight, highest pi and largest sequence length showing the interdependency of these characters on each other. This is in addition to the highest number of both positively and negatively charged amino acids for the same serotype. Among all four serotypes, DENV-4 was observed with relatively high percentage of GC content i.e. 47.1% which indicates that the genome of this serotype is more stable as compared to other serotypes due to the increased percentage of hydrogen bonds between G and C nucleotides. Therefore, this serotype is thermally more stable and high energy is required in order to denature its genome as compare to other serotypes. Contrary to this, the genome of DENV-2 is least thermally stable and cannot tolerate high temperatures and pressures as compared to other three serotypes as its genome contains the less GC content i.e. 45.8%.

REFERENCES

- Adams B, Boots M (2006) Modelling the relationship between antibody-dependent enhancement and immunological distance with application to dengue. *J Theor Biol* 242: 337-346
- Koonin EV, Senkevich TG, Dolja VV (2006) The ancient Virus World and evolution of cells. Biol Direct 1: 29
- Melo PR, Reis EA, Ciuffo IA, Goes M, Blanton RE, Reis MG (2007) The dynamics of dengue virus serotype 3 introduction and dispersion in the state of Bahia, Brazil. Mem Inst Oswaldo Cruz 102: 905-912
- Prangishvili D, Garrett RA, Koonin EV (2006) Evolutionary genomics of archaeal viruses: unique viral genomes in the third domain of life. Virus Res 117: 52-67
- Seligman SJ, Gould EA (2004) Live flavivirus vaccines: reasons for caution. *Lancet.* 363: 2073-2075
- Shen HB, Chou KC (2010) Virus-mPLoc: a fusion classifier for viral protein subcellular location prediction by incorporating multiple sites. *J Biomol Struct Dyn* 28: 175-186
- Somvanshi P, ., Seth PK (2009) Comparative Proteome Analysis Of Distinct Variants Of Dengue Virus Using Insilico Approach. *The Internet Journal of Genomics and Proteomics* 4.
- Thomas S, Redfern JB, Lidbury BA, Mahalingam S (2006) Antibody-dependent enhancement and vaccine development. *Expert Rev Vaccines* 5: 409-412
- van der Most RG, Sette A, Oseroff C, Alexander J, Murali-Krishna K, Lau LL, Southwood S, Sidney J, Chesnut RW, Matloubian M, Ahmed R (1996) Analysis of cytotoxic T cell responses to dominant and subdominant epitopes during acute and chronic lymphocytic choriomeningitis virus infection. *J Immunol* 157: 5543-5554

Characterization of Sic by Means of C-V Measurement of Respective Schottky Diode by DLTS

Noor ul Huda Khan Asghar[1*], Zaheer Abbas Gilani[1], Muhammad Saifullah Awan[2], Irshad Ahmad[3], Wahab Q [4] and Muhammad Asghar [5]

[1] Department of Physics, Balochistan University of Information Technology, Engineering & management Sciences, Quetta, [2] Department of Physics, COMSATS Institute of Information Technology, Islamabad, [3] Govt. Technical Training Institute, Multan-Pakistan, [4]IFM, Linkoping University, Sweden, [5]Department of Physics, The Islamia University of Bahawalpur

Abstract

Silicon Carbide (SiC) has been characterized by means of capacitance spectroscopy. The capacitance voltage measurement of respective schottky diode is performed by standard method available in our DLTS setup. The capacitance voltage measurements of SiC are obtained at various temperatures under the similar reverse biasing conditions for material. From these measurements the following parameters were evaluated: The doping concentration of SiC at room temperature was calculated 5.2061×10^{12} cm^{-3}. Its value increased with increase in temperature and showed no significant temperature effect. The built-in potential calculated for SiC at room temperature was 1.49V. Its value gradually decreased with increase in temperature. The depth profile of SiC became more uniform with increase in temperature and showed no change as the temperature varied from room temperature to lower values. Comparison of the data with the literature showed that the sample was affected by native and/or intrinsic point defects developed during growth or metallization process.

Keywords: Semiconducting Silicon Carbide materials, C-V characteristics, Deep level transient Spectroscopy of the material, Schottky Diode.

[*]*Corresponding Author's email: noorulhudakhan@gmail.com*

INTRODUCTION

There is significant interest in developing semiconductor electronic devices capable of operating over a higher temperature range and with higher tolerance against ionizing radiation than currently available. Wide band gap materials are the potential candidates to fulfill such requirements and SiC is one of them. SiC include high-power high-voltage switching applications, high temperature electronics, and high power microwave applications in the 1 - 10 GHz region. SiC is attractive for these applications because of its extreme thermal stability, wide band gap energy, and high breakdown field (Powell and Rowland, 2002). Because of the wide band gap energy (3.0 eV and 3.25 eV for the 6H and 4H poly types respectively), leakage currents in SiC are many orders of magnitude lower than in silicon. Furthermore, SiC is the only compound semiconductor which can be thermally oxidized to form a high quality native oxide (SiO_2). This makes it possible to fabricate MOSFETs, insulated gate bipolar transistors (IGBTs), and MOS-controlled thyristors (MCTs) in SiC (Ikeda, 1988; Hidayet and Enise, 2005).

MATERIALS AND METHODS

Sample preparation

The sample wafer used for this research was 6H-SiC n-type wafer prepared at Linkoping

(Sweden). An epilayer of ~35 μm thick was grown on the SiC substrate by chemical vapor deposition (CVD) growth. Nitrogen dopant atoms were incorporated during the epitaxial growth sequence (Lin and Chang, 1995; Suzuki and Koizumi, 2004). Circular Schottky contact of 0.8mm diameter using Au and Ni separately was made by thermal evaporation.

Capacitance-Voltage C-V Measurements

The C-V measurements are necessary to determine the diode quality as well as to determine depth profile. At different temperatures capacitance voltage measurements were taken for various materials. From the C-V measurement we find the carrier concentration, built-in-potential and depth profile: Doping concentration 'N_d', Built-in potential 'V_{bi}' and Depth profile 'depth vs. N_d,

$$N_d = 2/[q\varepsilon_m * \text{slope}] \quad (1)$$

$$V_{bi} = [\text{intercept} * q\varepsilon_m N_d]/2 \quad (2)$$

$$Nd = [2(V_a + V_{bi})]/ [q\varepsilon_m d/dv(A^2/C^2)] \quad (3)$$

And

$$D(C) = \varepsilon_m A/C$$

Where

V_a = Applied voltage, V_{bi} = Built-in potential, q = Electron charge,

ε_m = Relative permittivity of the material, D = Depth

RESULTS AND DISCUSSION

Capacitance-Voltage C-V Measurements of SiC

The typical C-V characteristics of n-type 6H-SiC as grown at different temperatures 295K to 400K are shown in Figures 1 to 12. In the graphs of Voltage (V) and (A/C the straight line is taken as the theoretical linear fitting of the curves. The graphs of depth profiles have taken between depth and doping concentration shown in Figures 13 and 14. Using equations (1) and (2) and for depth profile using equation (3) we calculated the following parameters shown in table below.

Temperature (T) K	Doping Concentration (N_d) cm^{-3}	Built in potential (V_{bi}) V
295K	$5.2061' 10^{12}$	1.49
320K	$1.1402' 10^{13}$	0.90
340K	$2.8920' 10^{13}$	0.72
360K	$7.8894' 10^{13}$	0.52
380K	$1.3945' 10^{14}$	0.60
400K	$2.5968' 10^{14}$	0.54

Table: 1 Parameters calculated from CV measurements of 6H-SiC

From table 1 we observed that the doping concentration and built-in potential was effected by temperature. The value of Nd at room temperature was determined 5.2061 $' 10^{12} cm^{-3}$ which increased with the increase in temperature. While the value of Vbi at room temperature calculated as 1.49V and gradually lowered on increasing temperature and measured 0.54V at 400K also an unsequence value of Vbi determined at 360K.

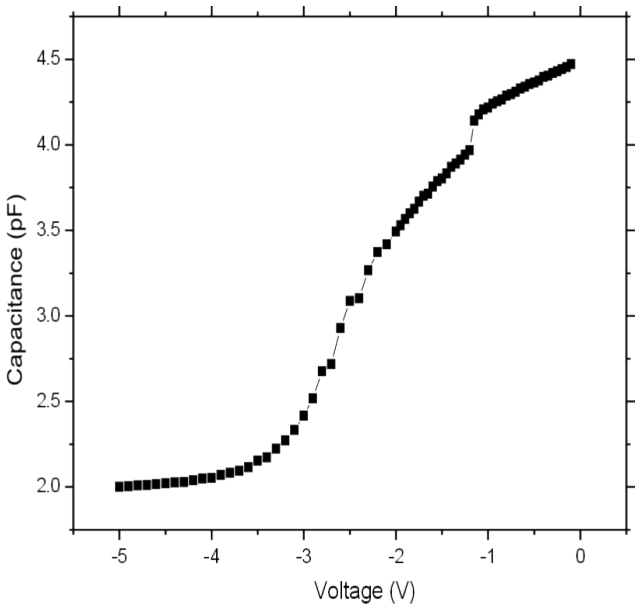

Fig 1. The graph between C-V of SiC at T=295K.

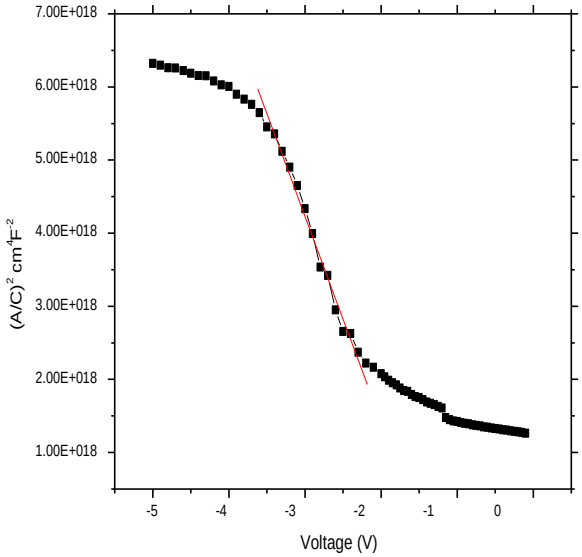

Fig 2. The graph between V and $(A/C)^2$ of SiC at T=295K.

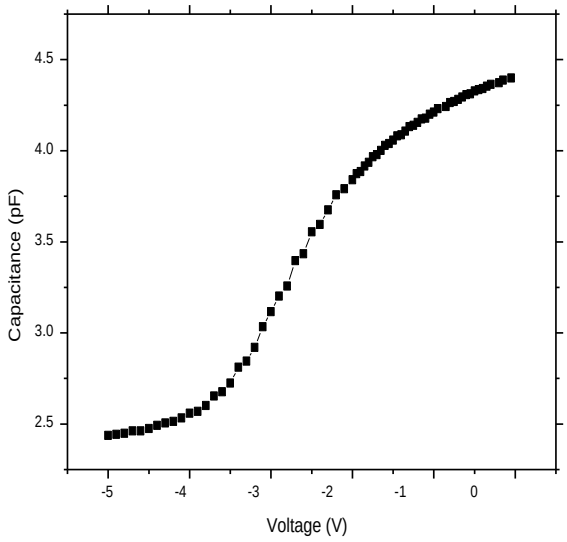

Fig 3. The graph between C-V of SiC at T=320K

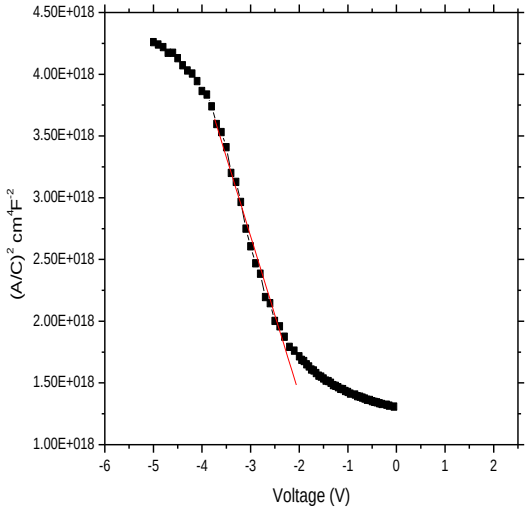

Fig 4. The graph between V and $(A/C)^2$ of SiC at T=320K

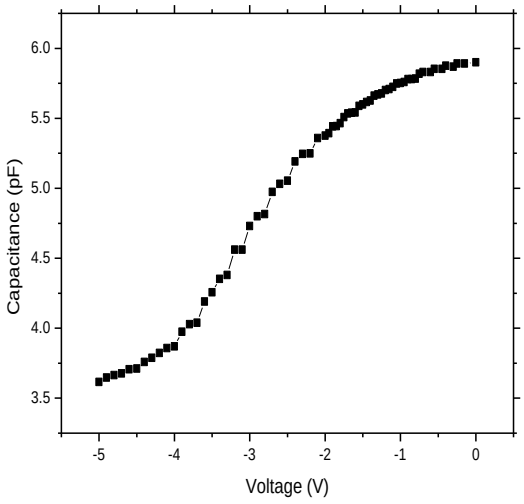

Fig 5. The graph between C-V of SiC at T=340K.

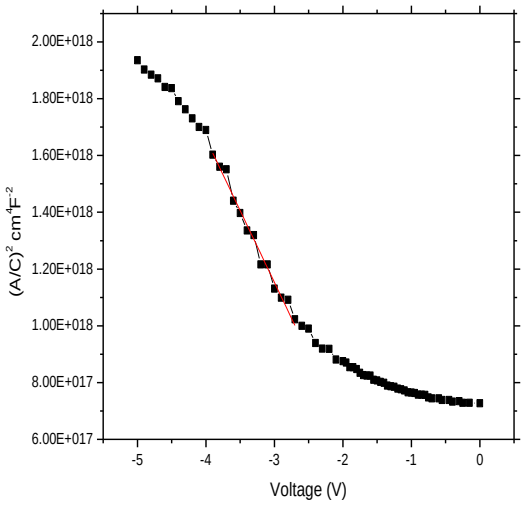

Fig 6. The graph between V and $(A/C)^2$ of SiC at T=340K

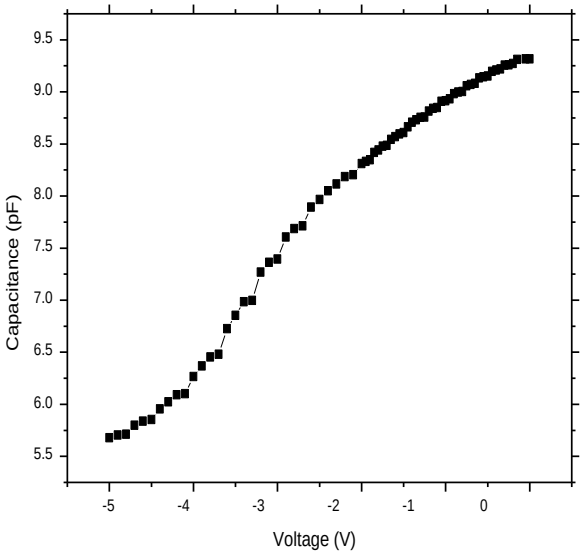

Fig 7. The graph between C-V of SiC at T=360K.

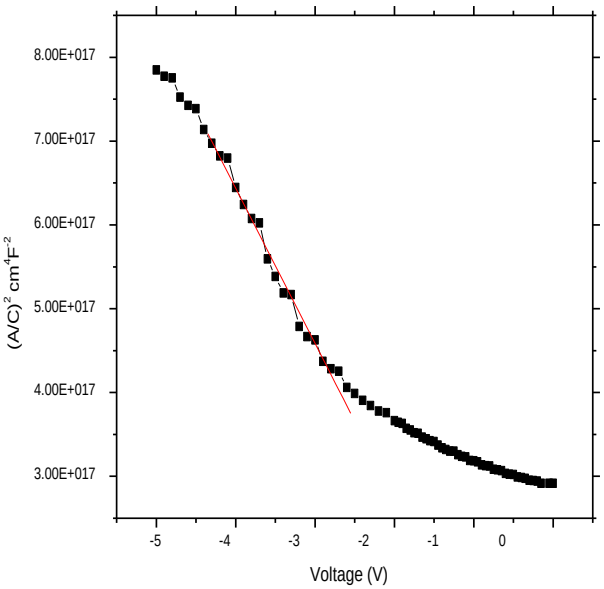

Fig 8. The graph between V and $(A/C)^2$ of SiC at T=360K.

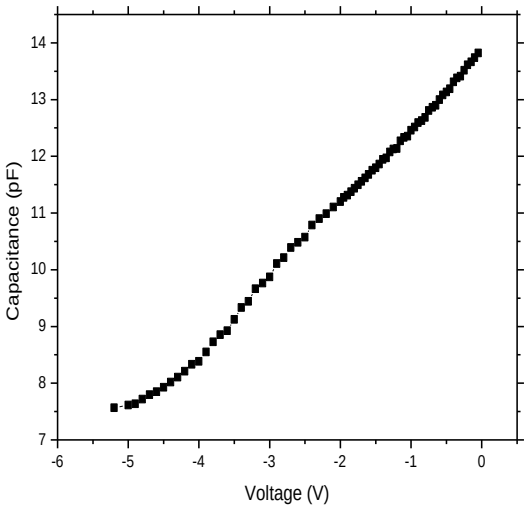

Fig: 9 the graph between C-V of SiC at T=380K.

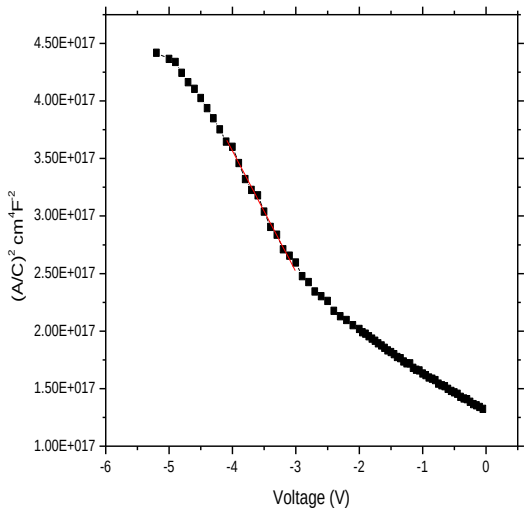

Fig: 10 the graph between V and $(A/C)^2$ of SiC at T=380K.

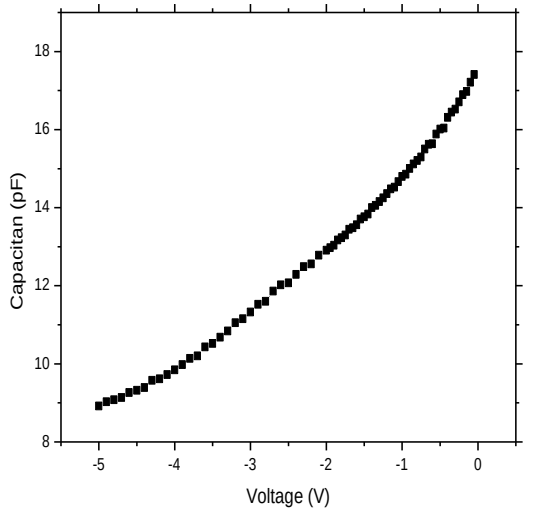

Fig: 11 the graph between C-V of SiC at T=400K.

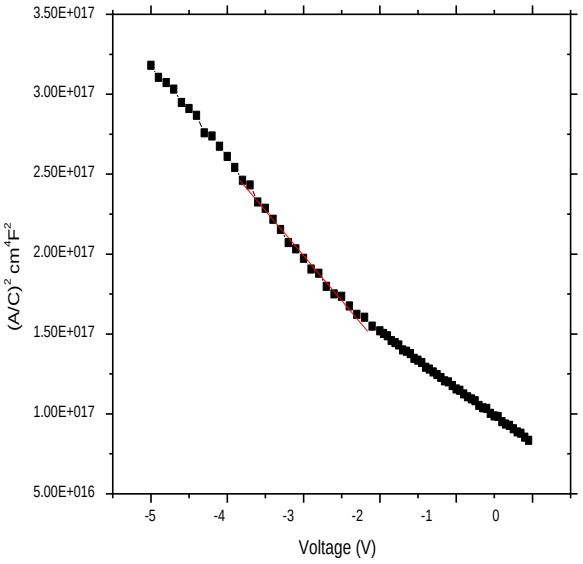

Fig:12 the graph between V and $(A/C)^2$ of SiC at T=400K.

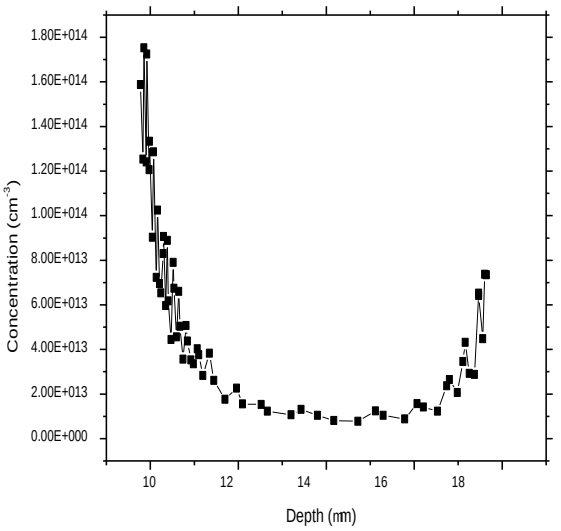

Fig 13 Depth profile of SiC at 320K.

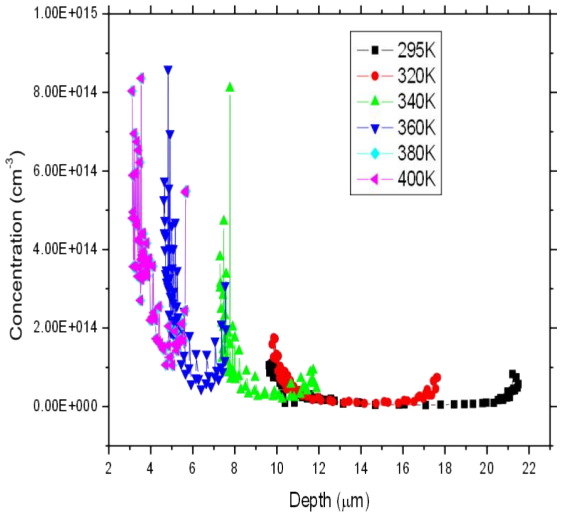

Fig: 14 Depth profile of SiC at various temperatures.

CONCLUSION

We studied the characterization of SiC by means of capacitance spectroscopy. The I-V characterization was performed to evaluate the rectifying behavior of the diode. The ideality factor (n), reverse saturation current (I_s) and barrier height (φ_B) of the diodes at various temperatures were evaluated. Doping concentration (N_d), built-in potential (V_{bi}) and depth profile were determined by C-V measurements.

The n-type 6H-SiC sample was grown on SiC substrate ~35μm thick by chemical vapors deposition technique. I-V and C-V measurements were taken at 295, 320, 340, 360, 380 and 400K. The calculated values of n, I_s, and φ_B at room temperature (R_T) were 1.9894, 6.57´ 10^{-13}A and 0.995eV respectively. N_d and V_{bi} at R_T were 5.2061 ´ 10^{12}cm^{-3} and 1.49V respectively. Over the temperature range, investigated I-V characteristics confirm that the conduction mechanism of the diode is controlled by thermionic field emission.

I-V measurements of SiC show ideality factor (n) to be close to unity at room temperature (R_T) indicating the main mechanism of current flow was thermionic emission. However, below the R_T, the ideality factor was bit higher which is understandable due to the freezing of carriers [3, 4, 5]. From C-V measurements the depth profiles of material remain uniform.

REFERENCES

Ÿ Powell AR and Rowland LB, (2002). SiC Materials Progress, Status, and Potential Roadblocks. Proceedings of IEEE. 90 (6): 942-955

Ÿ E.Ikeda, Jpn, J.Appl. Phys., 127, 180 (1988). And A.Gumus, journal of applied Phys., 91, (1).

Ÿ Hidayet Cetin and Enise Ayyildiz, Semicond. Sci. Technol 20, 624 (2005).

Ÿ C. F. Lin and Y. A. Chang, Appl. Phys. Lett., 67, 24 (1995).

Ÿ Marcio Suzuki and Satoshi Koizumi, Diamond and Related Material 13, 2037 (2004).

Reduction of Fibrillation of Lyocell Fabric in Continuous Dyeing

Noor Ahmed* and Nazakat Ali
Department of Textile Engineering, Balochistan University of Information Technology, Engineering & Management Sciences, Quetta

Abstract

Lyocell is one of the recent regenerated cellulosic fibres. It is produced by an environmentally-friendly process from wood pulp. Chemical structure of lyocell is similar to that of cotton and other regenerated fibres. The main difference is of the length of polymer chains (degree of polymerization).The main technical problem with this fiber is its ease of fibrillation. Fibrillation becomes apparent when fiber is abraded in wet state during pre-treatment and dyeing. The reason of such change of lyocell fibre surface is due to its physical structure (i.e. arrangement of polymer chains in amorphous and crystalline regions). Lyocell fabrics were processed by continuous dyeing method to observe the fibrillation effects. Cross-linking agents were applied before and after dyeing to see their effect on fibrillation. The fibrillation was assessed by observing the fiber morphology on Scanning Electron Microscope (SEM). The samples were also tested for color fastness to washing. Further, the color assessment k/s was performed to compare color yield of dyed, dyed cross-linked and cross-linked samples. The cross-linked dyed and dyed cross-linked samples were found to have reduced fibrillation. There was not any significant difference in colorfastness of dyed, dyed cross-linked and cross-linked dyed fabrics and the fastness was generally very good to excellent.

Key words: Lyocell, Fibrillation, Cross-linking agent, Continuous Dyeing.

Corresponding Authors' email: noor.ahmed@buitms.edu.pk

INTRODUCTION

Lyocell is the first in new generation of cellulosic fibers. TENCEL® is the registered trade name for lyocell which is a biodegradable fabric made from wood pulp Cellulose. It is produced by environmentally-friendly process from wood pulp. It is comfortable and popular in clothing because of absorbent nature and high strength. Lyocell is regenerated and it is 100% cellulosic fiber (Patrick, 2001). It is durable and has low shrinkage as compare to other regenerated cellulosic fibers (Bates et al., 2008). Lyocell is a fiber spun from organic solvents. Commercially, lyocell fibers are regenerated cellulose fibers spun from a cellulose solution in a mixture of N-methylmorpholine N-oxide (NMMO) and water. Lyocell is more environment friendly fiber (Renfrew and Philips, 2003). The method involves dissolving cellulose in N-methyl morpholin-N-oxide (NMMO) and filament is extruded into spinning bath solution followed by washing, drying and cutting (Bates et al., 2004). After drying material is passed to finishing section for the application of lubrication. This may be silicon, soap or any other agent (Martin et al., 1998). In wet state lyocell fibers fibrillates when they are rubbed or agitated during wet-processing, the micro fibrils are formed on the fiber surface. It affects lyocell to greater degree than cotton, flax and viscose (Chaudemanche and Patrick, 2010). Dyeing with Bi- functional reactive dyes help to reduce fibrillation problem (Nicolai et al. 1996). Fibrillated lyocell produces darker shades which means higher color uptake as compare to non-fibrillated it may be due to low light scattering on fibrillated surface (Goswani et al., 2007).The fibrillation tendency of lyocell can be reduced by chemical reagent which contains at least two aliphatic aldehyde groups, capable of reacting with each other (Wang et al., 2003). Different types of finishes have been used for

cross-linking cellulose fibers. DMDHEU (*Dimethylol dihydroxyethyleneurea*) is most important reactant resin. DMEU (*Dimethylol ethylene urea*) is a reactive resin of high reactivity. It is suitable for the production of resin finishes on cotton /polyester blends. DMDHEU is very stable to hydrolysis, having bad colour fastness against chlorine. The finished effects are fast to boiling wash treatments. (Rouette, 2000). The aim of this research work was to control the problems of fibrillation during wet processing of lyocell fabric and minimize the fibrillations by using cross-linking agents.

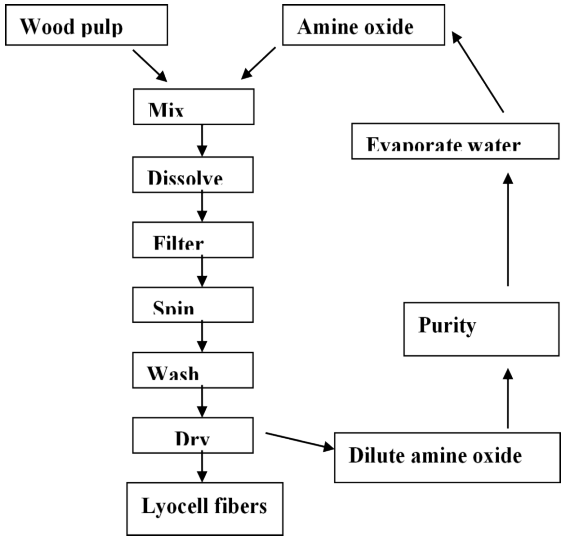

Figure 1: Schematic of Lyocell manufacturing (Patrick, 2001)

MATERIALS AND METHODS

Fabric

Gray 100% lyocell woven fabric (223 grams per square meter after preparation) was used in this study. The fabric construction was 16x16/102x66, twill.

Dyes and chemicals

Drimaren CL, bi-functional, and Drimaren K, di-fluorochloropyramidine, dyes of Clariant were used in this study. Trichromatic colours of Drimaren CL and Drimaren K reactive dyes and their percent concentrations used for dyeing are given in below table. Arkofix XLF (Clariant) was used as an inter-polymer cross-linking agent. Chemicals, sodium carbonate and Magnesium chloride used were analytical grade and the sodium hydroxide (48°Be) and H_2O_2 (50%) were commercial grade.

Table 1: The specific dyes for Tri-chromatic combination and their grams per liter

Grams /liter	Drimaren K dyes	Drimaren CL dyes
1.7 g/l	Yellow K2R = 1 g/l Red K4BL = 0.5 g/l Blue K2RL = 0.2 g/l	Yellow Cl2R = 1 g/l Red Cl4BN = 0.5 g/l Navy CLR = 0.2 g/l
13 g/l	Yellow K2R = 6 g/l Red K4BL = 3 g/l Blue K2RL = 4 g/l	Yellow Cl2R = 6 g/l Red Cl4BN = 3 g/l Navy CLR = 4 g/l

Preparation of Gray Lyocell Fabric for Dyeing

Desizing and bleaching.

Desizing process was carried out by pad-batch process using Desizer HT 100 (Enzymatic). Lyocell fabric rolled in the form of small batch for 12 hours. After 12 hours washing cycle was carried out in multiple sections; such as hot wash (90 - 95C) for 15 min, warm wash (60 - 70C) for 10 min. Finally the fabric dried in dryer. The bleaching process of the fabric was carried out using mild chemical concentrations as per recommendation of Clairant Pakistan Ltd.

Process Sequences for Dyeing and Finishing of Lyocell Fabric.

The process sequences for dyeing and finishing in this study are given by chart.

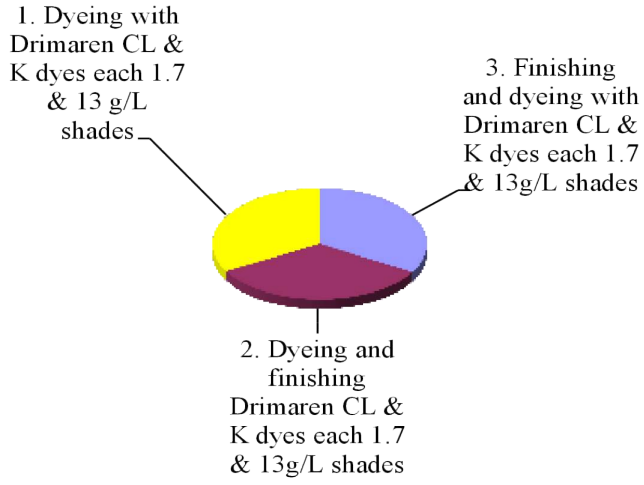

Figure 2: process sequence for dyeing and finishing of lyocell fabrics by chart.

Dyeing of Lyocell Fabric with Reactive Dyes

Continuous dyeing was carried out for assessment of fibrillation properties. Drimaren K and Drimaren CL dyes were applied for comparative analysis. Continuous dyeing process was carried out on the fabric which was pre-treated. Twelve samples were dyed through continuous dyeing. Six samples of each Drimaren K dyes and Drimaren CL dyes dyed in two different concentrations 1.7g/l and 13g/l. Drimaren K and Cl dyes auxiliaries; wetting agent (Leonil EHC) anti migrating agent (Solidikol N), fixing agent (Na_2CO_3) and the dyes were used. The Fabric Was Padded at 75 % Pick up. It Was Dried at 120^{o}c for 2 Min and Cured at 160^{o}c for 1 Min.

Finishing of Lyocell Fabric

Fabric Was Padded in the Recipe Containing Arkofix XLF, $Mgcl_2$, and Ceranine HCS at 75% Pick up. After Drying of Lyocell Fabric at 120^{o}c, It Was Cured for 3 Minutes at 185 ^{O}c.

Color Fastness to Washing Test (ISO 105-c03)

Samples Were Treated According to ISO 105-CO3. First Bulk Solution for Washing Prepared with 50:1 in Each Washing Container. Then Fabric Pieces (10x4 Cm^2) Dipped in Containers and These Containers Fixed into the Laundro-meter. Machine Was Run at 60^{o}c for 30 Minutes. After That, Samples Taken Out, Rinsed with Cold Water and Dried.

Colour Difference Test (Aatcc 173-2005)

Dyed and Finished Samples Were Tested on Spectrophotometer after Conditioning at 21$\pm$1^{o}c Temperature and 65$\pm$2% Relative Humidity. Spectrophotometer Was Calibrated First with White, Black and Green Colored Tiles. The Samples Sequentially Assessed for the Color Strength (K/s) Values.

Scanning Electron Microscope (Sem) Analysis

The Images of Lyocell Samples Were Captured on Scanning Electron Microscope (JEOL Japan Model No. JSM- 6380A) at the Magnification of 100-500. Samples for SEM Analysis Were Coated on Auto Coater (JEOL Japan Model No. Jfc- 1500). The Coating Was of Gold and Samples Were Coated up to 300^{o}a.

RESULTS AND DISCUSION

This Section Presents Experimental Results and Analytical Discussion on Technical Fibrillation Problem of the Lyocell Fabric. The Section Focused on the Effect of Dyeing Processes on Fibrillation and Other Related Properties of Lyocell Dyed Fabric. The Improvements by Pre and Post Cross-linking Processes Have Also Been Reported in This Section.

Comparative Study of Dyed, Dyed Cross-linked and Cross-linked Dyed Samples

Colour fastness to washing:

It was observed that up to 13 g/l of dark shades lyocell dyed samples gave good results. Reasons of good result were due to stable covalent bond formation between cellulose and reactive dyes. It was also observed that Drimaren K dyed samples have better washing results in comparison to Drimaren CL dyes on lyocell fabrics.

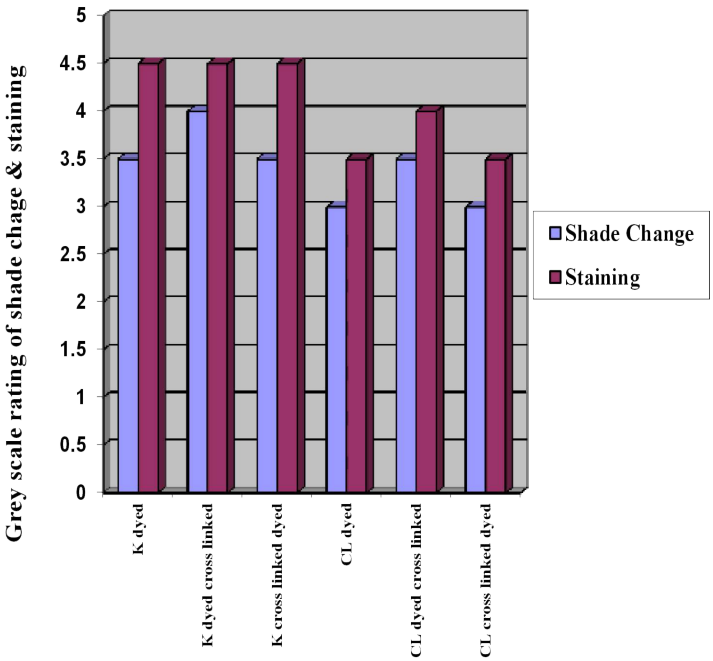

Figure 3: colour fastness to washing by chart Drimaren CL and K dyes.

Color strength (K/S)

It was observed that, in general colour strength values increases by the increasing in concentration of dye applied. It was generally observed that dyed and cross-linked dyed display higher colour yield.

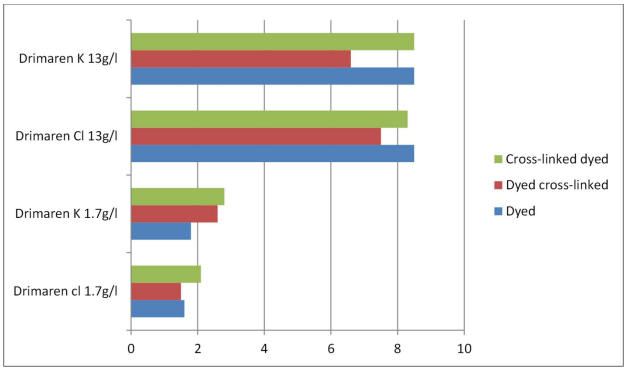

Figure 4: colour strength at maximum absorption of dyed, dyed cross-linked and cross- linked dyed samples by chart.

Surface Analysis of Lyocell Fabric:

It was observed from following figures that at magnification of x100 and x 500 dyed samples have higher fibrillation problem as compare to dyed cross-linked and cross-linked dyed lyocell samples. In both types of dyes (CL and K) at different concentrations fibrillation of dyed samples was higher. The problem of fibrillation was reduced, using cross-linking agents. Reason of this was that Reactive dyeing processes and resin finishing reduce fibrillation of lyocell fibers (Wang et al., 2003).

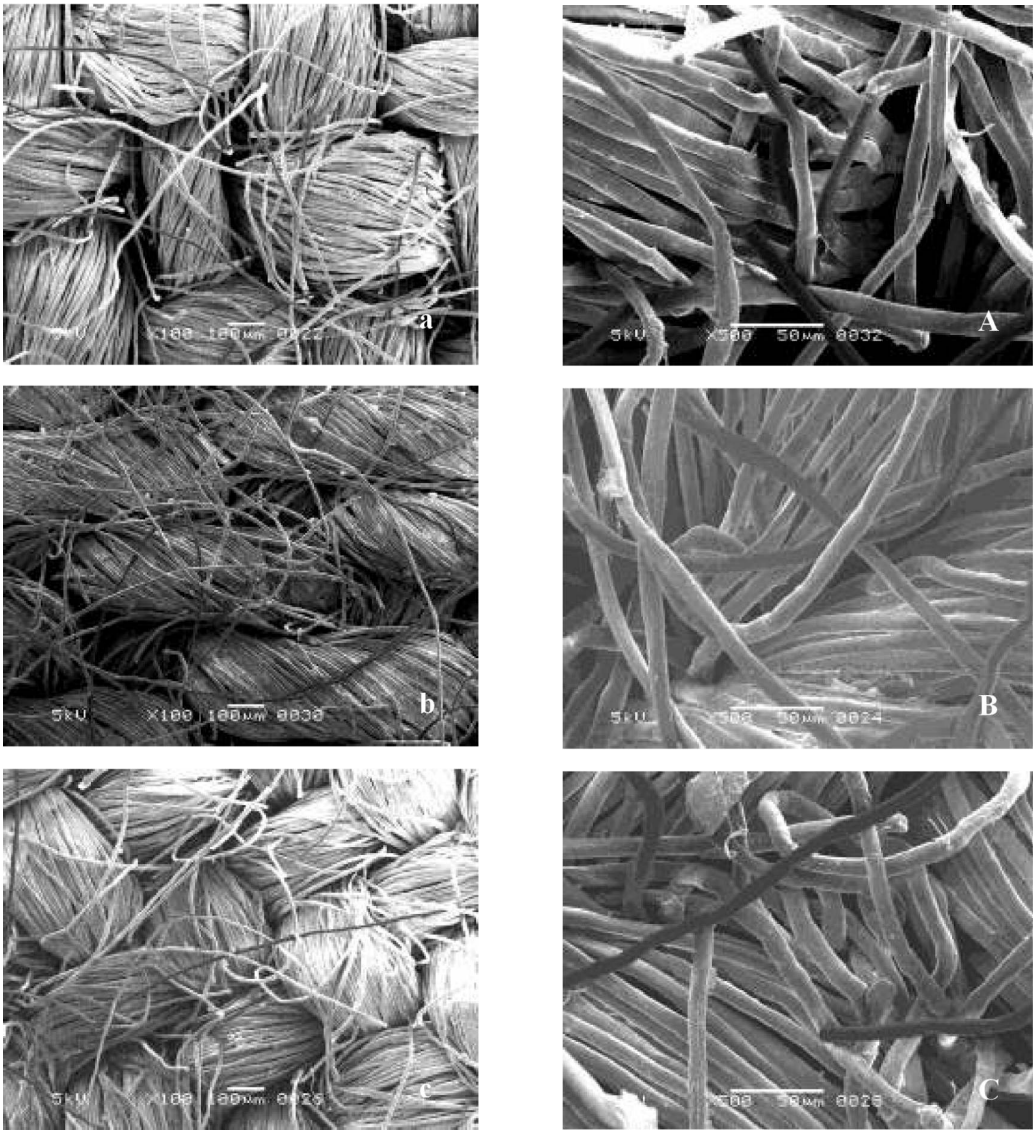

Fig. 5: Scanning electron micrographs of Drimaren K 1.7g/l (a) dyed, (b) dyed cross-linked (c) cross-linked dyed at magnification of x100 and (A) dyed, (B) dyed cross-linked (C) cross-linked dyed at magnification of x500.

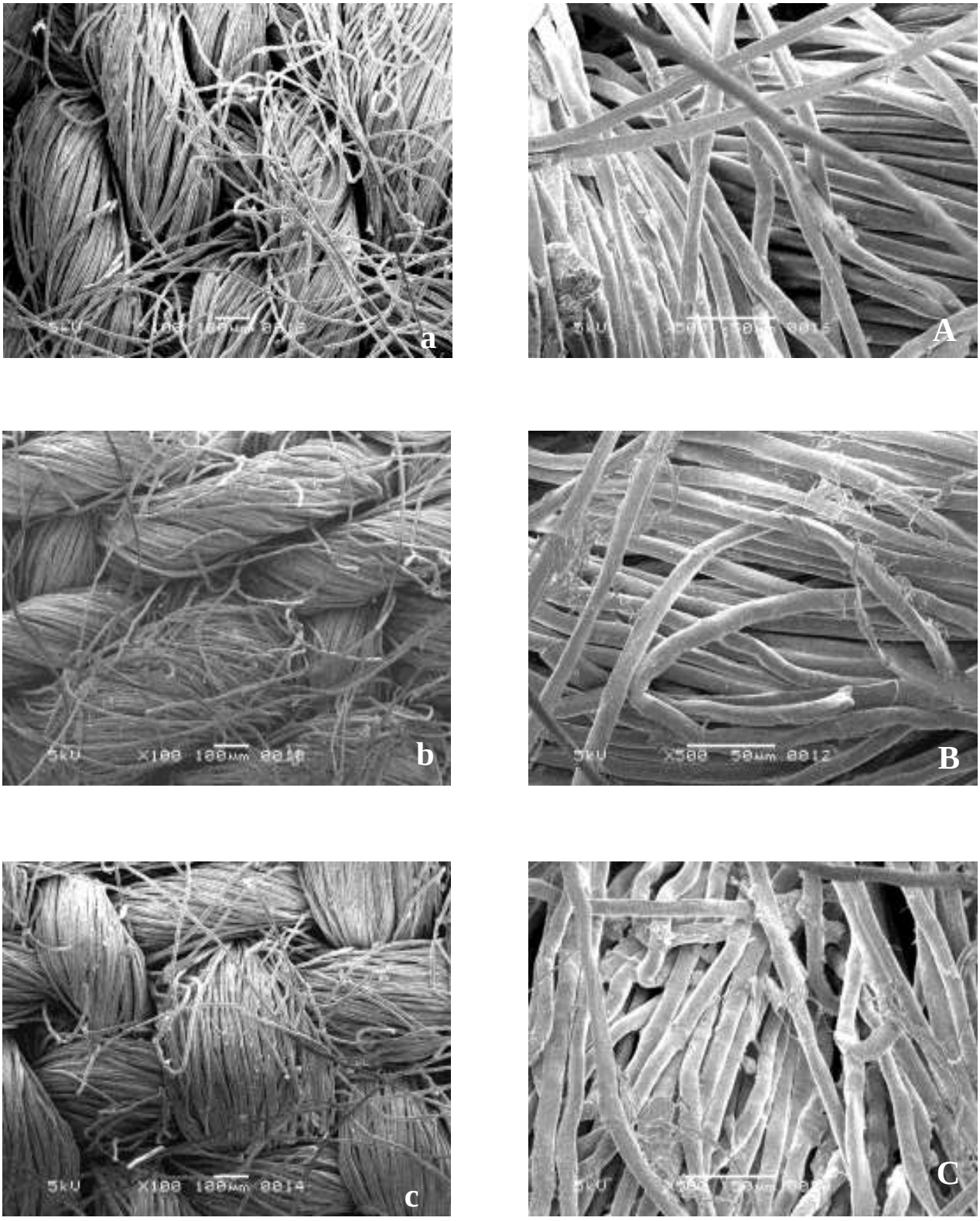

Fig 6: Scanning electron micrographs of Drimaren CL 1.7g/l (a) dyed, (b) dyed cross- linked (c) cross-linked dyed at magnification of x100 and (A) dyed, (B) dyed cross-linked (C) cross-linked dyed at magnification of x500.

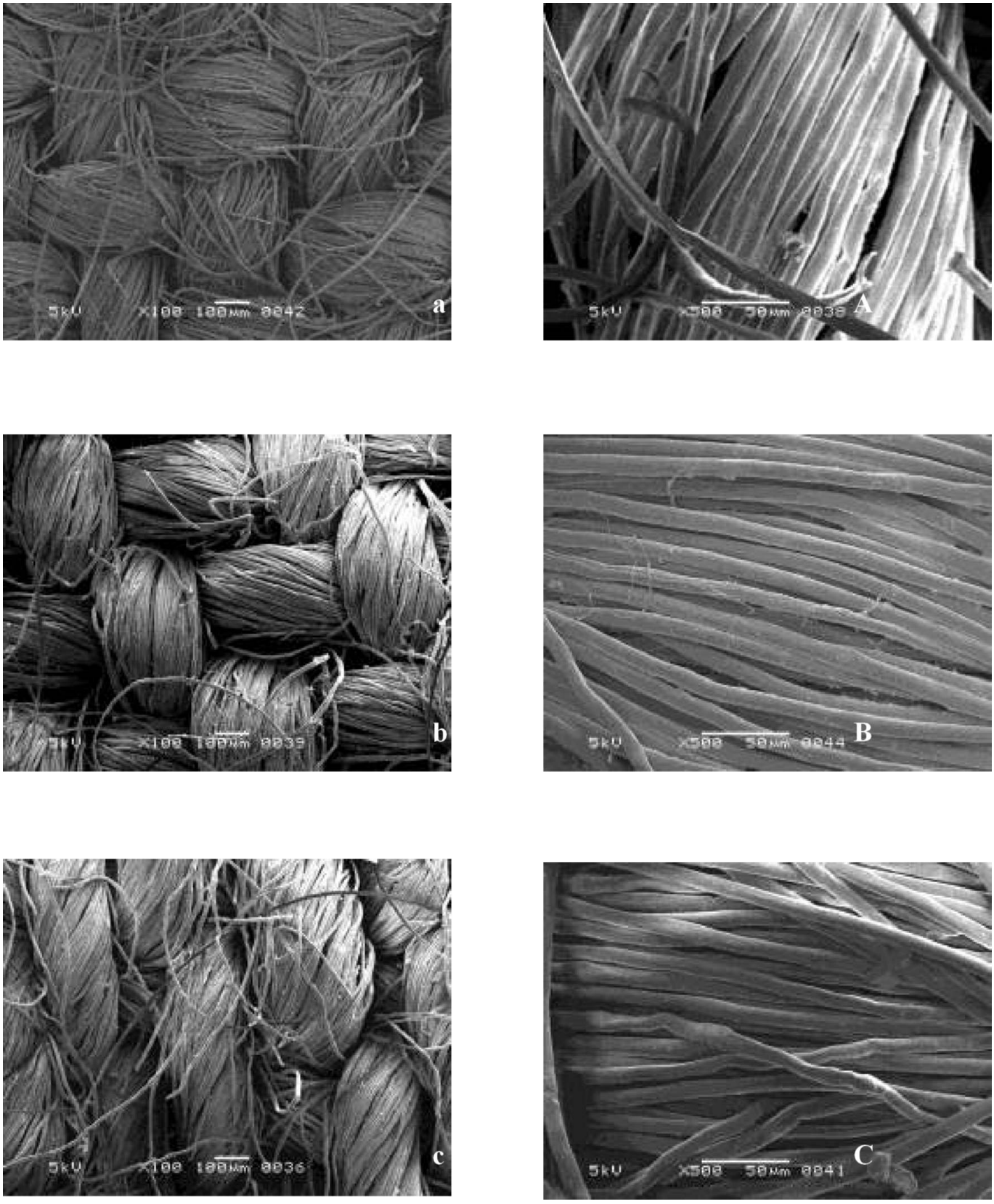

Fig 7: Scanning electron micrographs of Drimaren K 13g/l (a) dyed, (b) dyed cross-linked (c) cross-linked dyed at magnification of x100 and (A) dyed, (B) dyed cross-linked (C) cross-linked dyed at magnification of x500.

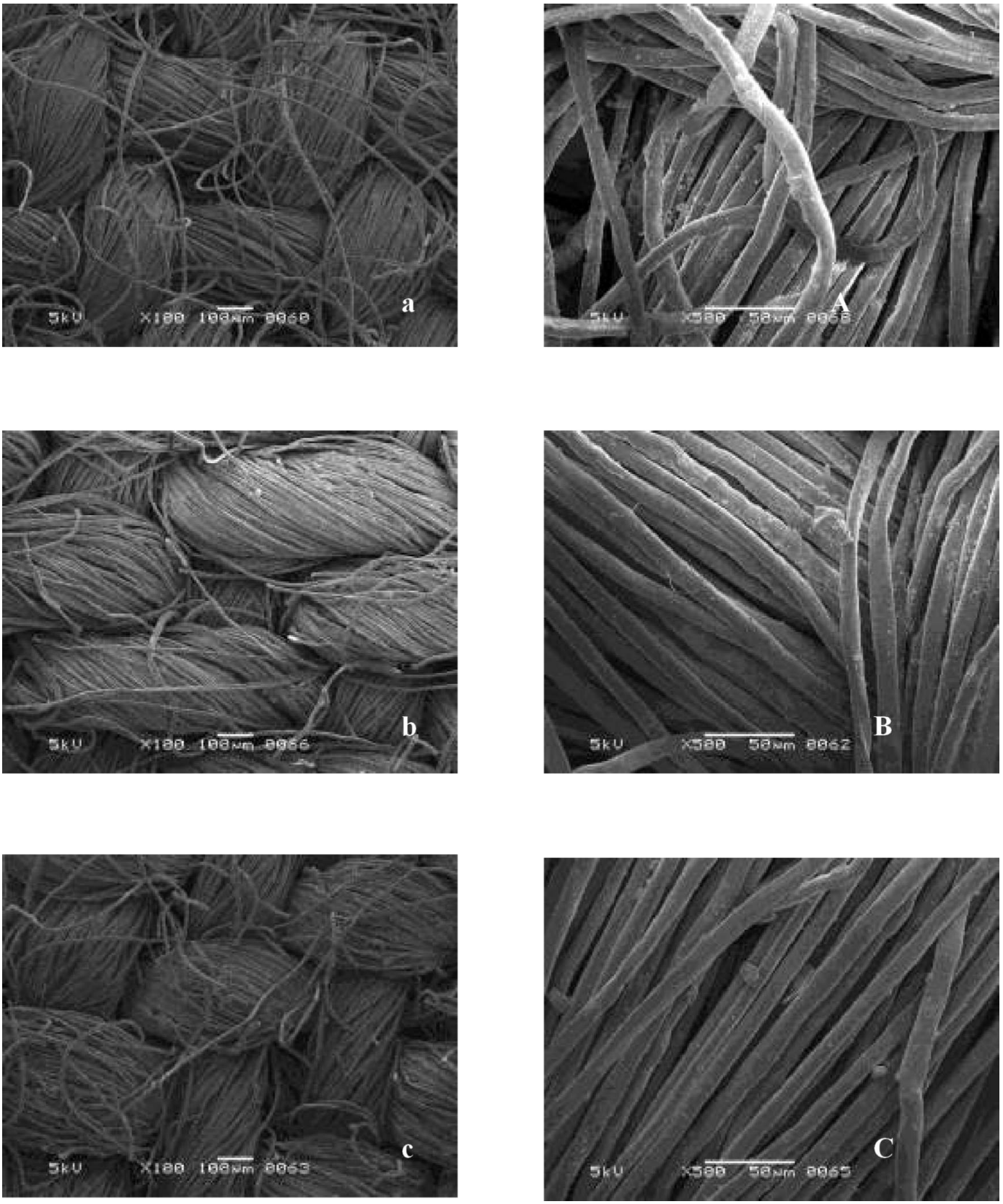

Fig 8: Scanning electron micrographs of Drimaren CL 13g/l (a) dyed, (b) dyed cross- linked (c) cross-linked dyed at magnification of x100 and (A) dyed, (B) dyed cross-linked (C) cross-linked dyed at magnification of x500.

CONCLUSION

This study showed that regenerated cellulosic lyocell fiber has the technical problem of fibrillation generation during processing. Pre-treated lyocell fabric was found to have excellent absorbency. It was found in this study that the fibrillation problem increased as the lyocell fabric passed through further processes such as dyeing and washing. It was further concluded from the results obtained that the fibrillation can be controlled by the application of internal polymer cross-linking agent, which acts as a linking bridge between cellulosic polymer chains. After application of cross-linking agent, dye sites are disturbed because cross-linking agents attach at hydroxyl group of cellulose which is also the dye site for reactive dye. Thus, there are always chances for cross-linking agent to occupy the dye site and compete with reactive dye molecules. This may affect the color strength. fiber surface analysis showed that the surfaces of fibres were smoothened after application of cross-linking agents but shade depth and hue changed slightly. If pre-treatment cost of natural cellulosic fabrics and lyocell fabrics is compared for similar whiteness and absorbency level then it can be concluded that lyocell pre-treatment was economical. This is because of less processes and low chemical concentrations required for pre-treatment of lyocell fabric. Further, lyocell fabric has higher absorbency, thus, having more dye-uptake and less dye wastage than the other cellulosic fibres. The lyocell fabrics attained peach-skin effect during wet-processing, which is an advantageous factor over natural cotton and other regenerated cellulose fibres.

REFERENCES

- Bates I, Riesel, R and Renfrew AHM. (2008). Protection of LyocellFibers Against Fibrillation, Influence of Dyeing with Bis- Monochloro-s-Triazinyl Reactive Dyes. *Colour Technology.* 124: 252-258.
- Bates I, Maudru E and Phillips DAS. (2004). Cross-linking Agents for the Protection of Lyocell against Fibrillation: Synthesis, Application and Technical Assessment of 2, 4-Di-acrylamidobenzene Sulphonic Acid. *Coloration Technology.* Society of Dyers and Colourists. 120: 293- 300.
- Chaudemanche C and Patrick N. (2010). Swelling and Dissolution Mechanism of Regenerated Lyocell Cellulose Fibers *Springer,* 18: 1-15.
- Goswani P Taylor J and Patrick M.W. (2007), “Dyeing Behavior of Lyocell Fabric: Effect of Fibrillation”, *Coloration Technology*, Society of Dyers and Colourists, V. 123, September 2007, pp.387-393.
- Martin James, Graveson Ian and Ashley S. (1998). Process For the Manufacturing Lyocell Fibers. *United States Patent Number 5,725,821.* 1-8.
- Nicolai M, Nechwatal A and Mieck KP. (1996). Textile Cross-linking Reactions to Reduce the Fibrillation Tendency of LyocellFibers. *Textile Research Journal.* 66: 575-580.
- Patrick, M.B.E. (2001), *Lyocell: The Production Process and Market Development, Regenerated Cellulose Fibers*, 1st edition, wood head publishing limited, Cambridge England, pp.62-86.
- Renfrew AHM and Philips DAS. (2003). Protection of Lyocell Fibers Against Fibrillation: Mode of Action of Cross-linking Agent 2, 4 - Dichloro-6-(Sulphatoethylsulphonyl) Anilino-s-Triazine. *Colouration Technology.* 119: 116-120.
- Rouette HK. (2000). *Encyclopedia of Textile Finishing*, New York, Springer Science, Business Media, L.L.C, pp. 130- 156.
- Wang Young- Soo, Koo Won-Mi and Kim H. (2003).Preparation and Properties of New Regenerated Cellulose Fibers. *Textile Research Journal.* 1-9.

Handshaking vs. Instant Broadcast in VANET Safety Message Routing

Faisal Khan[1], Yusun Chang[1], SungJin Park[1], Ehsanullah Kakar[2], John Copeland[1]
[1]School of Electrical and Computer Engineering, Georgia Institute of Technology, Atlanta, USA
[2]Department of Civil Engineering, Balochistan University of Information Technology , Engineering & Management Sciences, Quetta

Abstract

Vehicular ad hoc networks (VANETs) rely on multihop communication in order to disseminate information to locations beyond the transmission range. In this paper, the use of handshaking mechanism is evaluated against instant transmission for safety message routing in VANETs for the first time. It is argued that due to the small size of VANET safety message (mean payload size of 100 bytes), handshaking may not be advantageous to avoid hidden node problem and may incur overhead delay. The simplified instant broadcast routing without the use of handshake mechanism is recommended. Theoretical analysis of message propagation delay using instant broadcast routing is shown which can be easily extended for any broadcast method. Two prominent handshake based broadcast routing schemes are implemented in ns-3 along with instant broadcast scheme. The simulation results reveal that the instant broadcast effectively lowers the message propagation delay by half, and guarantees reliable dissemination of safety messages to all endangered vehicles on the road. Index Terms—VANETs, roads, vehicular traffic, broad.

Keywords: Handshaking, Instant Broadcast in VANET, Road-width, Sectoring

* *Corresponding Author's email: ehsan@buitms.edu.pk*

INTRODUCTION

In recent years, we have witnessed a large increase of research interest in the area of Vehicular ad hoc networks (VANETs). A number of factors have contributed to the growing interest including serious aim of vehicle manufacturers to incorporate information technology to ensure safety, environmental and comfort issues of their vehicles; and the concern of governments for adoption of innovative technologies to provide road safety. One of the important safety applications in VANETs is Cooperative Collision Warning System (CCWS) that disseminates safety alert messages to prevent potential accidents (Yan et al., 2010). Several messages in this category need to be propagated to vehicles beyond the immediate transmission range, e.g. safety alert messages about hazardous driving situations such as dangerous road surface, unexpected road block, accidents, unexpected fog banks, and so on (Fasolo et al., 2006; Rudack et al., 2003). Dissemination of such messages requires the design of effective propagation algorithms that can provide reliable message delivery to all the relevant vehicles with minimum delay. Propagation of message beyond the immediate transmission range involves multi-hopping in the highly dynamic network. Consequently, the propagation scenario becomes much more complex as multi-hop increases the chances of collision and also causes over consumption of radio resource due to unnecessary retransmissions (Korkmaz and Ekici, 2004) . Considerable research has been carried to address the complex routing mechanism in VANETs. In this regard, significant effort is directed on providing feasible solutions using broadcast routing techniques. Broadcast routing accomplishes the critical requirement of VANET safety messages by reliably transmitting the message to all relevant

vehicles. Urban Multi-hop Broadcast (UMB) (Korkmaz and Ekici, 2004) BROADCOMM (Durresi et al., 2005) and Smart Broadcast (SB) (Fasolo et al., 2006) are among prominent works using broadcast technique. Most broadcast methods adopt the conventional 802.11 like RTS/CTS handshake before transmitting the actual safety message. RTB/CTB (request to broadcast/clear to broadcast) handshake in VANETs (substitute for RTS/CTS handshake in 802.11) is used to mitigate the hidden node problem. Unlike 802.11, here the safety message initiator exchanges RTB/CTB with only one of the recipients among its neighbors. However, note that due to the small size of VANET safety message payload length of 100 bytes on average(Xu et al., 2004), each safety message transmission occupies the radio channel for a very brief amount of time as opposed to a data stream. Consequently, in case of message transmission without RTB/CTB handshake, the likelihood of message collision due to hidden node is virtually equal to that with the use of RTB/CTB exchange. Also importantly, since vehicular topology has mostly extended distribution of vehicles and multihop transmission, the so called gagged terminal problem and masked terminal problem are acute in VANET scenario. Moreover, the extended distribution of vehicles also has frequent instances of hidden terminals outside the transmission range of receivers i.e. the CTB message from receivers is unheard by those hidden terminals, thus causing handshaking ineffective. Several works in the literature evaluate the efficiency of handshaking mechanism in infrastructure based 802.11 networks (Sobrinho, 2005) and general ad hoc networks (Xu et al., 2002). However, to the best of our knowledge, there does not exist any work in hitherto literature that concerns the evaluation of handshaking mechanism with regards to VANETs.

In this paper, the efficiency of safety message dissemination using handshake based broadcast in VANETs is evaluated. Instant broadcast, a simplified version of Smart Broadcast technique, is recommended where safety message is propagated without using handshaking mechanism and related control packets. Analytical model based on Markov chain modeling is also developed for message propagation delaying instant broadcast. Thorough evaluation and comparisons performed in ns-3 simulator show that lower propagation delay can be guaranteed by avoiding handshaking mechanism and at the same ensuring reliability of reception by all the relevant nodes. The main contributions of this work are: evaluating the effectiveness of handshake mechanism in VANETs for the first time, improved end to end propagation speed by 100% each hop through avoiding handshake, theoretical analysis of delay for the instant broadcast method which can be easily extended for delay in any broadcast method in VANETs, and profound simulation results by modeling the communication architecture in ns-3 simulator.

Handshake Based Routing Techniques in Vanets

Several handshake based routing techniques have been proposed for VANETs. However, safety message dissemination in VANETs imposes strict constraints of minimized propagation delay and guaranteed delivery to all relevant vehicles. Therefore, we will focus our discussion to two solutions that comply best with these requirements (Li and Wang, 2007; Yang and Chou, 2008). In the following, we detail the functionality of Urban Multi-hop Broadcast and Smart Broadcast routing solutions.

Urban Multi-hop Broadcast (UMB)

In UMB protocol, node that is furthest away from the sender is selected for the message relay and is engaged in RTB/CTB handshake. To select the relay node, the coverage area of the sender is divided into equal size sectors in the direction of dissemination of message. The relay node is selected in the furthest sector. The sender node broadcasts a control packet called Request to Broadcast (RTB) which contains the geographical location of the source and sector size. When the nodes in the direction of dissemination receive this RTB packet, they compute their distance to the source.

Based on this distance they send a channel jamming signal called black burst: the further the distance of the respective sector the longer the burst. Once a node completes its burst it senses the channel. If the channel is busy the node exits the contention phase. However, if the channel is idle the node identifies itself as the next relay node and returns a control packet Clear to Broadcast (CTB) containing its ID. Note that CTB would collide if there were more than one node in the furthest sector. In that case the process will reiterate by dividing the sectors into sub sectors of smaller widths. After successfully receiving a CTB packet the source node sends its broadcast packet that also contains the ID of the node which successfully sent the CTB (the relay node). The relay node will now become the new source and repeat the process for next hop.

Smart Broadcast (SB)

Smart broadcast is an extension of UMB protocol that attempts to minimize the excessive delay caused by iterative collision resolution method in UMB. Similar to UMB, SB uses the assumption that coverage area can be partitioned in Adjacent sectors and that node are capable of estimating the sector they belong to. Hence a contention resolution procedure is performed. Source broadcasts the control RTB packet to seek the corresponding CTB packet. The receiving nodes Contend to return the CTB packet based on their corresponding sector. In case of CTB collision, unlike in UMB, the process will not be iterated again but rather the nodes would remain in contention phase and the node with the next minimum back off will send the CTB.

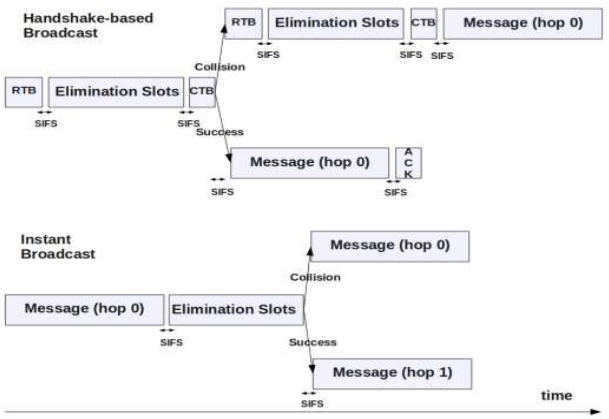

Figure 1. Sequence of packets in Handshake and Instant Broadcast schemes (figure drawn to scale considering packet sizes (Message = 112 bytes, RTB=20 bytes, CTB=14 bytes, ACK=12 bytes); transmission delay is ignored)

Instant Broadcast

In this section a simplified version of Smart Broadcast protocol is suggested that avoids the use of handshake mechanism. Detailed description with analytical model for propagation delay is presented for Instant Broadcast method.

Motivation

UMB and SB protocols rely on the exchange of RTB/CTB messages each hop before the transmission of actual safety message. Both the protocols may perform well for the case of non-safety data transfer in VANETs where a typical data transfer carries more than 2312 bytes. However, the small size of VANETs safety message (100 bytes payload on average) may not be adequate to employ RTB/CTB exchange which can incur excessive delay (Li and Wang, 2007). In particular for a multi-hop propagation, the overall end to end delay would severely deteriorate as the delay overhead due to RTB/CTB multiplies each hop.

Protocol Description

Instant Broadcast is the simplified extension of Smart Broadcast protocol that avoids the usage of handshake mechanism. The sender (message originator) gains access to the medium by following the 802.11 CSMA/CA policy and broadcasts the entire safety message. Collision for the message originator is dealt by following the exponential back off mechanism. The position, direction of broadcast, and sectoring information is appended in the safety message packet as a small overhead of about 12 bytes. This overhead is not specific to Instant Broadcast protocol as it is also used in both UMB and SB protocols. The position information comprises 4 bytes each for longitude and latitude of the sender (acquired from the on-board GPS device), hop count and intended broadcast distance comprise 2 bytes, direction of broadcast is 2 bits, while sectoring information comprises 1 byte each for sector width (in meters) and number of sectors. Receiving nodes will follow the same SB contention procedure and the relay node will rebroadcast the safety message. In case of collision the vehicle with the next minimum back off value will rebroadcast the message.

The rebroadcast from the relay node is overheard by the sender; this will confirm the successful reception of safety message. In case the rebroadcast message is not heard by the sender within the specified time (timeout), the broadcast is repeated by the sender. Note that the movement of vehicle (50 miles per hour on average) relative to message propagation speed (25 meters per millisecond on average according to simulations in section IV) is negligible to affect the message overhearing mechanism. In the last hop the message is retransmitted twice, once by the actual forwarder and the second time (after the first retransmission is received) by the furthest receiving node for the purpose of acknowledgement.

Figure 1 shows a general sequence of packets in handshake based broadcast and instant broadcast methods. The figure gives an intuitive comparison between the two methods in terms of delay while considering collisions. Here, elimination

slots account for the time during which surroundings nodes decide the next forwarder among themselves. It can be observed from the figure that by the time handshake method broadcasts the message in one hop, instant broadcast would have almost completed two hops in case when there is no collision. Interestingly, even while comparing collision case for instant broadcast to successful case for handshake broadcast, the delay of instant broadcast does not exceed drastically and it completes its one hop in almost the same time as handshake based broadcast. The delay gain of instant broadcast in figure 1 may seem improbable; however, we will also show in our simulation analysis in section IV that the delay gain of instant broadcast is effectively twice as the handshake based methods under practical assumptions. UMB, SB and the suggested extension of SB use the concept of equally partitioning the coverage area into adjacent sectors around the sender node, to decide the next relay node. Each receiving node in the range decides its corresponding sector by estimating its distance from the sender node using the location information. Each sector is assigned a contention window containing equal number of time slots:

$$Wn = ft1; t2; t3; :::; tlg + (N - n); n = 1; 2; :::;N \quad (1)$$

Where Wn denotes the contention window for sector n. The number of time slots l is equal for all sectors and its value depends on traffic congestion. The more congested the traffic the more the number of time slots. Each window is offset by N - n, where N is the total number of sectors, thus making sure that nodes in the further sectors always transmit before nodes in the other sectors. The optimization of parameters N and l will be shown with the help of simulations in section IV.

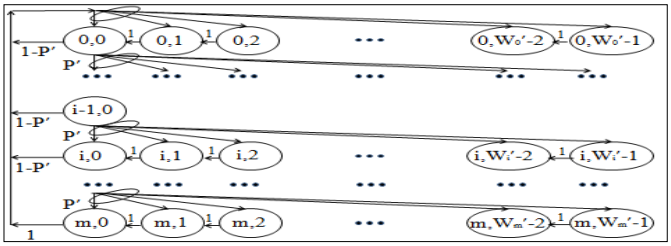

Figure 2. Markov chain model with hidden node collision

Delay Analysis

The delay analysis for the vehicular multi-hop scenario using Instant Broadcast method is formulated here. As explained above the sending mechanism in the first hop (message origination) is different from the sending (forwarding) mechanism in the following hops. In the former the sender increases its back off window size in case of collision until successful transmission occurs, while in the latter the sender gives up in case of collision and the node with the next minimum Back off value will forward the message. As a result, in the delay analysis, we deal the delay for the first hop separately from the delay of the following hops. The analysis for the message origination hop is presented first. In this analysis, a Bianchi's Markov chain is used with the assumption that the traffic distribution is uniform and that there are fixed number of contending nodes (CN) (excluding the sender) and fixed number of hidden nodes (HN) for each sender. In the Bianchi's Markov chain model (Bianch, 2000), the author defines the probability p as a probability that a transmitted packet collides and thus increases current window size to

double. The collision, as considered in (Bianch, 2000), occurs when contending nodes choose a time slot at the same time. However, in our scenario we also consider collisions due to hidden nodes. To incorporate this effect, a modified Markov chain model is depicted in Fig.2 . b(t) and s(t) are stochastic processes representing the back off time counter and back off tage, respectively, for a given node at time t. P0 is the packetollision probability at state s(t). Let tr be the transmission
Time of the packet given by

$$t_r = \frac{H_{PHY} + H_{MAC} + Payload}{R_b} + \delta \qquad (2)$$

Where HPHY and HMAC are the PHY and MAC headers MAC header also includes our protocol overhead). Rb is he data rate while is the propagation time. Here, we assume the same data rate for payload, PHY and MAC headerTransmission.

We represent the interval, in terms of the number f back off slots, that a hidden node does not transmit a packet during time tr by

$$t_\alpha = \left\lceil \frac{t_r}{slot\ time} \right\rceil \qquad (3)$$

Let Tc be the transmission probability of a contending node and Th be the transmission probability of a hidden node. The probability that a hidden node does not transmits during the sender's transmission is $(1 - \tau)^{t\alpha .HN}$. Consequently, by incorporating these collisions, the probability of unsuccessful transmission becomes

$$P^r = 1 - (1 - \tau_C)^{C N} (1 - \tau_h)^{t\alpha .HN} \qquad (4)$$

From (Bianchi, 2003), the probability that a node starts its transmission in a given time slot is given by

$$\tau = \frac{2(1 - 2P^r)}{(1 - 2P^r)(W^r + 1) + P^r W^r (1 - (2P^r)^m)} \qquad (5)$$

where W^r is the minimum window size and m is the maximum backoff stage. τ_C and τ_h can be computed from (Bianchi,2003), and equation (4) using numerical analysis. The probability that a transmission occurs among contend- ing nodes in a given time slot is

$$P_{tr} = 1 - (1 - \tau_c)^{C N + 1} \qquad (6)$$

The probability that a packet is successfully transmitted given P_{tr} (probability that transmission occurs among con- tenders) is given by

$$P_s = \frac{(CN + 1)\tau_c (1 - \tau_c)^{C N} (1 - \tau_h)^{t_\alpha HN}}{P_{tr}} \qquad (7)$$

From (Chatzimisiouet al., 2003) and the above equations, we can write the average delay for message transmission in the first hop (message origination hop) $E[D]$ as

$$E[D] = E[S]E[slot] \qquad (8)$$

$$E[S] = \frac{(1 - 2P^r)(W^r + 1) + pW^r (1 - (2P^r)^m)}{2(1 - 2P^r)(1 - P^r)} \qquad (9)$$

$$E[slot] = (1 - P_{tr})\sigma + P_{tr} P_S T_S + P_{tr} (1 - P_S) T_C \qquad (10)$$

$E[S]$ is the average number of slot times for a successful transmission and $E[slot]$ is the average length of a slot time; σ is the duration of empty slot, T_S and T_C are the average time the medium is sensed busy because of a successful transmission or a collision respectively.

$$T_s = DIFS + \left(\frac{H_{PHY} + H_{MAC} + Payload}{R_b} + E[D^r] + \delta\right) \qquad (11)$$

$$T_c = DIFS + \left(\frac{H_{PHY} + H_{MAC} + Payload}{R_b} + timeout + \delta\right) \qquad (12)$$

As explained in the protocol description, we consider re-transmission in the next hop as acknowledgment for transmis- sion in the previous hop. Therefore, in (11), we include the average next hop delay $E[D^r]$ as the acknowledgement delay in (12), however, we include the acknowledgment timeout of the message originator. Now, we briefly describe the analysis for the average delay $E[D^r]$ of the forwarding hop. Here we assume the transmission probability τ_h of a hidden node is the same as considered above. Also, we assume from our sectoring method that the contention window size I is fixed for each

sector in the propagation scenario. Since the traffic distribution is assumed as uniform, the number of hidden nodes and the number of contending nodes are assumed to be the same for each sector. Note that unlike in the first hop, here the sender does not use exponential backoff and rather gives up transmission in case of retransmits the message. The probability of transmission in a given slot time is given by $\tau c_{t} = \frac{1}{I}$.

Using (7), we get probability $P_S t$ that packet is successfully transmitted. The average delay $E[D^r]$ for a forwarding hop can be finally written as

$$E[D^r] = E[d]X \qquad (13)$$

where $E[d]$ is the average delay for a retransmission at-tempt, which can be computed by using (8), (9) and (10) with $m = 1$, while X is the average number of retransmission attempts in theforwarding hop given by

$$X = \sum_{n=0}^{W-1} (1 - P_{s^t} P_{tr})^n P_{s^t} P_{tr} n \qquad (14)$$

Note that while calculating the forwarding hop delay, we include the average next hop delay to account for acknowl- edgment in (11). Therefore, the average next hop delay will be included in each forwarding hop until the retransmission in the last hop. In the last hop, as explained in the protocol de- scription, there is a retransmission after the initial forwarding that specifically serves as acknowledgment without requiring any further confirmation.

Simulation setup

To analyze the comparison of handshake based broadcast method and instant broadcast method, IB is fully implemented along with UMB and SB broadcast schemes in ns-3 simulator, version 3.9 (The NS-3 Network simulation). The traffic mobility is generated using TraNS (Traffic and Network Simulation Environment) (Traffic and Network Simulation Environment). The common simulation parameters are summarized in Table 1. We have used 4 km road length scenario with unidirectional roads having two lanes. Ten different vehicle densities are tested with density from 5 to 50 nodes per 300 meters length of the road (i.e. one hope distance), and having Gaussian randomly assigned speed with mean 50 miles/h and standard deviation 3 miles/h. The minimum safe time headway between vehicles is kept 1.5 seconds. We use Jakes model to estimate Rayleigh fading for the channel (Blaszczyszyn et al., 2009). To best study the performance of algorithms in the existence of hidden nodes, the scenario is tested for different message generation rates of 0.01 to 1 message per vehicle per second, where 1 message per vehicle per second has a high likelihood of hidden nodes existence at almost every broadcast instance. Moreover, to account for randomness each simulation test is run for three runs to acquire thorough results.

Figure 3. Parameter optimization, throughput and reliability evaluation

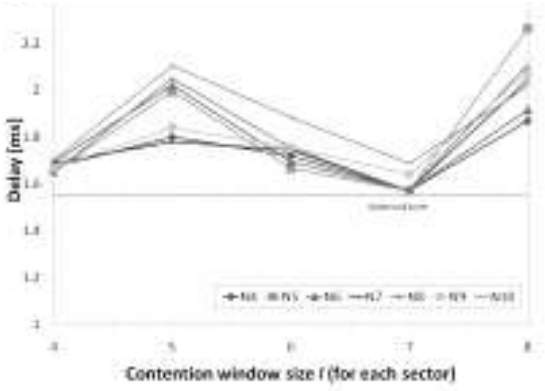

(a) Average one hop delay with variable settings of I and N

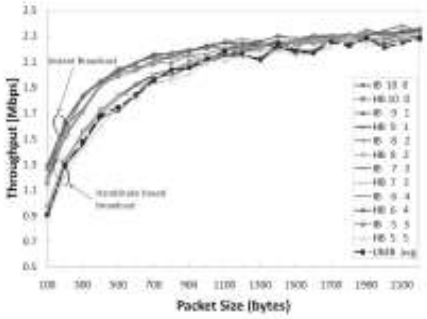

(b) Throughput for Instant Broadcast vs Handshake-based Broadcast (Legend indices represent number of Contending nodes (Left) and number of Hidden nodes (Right))

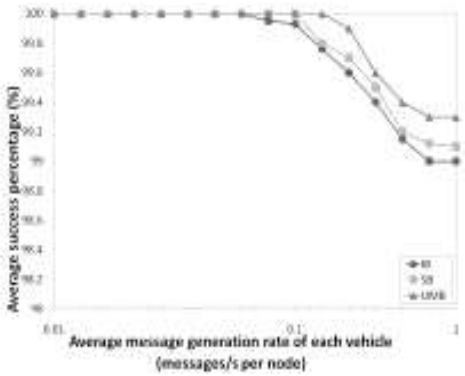

(c) Average success rate

SIMULATION PARAMETERS

Description	Value
Transmission range	300 meters
Data rate	3 Mbps
Message payload size	100 Bytes (except for experiment in Fig 3(b))
Protocol overhead	12 bytes
MAC header size	34 bytes
PHY header size	26 bytes
Base protocol	802.11p
RTB, CTB, ACK	20, 14, 12 bytes
Time slot, DIFS, SIFS	20, 50,10 μSec
Road length	4 km (2 lanes)
Vehicle density	5-50 vehicles/300 meters
Vehicle speed	50 miles/h (mean)
Message generation rate	0.01-1 message per vehicle/second
Path loss model	Two Ray model
Fading model	Rayleigh fading model
Simulation time	100 seconds (each run)

RESULTS AND DISCUSSION

Figure 3(a) shows average one hop propagation delay for instant Broadcast using different contention window sizes l and number of sectors N. The plot is based on mean delay with variable node densities. From the figure it can be observed that both l and N are influential on the propagation delay. The higher values of each parameter may avoid collisions, however, it would incur higher delay. On the contrary, the smaller values incur excessive delay due to collisions and the resulting retransmission. The parameter setting of l = 7 and N _ 8 seems optimal for minimum propagation delay. Also, since the sectoring approach is identical in all the three protocols under discussion, we keep the optimum values of window size l = 7 and number of sectors N = 8 in the rest of the simulation experiments. Figure 3(b) gives an explicit comparison between handshake based method and instant broadcast method in the presence of variable number of hidden and contending nodes under saturation condition. Here, average one hop network throughput is reported against variable packet payload size from 100 to 2200 bytes. For the sake of clarity in the plot, we depict Smart Broadcast (being the closer counterpart of IB) in detail, while for UMB, the average throughput curve is shown. Clearly, the IB method achieves higher throughput compared to handshake based broadcast for message sizes up to 1000 bytes. The throughput gain of IB, for the smaller message sizes, is almost constant regardless of the increase of the number of hidden nodes. The throughput gain is understandable for a number of reasons. Firstly, due the fact that handshake based method aims to exploit the small size of RTB to reserve the channel prior to sending the actual message packet. However, for the smaller message size, the message itself has less likelihood of collision like an RTB packet. Thus the handshake serves as an overhead, resulting in lower throughput. Secondly, the extended vehicle distribution (topology) on the road has a high likelihood of gagged station problem. In a gagged station problem the RTB/CTB exchange unnecessarily prevents simultaneous (non-interfering) communication among neighboring nodes, thus effecting the overall network throughput. Thirdly, the extended distribution of vehicles on the road causes the masked station problem in high packet generation rates, where RTB/CTB virtually becomes ineffective and rather incursive delay. For message sizes above 1000 bytes, however, the handshake mechanism can be effective as shown in the plot and can improve the overall throughput. Figure 3(c) shows the success rate of the three protocols. Success rate is the ratio of the number of nodes that receive the safety message to the total number of nodes that are present in the multi-hop coverage range. Here, reception by any node is the final successful reception of message regardless of the Number of retransmission due to collisions. As discussed earlier, the existence of hidden nodes is directly proportional to packet generation rate. Here, we see that IB performs equally well with a very negligible loss (about 0.2% more than handshake based method) over higher packet generation rate. Thus, IB maintains equal reliability as protocols with handshaking overheads, while at the same provides lower propagation delay as we show in the following figures. Figure 4(a) shows mean delay with respect to message generation rate using safety message payload length of 100 bytes. From the figure it is obvious that instant broadcast method provides considerable improvement over SB and UMB protocols in terms of mean one hop delay. The delay gain is consistent with message generation rate until slightly above

0.1 message per second per vehicle where the hidden node problem may be acute, resulting in the handshake methods performing equally well. However, retransmission due to hidden node collisions in the higher message generation case do not significantly affect the IB performance as the delay (even in the higher rates) is close to the handshake based methods. Figure 4(b) depicts mean delay with respect to distance. We observe considerable delay gain of IB again over SB and UMB protocols with respect to distance. Note that the distance interval (300 meters) on x-axis roughly represents one hop communication range. Therefore, we observe that the delay gain of IB over the other two protocols doubles every hop, and it can be seen in the fourth hop that the delay gain of IB is about a significant 12 milliseconds.

Figure 4(c) depicts average load generated by each message in the network against vehicle density. The figure highlights an important achievement of IB protocol over the other two protocols. It provides the total number of bits transmitted in the network in order to disseminate a safety message to related nodes. In other words, it shows the channel reservation per safety event. The average load generated per message increases slightly with increasing vehicle density for all the three protocols due to retransmission triggered by collisions in the high density traffic. However, since IB involves only the actual message in the propagation mechanism, it generates the least amount of load in the network per message. Since the handshake based methods involve RTB and CTB overhead packets, and also, due to their resulting retransmission because of gagged station problems and masked station problems, their overall load generated per message is higher. The evaluation results show that Instant Broadcast offers equal reliability as the methods using handshaking mechanism, and at the same time improves the overall safety message propagation delay by avoiding overhead messages.

CONCLUSION

In this paper, we have analyzed the use of handshaking mechanism for safety message dissemination in VANETs. Instant Broadcast routing without using handshaking is asserted to be used for multi-hop safety message dissemination in VANETs. Our extensive simulation results using ns-3 simulator suggest that Instant Broadcast significantly improves the message propagation delay and ensures reliability of reception by all the nodes in the multi-hop range. The evaluation of handshaking mechanism presented in this paper will assist future researchers in considering handshaking while designing VANET communication protocols. Theoretical delay analysis for instant broadcast method is also developed in this paper, which can be extended for delay calculation of any broadcast method in VANETs. Future work can be directed towards further investigation of the contention resolution mechanism and exploit some novel parameters such as vehicle type and lane number with respect to message originator. In this paper, we have presented a new technique for sectoring the broadcast range for safety message routing in VANETs. Rush hour traffic scenario is considered where most of the hitherto mechanisms are severely affected with collisions and consequent high message propagation delays. The hitherto neglected factor of road width is introduced to be used as a second dimension for sectoring the transmission range of the message sender. Collision gain of the proposed technique is evaluated using Marchov chains. Extensive simulation evaluation is performed using ns-3 simulator, and the results suggest that Lane based sectoring significantly improves the message propagation delay by as much as 9 ms for rebroadcast in each hop while at the same time improves reliability of message propagation by reducing rebroadcast collisions by 2% over the existing sectoring technique even in worst traffic scenario. Uncovering the importance of road width for VANETs in this paper will assist future researchers in understanding a more detailed road topology that influences VANET

communication. The idea of segmenting transmission range into manageable units can also be replicated in service channel allocation strategy in VANETs where there is an equally critical concern about effective channel utilization. Theoretical delay analysis for rebroadcast stage developed in this paper can be extended for delay calculation of other broadcast methods in VANETs. Future work can be directed towards investigation sectoring in road intersection scenarios, and further study of the vehicle density and topology learning mechanism on the road.

REFERENCES

- Bianchi G. (2000). Performance analysis of the IEEE 802.11 distributed coordination function, IEEE JSAC, vol.18, no.3, pp.535-547.

- Blaszczyszyn B, Muhlethaler P and Toor Y. (2009). Performance of MAC protocols in linear VANETs under different attenuation and fading conditions, in Proc. of 12th International IEEE Conference on Intelligent transportation Systems, pp.1-6, 4-7.

- Chatzimisios P. (2003). A.C. Boucouvalas and V. Vitsas, "Packet delay analysis of IEEE 802.11 MAC protocol," Electronics Letters. 39(18):1358- 1359.

- Durresi M, Durresi A and Barolli L. (2005). Emergency broadcast protocol for inter-vehicle communications, in Proc. of the 11th IEEE International Conference on Parallel and Distributed Systems (ICPADS'05), pp.402-406.

- Fan L and Yu W. (2007). Routing in vehicular ad hoc networks: A survey, IEEE Vehicular Technology Magazine. 2: 12-22.

- Fasolo E, Zanella A and Zorzi M. (2006). An Effective Broadcast Scheme for Alert Message Propagation in Vehicular Ad hoc Networks," in Proc. of ICC '06. 9:3960-3965.

- Kaixin Xu, Gerla M and Bae S. (2002). How effective is the IEEE 802.11 RTS / CTS handshake in adhoc networks, in Proceedings of Global Telecommunications Conference, GLOBECOM '02. 1: 72- 76, 17-21.

- Korkmaz G, Ekici E, Ozguner F and Ozguner U. (2004). "Urban multi-hop broadcast protocol for inter-vehicle communication systems, in Proc. of the first ACM workshop on VANETs.

- Qing Xu, Mak T, Jeff Ko and Sengupta R. (2004). Vehicle-to-vehicle safety messaging in DSRC, in Proc. of the 1st ACM international workshop on Vehicular ad hoc networks, pp. 19-28.

- Rudack M, Meincke M, Jobmann M and Lott M. (2003). On traffic dynamical aspects of inter vehicle communications (IVC)," in Proc. of VTC '03. 5: 3368- 3372.

- Sobrinho J, de Haan R and Brazio J. (2005). Why RTS-CTS is not your ideal wireless LAN multiple access protocol. Wireless Communications and Networking Conference, 1: 81- 87.

- The ns-3 network simulator http://www.nsnam.org/

- Traffic and Network Simulation Environment (TraNS) http://lca.epfl.ch/projects/trans

- Yan G, Yang W, Weigle M, Olariu S and Rawat D. (2005). Cooperative Collision Warning through mobility and probability prediction in Proc. of Intelligent Vehicles Symposium (IVS), pp.1172-1177.

- Yang Y and Chou L. (2008). Position-Based Adaptive Broadcast for Inter-Vehicle Communications," IEEE ICC workshop on Communications, pp.410-414, 19-23.

Orange Peel as an Adsorbent for the Removal of Reactive Blue Dye from Textile Waste Water

Nazakat Ali* and Noor Ahmed

Department of Textile Engineering, Balochistan University of Information Technology, Engineering & Management Sciences, Quetta

Abstract

In this study the capable use of the low cost and eco-friendly material orange peel as a biosorbent for the removal of dichlorotriazine Reactive Blue (RB-Drimarine-K2 RL) dye from aqueous solutions was studied, containing equilibrium and dynamic studies. Experiments were performed on different dye concentrations, particle sizes, adsorbent doses, pH, shaking speed and shaking time. It was revealed that the adsorption capacities of orange peels were comparatively high for the reactive dyes. The adsorption equilibrium data could be best plotted by applying the Langmuir and Freundlich isotherms. The experimental results were labeled by both isotherm. Adsorption results were analyzed using the linear models and the regression results showed that the adsorption was more accurately described by a Lngumuir model.

Key words: Reactive Blue (RB), Dicholortiazine (DCT), Monochlorotriazine (MCT), adsorption.

* *Corresponding Author's email: nazakat.ali@buitms.edu.pk*

INTRODUCTION

The textile industry is one of the largest production industries, having significant role in manufacturing sector global industry. It provides enormous masses of materials for clothing and furnishings, with their specialties and end-uses (Broadbent, 2001). The dyeing procedures may be divided into two major classes of immersion exhaustion (exhaust dyeing) and pad impregnation (pad dyeing) processes (Khatri, 2010). The degree of fixation is variable in different classes of dyes; the reactive dye has 50-80% of fixation, the remaining components are unfixed dyes. The dyeing process produces huge amount of colored wastewater; the amount of color pick up varies from material to material and amount of dye to be hydrolyzed in water. The wet pick up for polyester cotton blends for reactive dyes is 40-45% and it is 60-70% for cotton, cellulosic fibers, the remaining amount of unfixed hydrolyzed disposed in water streams (Broadbent, 2001). The reactive dyes react with hydroxide ions present in the aqueous dyebath under alkaline pH conditions. This produces nonreactive hydrolysed dye which remains in the dyebath as well as in the fiber. In order to obtain the required levels of washing fastness, it is necessary to remove all unreacted and hydrolysed (unfixed) dye from the cotton fiber. This is achieved by 'washing-off'; a series of thorough rinsing and 'soaping' steps. The dye fixation efficiency is typically in the range of 50–80%; i.e. 20 to 50% of the dye of the desired shade of color is discharged to the environment. (Khatri, 2010). Irrespective of the dyeing method and the type of reactive group, almost all of the potentially toxic non biodegradable inorganic electrolyte, alkali and unfixed dye are discharged to dyeing effluent. This creates potential environmental problems from a highly-colored effluent with high levels of dissolved solids and oxygen demand. (Khatri , 2010). There are different conventional methods available for the treatment of such industrial waste; physical, chemical, physico-chemical, biological, and membrane technology are the methods that are widely used for the control of these effluents. Adsorption is one of the best methods for the removal or reduction of dye containing water effluents. Amongst all the sorbent materials

proposed, activated carbon is the most popular for the removal of pollutants from wastewater (Derbyshire *et al*., 2003). There are different methods for the removal of colorants such as chemical oxidation, coagulation and reverse osmosis (Ahalya et.al, 2006). The adsorption method has an advantage over the other methods because of sludge free process for the removal of dyes ta a great extent from dissolved solution as compared to other commercial methods and their application in color removal (Ramchandra et.al, 2008).

Though, commercially accessible adsorbent materials are found to be very expensive. the use of low cost adsorbent materials is increasing in the application of the adsorption technology, for the removal of coloring substances and other compounds from waste as well as from underground water (Ramakrishna K.R. and Viraraghavan T., 1997). It has been considered that low-cost and biodegradable alternate materials are obtained from natural resources to remove organic impurities; some of them are sugar-cane bagasse, rice husk, straw, coconut husk, saw dust, and fly ash. By using bio-degradable biosorbent materials the waste can be minimized due to bio-degradable nature of materials (Ramchandra et.al, 2008).

Therefore, orange peels are found to be best adsorbent material and used in this study for the removal of reactive blue dye (Di-Chlorotriazine) from textile effluent. Different working parameters were optimized and used. The following parameters were used: adsorbent dosage, dye concentration, particle size, shaking speed; shaking time and pH to calculate the adsorption capacity of orange peel and removal percentage of adsorbate on adsorbent under these optimized parameters.

MATERIALS AND METHODS

The following chemicals were used for the experimental work: Reactive dye; (H_2SO_4) Sulphuric Acid, Hydrochloric Acid, (HCL) Alkali (NaOH), Sodium bi-carbonate ($NaHCO_3$) and Distilled water were used. The reactive blue dye (Dri-marine K_2-RL) from Clairant was used for this study. The dye has high rate of reactivity and dark color with good fixation properties as compared to other type of reactive dyes such as MCT (Mono choloro-triezene) and Fluorine containing dyes.

Table: 1 shows the general characteristics of Reactive Blue K 2 RL

Dye	Type	Form	Color	Molecular weight(g/mol)	Wave length (λmax) nm	Color Index
Drimarine	Reactive	Granular	Blue	968.52	589	18103

Machinery

Electronic weighing balance of (AFD-300) with range of 0.01-300 grams , Universal pH strips range of 1.0-14.0, Oven dryer (WTB-Binder), Biochrom Lis S-22 Double beam Spectrophotometer, Filter paper(Whatman), Oscillating dyeing machine, Manual cutters, Millers/Manual and Sieves (Tyler manufacturers USA) were used to prepare adsorbent, adsorbent particle sizes.

In this research work the orange peel was collected from local market and used as biosorbent material for the removal of reactive Blue dye from aqueous solution after following process.

Preparation of adsorbent: The adsorbent material was washed with tap water, followed by chopping, drying under sunlight, distilation washing, oven drying, grinding, and sieving.

Preparation of aqueous solution: The aqueous solution was prepared by mixing different doses of dye 25, 50, 75, 100 and 125 mg/L respectively in distilled water.

Optimization of parameters: Following parameters were optimized to get the maximum sorption of dye on orange peel.

Adsorbent dose

Different doses 10.0, 20.0, 30.0, 40.0 and 50.0 respectively were used and optimized.

Particle size

Different particle sizes of adsorbent were made by sieving the grinded material with 600 µm, 1200 µm, 3.0, 4.0, and 5.0 mm respectively.

Shaking speed
Different shaking speeds 80, 100, 120, 140, and 160 rpm were used and optimized.

Shaking time
Different amount of shaking time i.e 15, 25, 35, 45 and 55 minutes were used and optimized.

pH
Different levels of pH under acidic levels of 2.0, 4.0 and alkaline levels of 8.0, 9.0, 12.0 were used and optimized**.**

Preparation of Adsorbent
Orange peels were collected from the local market and Juice Centers of Hyderabad City and washed several time with tap water to remove the adhering dirt. Further the samples were dried under sunlight for 4-6 days and chopped by manual cutters into small pieces. Later on they were crushed with manual miller to obtain different particle sizes and finally sieved with different mesh sizes ranging from 600um to 1200 um and 3.0 mm, 4.0mm, and 5.0 mm. The mesh sizes again washed with distilled water to remove any acidity or basicity and was oven dried at 80 ^{0}C for 2-4hrs. Oven dryer (WTB-Binder) was used for drying purpose. The chopped peels were further grinded to achieve the different particles size. Finally different mesh sizes of the Sieves were used to obtain the different particle sizes of the grouned material for the experimental work. The mesh sizes of 3.0, 4.0, 5.0, and 600 µm and 1200 µm were used in this study.

Preparation of Aqueous Dye Solution
The Drimarine Reactive Blue dye (DCT) was used for the preparation of aqueous solution. The dye was obtained from Clairant. Aqueous solution of Reactive Blue-(DCT) dye with different concentration was prepared and used in all batch experiments. The dye solution was prepared by dissolving the different amount of reactive blue dye in distilled water at various concentrations. Batch experiments were carried out at concentrations of 25, 50, 75, 100, and 125 mg/l of the dye using the different doses of the adsorbent to attain equilibrium conditions.

Optimization of Parameters
The following parameters were optimized to get maximum removal percentage of reactive blue dye, for further experimental procedure.

pH and Dye Concentration
Dye solutions with different concentrations (25 mg/L, 50 mg/L, 75mg/L, 100 mg/L, and 125 mg/L) were prepared by diluting the stock solution accordingly. Batch biosorption experiments were carried out for each of the dye concentration prepared. The dyes solution was prepared by dissolving these doses in 1000 ml of distilled water to make the aqueous solutions of different concentrations.
The pH value of the samples was adjusted using 2.0 M HCl solution in 1000 ml of dye solution and 2.0 ml of NaOH solution in 1000ml of dye solution for Acid and alkaline ranging from pH 2.0-12.0. The parameters were optimized as minimum dye concentration of 25 mg/L at pH of 8.0-9.0, where maximum dye removal was found and used for further experiments.

Particle Size
Different particle sizes were used to optimize the adsorbent size, 1200 um, 600um, 3.0 mm, 4.0 mm, and 4.0 mm were used to find the particle size. These mesh sizes were used to sieve the material and batch adsorption experiments were conducted. The particle size of 600 um and 1200 um were found to be the best, where maximum adsorption was achieved and used for further experiments.

Adsorbent dose
Different adsorbent doses were used to optimize the adsorbent dose, 10 g/L -50g/L were used and it was found that the increase of adsorbent dose increased the removal percentage more than 85% at initial dye concentration and decreased to 25-35% when dye concentration was increased 25-125mg/L. Therefore maximum adsorbent doses of 40 and 50 g/L were found to be satisfactory and used for further experimental trials.

Shaking time

The different amounts of shaking time were used to obtain the maximum removal of color from the aqueous solution, the shaking time for 15, 25, 35, 45 and 55 minutes were used. The dye removal of 76-92% was obtained with maximum contact time of 55 minutes and was used for further experimental trials.

Shaking Speed

The different shaking speed were used to obtain the maximum removal of color from the aqueous solution, The shaking speed of 80, 100, 120, 140 and 160 rpm were used. It was found that on the maximum shaking speed of 55 rpm, the maximum dye removal of 84-89% was obtained and used for further experimental trials.

The tests were performed in triplicate on lab scale for the removal of color from aqueous solution of reactive blue dye with different dye concentrations on orange peel. The solution was prepared by putting different doses 25, 50, 75, 100, and 125 mg/L of dye into 1000 ml of distilled water. Different experimental parameters were optimized first and used to get the best results of adsorption for reactive blue dye on orange peel. The adsorbent dose of (50 mg/L), size of 600 and 1200 um, shaking time (55 minutes), pH (8.0-9.0), shaking speed (160 rpm) were found to be satisfactory where the adsorption was maximum. The dye solution with pH of 8.0 and 9.0 was poured in to glass flasks. Different particle size and doses of orange peel were used and shaken in with oscillating dyeing machine at different rpm and shaking time; then the samples were taken for color removal analysis.

The solution was filtered with Whatman filter paper to separate the solution and peels. The UV-Light Spectrophotometer (Biochrom-Libra S22) was used to analyze the color removal percentage. The five serum flasks four of them were filled with dye solution after adsorption process and one with initial dye concentration. The obtained results were compared and calculated by Bear-Lambert law; the obtained values were plotted on linear graphs to show the isotherms analysis. The Langumir and Freundlich isotherms were used to show the color removal percentage of reactive blue dye on different parameters.

RESULTS AND DISCUSSION

Effect of pH and Dye Concentration

Table: 2 Shows the effect of pH and dye concentration on dye removal

pH	25mg/L	50mg/L	75mg/L	100mg/L	125mg/L
2.0	12.4	14.9	16.2	19.3	22.4
4.0	19.3	20.2	24.9	28.4	32.3
8.0	84.4	74.2	66.3	58.7	43.2
9.0	90.7	88.4	71.8	64.2	57.7
12.0	14.4	16.8	26.5	30.7	36.6

The effect of pH on the adsorption percentage of dye by orange peels was examined over a range of pH values from 2.0 –12.0, as the results showed that the amount of adsorption decreases when the pH is decreased to 2.0-4.0, as shown in in Graph.1. With initial dye concentration of 25mg/L adsorption was maximum and decreased when the dye concentration was increased to 100 and 125mg/L. The dye removal was maximum at pH of 8.0 to 9.0 and decreased as the pH increased to alkaline pH of 9.0-12.0 at initial concentration of 25 mg/L.

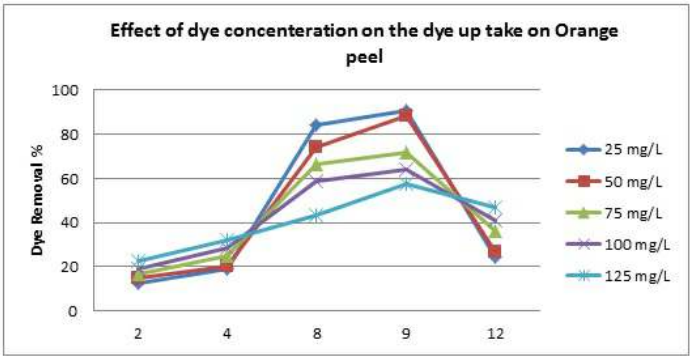

Figure: 1 shows the percentage of dye removal at different concentrations

On observing the effect of dye concentration, it was found that the maximum dye concentration gave slow adsorption on orange peel. Because after a definite time the dye concentration came to equilibrium level, where further adsorption was minimum or zero. The results showed that maximum

adsorption of 91.7% and 84.4% of adsorption were obtained at 25 and 50 mg/L respectively.

Effect of adsorbent dose

From experimental results it was found that the increase of adsorbent dose from 10-50 g/L increased the adsorption at optimized pH levels of 8.0 –9.0, with mesh size of 600 um and 1200 um respectively, at the shaking speed of 160 rpm and contact time of 55 minutes. Furthermore it was found that the maximum adsorption capacity was 84.6%-92.2% at 40g/Liter and 50 g/L of adsorbent dose with 600 um and 1200 um mesh sizes at initial dye concentration of 25mg/L.

Table: 3 Shows the effect of adsorbent dose on percentage of dye removal

Adsorbent Dose g/L	25mg/L	50 mg/L	75 mg/L	100 mg/L	125 mg/L
10	60.7	52.9	48.6	36.3	24.9
20	68.3	62.2	58.6	52.4	46.3
30	82.4	76.8	64.5	54.7	42.6
40	84.6	78.7	70.6	58.2	48.4
50	92.2	86.2	78.9	64.7	59.2

Figure:: 2 Shows the percentage of dye removal at different doses

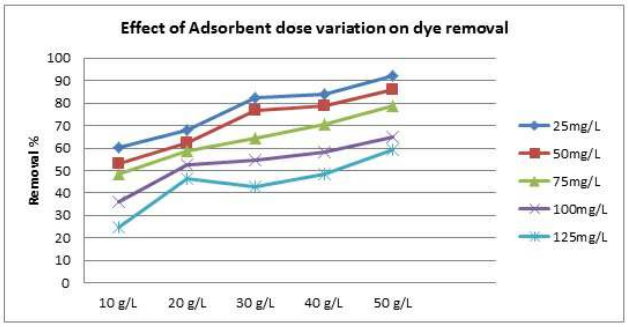

Maximum color removal was obtained at 25 mg/L of dye concentration; the 60% color was removed at 10g/L as initial adsorbent dose and removal percentage was increased as dose increased up to 50 g/L on which color removal was found to be 90-92%. It is clear from the above results that the increase in adsorbent dose increased the adsorption and decrease in color removal when adsorbent dose eas reduced.

Effect of particle size

The particle size also plays a major role in adsorption due to the surface of the adsorbent material, higher the surface area higher the adsorption, lower the surface area lower the adsorption. Particle sizes were varied from (600-1200 um) and (3.0-5.0 Mesh sizes) microns. For different particle sizes, the removal percentages of dye on orange peel were measured; the values are given Table.2 Shows the results for maximum color removal of dyes at different particle sizes.

Table: 4 Shows the effect of particle size on percentage of dye removal

Dye Concentration	600 um	1200 µm	3.0 mm	4.0 mm	5.0 mm
25 mg/L	92.4	89.9	86.6	84.3	82.4
50 mg/L	78.3	70.2	64.9	58.4	52.3
75 mg/L	64.4	52.2	46.3	38.7	32.2
100 mg/L	50.7	42.4	31.8	24.2	17.7
125 mg/L	40.2	34.8	26.5	20.7	14.6

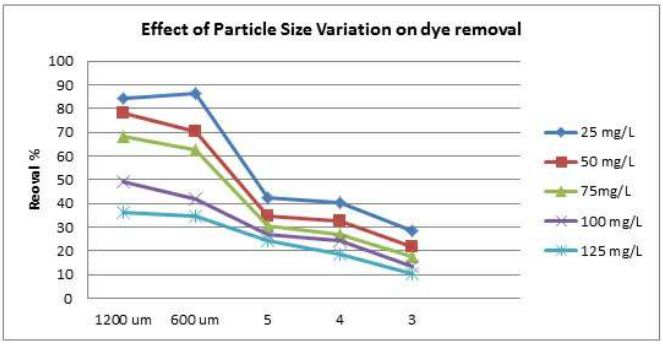

Figure: 3 Shows the percentage of dye removal on different particle sizes

The results clearly showed that the maximum adsorption was obtained at a concentration of 25 mg/L with particle size of 600 um and 1200 um. As the concentration of dye increased in the adsorption of dye on the orange peel decreased and when the dye concentration was reduced to 25mg/L, the maximum color removal 82-88% was obtained.

Increase in particle size gave the lower adsorption due to the low surface area and decrease in particle size gave the higher adsorption due to the more surface area. It was concluded from the observation that the

mesh size of 600-1200 um were found to be best for adsorption.

Effect of shaking time

Shaking time or contact time was used from 15-55 minutes; the shaking time was varied to analyze the maximum adsorption for optimization of contact time.

Table: 5 Shows the effect of shaking time on percentage of dye removal

Shaking Time min	25mg/L	50mg/L	75mg/L	100mg/L	125mg/L
15	44.8	35.3	28.6	21.9	16.4
25	48.3	38.6	42.4	34.2	29.2
35	67.1	56.5	62.7	51.5	46.3
45	89.4	84.6	86.2	76.3	74.6
55	92.6	85.9	88.7	79.2	76.4

The effect of shaking time on adsorption was conducted on various contact time and the results show in Graph.4, that the adsorption increased with the increase of contact time and decreased with the decrease of time, caused by the diffusion of dye molecules towards the surface of orange peel. In some cases it was found that more contact time gives reversible reaction of dye diffusion from orange peel surface to solution, so the maximum time of best adsorption results was found to be 45-55 minutes, where 89.4%-92.6% dye was removed and adjusted for further experiments.

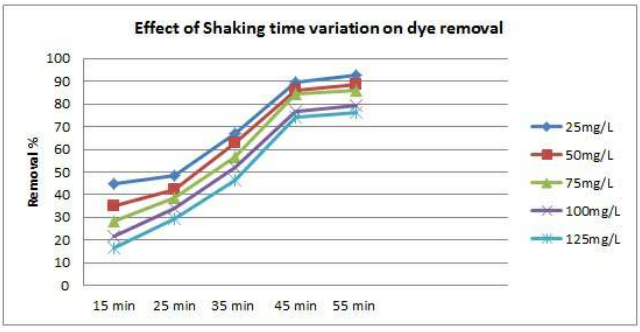

Figure**:** :4 Shows the percentage of dye removal on different shaking time

Effect of shaking speed

Different Shaking speeds ranging from 80-160 rpm were used and optimized to find the maximum color removal of reactive dye. The other parameters such as pH, adsorbent dose, dye concentrations, and shaking time were kept constant after optimizing. It was found that the maximum color removal was obtained on maximum contact time of 55 minutes. The color removal percentage was found 83-86% on 140-160 rpm.

Table: 6 Shows the effect of shaking speed on percentage of dye removal

Shaking Rpm	25mg/L	50mg/L	75mg/L	100mg/L	125mg/L
80	68.4	62.9	58.6	46.3	40.4
100	73.7	69.2	65.6	60.4	56.3
120	79.4	74.8	70.5	68.7	62.1
140	83.8	80.3	75.6	70.2	66.4
160	86.4	84.2	82.9	79.7	72.6

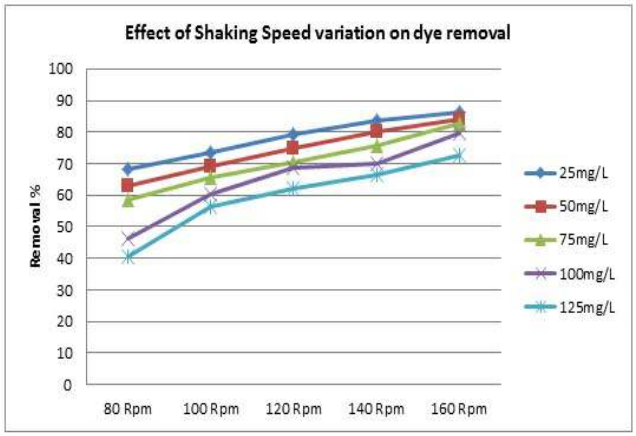

Figure**:** : 5 Shows the percentage of dye removal on different shaking speed

Adsorption Isotherms Analysis

The dye removal percentage was studied on different dye concentrations at optimized parameters adsorbent dose of 50 g/L, particle size of 1200 um, pH of 8.0-9.0, with shaking speed of 160 rpm and contact time of 55 minutes and plotted on Langumir and Freundlich isotherms. The initial and final concentrations were measured and obtained results were plotted. It was found that Langumir and Freundlich isotherms fit the obtained results. Isotherm constants and coefficient of correlation of both are given in table 6. The adsorption kinetics showed that the adsorption was maximum at initial dye concentration of 25 mg/L.

Table 6: Shows the Isotherms constant and coefficient of correlation of Langumir and Freundlich

S.No	Adsorbent dose mg/250 mL	Langumir isotherm constants			Freundlich isotherm constants		
		Q_m (mg/g)	K_a (l mg^{-1})	R^2	K_f (mg/g)	1/n	R^2
1.	2.5	17.52	0.12	0.997	7.23	0.146	0.995
2.	5.0	20.67	0.18	0.999	8.04	0.259	0.983
3.	7.3	24.26	0.24	0.996	6.53	0.275	0.971
4.	10.0	32.58	0.32	0.994	4.21	0.384	0.964
5.	12.7	38.72	0.39	0.995	2.82	0.553	0.952

Table 7: Shows the removal percentage of color at 2.5 g/250 ml

S.No	M.AC (g/250 ml)	Initial C_o (mg/L)	Final C_f (mg/L)	X= C_o - C_f (mg/L)	Removal %	X/M mg/g	1/C mg/L
1.	2.5	25.0	15.0	10.0	60.0	0.25	0.04
2.	2.5	50.0	24.0	26.0	52.2	0.091	0.02
3.	2.5	75.0	38.5	36.5	48.7	0.068	0.013
4.	2.5	100.0	61.4	38.6	38.6	0.064	0.01
5.	2.5	125.0	94.5	30.5	24.4	0.081	0.008

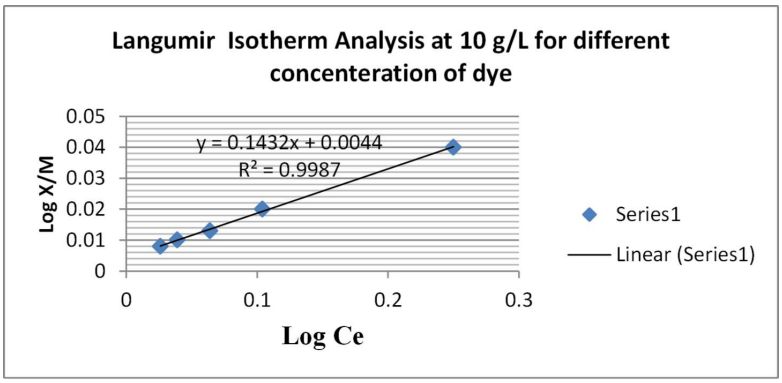

(a)

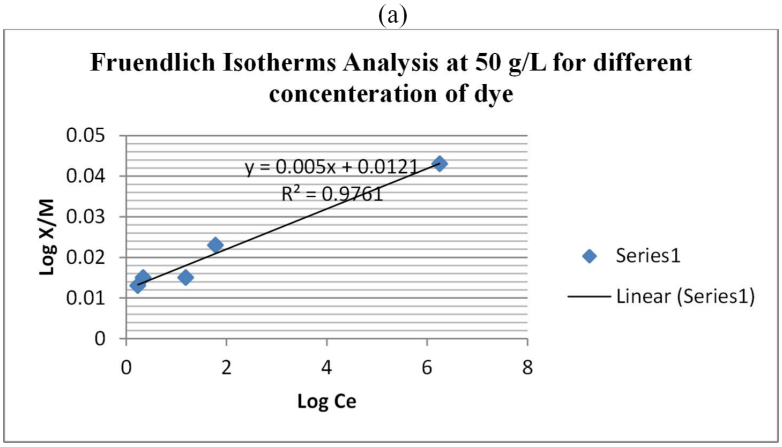

Figure:: 6 Shows the (a) Langumir and (b) Freundlich Isotherm analysis of adsorbate removal (X/M) mg/g on adsorbent at different concentration **for RB (C_0**= 25, 50, 75, 100, 125& 150 mg/L; M_{Ac}= 10 g/L; particle size: 600-1200µm; Shaking speed = 80-160 rpm; initial pH~8.0-9.0; Shaking time = 15-55 min.

Table 8: Shows the removal percentage of color at 5.0 g/250 ml

S.No	M.AC (g/250 ml)	Initial C_o (mg/L)	Final C_f (mg/L)	X= C_o - C_f (mg/L)	Elimination %	X/M	1/C
1.	5.0	25.0	19.8	5.15	79.4	0.970	0.04
2.	5.0	50.0	30.8	19.2	61.6	0.260	0.02
3.	5.0	75.0	42.2	32.7	56.3	0.152	0.013
4.	5.0	100.0	52.9	47.1	52.9	0.106	0.01
5.	5.0	125.0	71.0	54.0	56.8	0.092	0.008

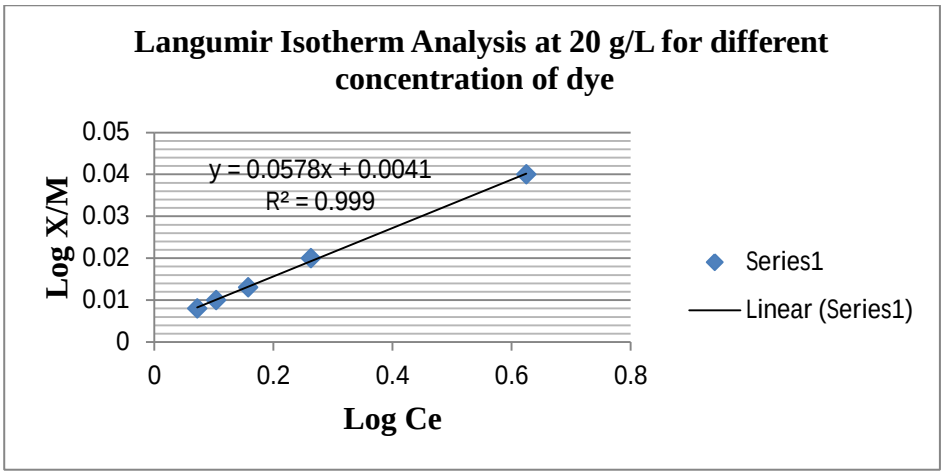

(a)

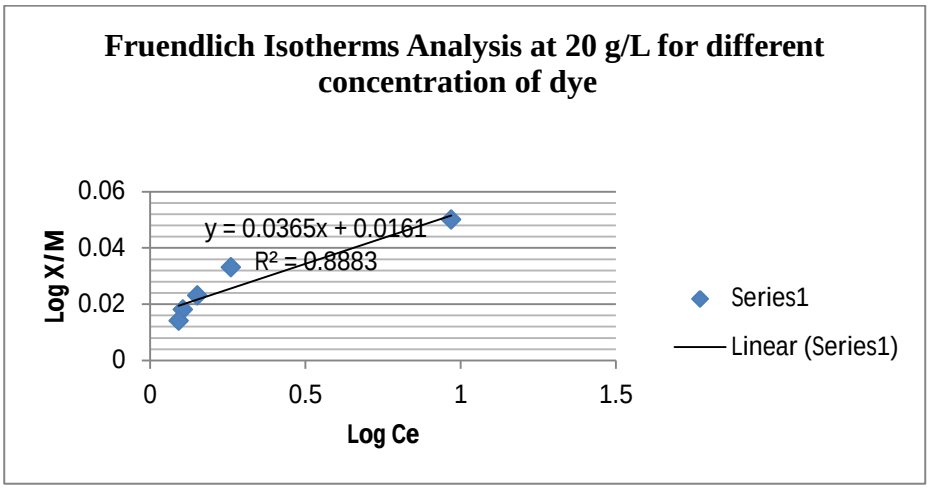

(b)

Figure: 7 Shows the (a) Langumir and (b) Freundlich Isotherm analysis of adsorbate (dye) removal (X/M) mg/g, on adsorbent at different concentration **of RB (C_0**= 25, 50, 75, 100, 125& 150 mg/L; M_{Ac}= 20 g/L; particle size: 600-1200µm; Shaking speed = 80-160 rp m; initial pH~8.0-9.0; Shaking time = 15-55 min.

Table 9: Shows the removal percentage of color at 7.3 g/250 ml

S.No	M.AC (g/250 ml)	Initial C_o (mg/L)	Final C_f (mg/L)	X= C_o - C_f (mg/L)	Elimination %	X/M	1/C
1.	7.3	25.0	20.5	4.5	82	0.622	0.04
2.	7.3	50.0	39.0	11.0	78	0.663	0.02
3.	7.3	75.0	46.5	28.5	62	0.265	0.013
4.	7.3	100.0	54.0	44.0	54	0.165	0.01
5.	7.3	125.0	52.5	72.5	42	0.100	0.008

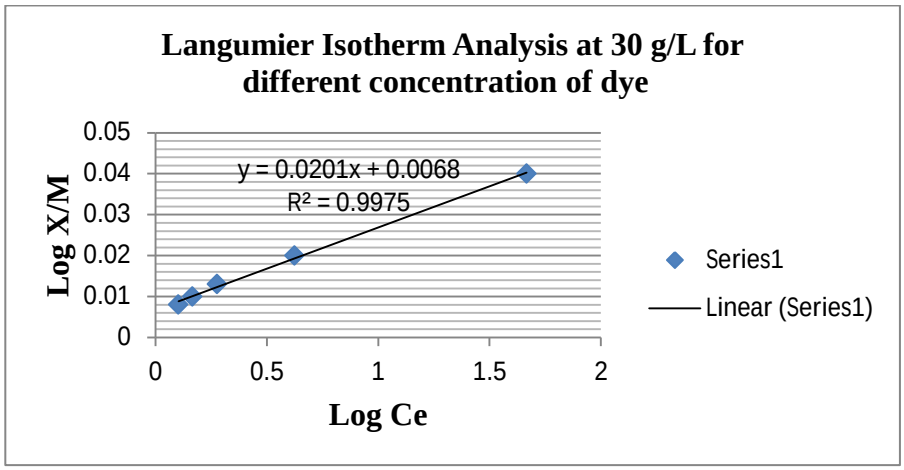

(a)

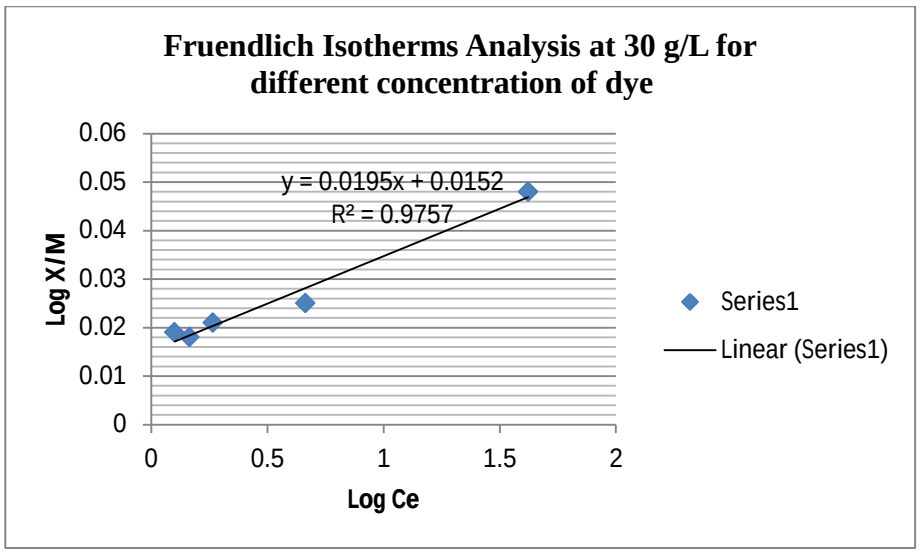

(b)

Figure: :8 Shows the (a) Langumir and (b) Freundlich Isotherm analysis of adsorbate removal (X/M) on adsorbent at different concentration **for RB (C_0**= 25, 50, 75, 100, 125& 150 mg/L; M_{Ac}= 30 g/L; particle size: 600-1200µm; Shaking speed = 80-160 rpm; initial p H~8.0-9.0; Shaking time = 15-55 min.

Table 10: Shows the removal percentage of color at 10.0 g/250 ml

S.No	M.AC (g/250 ml)	Initial C_o (mg/L)	Final C_f (mg/L)	X= C_o - C_f (mg/L)	Elimination %	X/M	1/C
2.	10.0	50.0	10.5	39.5	79.0	0.25	0.02
4.	10.0	100.0	41.0	59.0	59.0	0.16	0.01
5.	10.0	125.0	65.0	60.0	48.0	0.16	0.008

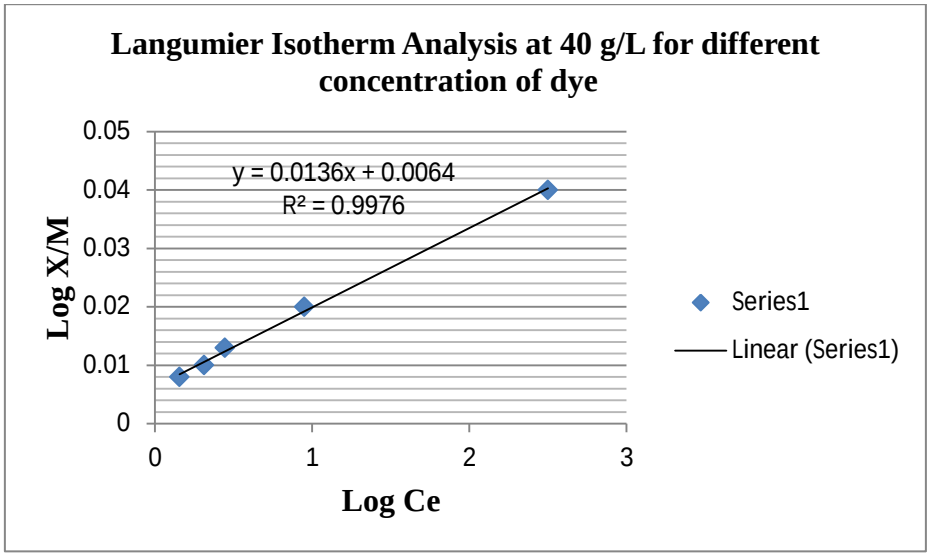

(a)

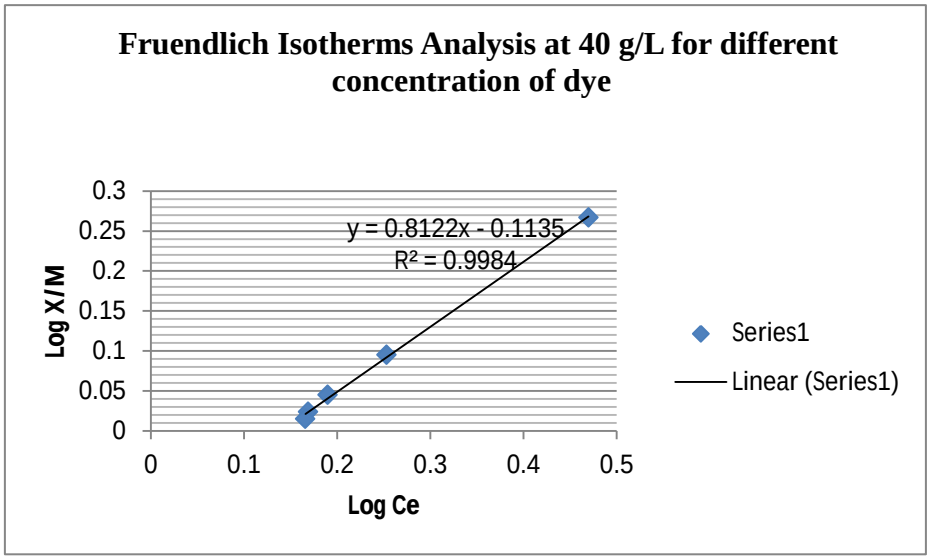

(b)

Figure: :9 Shows the (a) Langumir and (b) Freundlich Isotherm analysis of adsorbate Re moval (X/M) mg/g on Adsorbent at different concentration of RB (C_0= 25, 50, 75, 100, 125& 15 0 mg/L; M_{AC}= 40 g/L; particle size: 600-1200µm; Shaking speed = 80-160 rpm; initial pH~8.0-9.0; Shaking time = 15-55 min.

Table 11: Shows the removal percentage of color at 12.5 g/250 ml

S.No	M.AC (g/250 ml)	Initial C_o (mg/L)	Final C_f (mg/L)	X= C_o - C_f (mg/L)	Removal %	X/M	1/C
1.	12.5	25.0	23.0	2.0	92	2	0.04
2.	12.5	50.0	43.0	7.0	86	4	0.02
3.	12.5	75.0	64.5	10.5	78	6	0.013
4.	12.5	100.0	64.0	36.0	64	8	0.01
5.	12.5	125.0	72.5	52.5	58	10	0.008

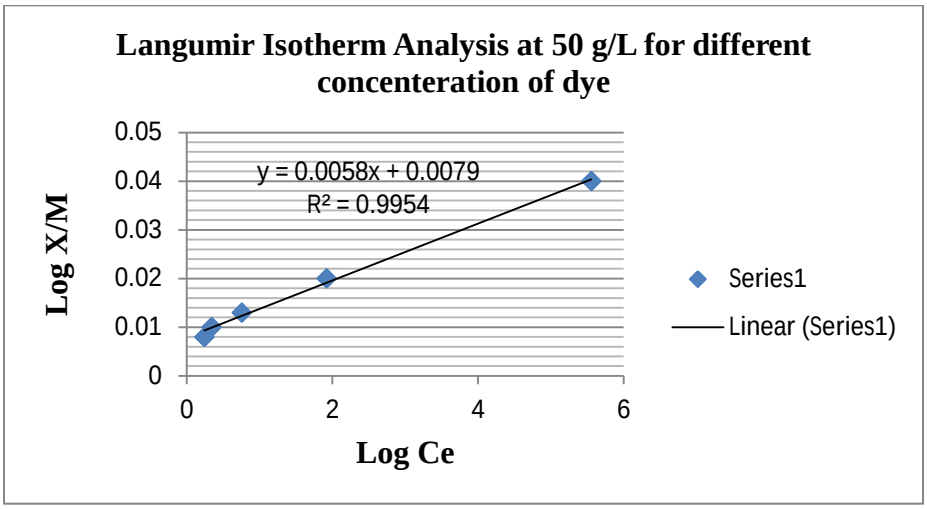

(a)

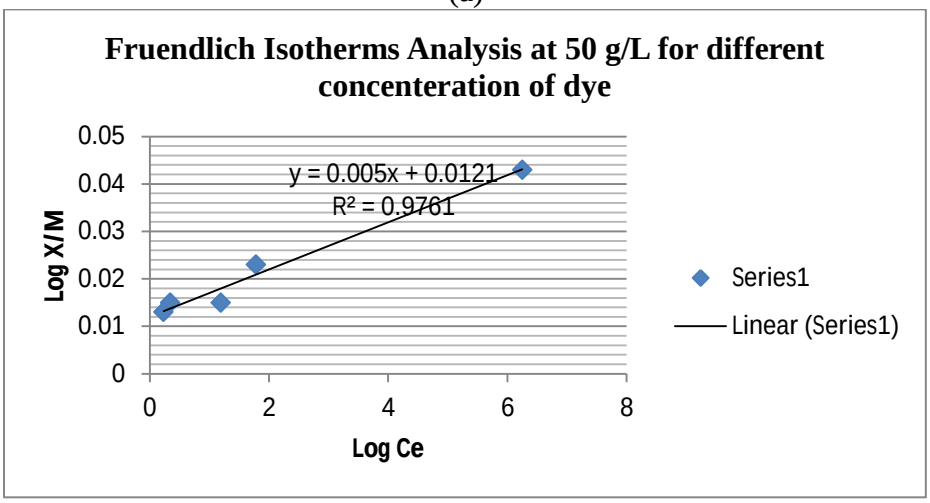

(b)

Figure: 10. Shows the (a) Langumir and (b) Freundlich Isotherm analysis of adsorbate removal (X/M) on adsorbent at different concentration for RB (C_0= 25, 50, 75, 100, 125& 150 mg/L; M A.c = 50 g/L; particle size: 600-1200µm; Shaking speed = 80-160 rpm; initial pH~8.0-9.0; Shaking. time= 15-55 minutes. The most common isotherms used for the design and study of adsorption are Freundlich and Langumir isotherms. These two isotherms are based on the analysis of monolayer formation of adsorbate over the surface of adsorbent.

It was found from the above plotted linear graphs of Langumir and Freundlich isotherms for the different dye concentrations of 25, 50, 75,100 and 125 mg/L at different doses of adsorbent 10,20,30,40, and 50 g/L, that the maximum adsorption was found on 25 mg/L on adsorbent dose of 50 g/L. The Langumir isotherms show more linear graphs as compared to the Freundlich isotherms, the isotherms constant and coefficient of correlation are tabulated in Table .6. The coefficient of correlation was found ($R^2 \geq 0.99$) and the value of K_f decreased with the increase of concentration from 25-125 mg/L in aqueous solution. The adsorption isotherm kinetics show that the maximum, easy and well in time adsorption of reactive blue dye on orange peel was achieved on 25 mg/L.

CONCLUSION

The use of orange peel as bio- serpents for the removal of reactive blue dyes from aqueous solution was studied; the following results were obtained after batch experiments. The amount of adsorption increased when the pH was increased to 8.0-9.0, at the adsorbent dose 50 g/ L; at 160 rpm of shaker for initial time of 55 minutes, with particle sizes 1200 µm of mesh size; with initial dye concentration of 25mg/L. Further it was found that the optimized pH of 8.0, and 9.0 were ideal to obtain maximum sorption of dye from the solution, the maximum adsorption was 92.35% and 86.64%. It is clear from the obtained results that the dye concentration is inversely proportional to adsorption and removal percentage, As dye concentration was increased from 25 mg/L to 125 mg/L, the maximum color removal was found at 25 mg/L that is 90-92%. On the other hand when dye concentration reached 125 mg/L the color removal percentage was reduced to about 30-38%. Whereas, the adsorbent dose is directly proportional to adsorption and removal percentage; when the adsorbent dose was 10g/L the minimum percentage of dye removal was found, as the adsorbent dose increased up to 50 g/L the maximum adsorption was established. Further the optimized shaking speed 160 rpm, and optimized particle size found to be 1200 µm, and maximum contact time of 55 minutes were found to be satisfactory to get the maximum results. The adsorption percentage decreased with the increase of particle size, Smaller the particle size, the greater was the contact surface area for adsorption. The results showed that the adsorption isotherms fits both the Fruendlich and Langumir isotherms. The isotherm analysis graph shows the linear slope that best fits the Langumir for the removal of reactive blue dye on orange peel.

REFERENCES

- Ahalya N, Ramachandra TV and Kanamadi RD (2006). Removal of hexavalent chromium using coffee husk. Bioresource Technology 167-191
- Aurthur BD. (2001). Basic Principles of Coloration, 2nd edition, Society of Dyers and Colorists. 56-89.
- Derbyshire F, Jagtoyen M, Andrews R, Rao A, Martin-Gullon I and Grulke E (2003). Carbon Materials in Environmental Applications. In: Radovic, L.R. Ed., Chemistry and Physics of Carbon. Marcel Dekker, New York, 27, 41–66.
- Khatri A. (2010). Pad-steam Dyeing of Cotton with Reactive Dyes Using Biodegradable Alkaline Organic Salts, Textile Technology Discipline School of Fashion and Textiles Design and Social Context RMIT University, Australia, 30-78.
- Puthiya V, Nidheesh, Rajan G, Sreekrishnaperumal T, Ramesh, Tangappan S, Anantha S. (2011). Kinetic analysis of crystal violet adsorption on to bottom ash, Department of Civil Engineering, National Institute of Technology, Tiruchirappalli, Tamilnadu-INDIA. 68-89.
- Ramachandra TV, Rajasekaramurthy C and Ahalya N. (2008). Biosorption, Techniques and Mechanisms Restoration of Lakes and Wetlands. Allied Publishers (P) Ltd., India. RD, CES Technical Report 110, pp.146-158.
- Ramakrishna KR and Viraraghavan T. (1997). "Dye removal using low cost adsorbents", Journal of Water Science Technology. 36:189–196.

Investigating the Mechanical Properties and Drill-ability of Rocks

Abdullah Rasheed Qureshi[1*], Adnan Aftab[2], Zaheer Kasi[1], Abdul Sami Gahejo Abro[1]

[1]Department of Mining Engineering, [2]Department of Petroleum & Gas Engineering, Balochistan University of Information Technology, Engineering & Management Sciences, Quetta

Abstract

Drilling is the primitive and common operation in rock excavation industry, starting from exploration to exploitation. Effect of mechanical properties of the formation on drilling operation is a big challenge to mining engineers. The primarily problem is rock drill-ability. The objective of this paper is to correlate the drill-ability of certain rocks with their mechanical properties including Compressive strength, Tensile strength, Schmidt hammer rebound number and Shore Hardness number, in order to establish rate of penetration. This paper contains investigation of both laboratory experiments and Field examination of drilling equipment. Laboratory work includes the determination of various mechanical properties of rock specimen, determined according to ASTM procedure using Universal Testing Machine. Schmidt hammer test conducted on the rock specimen by clamping into the UTM loading platens. Shore hardness test performed on disc specimen carefully prepared for the purpose. The test was conducted as per standard procedure.

Keywords: Drill-ability, Mechanical Properties, Schmidt Hammer Test, Rate of Penetration, Universal Testing Machine.

[*]*Corresponding Author e-mail: adnan.aftab@buitms.edu.pk*

INTRODUCTION

Drilling is the prehistoric and common operation in rock excavation industries, starting from exploration to exploitation of mineral, oil and water. Rocks are drilled for several purposes. such as, geological exploration, blast hole for mineral production, for rock bolting, rock cores for determining geotechnical parameters and rock excavation for civil constructions (Akun and Karpuz, 2005; Kahraman et al., 2003).

In addition, energy applied to the rock affects the type of fracture and breakage develops in rock. No single rock property is a measure of drill-ability of the rocks; infact all the geotechnical properties of rock in some way or the other contribute to the drilling performance (American Society of testing and Material 1974; Brady and Brown, 1985) The most influencial parameters for drilling are mechanical property of the rock, cutting tools and their shapes, magnitude of forces influenced at the bit, rock interface and flushing rate. The performance of a drilling system is usually represented by the drill-ability of rocks which is defined as the real or projected rate of penetration in a given rock type. Thus, a study which describes relationship between penetration rate and the various rock properties for drilling parameters is required to perform economical and efficient drilling (Hardy, 1957; Hetenyi, 1966; Olgay and Eren, 2011).

MATERIALS AND METHODS

The behavior of rock mass is governed by the defects existing in the rock mass. Because rock mass in general is non-homogeneous and the properties of the samples are taken from one portion of rock, the rock mass may be different from another portion. Therefore, sample collected must truly represent the rock mass, the properties of which are to be determined. Samples

collected for laboratory testing should be in the form of large blocks from the field [11]. In instances where substantial drilling is required to evaluate a deposit, it is usually considered to be good practice to core a certain percentage of holes in the drill program. The actual percentage will vary with the available budget and the degree of complexity of the geology, but usually average about 10% core samples offer the advantage that sample location can be closely defined, and there is little possibility of contamination or loss of values as long as recovery is good. On the negative side, core drilling is expensive and usually the sample obtained is relatively small. In case where the ore boundaries are fairly well known, the cost can sometimes be lowered by rotary drilling to near the ore boundary and then continuing with core. Rebound and rebound of diamond tipped impactor hardness is calculated by Shore Sceleroscope Hardness Test (Figure 1) .Rebound hardness is calculated by Schmidt Hammer Hardness Test (Figure 2) which impacts the piston striking. This test was first used for rapid examination of compressive strength of concrete and later it was used to calculate the hardness of rock. UTM (Universal testing machine) (Figure 3) is used to determine UCS (UNI-AXIAL COMPRESSION TESTING) which is the most basic parameter of rock strength, and the bore ability prediction is performed by using UTM [8]. It is calculated in accordance with instructions given in ASTM (American Society for Testing and Materials).

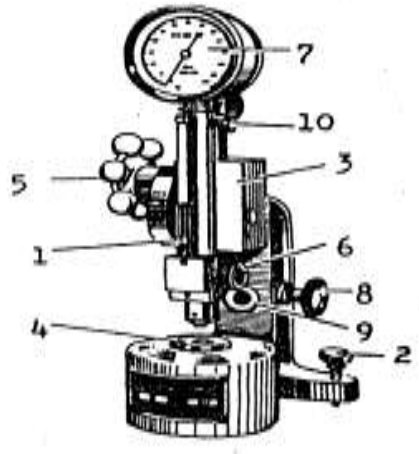

Figure 1 – Shore Sceleroscope

1. Level Rod
2. Level Adjust Screw
3. Main Body
4. Table
5. Control Knob
6. Operation Knob
7. Indication Scale
8. Butt Gage Fixed Handle
9. Hole For Butt Gage
10. Dial Gauge Fixed Screw

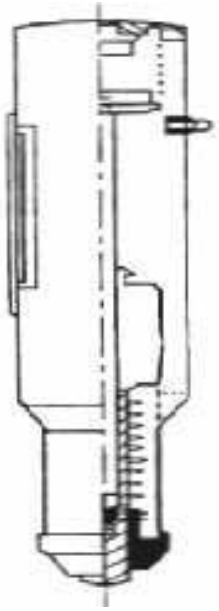

Figure 2 – Schmidt Hammer

Figure 3 - Universal Testing Machine (UTM)

In laboratory, the test specimens are required to be prepared from the rock sample brought from the field. The shape and size of specimen depend upon the type of the test to be conducted. Most of the test specimens to Mechanical Properties are of regular shape (i.e. Cylindrical). Typical diameter range used for Cylinder sample are 25mm to 50mm. As a standard, however, unconfined compressive strength tests require that test specimen be right circular cylinder with a diameter not less than (54mm) core size and the ratio of length and diameter is 2.0 to 2.6 to avoid the stress concentration at the time of testing (Olgay and Eren, 2011)s. The specimen sides should be regular in order to avoid abrupt irregularities. The specimen ends should be cut parallel to each other and of normal to longitudinal axis. The ends should be ground and end lapped. The result obtained from testing a single specimen may not represent the property of rock mass. Therefore, in order to limit the testing work, at least four specimens should be tested to get an absolute value.

The strain, corresponding to each stress level (or equivalent load level), is obtained by multiplying the apparent strain by the calibration constant of the compress meter. The uni-axial compressive strength is calculated by Qu = Pu/A, Pu = the maximum load carried out by the specimen while the testing, and A = the actual cross sectional area calculated in accordance with the specification (Hartman, 1987). Indirect tensile strength of a substance can be obtained by the ratio of multiplication of failure load with 2 and multiplication of constant (π) into diameter and thickness of the specimen. Tensile strength is calculated by σt= 2P/DT, σt= indirect tensile strength, P= failure load, D = diameter of specimen (disc), and T = thickness of specimen disc (Lewis, 1964).

RESULTS AND DISCUSSION

The rate of penetration (ROP) is an essential parameter for the calculation of drillability. Causing the rock to break during drilling is a matter of applying sufficient force with a tool to exceed the strength of the rock. This resistance to penetration of rock is termed as its drilling strength, an empirical property; it is not equivalent to any of the well-known strength parameters.

Experimental work involves three samples from three different sites. The rate of penetration data of sample 1 and Sample 2 are shown in Table 1 and Table 2.

Table 1- Rate of penetration of Sample 1

HOLE ID	STARTING TIME	STOPPING TIME	TIME ELAPSED	METER DRILLED
2 JULY 01	10:25AM	10:40AM	15 MIN	17 METERS
2 JULY 02	10:56AM	11:17AM	26 MIN	19 METERS
7 JULY 03	11:05AM	11:23AM	18 MIN	21 METERS
14 JULY 04	10:26AM	10:42AM	16 MIN	17 METERS
15 JULY 05	11:50AM	12:06PM	20 MIN	12 METERS
TOTAL			95 MIN	80 METERS

Table 2- Rate of penetration of Sample 2

HOLE ID	STARTING TIME	STOPPING TIME	TIME ELAPSED	METER DRILLED
3 NOV 01	11:20AM	11:34AM	14 MIN	11 METERS
3 NOV 02	12:16PM	12:33PM	17 MIN	13 METERS
4 NOV 03	11:05AM	11:20AM	15 MIN	10 METERS
4 NOV 04	11:26AM	11:41AM	15 MIN	12 METERS
4 NOV 05	11:50AM	12:06PM	16 MIN	12 METERS
TOTAL			77 MIN	58 METERS

Table 3- Rate of penetration of Sample 3

HOLE ID	STARTING TIME	STOPPING TIME	TIME ELAPSED	METER DRILLED
10 NOV 01	10:23AM	10:59AM	36 MIN	7 METERS
11 NOV 02	10:35AM	11:18AM	43 MIN	8 METERS
12 NOV 03	10:15AM	10:57AM	42 MIN	7 METERS
13 NOV 04	10:26AM	11:02AM	36 MIN	6 METERS
14 NOV 05	10:30AM	11:10AM	40 MIN	7 METERS
TOTAL			197 MIN	35 METERS

The uni-axial compressive strength tests of the limestone rock specimens are calculated by dividing maximum load carried by the specimen (i.e. failure load) during the test, by the actual cross-sectional area. Three samples were tested to determine UCS of lime stone as shown in Table 3. The tensile strength of limestone rock specimen is calculated as shown in Table 4.

Table-4 Results of UCS Tests of Limestone

Test No.	Length cm / (m)	Diameter cm / (m)	X-sectional Area (m^2)	Failure Load (N)	UCS $_c$ MPa
Sample 1	11.5 (0.115)	4.7 (0.047)	0.001734	112710	65
Sample 2	11.5 (0.115)	4.7 (0.047)	0.001734	100572	58
Sample 3	11.5 (0.115)	4.7 (0.047)	0.001734	147390	85

Table-5Results of Tensile Strength of Limestone

Test No.	Thickness cm / (m)	Diameter Cm / (m)	Failure Load (KN)	Tensile Strength $_t$ MPa
Sample 1	2.5 (0.025)	4.7 (0.047)	22.148	**11.98**
Sample 2	2.5 (0.025)	4.7 (0.047)	23.847	**12.91**
Sample 3	2.5 (0.025)	4.7 (0.047)	38.799	**21.00**

Shore hardness has to be determined by the shore hardness testing instrument. The 2cm thickness sizes of specimens were prepared in the laboratory by means of cutter and grinder from the each sample of the sites. The readings of the shore hardness test of each specimen are shown in the tables 5 and Summary of Mechanical properties is shown in Table 6.

Table-6 Shore hardness test

ITERATIONS	Sample 1		Sample 2		Sample 3	
	Side1	Side	Side1	Side2	Side1	Side2
01	20	28	43	45	54	47
02	31	31	46.5	48	57	49
03	26	08	46	39	47	42
04	35	36.5	53.5	35	49	40
05	38	47	46	37	63	51
06	46	32.5	47	24	46	43
07	33	42.5	38	36	49	57
08	21	14.5	22.7	31	52	58
09	28	23	36.5	35	51	52
10	10	32	39	37	58	54
11	16	39	39	47	48	42
12	34	31	39.5	49	53	40
13	43	32	41	51	52	42
14	45	31	46.4	47	51	49
15	46	39	44.5	52	62	60
AVERAGE	**31.46**	**31.13**	**41.90**	**40.86**	**52.08**	**48.04**

Table-7 Summary of Mechanical properties

Sr. No	Sample ID	UCS (MPa)	Tensile Strength (MPa)	Shore Hardness No.	Rate of Penetration meters/hour
1	Sample 1	65	11.98	31.58	50.5
2	Sample 2	58	12.91	43.77	45
3	Sample 3	85	21.00	50.64	10.8

Drill-ability of rock manifests the various mechanical properties of rock. Assessment of drill-ability or penetrability is the most serious issue among the drilling equipment manufacturers and operators. Unfortunately there is no direct method of drill-ability measurement but it could be measured through empirical correlation of various mechanical properties of rocks [11]. Correlation of UCS (Uni-axial Compressive strength) & ROP (Rate of penetration), Correlation of Tensile Strength & ROP, and Correlation of Shore Hardness & ROP are shown in Figure 4, 5, and 6.

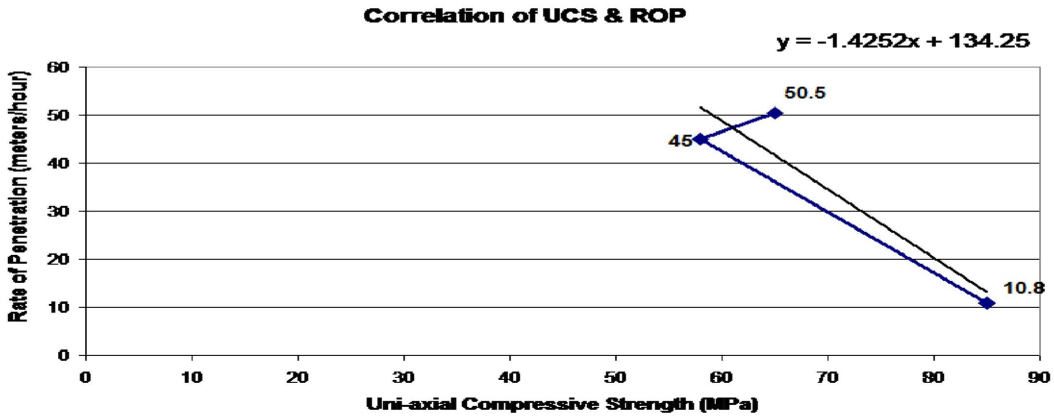

Figure 4 – Correlation of UCS & ROP

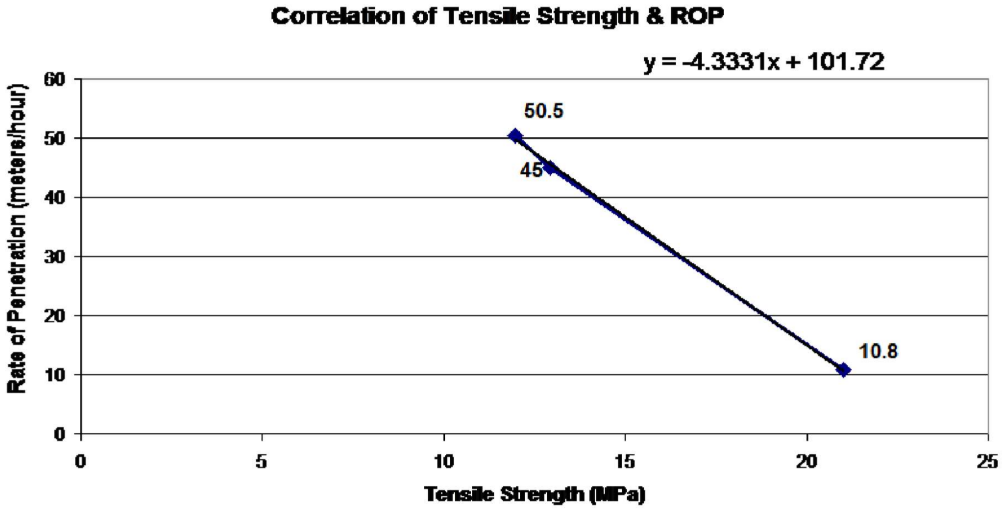

Figure 5 - Correlation of Tensile strength and ROP

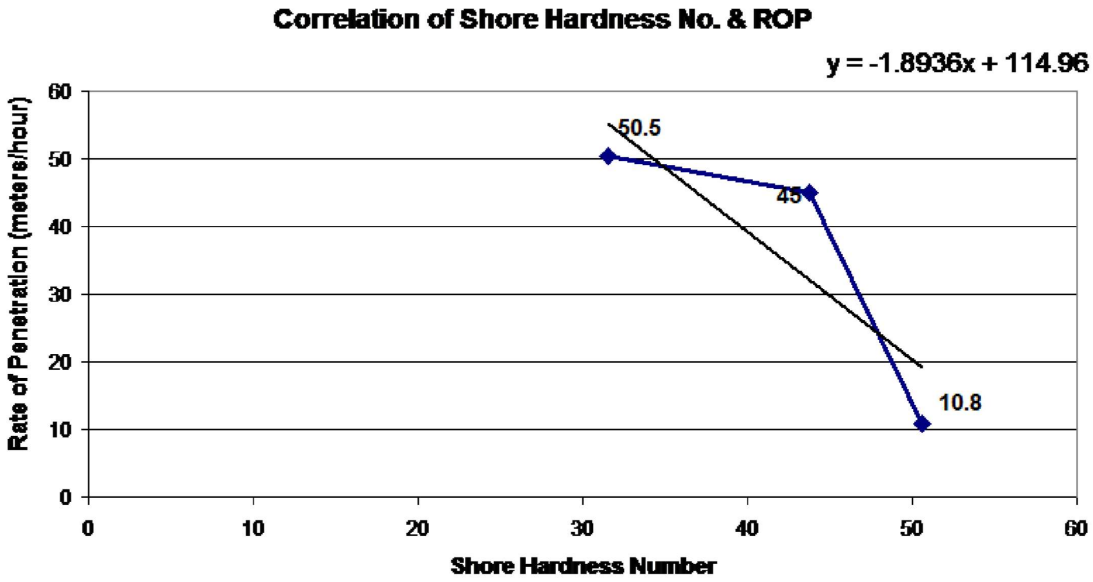

Figure 6 - Correlation of Shore Hardness & ROP

CONCLUSION

In this paper attempts have been made to correlate the rate of penetration in the rocks having different mechanical properties. Following conclusions were drawn from the experimental data. The limestone samples obtained from the three different sites were analyzed for Uni-axial Compressive Strength, Tensile Strength and Shore Hardness Number. Compressive Strength test shows that all three rocks fall under the category of Medium Hard Rock.

ACKNOWLEDGMENT

Authors are thankful to Dr. Syed Abid Hussain and Dr. Syed Muhammad Ali Shah who have contributed their knowledge and field experience in writing this research paper.

REFERENCES

Ÿ Akun ME, Karpuz C. (2005). Drill-ability studies of surface-set diamond drilling in Zonguldak Region sandstones from Turkey. *Int. J. Rock Mech. Min. Sci.* 42: 473-479.

Ÿ American Society for testing and material (1974). Standard method of test for tri axial compressive strength of undrained rock core specimens without pore pressure measurements. Annual book of ASTM standards, USA.

Ÿ Braddy BHT and Brown ET. (1985). Rock Mechanics. Division of Geomechanics, Australia and Imperial College of Science and Technology, London.

Ÿ Hardy. (1957). Standard procedures for determination of the physical properties of mine rock under short period uni axial compression. Unpublished fuel division report. FRL – 242.

Ÿ Hetenyi M (1966). Handbook of experimental stress analysis. Wiley, New York.

Ÿ Hartman HL. (1987). Introductory Mining Engineering. The University of Alabama, Alabama.

Ÿ Huang SL, Wang ZW. (1997). The mechanics of diamond core drilling of rocks. *Int. J. Rock Mech. Min. Sci*. Geomech. Abst., 34: 6-12.

Ÿ Kahraman S, Bilgin N, Feridunoglu C. (2003). Dominant rock properties affecting the penetration rate of percussive drills. *Int. J. Rock Mech. Min. Sci.*, 40: 711-723.

Ÿ Lewis RS. (1964). Elements of mining engineering. University of Utah, USA.

Ÿ Vani Prakashan (1989) Concise Mining Manual. Indian School of Mines Dhanbad, India.

Ÿ Olgay Y and Eren S. (2011). The effect of mechanical rock properties and brittleness on drillability. *Scientific Research and Essays* 6(5): 1077-1088.

Extraction of Active Components of Aloe Vera to Treat Acne/pimple in Population of Quetta City

Asma Yousafzai*, Saima Saleem, Nusrat Jahan, Fariha Javed, Muhammad Waseem Khan, Razia Kanwal

Department of Biotechnology and Informatics, Balochistan University of Information Technology, Engineering & Management Sciences, Quetta

Abstract

Comprehensive study of local aloe vera and its effects on acne/pimple was performed. The work mainly describes the chemical investigation of aloe vera by traditional methods to check its efficacy in the treatment of acne. Local aloe specie was gown and solutions of different concentration were made. Samples of acne were collected from different acne sufferers to identify the microbe which is major cause of acne infection. Doses of different concentrations of aloe vera were tested on the acne causing microorganism. In the present work traditional methods of plant extraction were used to find the relationship between aloe vera and acne treatment. Doses of different concentrations were calculated and analyzed to treat acne.

Key Words: Aloe vera, Acne, Pimple, Traditional treatment, Medicinal plant

**Corresponding Author's email: asmakhan@buitms.edu.pk*

INTRODUCTION

Aloe barbadensis miller (Aloe vera) belongs to the Liliaceal family,of wich there are about 360 species. It is a cactus-like plant that grows readily in hot, dry climates and currently, because of demand is cultivated in large quantities (Newall *et al.,* 1996). Succulent almost sessile perennial herb, has leaves 30-50 cm long and 10cm broad at the base, color pea green (when young spotted with white), bright yellow tubular flowers 25-35 cm in length arranged in a slender loose spike, stamens frequently project beyond the perianth. Its thick leaves contain the water supply for the plant to survive long periods of drought (Foster, 1999). Due to the increasing development of antibiotic resistance, the emphasis of the present study is being given on the use of *Aloe* vera as a natural remedy for the inhibition of various infections and to identify the different compounds. (Agarry et al., 2005)

Among these the most popular is Aloe Barbadensis Miller which has most therapeutic value and referred to as 'True Aloe'. After all the research, it has been accepted that Aloe Barbadensis Miller is the best, as it is the most consistent of all varieties. Aloe Vera is generally propagated by root suckers by carefully digging out without damaging the parent plant and planting it in the main field. It can also be propagated through rhizome cuttings by digging out the rhizomes after the harvest of the crop and making them into 5-6 cm length cuttings with a minimum of 2-3 nodes on them. Then they are rooted in specially prepared sand beds or containers. (Boudreau and Beland, 2006; Oala et al., 2007).

Its thick leaves contain the water supply for the plant to survive long periods of drought. These leaves have a high capacity of retaining the water. When a leaf is cut, an orange yellow sap drips from the open end which has a very strong laxative effect. When the green skin of a leaf is removed a clear mucilaginous substance appears that contain fibers, water and the ingredients to retain the water in the leaf. These ingredients give this "gel" its special qualities as they are known now for many centuries. Among the uses for this gel is acceleration of wound healing, use

on skin burns, moisturizing dry skin and it is taken internally for peptic ulcers or gastritis. (Rabe and Staden, 1997).

Chemical investigations of different parts of leaf

The detailed chemical investigation of Aloe Vera distinguishes between the different parts of the leaf. The leaf pulp separately analyzed from the rind. The pulp was found to contain 98.5% water, and its alcohol-insoluble was mucilage with high content of uronic acid, fructose and hydrolysable sugars. Enzymes such as an oxidase, a catalase, a cetalase and an amylase were reported to be present, but small nitrogen content. The leaf pulp did not respond to tests for “aloin”. The chemical components of the gel scraped from the leaves after the exudate had been drained off, were examined. The crude gel had an ash content of 12.9%, removable by dialysis. White water-soluble mucilage was purified which on hydrolysis was found to contain equal amounts of glucose and mannose as the main constituents, with a small amount of uronic acid (2.37%). Ketoses were thought to be absent. They also reported that some aloin was present in the crude gel, despite bleeding off the exudates from the leaves.

MATERIALS AND METHODS

Collection of plant material

Pakistani and Irani Aloe vera leaves were collected from the Botanical garden of Balochistan University, Quetta, Balochistan, Pakistan.

Test organisms

Pure cultures of bacterial strains of Escherichia coli, Staphylococcus aureus, Bacillus subtilius, and Salmonella typhie were used as test organisms. The organisms were maintained on agar slants stocks and were subsequently subcultured into newly prepared macConky agar slants.

Plant extraction and fractionation

The leaves (2 kg) each were dried in shade, ground and soaked in ethanol for 10 days separately. Thick dark crude extracts were yielded after evaporating the solvent through rotary evaporator. Fractionation of the methanolic extracts was carried out to find the antibacterial activities. The extracts were dissolved in Di-Methyl Sulfoxide (DMSO) and used for the antimicrobial susceptibility testing.

Antimicrobial susceptibility testing

The antibacterial activities of four plants extract were determined against bacterial strains by agar well diffusion Technique (Agarry et al; 2005). Sterile agar (at 45°C) was poured into sterile Petri dishes, which had been inoculated with the test organisms. The plates were allowed to gel for an hour. Wells (10 mm diameter) were made with the aid of flamed cork borer on the surface of the agar plates. 0.1 gram of ethanol extracts of aloe vera plants were dissolved in (DMSO).From this 10 µl, 15 µl was pipette out and added to the respective wells. These were incubated at 37°C for 24 h. The presence of zones of inhibition was regarded as the presence of antimicrobial action. From the inhibition zones seen, antimicrobial activity was expressed in terms of average diameter of the zones of inhibition measured.

RESULTS AND DISCUSSION

Different doses for 75% Aloe vera solution gave variety of results. Doses of 0.1, 1.0, 1.5, 2.0 and 2.5 didn’t give any result on acne vulgaris caused by propionibacterium acnes on body of mice for 3 days. 3ml does for 3 days caused the diameter of lesion to reduce about 4.5 mm, 3.5ml does for 3 days caused the diameter of lesion to reduce about 4.3 mm, 4ml does for 3 days caused the diameter of lesion to reduce about 4.1 mm, 4.5ml does for 3 days caused the diameter of lesion to reduce about 3.9 mm best results were obtained at 5ml does for 3 days caused the diameter of lesion to reduce about 3mm. (Table 1, Figure 2). Different doses for 80% Aloe vera solution give variety of results. 0.1ml does for 3 days caused the diameter of lesion to reduce about 4.6 mm, 1ml does for 3 days caused the diameter of lesion to reduce about 3.9 mm. 1.5ml does for 3 days caused the diameter of lesion to reduce about 3.2 mm, 2ml does for 3 days caused the diameter of lesion to reduce about 2.2 mm, 2.5ml does for 3 days caused the diameter of lesion to reduce about 1.45 mm, 3ml does

for 3 days caused the diameter of lesion to reduce about 1.15 mm, 3.5ml does for 3 days caused the diameter of lesion to reduce about 0.9 mm, 4ml does for 3 days caused the diameter of lesion to reduce about 0.65 mm, 4.5ml does for 3 days caused the diameter of lesion to reduce about 0.45 mm, 5ml does for 3 days caused the diameter of lesion to reduce about 0.3 mm. so the best results were obtained at 5ml in 80% aloe Vera concentration. (Table 2, Figure 3). (Reynolds and Dweck, 1999).

Different doses for 85% Aloe vera solution give variety of results. first dose of 0.1ml for 3 days caused the diameter of lesion to reduce about 4.4mm, second dose of 1ml for 3 days caused the diameter of lesion to reduce about 3.5mm, third dose of 1.5ml for 3 days caused the diameter of lesion to reduce about 2.9mm, fourth dose of 2ml for 3 days caused the diameter of lesion to reduce about 2.1mm, fifth dose of 2.5ml for 3 days caused the diameter of lesion to reduce about 1.2mm, sixth dose of 3ml for 3 days caused the diameter of lesion to reduce about 0.8mm, seventh dose of 3.5ml for 3 days caused the diameter of lesion to reduce about 0.5mm, eighth dose of 4ml for 3 days caused the diameter of lesion to reduce about 0.2mm, ninth dose of 4.5ml for 3 days caused the diameter of lesion to reduce about 0.1mm, tenth dose of 5 ml for 3 days eliminated all kind if lesions with improved texture of skin. (Table 3, Figure 4).

Different doses for 90% Aloe vera solution give variety of results. first dose of 0.1ml for 3 days caused the diameter of lesion to reduce about 4.2mm, second dose of 1ml for 3 days caused the diameter of lesion to reduce about 3.1mm, third dose of 1.5ml for 3 days caused the diameter of lesion to reduce about 2.4mm, fourth dose of 2ml for 3 days caused the diameter of lesion to reduce about 1.9mm, fifth dose of 2.5ml for 3 days caused the diameter of lesion to reduce about 1.1mm, sixth dose of 3ml for 3 days caused the diameter of lesion to reduce about 0.6mm, seventh dose of 3.5ml for 3 days caused the diameter of lesion to reduce about 0.3mm, eighth dose of 4ml for 3 days caused the diameter of lesion to reduce about 0.1mm, ninth dose of 4.5ml for 3 days eliminated all kind if lesions with improved texture of skin(Rubina et al., 2009).

(Table 4, Figure 4)

Table 1: Results for 75% dose of Aloe vera solution

Dose (ml)	Size (mm)	Other effects
0.1	NIL	NA
1.0	NIL	NA
1.5	NIL	NA
2.0	NIL	NA
2.5	NIL	NA
3.0	4.5	Slight decrease in redness, no affect on pus filled lesions and hard cysts
3.5	4.3	Dryness of pus filled lesions, no affect on hard cysts
4.0	4.1	Redness disappeared completely, pus filled lesions healed, no affect on hard cysts
4.5	3.9	Hard cysts softened
5.0	3	Decrease in lesion's size and inflammation

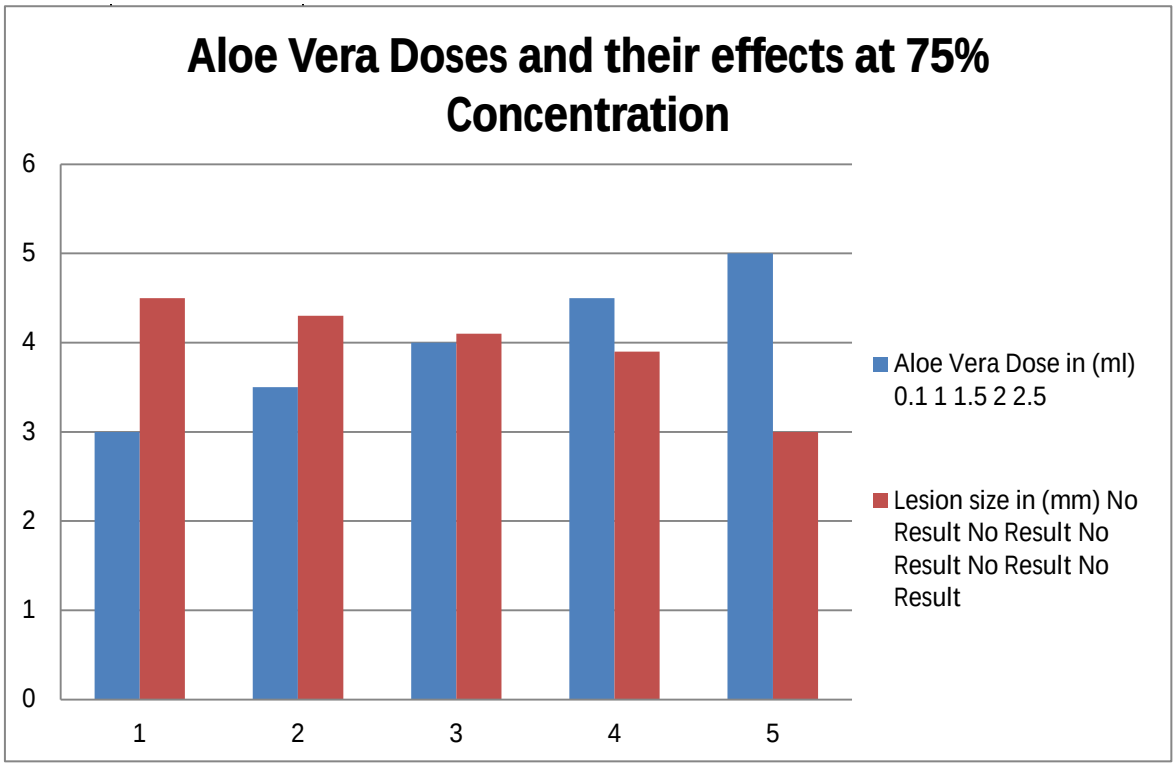

Figure 1: Aloe Vera Doses and their effects at 75% Concentration

Table 2: Results for 80% dose of Aloe vera solution

Dose (ml)	Size (mm)	Other effects
0.1	4.6	Redness reduced, no affect on inflammation, pus filled lesions & hard cysts
1.0	3.9	Redness disappeared, inflammation reduced, pus started to dry
1.5	3.2	Inflammation further reduced, cysts softened, pus reduced
2.0	2.2	Cysts reduced
2.5	1.45	Cysts further reduced
3.0	1.15	Pus filled lesions further reduced
3.5	0.9	Pus filled lesions more reduced
4.0	0.65	Pus filled lesions further reduced disappeared
4.5	0.45	Open mouth lesions reduced
5.0	0.3	All types of lesions reduced remarkably

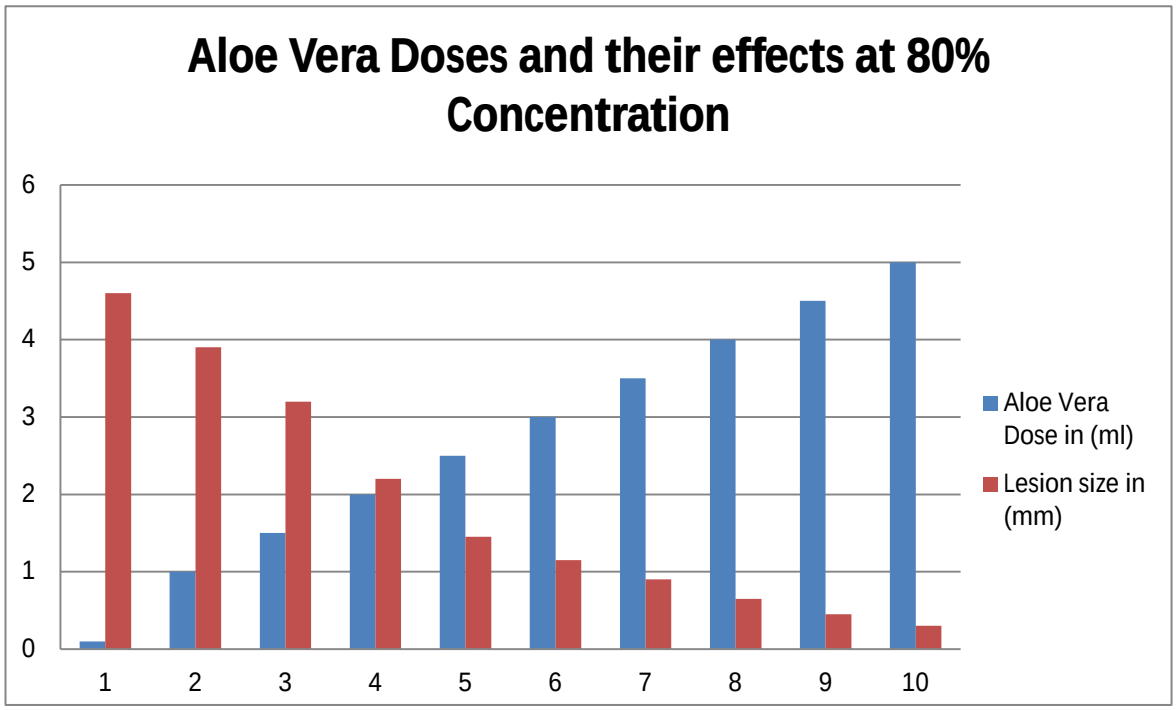

Figure 2: Aloe Vera Doses and their effects at 80% Concentration

Table 3: Results for 85% dose of Aloe vera solution

Dose (ml)	Size (mm)	Other effects
0.1	4.4	Redness reduced, no affect on inflammation, pus filled lesions and hard cysts (white & black heads)
1.0	3.5	Redness disappeared, inflammation reduced, pus started to dry, no affect on hard cysts (white & black heads)
1.5	2.9	Inflammation disappeared, pus further dried, hard cysts further reduced
2.0	2.1	Pus further dried, Cysts more reduced
2.5	1.2	Open mouth lesions healed completely, pus further dried, and hard cysts reduced
3.0	0.8	Pus filled lesions disappeared completely, cysts more reduced
3.5	0.5	Open mouth lesions disappeared completely, cysts completely disappeared
4.0	0.2	All lesions reduced to like just spots
4.5	0.1	Some dried lesions left
5.0	0.00	All lesions disappeared completely

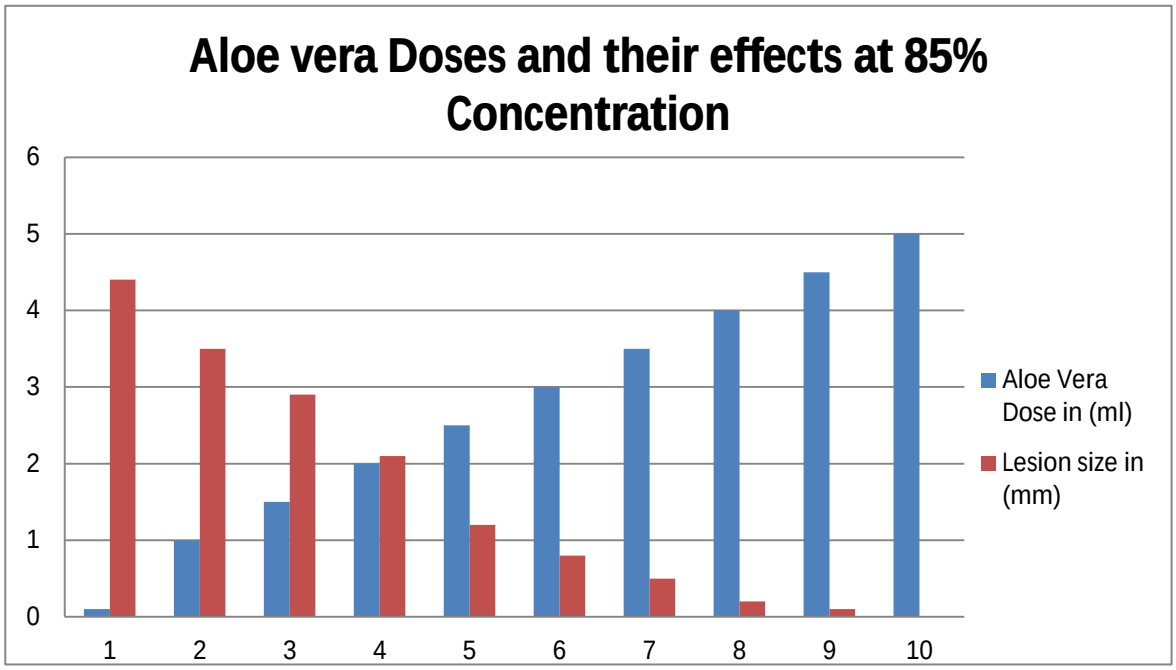

Figure 3: Aloe Vera Doses and their effects at 85% Concentration

Table 4: Results for 90% dose of Aloe vera solution

Dose (ml)	Size (mm)	Other effects
0.1	4.2	Redness reduced, inflammation reduced, no effect on open mouth lesions, pus filled lesions and hard cysts (white & black heads)
1.0	3.1	Redness disappeared completely, inflammation reduced, open mouth lesions healed partially, pus dried slightly and no affect on hard cysts (white & black heads)
1.5	2.4	Inflammation disappeared completely, open mouth lesions healed to a comparatively smooth texture, puss dried and lesions reduced, cysts softened
2.0	1.9	Pus filled lesions more reduced, hard cysts (white heads) softened and started to dissolve
2.5	1.1	Pus filled lesions almost disappeared, white heads completely disappeared, hard cysts (black heads) reduced
3.0	0.6	Pus filled lesions completely dried, hard cysts (black heads) further reduced
3.5	0.3	Hard cysts (black heads) almost disappeared, skin texture smoothened
4.0	0.1	All lesions healed with very smooth texture with breakouts
4.5	0.0	
5.0	0.00	

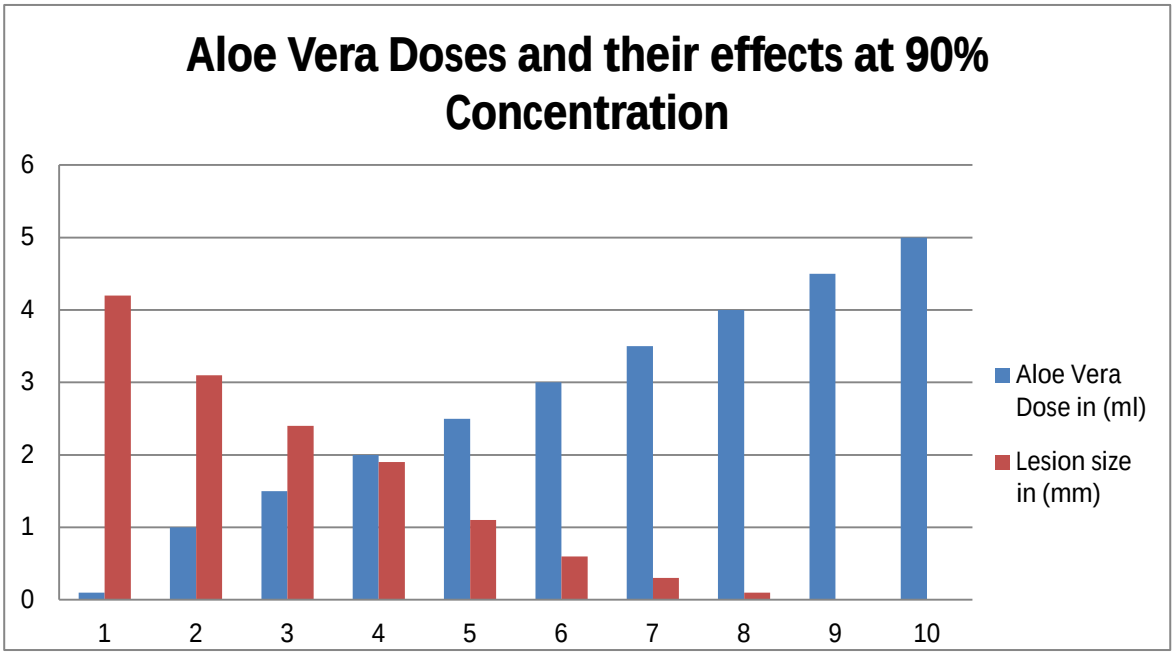

Figure 4: Aloe Vera Doses and their effects at 90% Concentration

CONCLUSION

Aloe vera plant extracts were found effective against skin acne and skin pimples. Different concentrations of Aloe vera have different results and effects on skin lesions. At higher doses of Aloe vera concentrations the skin lesions healed completely, pus filled lesions dried and cysts disappeared completely.

REFERENCES

Ÿ Agarry I, Olaleye M and Bello M. (2005). Comparative antimicrobial activities of aloe vera gel and leaf. African Journal of Biotechnology. 4 (12): 1413-1414.

Ÿ Boudreau MD and Beland FA. (2006). An evaluation of the biological and toxicological properties of Aloe barbadensis (miller), Aloe vera. Environ Sci Health C Environ Carcinog Ecotoxicol Rev. 24:103–154.

Ÿ Foster S. (1999). Aloe vera: The succulent with skin soothing cellprotecting properties. Herbs for Health magazine. Health WorldOnline. http://www.healthy.net/library/articles/hfh/aloe.htm

Ÿ Newall CA, Anderson LA, Phillipson JD. (1996). Herbal medicines. A guide for health-care professionals. The Pharmaceutical Press, London. 25.

Ÿ Oana RC, Marcel P, Laurian V and Mircea T. (2007). Antifungal activity of Aloe vera leaves. Fitoterapia. 78: 219-222.

Ÿ Rabe T and Staden JV. (1997). Antibacterial activity of South African plants used for medicinal purposes. *Journal of Ethnopharmacology*, 56 (1): 81-87.

Ÿ Reynolds T and Dweck AC. (1999). Aloe vera leaf gel: a review update. J. Ethnopharmacol. 68: 3-37.

Ÿ Rubina Lawrence, Priyanka Tripathi, Ebenezer Jeyakumar. (2009). Isolation, purification and evaluation of antibacterial agents from Aloe vera. Brazilian Journal of Microbiology. 40: 906-915.

Effects of Trade Liberalization on Economic Growth of Pakistan

Usman Azhar

Department of Environmental Management and Policy, Balochistan University of Information Technology, Engineering & Management Sciences, Quetta

Abstract

Trade policy is gaining an increasing importance in developing economies as a strategy for economic development. The rapidly growing world market offers. Realizing the importance of trade policy as a tool for economic development, the government of Pakistan began to restructure its trade policy from a protectionist regime to a more liberalized regime with the introduction of wide ranging structural reforms in late 1980s. Successive trade policies attempted to diversify the export base and to improve export infrastructure and to increase exports. This research explores the impact of trade liberalization on the economic performance of trade in Pakistan for the period 1977-2008. By using multiple linear regression estimation technique the aggregate production function for Pakistani economy is estimated. The findings indicate that the trade liberalization is having positive impact on the growth of economy. One interesting finding of this research is negative but statistically significant coefficient for Foreign Direct Investment in Pakistan. Extensive privatization of state owned enterprises could be one major reason behind this negative sign. This research suggests the continuation of trade liberalization policy for long term sustainable economic growth of the country.

Keywords: Trade liberalization, Imports substitution, Economic growth, Pakistan

Corresponding Author's Email: usman@buitms.edu.pk

INTRODUCTION

Trade has become an increasingly important global economic activity, with annual trade volumes increasing sixteen fold over the last fifty years and the ratio of world exports to Gross Domestic Product (GDP) now approaching twenty percent. Trade policy is gaining an increasing importance in developing economies as a strategy for economic development. The rapidly growing world market offers a window of opportunity for the developing world to accelerate their industrialization. With the increasing size of the world market and acceleration of international trade, developing countries throughout the world have been drawing foreign direct investment and technology transfer, and increasing employment and income growth (Frankel et al., 1999; Hinkel et al., 1999).

Realizing the importance of trade policy as a tool for economic development, the government of Pakistan began to restructure its trade policy from a protectionist regime to a more liberalized regime with the introduction of wide ranging structural reforms in late 1980s. Successive trade policies attempted to diversify the export base and to improve export infrastructure and to increase exports. The purpose of study is to explore the impact of this important policy change on the process of industrialization and economic growth. The early years of Pakistan's economy can be characterized by a weak industrial base, dominance of the agriculture sector, lack of well-organized infrastructure, and above all eco-political instability. The main objective of the policies of those years was to strengthen the industrial base. To this end, Pakistan adopted a restricted trade regime and protected its

domestic industries with high tariff and non-tariff barriers. The period of the sixties was the period in which the industrial base was laid and in which rapid expansion of large scale manufacturing industries started in the country. While the highly protected trade regime remained effective in this period, some additional policies were introduced to encourage industrial exports from the country, like an overvalued exchange rate, export bonuses, preferential credit access to industries with export potential and automatic renewal of import licenses. Consequently, both industrial production and exports registered a reasonable increase during the 1960s. However, industrial expansion did not continue at the same rate in the following decade of seventies. In fact, it suffered a setback in the following decade due to the nationalization of industries (Narayan et al., 2004; Onafowora et al., 1998). Although the government nationalized different types of industries in the country, it took three additional trade liberalization measures to encourage exports during this period, these were:

- Devaluation of the Pakistani Rupee by 57% in 1972.
- Elimination of the export bonus scheme.
- The discontinuation of restrictive licensing scheme.

These steps stimulated exports especially of manufactured products. Substantial trade liberalization has taken place in Pakistan since the late 1980s at a pace that has been accelerating over time. Import taxes have been reduced, the Statutory Regulatory Orders (SROs) have now been mostly withdrawn and Non-Tariff Barriers (NTBs) have been largely dismantled. In particular, the average tariff rate has declined sharply from 77 percent in 1985 to about 17 percent. Although trade policies were modified continuously in Pakistan, changes of particular significance were made after the formulation of the new trade policy in 1987. After the incorporation of the other changes, the trade policy led, inter alia, to a reduction in tariff slabs from 17 to 10 and introduction of a uniform tax in place of commodity based sales taxes. In fact, the government focused in this decade mainly on enhancing the role of private sector in the economy, increasing the competitiveness and efficiency of the domestic industrial sector, and promoting exports. The specific measures that the government took in pursuance of these objectives, related to the provision of different fiscal incentives such as tax holidays, tariff cuts, and other profit augmenting opportunities to the exporters. The maximum tariff was reduced from 225 percent in 1986-87 to 70 percent in 1994-95. Additionally the number of custom duty slabs were reduced from 13 to 5. Flexible exchange rate system introduced earlier was kept in effect during this decade. The response of economy to trade liberalization policy was mixed, in 1980s the average GDP growth rate was about 6 %, which reduced to 4 % in 1990s and 3.8 % in 2000s. On the other hand, if we analyze the patterns of international trade for the same decades, we can see a relatively different story. In 1980-81 the share of primary and manufactured products was 44 and 45 percent respectively. The share of manufactured products was 78 percent of total exports in 2006-07, while the share of primary products decreased to 11 percent for the same period of time. Likewise, the import of capital goods also increased considerably. It was 28 percent of the total imports in 1980-81, which reached to 36 percent in 2006-07. It is really interesting to see that the aggregate economic performance was relatively slow, reflected by lower GDP growth rates, but for the same period the share of manufactured goods was increased considerably in Pakistani exports. These two contrasting scenarios provide a good justification to analyze the impact of trade liberalization on economic growth. This study is focused to explore the impact of trade liberalization on the economic performance of a country endowed with labor but deficient in capital (Paulino et al., 2004; Rigobon, 2005).

Historical Analysis of Trade Regimes in Pakistan

After the independence in 1947 from British Rule, Pakistan established protectionist trade regime by emphasizing import substitutions as a way to spur the growth of

industrialization. This protectionist trade policy continued for almost three decades, from the 1950s to 70s. Although the protectionist regime proved to be relatively effective in protecting fledging domestic industries, the lack of foreign competition permitted the Pakistani investors to invest in safe but less efficient industrial sectors such as, automobile manufacturing, electronics, and electrical appliances industries. Consequently, many industries in Pakistan became gradually inefficient and vulnerable to the import substitution regime. It became difficult for local products to compete imported products on the basis of price or quality. The ultimate outcome is that the industries continued to enjoy the government protection are now finding it difficult to survive and compete with foreign products even in local market (Rodriguez and Rodrik, 2001). Protection from foreign competition is not a new phenomenon in Pakistan. Since 1952, a multifarious system of trade policy was maintained in Pakistan and different tariff rates were adopted for different commodities. The major reason was not only to protect the newly established domestic industries but also to generate revenue. Many types of trade barriers like quota, import bans, high tariff rates, licensing requirements, and others were introduced to protect domestic industries. Unfortunately, owing to smuggling and corruption these objectives were not achieved. Until 1981, about 41 percent of industrial value added products were protected by the import bans and another 22 percent by various other forms of trade restrictions (Siddiqui and Kemal 2002).

Meanwhile, there has been considerable progress in trade liberalization in most developing countries, turning from import substitution strategy to export-oriented approach in the 1970s. Trade liberalization policy has actively contributed to enhance the economic performance of many developing economies. Hence, the Government of Pakistan also introduced few additional trade liberalization measures to encourage exports during that period. The devaluation of the Pakistani Rupee by 57% in 1972 and elimination of the export bonus scheme were few important measures to stimulate export. Additionally, the discontinuation of restrictive licensing scheme was another important policy step towards trade liberalization (Onafowora et al., 1998). In early 1980s, trade policy reforms were initiated in Pakistan with a view to create a competitive and efficient industry through easing the import of raw material, intermediate goods and capital equipment. In order to achieve the efficiency and competitiveness, the domestic market was liberalized and trade barriers were removed gradually. Instead of quantitative restrictions tariff is being used to protect domestic industries and tariff structure has also been rationalized. The customs duty itself was lowered substantially from 80 per cent in 1996 to 30 per cent in 2001 and to 25 per cent in 2002.The average applied tariff rate fell from 42.7 per cent in 1996-97 to 20.4 per cent in 2001-02. During 1983-84 to 1993-94, 724 items were removed from the negative list. Overall, the number of goods on the negative list was reduced from 142 to 16, 32 to 7 and 221 to 107, respectively. In 2002, only 57 items constituted the negative list of imports and 192 items remained on the restricted list due to health and safety concerns. Only an insignificant portion of total imports is subject to quantitative restrictions. All these changes resulted in a decline in protection rates.

Tariff structure was rationalized further in the 1988-91 by the Government of Pakistan (GOP) after reducing the quantitative restrictions by the reduction in tariff rates and their dispersion. Tariffs were reduced on 1134 items and increased on 462 items. The maximum tariff was reduced from 225 percent to 100 percent. In June 1995, the tariff was further reduced to 65 percent. During the same periods the number of tariff slabs was reduced to 10. Except for automobiles and alcoholic drinks, the maximum tariff rate was reduced to 25 percent and the number of tariff slabs has been reduced to four (Rodrick et al, 2004).

If we examine the structure of trade during the decades of eighties and nineties, we can see that the share of imported capital goods in total imports has increased from 28 percent in 1981 to 37 percent in 1985-86. However due to slow down in the industrial sector the import of capital good declined to 25 percent

by 2000-01 and in 2006-07 it was 36 percent. The share of raw materials for consumer goods also shows a declining trend over the entire period, in 180-81 it was 50 percent and declined to 40 percent in 1985-86, it was increased to 55 percent in 200-01 and then again declined to 47 percent in 2006-07. The share of imported inputs for capital good has remained less than 10 percent throughout the period. The share of imports of final consumer goods increased from 14 percent to 18 percent over the periods from 1980-86 and it was reduced to 10 percent in 2006-7
Over the time, significant changes can be observable in the structure of exports. The share of exports of primary goods in 2006-07 is even less than one third of the 1980-81 level. The share of exports of semi-manufactured goods has increased from 11 percent to 24 percent over the period of 1980-81 to 1990-91, but declined to 11 percent in 2006-07. However, the exports of manufactured goods show a consistently increasing trend. Its share increases from 45 percent to 72 percent over the 20 years period and it further increased to 78 percent in 2006-07 (Table 1)

Table 1: Share of Exports by Economic Classification (Percentages).

Years	Primary	Semi-Manufactured	Manufactured	Total
1980-81	44	11	45	100
1985-86	35	16	49	100
1990-91	19	24	57	100
1995-96	16	22	62	100
1999-00	12	18	70	100
2001-01	13	15	72	100
2005-06	11	11	78	100
2006-07	11	11	78	100

Source: Economic Survey of Pakistan (various issues)

On the basis of this discussion we can say that trade liberalization and natural resource endowments are not the major factors behind the economic growth. Institutional setup is also an important stimulator for the economic performance of any country. It will be an interesting study to explore the impact of trade liberalization on economic growth in case of Pakistan. The growth rates of post liberalization decades and export compositions are portraying two opposite scenarios. It will be exiting to explore the impact of trade liberalization on economic growth of Pakistan (World Development Report, 1989).

Estimation and Analysis

The endogenous growth theory provides a good theoretical framework for understanding the relationship between trade policies and economic growth. In order to explore the relationship between economic growth and trade liberalization, I am intended to use human capital model of endogenous growth model with little augmentation through incorporating two additional variables of trade liberalization and foreign direct investment. The present study examines validity of Lucas (1988) model in the context of Pakistan. Since, the functional form of our model is nonlinear in its nature; consequently, we will use the functional relation after taking the natural log on both sides. Hence our final model will be:

Where:
Y =Gross Domestic Product (Measured in billions of current US $).
L= Labor Force (Measured in millions)
K = Gross Capital Formation. (Measured in millions of current US $).
FDI = Foreign Direct Investment (Measured in thousands of current US $)
OT= (Import + Export/ GDP) (Economics openness or Trade intensity)
ln= natural log
e_t is the random error term.

We can estimate the quantitative linkage relationship between among different variables related to economic performance by estimating equation (1). The additional benefit of using natural log is that our estimated coefficient will provide us the information regarding the elasticity of independent variables and the GDP. Since, we need to satisfy different criterions while establishing a quantitative linkage among variables, all the procedures are explained in forthcoming lines.

Data sources

All the data on above mentioned variables was taken from World Development Indicators (World Bank) and Economic Survey of Pakistan.

Estimation and Empirical Results

Prior to estimating the Model, it is important to discuss the expected signs of coefficients of explanatory variables, the expected signs of coefficients are:

The expected sign for the slope coefficient of dependent variable i.e. ln Y and L(labor), expressed as ""in the Model is positive, because GDP will increase due to increase in labor force. . So our null and alternative hypothesis will be:

H_0: 0 and H_1: > 0 (One tailed test).

We are expecting the positive sign for ""which is the slope coefficient for dependent variable i.e. ln Y and K (Capital), any positive change in the capital stock of nation will effect GDP positively. In this case we will tests following hypothesis :

H_0: 0 and H_1: > 0 (One tailed test).

The expected sign for "" is positive, the empirically many researchers have reported that the trade liberalization (OT) have positive relationship with the overall level of economic activities (GDP growth). So our hypothesis will be:

H_0: 0 and H_1: > 0 (One tailed test).

The expected sign for is positive as a positive change in foreign direct investment (FDI) will have positive influence on ln Y (GDP growth). We will evaluate following null and alternate hypothesis:

H_0: 0 and H_1: > 0 (One tailed test).

By using the estimation software (MegaStat-2007) I have estimated the MLR model represented by equation (1). The estimated model is as follows.

Regression Analysis

R^2	0.775		
Adjusted R^2	0.772	n	32
R	0.788	k	4
Std. Error	0.101	Dep. Var.	**Ln GDP**

ANOVA table

Source	*SS*	*df*	*MS*	*F*	*p-value*
Regression	10.8968	4	2.7242	267.39	2.72E-21
Residual	0.2751	27	0.0102		
Total	11.1719	31			

Regression output

					confidence interval	
variables	*coefficients*	*std. error*	*t (df=27)*	*p-value*	*95% lower*	*95% upper*
Intercept	3.2518	0.3171	10.255	8.25E-11	2.6012	3.9025
L	0.0419	0.0078	5.389	1.07E-05	0.0259	0.0578
K	0.00006573	0.00001960	3.354	.0024	0.00002552	0.00010594
OT	2,822.2644	699.2994	4.036	.0004	1,387.4205	4,257.1083
FDI	-0.00027655	0.00006640	-4.165	.0003	-0.00041279	-0.00014030

Our estimated equation is:

(10.25) (5.389) (3.354) (4.036) (-4.165)

The results indicate that all the estimated signs, except for FDI, are consistent with the expected signs. The relatively smaller sign of coefficients is due to the use of macroeconomic data. One justification of the negative sign of the slope coefficient of FDI could be: that for last few years the FDI in Pakistan is directed towards privatization of state owned enterprises, so FDI is not contributing effectively in the growth of GDP. The t-values mentioned in the parentheses, which are indicates that all the coefficients are statistically significant at 95 % level of significance. The overall significance of the regression can be judged through the F-value which is 267.39 ($P<0.05$). The value of coefficient of determination R^2, the criteria to evaluate overall goodness to fit, is 0.775 or 77.5 %, indicating that all these variables jointly explains 77.5 % of the variation in GDP for Pakistan.

Appropriateness of OLS Method to Estimate the Model. In order to explore MLR 3 we have estimated the correlation coefficients between variables and error term, as:

Correlation Matrix

	L	*K*	*OT*	*FDI*	*OT*	*Residual*
L	1.000					
K	.916	1.000				
OT	.080	.257	1.000			
FDI	.793	.958	.275	1.000		
OT	.080	.257	1.000	.275	1.000	
Residual	.000	.000	.000	.000	.000	1.000

32sample size

± .349 critical value .05 (two-tail)
± .449 critical value .01 (two-tail)

All the correlation coefficients of independent variables with error term are zero. So, we can think that this model satisfies MLR 3(zero conditional mean). Furthermore, there is problem of multicollinearity, indicated by relatively higher values of correlation coefficients among the variables. The major reason behind this high level of multicollinearity is that we have used the time-series data in our analysis and time trend is the source of high multicollinearity as well as for higher value of R^2. Therefore this problem is not serious enough, we can use this model.

CONCLUSION

Though, both positive and negative effects are involved in the channels of transmission. However, on the basis of statistical trends we can say that trade liberalization has positively contributed to the economic growth. Trade liberalization has had a poverty-reducing effect through enhanced growth, productivity and investment and through price stability. However, it also has entailed some costs, in particular costs related to changes in the employment of factors of production, from labor to capital, which have been poverty-increasing impact on labor abundance country. In this regard, trade liberalization has contributed to the accentuation of income inequality in the country. This may be attributed to the poor performance of mediating factors in Pakistan. With respect to income inequality, the evidence suggests that although trade liberalization by itself leads to a slight reduction in inequality, a rise in FDI appears to increase it

It is vital to have consistent policy environment in order to take full benefit of this channel. Further more liberalization of trade can improve growth and reduce poverty in Pakistan under the right conditions. Merely, the liberalization of trade will not be helpful for poverty alleviation. As the government's intervention, in the form of industrial polices, are causing rural-urban bias. The massive disguised unemployment in agricultural sector could be effectively utilized if the investment is not channelized through policy interventions by the government. Some other measures associated with uplifting the productivity with the potential to increase the income of the poor in rural areas are also essential. For sustainability of exports, further advancement in improving institutions, attracting export-oriented FDI and developing new export markets is needed as well as making a better case for improving market access in existing markers.

REFERENCES

- Frankel, Jaffrey A and David Romer. (1999). Does Trade Causes Growth? *The American Economic Review.* 89(3): 379-399.

- Hinkle, Lawerence E and Peter JM. (1999). Exchange Rate Misalignment: concepts and Measurements for Developing Countries. *A World Bank Research Publication, New York, Oxford University Press.*

- Narayan, Parkash K and Russell S. (2004). Temporal Causality and Dynamics of Exports, Human Capital and Real Income in China. *International Journal of Applied Economics.* 1 (1):24-45.

- Onafowora, Olubenga A and Oluwole O. (1998). Can Trade Liberalization Stimulate Economic growth in Africa? *World Development.* 26(3): 497-506.

- Paulino, Amelia S and Thirwall AP. (2004). The Impact of Trade Liberalization on Exports, Imports, and Balance of Payments of Developing countries. *The Economic Journal.* 114(493): 50-72.

- Rigobon, Roberto and Dani R. (2005). Rule of Law, Democracy, Openness and Income. *Economics of Transition.* 13(3):533-564.

- Rodriguez and Dani R. (2001). Trade Policy and Economic growth: A skeptic's Guide to Cross National Literature. *Cambridge M.A. NBER.*

- Rodrik, Dani, Arvind S and Francesco T. (2004). Institutions Rule: The Primacy of Institutions over Geography and Integration of Economic Development. *Journal of Economic Growth.* 9(2):131-165.

Ÿ Siddiqui, Rizwana and Kemal AR. (2002). Remittances, Trade Liberalization, and poverty in Pakistan: the role of excluded variables in Poverty change analysis. *MPRA Paper (4228).*

- World Development Report. (1989). Financial System and Development, World Development Indicators. *The World Bank Research Publications, New York, Oxford University Press.*

Introducing Lane Based Sectoring for Routing in VANETs

Faisal Khan[1], Yusun Chang[1], SungJin Park[1], Ehsanullah Kakar[2], John Copeland[1]
[1]School of Electrical and Computer Engineering, Georgia Institute of Technology, Atlanta, USA
[2]Department of Civil Engineering Balochistan University of Information Technology Engineering & Management Sciences, Quetta.

Abstract

Vehicular Ad hoc Networks (VANET s) provide vehicle-to-vehicle and vehicle-to-infrastructure communication using Dedicated Short-Range Communications (DSRC). The core objective of VANET s is to provide safety message communication among vehicles. In dense urban traffic, safety message com- munication encounters severe packet collisions due to excessive number of nodes contending to access the control channel. In such a complex dense and mobile scenario, an ideal single vehicle per time slot has yet not been achieved. This paper introduces the use of lane level location information to achieve a single vehicle per time slot configuration. The transmission range of a message originator is divided into a grid using distance and lanes as the two variables. Each block within the grid houses a single vehicle at most that is assigned a unique time slot. The contention among nodes for the same time slot is virtually removed. Theory and ns-3 simulation justify the feasibility, and prove that the technique reduces packet collisions by 2%, and improves message dissemination speed by as much as 30% each hop.

Keywords:- VANETs, Road-width, Lanes, Sectoring

*Corresponding Author's email: ehsan@buitms.edu.pk

INTRODUCTION

With the exponential increase of vehicles on the road, driving has become increasingly difficult and risky. In order to ensure passenger safety in challenging road scenarios, car manufacturers together with government agencies are in pursuit of a solution called Vehicular Ad hoc Networks (VANETs). VANETs would allow drivers to anticipate hazardous traffic events and approaching bad traffic conditions through inter-vehicle communication. One of the critical de- sign issues in VANETs is the dissemination of safety messages beyond the immediate transmission range of a vehicle. The propagation requires multi-hop forwarding of the message by selected vehicles among a large number of contenders. The problem becomes severe in dense urban traffic where higher number of contending vehicles results in excessive packet collisions. Since these collisions greatly impact reliability of reception and overall message dissemination speed, it remains the core concern while developing ideas for message routing in VANETs (Yan et al., 2010).

Considerable work has been carried to address the safety message propagation problem in VANETs. One common approach used to provide multi-hop forwarding is to divide the transmission range of message originating vehicle into multiple geographical sectors based on distance (Korkmaz et al., 2004, Fasolo et al., 2006, Khan et al., 2011) Vehicles in each sector pick a random backoff value from a contention window assigned to that sector. Contention windows are assigned in such a way that vehicles in the furthest sector can transmit first. Forwarding task is assigned to vehicle with minimum backoff. Since contention within a sector is random, it is highly probable in dense traffic environments that two vehicles within the same sector pick the same backoff value, thus causing collision. Further narrowing the sector length may minimize the effect to a certain degree. However, even with minimum possible sector length—equal to the length of a

car and necessary safety following distance many potential time slot colliders are still present in adjacent lanes. Considering the effect of lanes in VANETs forms the core of this work.

This paper aims to uncover the role of lanes in VANET communication. With road widths fastly nearing 100 meters (more than ten lanes each direction) (Turnbull 2003), it has become indispensable to consider the effect of road width or more specifically lanes while designing message propagation al- gorithms for VANETs. This work primarily considers dense urban traffic environment where traffic in each lane behaves like train trails with constant speeds. The proposed technique is suggested to be incorporated with methods for regular traffic using the currently probed vehicle density learning mechanism. To the best of our knowledge, this is the first work that considers the worst case rush hour traffic, whereas the previous works deal normal urban traffic as the extreme case. The use of the prevailing Differential Geographic Positioning System (DGPS) is assumed to determine accurate vehicle location. The aforementioned transmission range of a message originator is finely dissected both length and width-wise using distance and lanes respectively, forming a grid like structure with each block containing a single vehicle at most. Unique backoff values are assigned to each block ensuring only one vehicle in the furthest range forwards the message. Long contention window as a result of fine dissection may suggest high transmission delay, however, in dense traffic there is always a forwarding vehicle present in the furthest range that transmits with minimal backoff (i.e. transmission in the beginning of the window), making the length of the window ineffectual on delay. Additionally, since the overhead delay of message retransmission due to forwarding collisions is reduced, the over all end to end message propagation time is remarkably minimized.

The proposed idea is studied using thorough simulations performed in network simulator-3 (ns-3) Considerable reduction in rebroadcast collisions is achieved by using the grid based technique and the total collision occurrence is contained to below 3% in the worst case, while the message forwarding delay for each hop is improved by 9 ms over the existing sectoring technique. The important contributions of this work are: reducing packet collisions due to visible (non-hidden) nodes to near zero by using the grid based unique backoff value assignment, improved propagation delay through instant and collision-free forwarding of the furthest node, greater coverage by ensuring the furthest node as the next forwarder, and bringing to light the hitherto disregarded factor of road width to the attention of VANET research community. The remaining of this paper is organized as follows. Section II gives a brief idea of the significance of road width in VANETs in related literature. Section III details the proposed technique with theoretical analysis. Section IV presents the ns-3 simulation environment, results and their discussion. Conclusion with a discussion on future work is given in Section V.

Road Width in Vehicular Communication

Road topology is one of the critical foundation elements considered while designing communication mechanisms for VANETs. Some of the important topology factors considered in hitherto VANET literature include vehicle density, vehicle speed, headway distance, road side clutter (for path loss cal- culation), while the road geometry is assumed either entirely linear or with the inclusion of intersections (Fesolo et al., 2006, Li et al., 2009, Blaszczyszyn et al., 2009, Korkmaz et al., 2004, Xu et al., 2004) consider road width, however, their consideration is limited to its effect on vehicle density i.e. geographical separation of lanes is not considered and instead parallel vehicles in different lanes are assumed to be at the same location. Road width is also neglected in VANET mobility pattern generator tools (Krajzewicz and Rossel, 2011, Haerri et al., 2006, Traffic & Network simulation, 2011), where multiple lanes only account for density while their geographical separation is still ignored. The exponential increase of vehicles on the road has resulted in the ever increasing road widths to maintain smooth flow of traffic. Consequently, the average width of busy roads in a metropolis has become above six lanes each direction (Bauer et al., 2004). I-10 East downtown Houston is a compelling example of the significance of road width where the road is as

wide as 13 lanes each direction (Turnbull, 2003). In such scenarios vehicles in parallel lanes will exacerbate channel contention, and in addition, may effect physical path for radio propagation on the road. This work, however, thoroughly takes into account road width and attempts to exploit vehicles' lane level location information to avoid channel contention problem in multi-hop routing. The goal is to achieve zero collision (due to visible nodes) in rush hour traffic in dense urban scenario.

Broadcasting Using Lane Based Sectoring

In the following we present an extension to our Instant Broadcast algorithm proposed in (Khan et al., 2011) by introducing lane based sectoring. Here we assume rush hour dense traffic scenario, however, later in our simulations we show that the idea is also applicable in normal highway traffic where linear car spacing is 17 meters. Since our technique characteristically makes use of road lanes, we restrict our scenario to the usual urban road width of four or above lanes (Bauer et al., 2004).

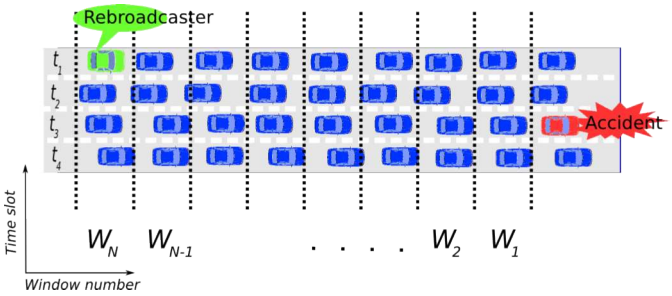

Figure 1. Backoff value assignment using Lane based Sectoring

Broadcasting Algorithm using Lane based Sectoring

The sender node (message originator) gains access to the medium by following the 802.11 CSMA/CA policy and broadcasts the entire safety message (with average VANET safety message size of 300 bytes (Khan et al., 2011)). The safety message is piggy backed with DGPS position of the sender, direction of broadcast and sectoring information for receiving nodes. Sectoring information, in turn, includes sectoring mode (i.e. linear or grid sectoring mode), and road width (at the sending instant). Sectoring mode is decided by considering current road density, which is learned through periodic beacon messages from surrounding vehicles or through keeping track of packet collision history where more collisions determine higher den- sity and vice versa. Withal sender's road width is considered to cater scenarios where different road widths exist within the multi-hop broadcast range e.g. road widening or narrowing within the multi-hop distance. The piggy backed information adds a minimal overhead of about 11 bytes. Similar size overheads are used in most broadcasting methods including UMB and SB protocols in (Korkmaz et al., 2004, Fasolo et al., 2006), The location information comprises 4 bytes each for longitude and latitude of the sender (acquired from the on- board DGPS device), direction of broadcast is 2 bits, while sectoring information comprises 2 bits for sectoring mode, 1 byte for road width (in number of lanes), and 1 byte for sector length (in meters).
Receiving nodes will enter a contention phase to rebroadcast the safety message and node with the smallest backoff value among the contenders will rebroadcast the safety message to the next hop. Since the receiving node furthest from the sender can provide longest relay, nodes in the furthest sector will have the least backoff values. In grid sectoring, in addition to lengthwise sectoring of the road based on the distance from the sending node, each sector is further subdivided width-wise into cells. Each sector is assigned a contention window with equal number of time slots:

$$W_n = \{t_1, t_2, t_3, ..., t_l\} + (N - n), \quad n = 1, 2, 3, ..., N \quad (1)$$

where W_n denotes contention window for sector n. The number of time slots l is equal for all sectors and its value is equal to the number of road lanes. Each window is offset by $N - n$, where N is the total number of sectors, thus ensuring that a node in further sector always rebroadcasts before a node in the nearer sectors.

Fig. 1 shows the sectoring mechanism and back off value assignment in lane based broadcast method. Transmission range of the safety message sender is divided into equal size sectors with increasing distance

from the sender along the road in the message forwarding direction. Each sector is assigned a fixed length contention window W_n as described in equation (1) . Within each sector, the road section is further subdivided width-wise into cells with cell width equal to that of one lane. Each cell is then assigned a fixed time slot from the corresponding contention window. Length of a cell (along the horizontal axis in Figure 1) is significant in the proposed mechanism. One cell in our scenario strictly spaces one vehicle in order to completely avoid collision. Therefore, we cautiously assume sector length (or cell length) as 13 meters, although (Bauer et al ., 2004) reports that the average vehicle spacing in a city freeway is about 16.8 meters (equal to four car lengths; average car length being 4 meters). Node within each cell backs off for its assigned amount of time. Consequently, in our scenario the node in N^{th} sector (furthest) sector with time slot t_1 will rebroadcast first. All the remaining nodes with higher back off values would overhear the rebroadcast and would subsequently quit their rebroadcast step. The rebroadcast from the relay node is also overheard by the original sender, this will confirm successful reception of the safety message. In case the rebroadcast message is not heard by the original sender within the specified time (timeout), the broadcast is repeated by the original sender. Note that the movement of vehicle (50 miles per hour on average) relative to message propagation speed (25 meters per millisecond on average according to simulations in section IV) is negligible to influence the message overhearing mechanism. The same mechanism is repeated in the remaining hops until the message propagates across the intended distance.

Delay Analysis

Since this work focuses on the rebroadcasting stage in VANET multi-hop safety message propagation, we confine our delay analysis to the rebroadcasting step in the message prop- agation scenario. The rebroadcast delay in a normal sectoring mechanism is formulated first, followed by the rebroadcast delay in lane based sectoring. We assume the traffic distribution is uniform and that there are fixed number of contending nodes (CN) for each sender. We follow Bianchi's Markov chain model (Bianchi, 2000) to formulate one hop delay for our broadcasting mechanism. Let t_r be the transmission time of the packet given by

$$t_r = \frac{h_{PHY} + h_{MAC} + Payload}{R_b} + \delta \qquad (2)$$

where $hPHY$ and $hMAC$ are the PHY and MAC headers (MAC header also includes our protocol overhead). Rb is the data rate and δ is the propagation time. We assume the same data rate for payload, PHY and MAC header transmission. Let τc be the transmission probability of a contending node. The probability of unsuccessful transmission becomes

$Pr = 1 - (1 - \tau c)^{CN}$ (3)

From (Bianchi, 2000), the probability that a node starts its transmission in a given time slot is given by

$$\tau = \frac{2(1-2P')}{(1-2P')(N+1) + P'N(1-(2P')^l)} \qquad (4)$$

where N and l are number of sectors and number of slots from (1). τc can be analytically computed from (Bianchi, 2000) and equation (4).

The probability that a transmission occurs among contender nodes in a given time slot is

$$P_{tr} = 1 - (1-\tau_c)^{CN+1} \qquad (5)$$

Probability that a packet is successfully transmitted given Ptr is

$$P_s = \frac{(CN+1)\tau_c(1-\tau_c)^{CN}}{P_{tr}} \qquad (6)$$

From (Blaszczyszyn et al., 2009) and the above equations, we can write the average delay for message rebroadcast $E[D]$ as

$E[D] = E[x]E[t]$ (7)

Where

$$E[x] = \frac{(1-2P')(N+1) + P'N(1-(2P')^l)}{2(1-2P')(1-P')} \qquad (8)$$

$$E[t] = (1-P_{tr})\sigma + P_{tr}P_sT_s + P_{tr}(1-P_s)T_c \qquad (9)$$

$E[x]$ is the average number of time slots for a successful transmission and $E[t]$ is the average length of a time slot; σ is the duration of empty slot, T_S and T_C is the average time the medium is sensed busy because of a successful transmission or a collision respectively.

$$T_S = DIFS + t_r + \delta + ACK \quad (10)$$

$$T_c = DIFS + t_r + timeout + \delta \quad (11)$$

In case of lane based sectoring method, the rebroadcast delay E [D] is strictly dependent on the density of nodes. Rush hour traffic has the lowest rebroadcast delay as the smaller back off value cells, like all other cells, are likely to be occupied, thus causing rebroadcast in the first few time slots of the contention window. Therefore, in rush hour traffic for lane based sectoring method, as Ptr becomes equal to c , and CN approaches zero, the probability of successful transmission Ps approaches nearly 1.

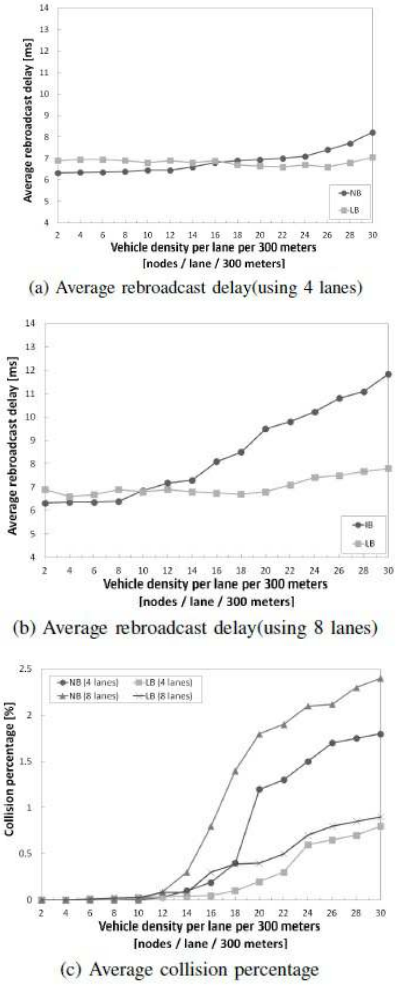

(a) Average rebroadcast delay(using 4 lanes)

(b) Average rebroadcast delay(using 8 lanes)

(c) Average collision percentage

Figure 2. Rebroadcast delay in 4 and 8 lanes, average collision percentage; (message size 300 bytes).

Simulation Analysis

Simulation setup

To analyze the comparison of normal sectoring broadcast and lane based sectoring broadcast, the general broadcast procedure followed by UMB, SB and IB in (Korkmaz et al., 2004, Fasolo et al., 2006, Khan et al., 2011) was fully implemented using both normal sectoring as well as lane based sectoring in ns-3 simulator, version 3.9. The traffic mobility is generated using the tool VanetMobiSim (Haeri et al., 2006).

Simulation parameters are summarized in Table 1. We have used 1 km road length scenario with unidirectional road having four and eight lanes. Fifteen different vehicle densities are tested with density ranging from 2 to 30 nodes per lane per 300 meters length of the road (i.e. one hop distance), and having Gaussian randomly assigned speeds with mean 50 miles/h and standard deviation 3 miles/h. The minimum headway between vehicles is kept as 10 meters to account for worst case scenarios. Jakes model has been used to estimate Rayleigh fading for the channel (Blaszczyszyn et al., 2009). To best study the performance of the proposed technique, the scenario is tested for different message generation rates of 0.01 to 1 message per vehicle per second.

Description	Value
Transmission range	300 meters
Data rate	3 Mbps
Message payload size	300 and 1000 Bytes
Protocol overhead	11 bytes
MAC header size	34 bytes
PHY header size	26 bytes
Base protocol	802.11p
Time slot, DIFS, SIFS	20, 50,10 μSec
Road length	1 km
Vehicle density	2-30 vehicles/lane/300 meters
Vehicle speed	50 miles/h (mean)
Vehicle spacing	10 meters
Message generation rate	0.01-1 message per vehicle/second
Path loss model	Two Ray model
Fading model	Rayleigh fading model

RESULTS AND DISCUSSION

Fig. 2(a) and 2(b) show average rebroadcast delay in 4 and 8 lane road configuration with variable vehicle densities. NB in the figure denotes

Normal sectoring Broadcast while LB denotes Lane sectoring based Broadcast. We use the average message size of 300 bytes to measure the performance here. In fig. 2(a) the behavior of both the methods remains unaffected in low density scenarios until the vehicle density of 16 nodes per lane per 300 meters. Among the two methods, LB however, slightly falls short in performance in low density range due to the usage of longer back off window than required. Note that the window size for LB has been kept as 120 slots as discussed in the algorithm, albeit it was also mentioned that a density learning technique can alleviate such additional time slot overhead. For the case of NB however, the window size has been varied depending on the density of vehicles. Therefore, NB maintains its advantage in low density scenarios. In fig. 2(a) as the vehicle density increases above 16 nodes per lane per 300 meters, the additional window size of LB pays off and there is a delay gain of about of 2 ms per rebroadcast as the density reaches 30. This effect clearly demonstrates the LB basic principle that as the vehicle density reaches rush hour traffic (i.e. as nearly every cell of the grid is being occupied with vehicles), there is high likelihood that least back off value slots are assigned to vehicles and rebroadcast takes place early in the back off window.

In Fig. 2(b) the delay gain of LB over NB becomes clearly compelling. Using 8 lanes road scenario the NB method sectors the transmission range with narrower sector length, however, the presence of nodes in the parallel lanes is disre- garded. Therefore, although the high density of nodes in each sector is considered, the likelihood of back off value collision among nodes grows astonishingly higher, thus resulting in resending attempts from the original sender and causing high delay. LB, on the other hand, is effected minimally with higher density and a near one time slot per node configuration is achieved and the delay gain reaches as high as 5 ms per rebroadcast over the normal broadcast method.

Fig. 2(c) depicts average collision percentage with variable vehicle densities in 4 and 8 lane cases. The figure explicitly depicts the collision improvement perspective of LB over NB method. Here collision percentage is the measure of the number of retransmission attempts by the sender. It can be discerned from the figure that the performance of normal sectoring method NB is severely degraded in high density road traffic. In rush hour traffic where vehicle density increases above 16, the collision rate steeply rises to as high as 2.4% in 8 lane scenario.

Higher collision directly incurs high retransmission rate, thus effecting overall end to end delay as well as message dissemination reliability. LB, in contrast, even in the worst case of 8 lane with 30 nodes per lane maintains collision percentage below 1, thus promising high reliability as required for safety communication in VANETs.

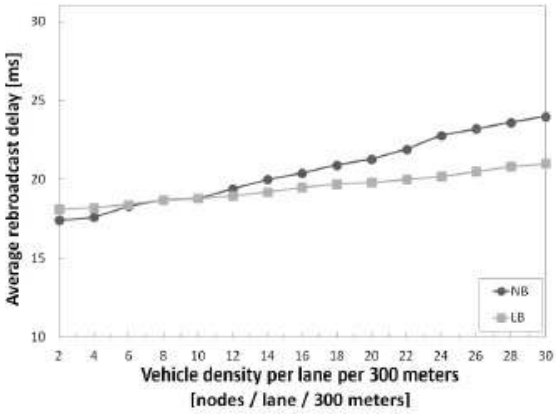

(a) Average rebroadcast delay(using 4 lanes)

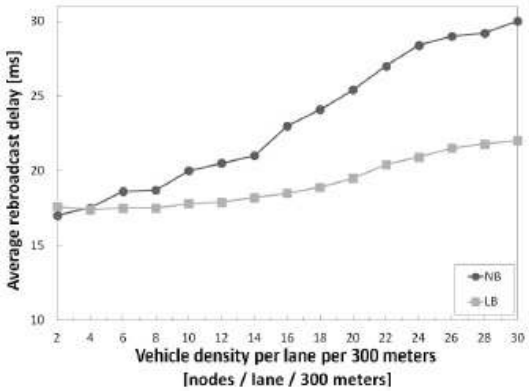

(b) Average rebroadcast delay(using 8 lanes)

Fig. 3 shows performance measure with message size of 1000 bytes. The general behavior of the two methods follow the same trend as in fig. 2 where the message size is 300 bytes. There are, however, two noticeable distinctions with higher message size. First, contention is slightly more sensitive to node density with higher message size; Second, the

overall collision rate is higher for the two methods in both 4 and 8 lane scenarios. The reason being the higher message size means longer medium occupancy by each sender, causing accumulated contenders, thus more collisions and its resultant longer overall delay. Importantly, the gain of LB over NB method remains significant even with higher message size both in terms of delay (by 9 ms in worst case) and collision rate (by 2% in worst case).

CONCLUSION

In this paper, we have presented a new technique for sector- ing the broadcast range for safety message routing in VANETs. Rush hour traffic scenario is considered where most of the hitherto mechanisms are severely effected with collisions and consequent high message propagation delays. The hitherto neglected factor of road width is introduced to be used as a second dimension for sectoring the transmission range of the message sender. Collision gain of the proposed technique is evaluated using Marchov chains. Extensive simulation evaluation is performed using ns-3 simulator, and the results suggest that Lane based sectoring significantly improves the message propagation delay by as much as 9 ms for rebroadcast in each hop while at the same time improves reliability of message propagation by reducing rebroadcast collisions by 2% over the existing sectoring technique even in worst traffic scenario. Uncovering the importance of road width for VANETs in this paper will assist future researchers in understanding a more detailed road topology that influences VANET com- munication. The idea of segmenting transmission range into manageable units can also be replicated in service channel allocation strategy in VANETs where there is an equally critical concern about effective channel utilization. Theoretical delay analysis for rebroadcast stage developed in this paper can be extended for delay calculation of other broadcast methods in VANETs. Future work can be directed towards investigation of sectoring in road intersection scenarios, and further study of the vehicle density and topology learning mechanism on the road.

REFERENCES

Ÿ Bauer M, Harwood D and Richard K. (2004). Safety effects of using narrow lanes and shoulder-use lanes to increase the capacity of urban freeways in *Transportation Research Board's Transportation Research Record: Journal of the Transportation Research Board No. 1897.*

Ÿ Bianchi G (2000). Performance analysis of the IEEE 802.11 distributed coordination function, IEEE JSAC, vol.18, no.3, pp.535-547.

Ÿ Blaszczyszyn B, Muhlethaler P and Toor Y (2009). Performance of MAC protocols in linear VANETs under different attenuation and fading conditions, in Proc. of 12th International IEEE Conference on Intelligent transportation Systems, pp.1-6, 4-7.

Ÿ Fasolo E, Zanella A and Zorzi M (2006) An Effective Broadcast Scheme for Alert Message Propagation in Vehicular Ad hoc Networks," in Proc. of ICC '06, vol.9, pp.3960-3965.

Ÿ Haerri, Fiore, Fethi and Bonnet. (2006). VanetMobiSim: generating realistic mobility patterns for VANETs. http://vanet.eurecom.fr/.

Ÿ Khan F, Chang Y, Park S and Copeland J. (2011). Handshaking vs. instant broadcast in vanet safety message routing, in *Proceedings of IEEE PIMRC'11*, pp. 709–714.

Ÿ Korkmaz G, Ekici E, Ozguner F and Ozguner U (2004). "Urban multi-hop broadcast protocol for inter-vehicle communication systems, in Proc. of the first ACM workshop on VANETs.

Ÿ Krajzewicz D and Rossel C. (2007). Simulation of Urban MObility (SUMO). http://sumo.sourceforge.net/index.shtml.

Ÿ Qing Xu, Mak T, Jeff Ko and Sengupta R (2004). Vehicle-to-vehicle safety

messaging in DSRC, in Proc. of the 1st ACM international workshop on Vehicular ad hoc networks, pp. 19-28.

- The ns-3 network simulator (ns-3.9). http://www.nsnam.org/, 2011.
- The ns-3 network simulator http://www.nsnam.org/
- Traffic and Network Simulation Environment (TraNS) http://lca.epfl.ch/projects/trans
- Turnbull KF. (2003). Houston managed lanes case study: The evolution of the houston hov system, *US Department of Transportation, Federal Highway Administration.*
- Yan G, Yang W, Weigle M, Olariu S and Rawat D. (2005) "Cooperative Collision Warning through mobility and probability prediction," in Proc. of Intelligent Vehicles Symposium (IVS), pp.1172-1177.

Flow Dynamics of Two Phase (air and water) Stratified Flow by a Simulation Package COMSOL MULTIPHYSICS

Muhammad Hashim[1*], Ali Nawaz Mengal[2]

[1]Department of Petroleum and Gas Engineering, [2]Department of Mining Engineering, Balochistan University of Information Technology, Engineering and Management Sciences, Quetta

Abstract

In this paper simulation of the two phase stratified flow is carried out by a Commercial Simulation Package Comsol Multiphysics version 3.4 using level set approach for tracking the movements of the interface. The problem involves the Simulation (based on Transient analysis) of two phase stratified flow between two planes in (2D) two Dimension. Some boundary problems arose in defining specific geometry, that is why a little different geometry approach is presented to overcome this problem. Further, gravity that usually stabilizes the flow by providing specific flow pattern (specially separation of the fluids in gravity field having different densities) when flow is occurring in gravity field was observed that gravity constant destabilize the flow (carrying simulation in Comsol Multiphysics) and convergence problem arises. That is why the flow has checked by keeping the value of gravity zero at first then, giving a much less value than the gravity really has, and increased gradually to a value beyond which again the flow did not converge. The effects of Surface tension Coefficient on the flow, are also observed and presented.

Key words: Stratified flow, Level Set Approach, Interface, Gravity, Surface tension

[*]*Corresponding Authors email: m.hashim@buitms.edu.pk*

INTRODUCTION

Two phase (gas, liquid) stratified flow occurs in many engineering design problem, such as long distance transportation of oil and gas, oil platforms, process industry, may be in horizontal section of horizontal Oil/Gas wells, reactors etc. To simulate or to calculate the flow pattern, shear forces(Wongwises and kalinithenko, 2002) involved and different aspect of flow are of the utmost importance in designing of such wide range of engineering problems (Yap et al., 2005; Ghorai and Nigam, 2000).

Multiphase/ two phase flow phenomenon has been a challenging task through all times and to understand this sort of flow, a wide range of research have been carried out for past several years.

In petroleum industry specially in surface gathering systems, in horizontal section of horizontal wells and in oil/gas transportation industry, in many cases gas and oil flows simultaneously either it is wanted to transport both at the same time or if condensation occurs in pipes. To avoid problems in such cases, the behaviours like forces, flow pattern and instabilities etc involved in the flow has been studied widely. Different approaches have been investigated to understand the stratified flow phenomenon.

A variety of CFD based Commercial simulation packages are available in industry to simulate the problem and to apply further in modelling of such designs

(Wongwises and kalinithenko, 2002).

The Simulation package Comsol Multiphysics with its built-in levelset approach is used here to simulate the two phase (air-water) flow between two plane transiently. The results may be applied to different two fluid flow problems, especially Oil-Gas (Moguedet et al., 2005).

2d Models Prepared in Comsol Multyphysics

The simulation is carried out in a commercial CFD (Computational Fluid Dynamics) based simulation package Comsol Multiphysics version 3.4.
Since, two phase (air-water) stratified flow is understudy, there for the level set approach is used in particular, tracking the moving interface.

An Overview of the Level Set Approach

A large number of fluid flow problems involve moving interfaces, like air-water, breaking surface waves, combustion and reacting flows etc. The interplay between the interface dynamics and the surrounding fluid motions is of great consideration in such many applications. Factors such as density ratios and temperature jumps across the interface, surface tension effects, topological connectivity and boundary conditions play significant roles in the dynamics (Berthelsen and Ytrehus, 2005).

To tackle some of the most complex problems in fluid interface, a class of numerical techniques have been built over the past several years. Relying on an implicit representation of the interface whose equation of motion is numerically approximated using schemes built from those for hyperbolic conservation laws, Osher and Sethian Level Set methods which are the computational techniques for tracking moving interfaces. The resulting techniques are able to handle problems in which the speed of the evolving interface may sensitively depend on local properties such as curvature and normal direction, as well as complex physics of the front and internal jump and boundary conditions determined by the interface location. In particular, Level Set methods are designed for problems in multiple space dimension in which the topology of the evolving interface changes during the course of events and problems in which sharp corners ad cusps are present (Rune, 2007).

Governing Equations

To simulate numerically the model a level set approach is coupled to the classical Navier-Stokes equations. Actually this method is very well studied to describe the motion of interface.

$$\rho\frac{\partial u}{\partial t}+\rho u.\nabla u=\nabla.\left[-pId+\eta\left(\nabla u+(\nabla u)^{T}\right)\right]+\rho g+\sigma\kappa\delta n \quad 5.1$$

$$\nabla.u=0 \quad 5.2$$

$$\frac{\partial\Phi}{\partial t}+u.\nabla\Phi=\gamma\nabla.\left[\varepsilon\nabla\Phi-\Phi(1-\Phi)\frac{\nabla\Phi}{|\nabla\Phi|}\right] \quad 5.3$$

Where in equation 5.1,

ρ is the density
η is the dynamic viscosity
g is the gravity constant
σ is the surface tension coefficient
κ = - .n the curvature of the fluid interface
δ is the delta function concentrated at the interface between the fluids
u is the velocity field
p is the pressure

The term σκδn defines the surface tension forces.
In equation 5.2, Φ represents the level set function and in this approach Φ at a point is the distance from the interface, such that an interface corresponds to a surface where Φ = 0. γ and ε are the level set parameters where γ is the reinitialization parameter and ε is the parameter controlling the interface thickness.

Moving Air and Water Concurrently between Two Interface

Air and water both are flowing co currently between two planes from left to the right. The interface and exit positions of the two fluids are not the same. The configuration consists of two sections (subdomains) water and air. The air (upper) section is a bit ahead of the

water (lower) section. The pressure at the two points at outlets is defined zero (see Comsol Model Reports). this is done to establish an interface between two fluids. While at the exit, the water exits first. This is done to avoid the problem that arises in defining the boundary condition.
The total length of the model is 4.5 with a common interface of 3.5. The length of each section is 4. The total height of the sections is 0.8, and each section with the height of 0.4.

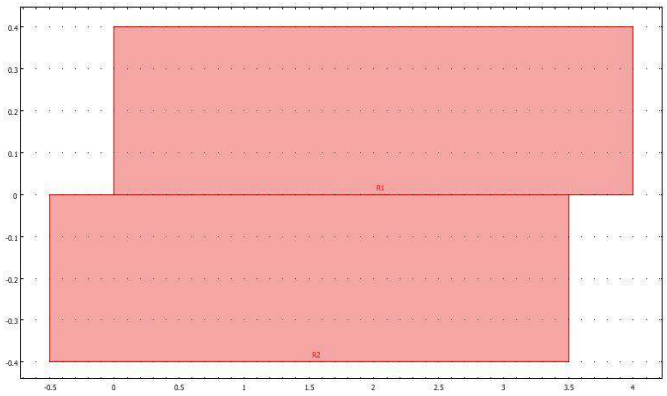

Figure.1. Basic geometry for the model of moving air and water co currently.

Subdomains
The model consists of two subdomains 1 and 2. Subdomain 1 is provided by water while subdomain 2 by air.

The following table describes the numerical values of functional parameters used in the simulation.

Parameter	Num. Value (air)	Num. Value (water)	Unit
Density: ρ	1	1000	kg/m^3
Dynamic viscosity: η	1e-5	1e-3	Pa.s
Gravity constant: gy (in y direction)	0 and -2		m/s^2
Surface tension coefficient: σ	0, 0.073		N/m
Mean inlet velocity	0.1	0.01	m/s
Parameter controlling interface thickness: ε	0.05		M
Reinitialization parameter: γ	0.2		m/s

The mesh statistics of the subdomains is given in the following table.

Number of degrees of freedom	16636
Number of mesh points	1321
Number of elements	2464
Triangular	2464
Quadrilateral	0
Number of boundary elements	228
Number of vertex elements	8
Minimum element quality	0.785
Element area ratio	0.218

Boundaries, boundary conditions and settings

Boundary	Boundary type	Boundary condition	Settings
1	Inlet	Velocity	$u= u_o$, $\varphi = \varphi_o$
2	Wall	No-slip	$u= 0$
3	Wall	No-slip	$u= 0$
4	Inlet	Velocity	$u= u_o$, $\varphi = \varphi_o$
5	Interior boundary	Initial fluid interface	
6	Wall	No-slip	$u= 0$
7	Outlet	Pressure	$p_o= 0$
8	Wall	No-slip	$u= 0$
9	Outlet	Pressure	$p_o= 0$

At boundary 1, the fraction of fluid 2(subdomain 2(air) is defined as fluid 2) is zero here. The velocity in x-direction is expressed as 6*V_mean*s*(1-s)+t. Multiplying V_mean by 6 and adding with t (time step) is done to increase (maintain) the velocity during the flow. At boundary 4, the fraction of fluid 2 is 1.

RESULTS AND DISCUSSION.

Result without effects of Gravity and Surface tension

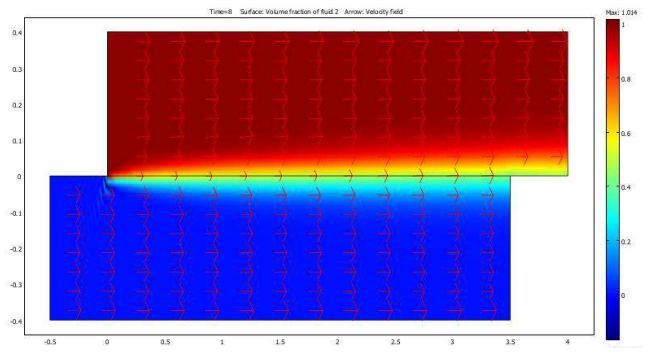

2. Result of simulation of moving air and water. The arrows are velocity field

The result showed above is obtained keeping the surface tension and gravity zero. Density plays an important role in fluid flow problems, flowing in gravity field. In our case giving to gravity a value of zero looks quite unrealistic. Also the water surface tension that differentiates between the water and air surface is kept zero to stabilize the flow at this stage.
Assigning a value of 9.81 m/s^2 to the gravity, the flow problem does not converge. Thus at this stage, it is tried here if no gravity acts on the flow.

Since the flow is transient, and is solved for the time of 8 seconds, the analysis of the flow pattern in different times show that initially when flowing air interacts with the flowing water, instability occurs and, a first water wave rises highly and approaches approximately the air wall contact which looks like forming a slug for a short interval of time. Then the first wave falls a little and a second water wave rises, but not so high as the first wave. At this stage the the interface rises quite high and much water flows out than air. No other wave rises, the second wave falls down slowly, and after some time a complete stratified smooth flow develops.

With each time step the velocity is defined to rise. With the rise in velocity of air and water both, the instability was considered to happen after some time but it is observed that flow stabilizes with a complete stratified smooth flow.

The pressure distribution (given in Appendix A) in two sections is almost uniform in the range of 1000 Pa approximately, except at the entrance of the water section, where the pressure is higher, in the range of 2000 Pa approximately.

The velocity distribution (given in Appendix A) shows that at the solid walls the velocity is zero. In air section, just below the wall the velocity of the air is quite high due to much lower pressure. Below this, the air velocity attains uniform value. But, just above the interface, it looks like water vapors rise in the air section and a pressure reduction in result. Due to this pressure reduction again velocity increases. At the Air-Water interface, the velocity decreases due to the shear forces acting at the interface. Below the interface the shear forces reduces and also the pressure due to the mixing air in water, and the velocity rises again. The velocity below this region is again decreased (less than the velocity in the air section). The velocity then gains a higher value just above the water-wall contact.

When surface tension was introduced, no difference was observed in flow patterns. The pressure and velocity distribution are also in the same pattern.

Result with a Small Gravity Value and Surface Tension Coeefficient

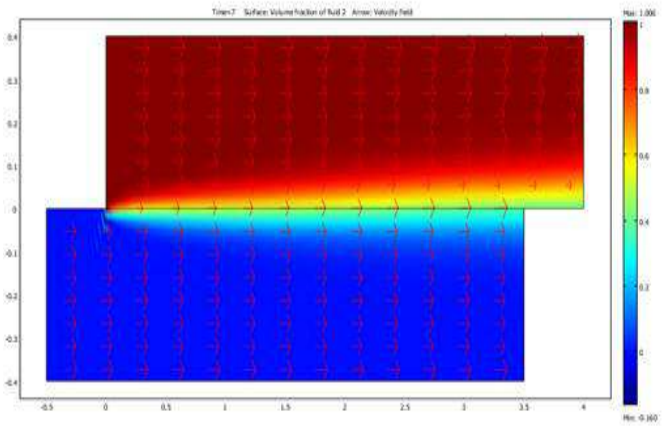

Figure 3. Air moving with an inlet mean velocity of 0.1 m/s^2 and water is flowing with an inlet mean velocity of 0.01 m/s^2. The arrows show the velocity field.

As the flow problem does not converge when introducing gravity, it is checked by introducing a little value of gravity that is 2 m/s^2 to observe the effect of gravity. This value obtained by starting from 1m/s^2 and the final convergence obtained at 2 m/s^2. The value of gravity more than this destabilizes the flow and the flow does not converge. But still we can check the effect of gravity if it has a small value though.

By introducing a little gravity keeping the value of surface tension coefficient as it is, it is observed that when the first water wave rises, at the same time water level falls down at the exit of the water section. When second water wave rises consecutive to the first one,

the water level at the exit of water rises again. As time passes the water level at the entrance falls down and water level at the exit rises up slowly. After some time again a stratified smooth flow develops but with an interface a little higher at the exit. This means that at the end of the interface the area of the flowing air reduces slightly. By introducing Gravity, the pressure distribution changes slightly (See appendix A). Pressure in the lower(water) section is a little higher than in the upper (air) section. The over all velocity of the model reduces by introducing gravity (See appendix A). At the solid walls, the velocities are zero. Just below the solid wall in air section, since a low pressure exists, the velocity gets a high value. Again at the interface, due to shear forces acting here, the velocity reduces. Checking the flow just with the gravity (2m/s2 here) and vanishing the effect of surface tension coefficient, it follows the pattern as just the surface tension was introduced.

Flowing Air over Water Which Is Initially at Rest but Provided an Outlet

The configuration consists of two sections; air (upper) and water (lower). In this configuration the air flows (left to right) over water which is at rest (no inlet for the water) but provided an outlet. The basic idea in modelling such configuration is to observe the drag applied by air to move the water.

The geometry is designed such that, initially the air flows as single phase to establish a stabilized flow, and then flows over water.

The length of the air section is 10 while the length of the water section is 8. The heights

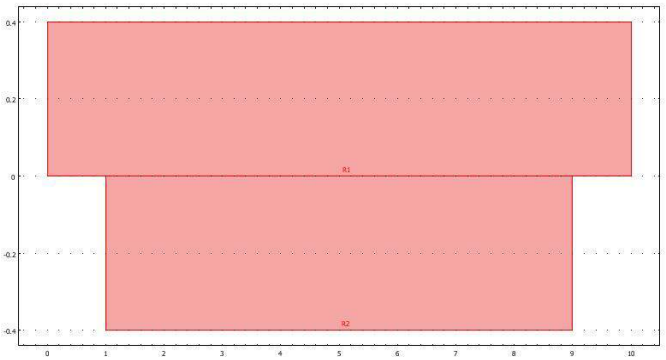

Figure 4. Basic geometry of the flow problem of flowing air over water which is initially at rest but provided an outlet. Mean inlet air velocity is 0.1m/s^2.

SUBDOMAINS

The configuration consists of two sub domains. Water is provided in subdomain 1 while air in 2. The following table describes the numerical values of functional parameters used in the simulation.

Parameter	Num. Value (air)	Num. Value (water)	Unit
Density: ρ	1	1000	kg/m^3
Dynamic viscosity: η	1e-5	1e-3	Pa.s
Gravity constant: gy (in y direction)	0 and -3		m/s^2
Surface tension coefficient: σ		0, 0.073	N/m
Mean inlet velocity	0.1	0.0	m/s
Parameter controlling interface thickness: ε	0.1		m
Reinitialization parameter: γ	0.1		m/s

The mesh statistics of the subdomains is given in the following table.

Number of degrees of freedom	14320
Number of mesh points	1141
Number of elements	2112
Triangular	2112
Quadrilateral	0
Number of boundary elements	228
Number of vertex elements	8
Minimum element quality	0.713
Element area ratio	0.438

Boundaries, Boundary Conditions and Settings

Boundary	Boundary type	Boundary condition	Settings
1	Inlet	Velocity	$u= u_0$, $\varphi = \varphi_0$
2	Wall	No-slip	$u= 0$
3	Wall	No-slip	$u= 0$
4	Inlet	Velocity	$u= u_0$, $\varphi = \varphi_0$
5	Interior boundary	Initial fluid interface	
6	Wall	No-slip	$u= 0$
7	Outlet	Pressure	$p_0= 0$
8	Wall	No-slip	$u= 0$
9	Outlet	Pressure	$p_0= 0$

The figure showing different boundaries is given in Appendix A.

Results without Surface Tension and Gravity

The figure below is the result of flow of air over water at rest but provided an outlet. Basically in this flow problem the water is shear driven, shear forces act at the interface of flowing air and still water.

With no gravity and surface tension coefficient, it is observed that when air flows over water, the water level falls at start of the water section. The fall in water section goes approximately to the water wall contact, forming slug, but the water level at the exit of the water section remains constant. It was expected since the cause of this pattern is the absence of gravity, as in the absence of gravity no external force acts on the flow and the water level does not falls at the exit. At the entrance when air just contacts the water surface, the fall of water is due to drag, as there is no inflow of water and, water flows to the exit by interfacial shear force.

The pressure distribution is quite different here (Appendix A). The pressure decreases with the flow from left to the right in three stages, in the beginning, in the middle and in the end of flow. All pressure reductions takes place suddenly. It means, no hydrostatic pressure acts here.

Initially in the water section, water is at rest with no inflow. When the flowing air with velocity interacts with water, the direction of the velocity changes to the down side due to the water displacement and creation of wave. Air moves the water with a little velocity. The air gets maximum velocity at the top of the wave due to pressure reduction by wave generation.

When, only Surface tension coefficient was introduced as in the first model, no effects were observed. It just behaves as it does without Surface tension coefficient.

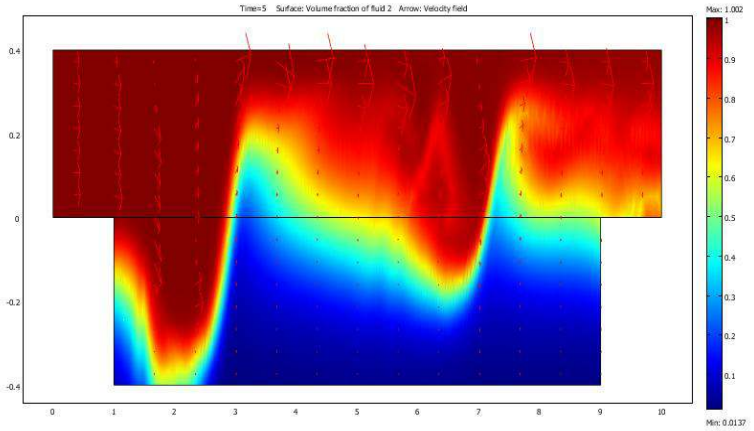

Figure 5. Result of the flow when Gravity and Surface tension are not considered.

Results with a Little Gravity and Surface Tension

Here again it was tried to check the effect of gravity(which must be taken into account) by introducing a little value of Gravity 2m/s2 and also by introducing Surface tension coefficient. Here the result is a bit satisfactory as the water level at the exit falls down mainly due to gravity and somewhat due to shear. As the water is shear driven, and is under effect of gravity, the water level falls abruptly at the exit and slowly at the start. If this goes on, the water will be drained out of the section. By introducing the gravity, the pressure distribution is quite natural here, higher at the bottom due to hydrostatic pressure of water and lower at the top wall (air-wall contact). (See appendix A) As the water falls down due to gravity, a decrease in pressure takes place above in the air zone and back flow of the air occurs. The result just by introducing a value of small gravity but keeping the surface tension zero, the flow pattern is as when both quantities were introduced.

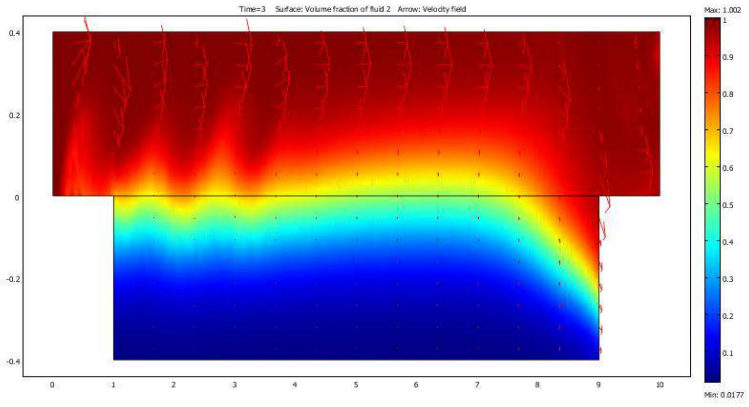

Figure 6. The result when Gravity and Surface tension are introduced.

CONCLUSION

Finally, the work shows the possibilities of Comsol Multiphysics to deal with two phase flow topics provided appropriate geometries, boundary conditions and parameters, since during the simulation, it is observed that Comsol Multiphysics is very sensitive to the above mentioned values and conditions. Minor changes to the boundary conditions, geometry and defined parameters cause the problem not to converge and thus no solution. The main conclusions we established on this work are, Without considering Gravity constant, the flow behaves in a different way, which does not show the natural way of fluid flow pattern. Thus Gravity plays vital role in establishing a natural and accepted flow pattern. Surface tension Coefficient, which is thought to have a role while stratified two phase (air-water) occurs, since its existence affects the surface of water in different way, but it is observed that it does not affect the flow. The level set method is a good approach when dealing with the moving interface, since the movement of fluid interface is a dynamic process and must be clearly observed to understand the flow.

The two fluids (air-water) used here may be displaced by Oil-Gas and different fluids having specific properties. The different flow problems which arise in the two phase flow industry/ Oil-Gas industry may be dealt in a good way.

Indeed, further works are needed to solve the two phase flow problem between two planes by Comsol. It looks quite possible to solve such problems by making further more and more good efforts. Further if the sensitivity issue of the Comsol Multiphysics is overcome, more possibilities will be attained to deal with such problems in a good time and wide range of parameters.

REFERENCES

Ÿ Wongwises S and Kalinithenko V. (2002). “Mean velocity distributions in a horizontal air-water flow”, *International Journal of Multiphase Flow.* 28:167-174.

Ÿ Yap YF, Chai JC, Toh KC, Wong TN, Lam YC. (2005). Numerical modelling of unidirectional stratified flow with and without phase change. *International journal of Heat and Mass Transfer*. 48:477-486.

Ÿ Ghorai S, Nigam KDP (2000). “CFD modelling of flow profiles and interfacial phenomena in two-phase flow in pipes” , Department of chemical Engineering, Indian Institute of Technology, Haus KHas, New Delhi 16 India.

Ÿ Rune W. Time “Two-Phase Flow in Pipelines (Course Compendium)”; Department of Petroleum Engineering, Faculty of Science and Technology, University of Stavanger, Norway, September 17th 2007.

Ÿ Berthelsen PA and Ytrehus T. (2005). Calculations of stratified wavy two-phase flow in pipes, The Fluids Engineering Group, Department of Energy and Process Engineering, Norwegian University of Science and Technology, Kolbjørn Hejes vei 2, N-7491 Trondheim, Norway

Ÿ Moguedet M, Namy P and Béreaux Y (2007). “ On the Use of Comsol Multiphysics® to Understand and Optimize the Filling Phase in Injection and Micro-Injection Molding Process. Excerpt from the Proceedings of the COMSOL Users Conference Grenoble.

RATIONAL DESIGN OF RETAINING WALLS

Babaev VN[1], Shmukler VS[1], Feirushah SH[2] , Kalmikov OA[1],
Zinchenko VM[1] , Ehsanullah [3]
[1]Kharkov National Municipal Academy Ukraine, [2]Department of Civil Engineering, College of Engineering Salahaddin University Hawler, Iraq, [3]Department of Civil Engineering, BUITEMS, Quetta

Abstract

Proposed a method and discussed the procedure for forming the structure of lightweight retaining wall. The method is based on the some new energy principles. Considered some examples for design of retaining walls. The construction of resulting structure is based on new technology.

Keywords: retaining wall, active pressure, strain energy density, stress-strain state.

Correspongding Authores Email. drehsan.buitems@gmail.com

INTRODUCTION

Analysis and design of the structures with positive properties is one of the priorities of modern engineering science. The above determines development of methods and tools of design of efficient systems, which minimize the cost of the construction, weight, adverse impact on the environment, and etc. In this regard, the traditional (indirect) approach of the design can not provide integrated solutions positivity. Information technology is an alternative, which based on general systems theory, including topics such as mathematical modeling, synergetics, and informatics. Finite element method (FEM) became the basic of the modeling of deformable structures. Finite-element modeling provides not only effective solution of indirect problems of mechanics of deformable solid bodies, but also is an excellent application apparatus for formulating and solving optimization problems, i.e direct problems. A special class is problems of regulation of parameters of structures and their state, and in particular, in conjunction with the finding of their extreme values. Gorodtsly et al 2003 reported that the mangement (control) of the behavior of structures is the tool that can be used not only to significantly improve its technical and economic parameters, but also, most importantly, improve reliability of service. The principal feature of the formation of controlled structures is dual process involving algorithms for obtaining the necessary characteristics and appropriate technological sequences of their production. In this paper, using described approach, was found complex solution (including the application in practice) of the direct design of retaining walls. In this case, design and technological procedures are founded on new energetical principles (Ishlinskii 2008, Vasilkov 2008). As a result, the algorithms for search of rational method of design of structure were constructed, the geometry of which provides:

the given transformation of the diagram of horizontal active pressure on the wall;

quasi-energetical equi-strength of system.

In addition, proposed and implemented an effictive method of construction of the discussed structure.

1 Geometry Generation of Ketaining Wall

1.1. Assumptions

The proposed formulation of the problem is founded on the hypotheses and assumptions of the corresponding Coulomb theories (Fig.1), namely (Klein 1996) the failure mode of biagregata consisting of retaining wall and held it soil, array is represented by the movement of the wall away from the soil, and simultaneously slipping of the some prism of the last along sliding surface - considered two sliding surfaces: the back side of the wall and a plane, which is the boundary of the stationary part of the soil; the slipping prism is absolutely rigid body, which allows to replace the existing volume and surface forces by their resultants of G; Q; R (G - self weight; Q - reaction of retaining wall; R - reaction of the fixed soil);

- The soil is a loose body, devoid of cohesion;
- Considered biagregat in the equilibrium limit state, corresponding to the initial stage of displacement of wall and sliding of the prism of soil. Therefore, it is assumed that reactive forces acting on the sliding prism by wall and the fixed part of the soil deviate from the vertical to the respective planes of φ_o and φ, equal to the angles of friction of soil on these planes;
- Considered the initial stage of the failure process, in this connection, the equilibrium conditions are written to its undeformed state;
- The problem is considered as planar.

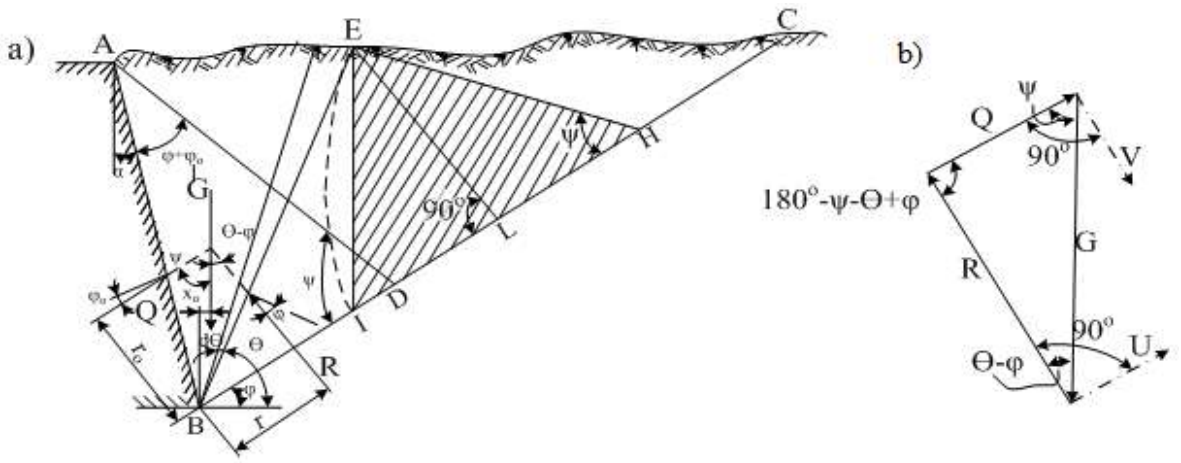

Figure1.1. The design scheme of the biaggregate.

The angles of force triangle (Figure 1.1) are:

$$\gamma = 90^{\circ} - \alpha - \varphi_{\tau};$$
$$\theta - \varphi; \qquad (1.1)$$
$$180^{\circ} - \gamma - \theta + \varphi,$$

where α - the angle between the vertical plane and the back face of the wall;
θ - the unknown angle between the horizontal plane and slipping plane.
From the above follows that the reaction of retaining wall is equal in magnitude to the required active pressure and opposite in direction. On the basis of the assumed hypothesis, the expression for the resultant of active pressure (Klein 1996) is:

$$Q = \frac{\gamma \times h^2}{2} \lambda, \qquad (1.2.)$$

where γ - specific weight of soil;
h – projection of height of wall on the vertical plane;
λ – the coefficient of active soil pressure is equal to

$$\lambda = \frac{\cos^2(\varphi - \alpha)}{\left[1 + \sqrt{\frac{\sin(\varphi + \varphi_o)\sin(\varphi - \bar{\beta})}{\cos(\alpha + \varphi_o)\cos(\alpha - \bar{\beta})}}\right]^2 \cos^2 \alpha \cos(\alpha + \varphi_o)}, \qquad (1.3)$$

where $\bar{\beta}$ – the angle of inclination of external surface of soil with respect to the horizontal (pitch angle).

Analysis of (1.3) allows considering the angle of inclination of the wall to the vertical α, as external regulating parameter (Ishlinskii 2008.) Further, given the logical direction of the problem, as well as to simplify its formulation (without loss of generality) we give:

The external surface of the soil is limited by horizontal plane, ie $\bar{\beta} = 0$;

The back side surface of the wall is considered perfectly smooth, then φ_o=0.
In this connection, (1.3) simplifies to:

$$\lambda = \left[tg\left(45 - \frac{\varphi + \alpha}{2}\right) + tg\alpha\right]^2 \cos\alpha \qquad (1.4)$$

1.2. Mathematical Model.

Rationalization of the system, to some extent, can be achieved by reducing the soil pressure on retaining wall. The latter may be realized by making a certain shape for back surface of wall. Taking the concept of the independent formation of the priori distribution of the horizontal pressure (eg, uniform distributed load), per unit surface of the wall, we can write:

$$\sigma = \lambda \times \gamma \times (z_o + z_1), \qquad (1.5)$$

Where: $z=z_o+z_1$ - current depth (Figure 1.2);
σ – intensity of normal pressure on the wall at depth z from the surface of the backfill; z_o – the depth, at which the horizontal pressure is taken as the initial (Figure 1.2).

$$I = \left[tg\left(45 - \frac{\varphi + \alpha}{2}\right) + tg\alpha \right]^2 \cos\alpha$$

The range of the angle α lies in the limit: $-\varphi < \alpha \le 0$, (1.6)

The limits set by the physical meaning of the problem.

Next, we introduce the notation:

$$\bar{\gamma} = 45^o - \frac{\varphi}{2},$$

$$I = \left[tg\left(\bar{\gamma} - \frac{\alpha}{2}\right) + tg\alpha \right]^2 \cos\alpha$$

Using the known trigonometric relationship: $\cos\alpha = \pm\sqrt{\frac{1}{1+tg^2\alpha}}$, Для дальнейших выкладок For further calculations need to choose the sign before the radical sign. So much so $\cos\alpha$ is an even function we take:

$$\cos\alpha = \sqrt{\frac{1}{1+tg^2\alpha}}.$$

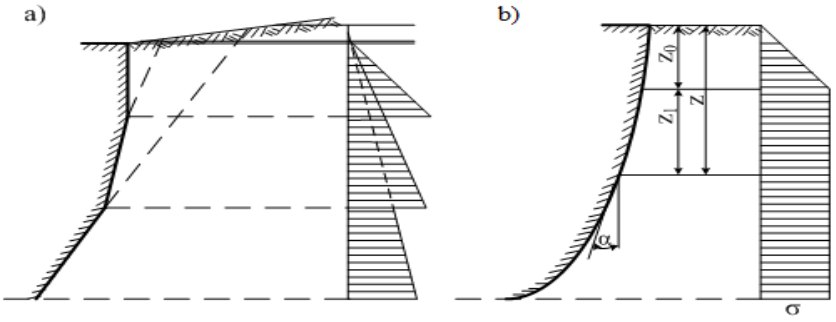

Figure 1.2. Search of geometry of wall.

Then:

$$I = \left[\frac{tg\gamma - tg\left(\frac{\alpha}{2}\right)}{1 + g\gamma \times tg\left(\frac{\alpha}{2}\right)} + tg\alpha \right]^2 \sqrt{\frac{1}{1+tg^2\alpha}}$$

Use the trigonometric relation: $tg\frac{\alpha}{2} = \pm\sqrt{\frac{1-\cos\alpha}{1+\cos\alpha}}$, where is also necessary to choose the appropriate sign. From (1.6) we see that the angle α - is negative, then the function $tg\frac{\alpha}{2}$ is also negative. In this connection:

$$tg\frac{\alpha}{2} = -\sqrt{\frac{1-\cos\alpha}{1+\cos\alpha}}$$

$$I = \left[\frac{tg\gamma + \sqrt{\frac{1-\cos\alpha}{1+\cos\alpha}}}{1 - g\gamma \times \sqrt{\frac{1-\cos\alpha}{1+\cos\alpha}}} - tg\alpha \right]^2 \sqrt{\frac{1}{1+tg^2\alpha}} = \left[\frac{tg\gamma + \sqrt{\frac{1-\sqrt{\frac{1}{1+tg^2\alpha}}}{1+\sqrt{\frac{1}{1+tg^2\alpha}}}}}{1 - g\gamma \times \sqrt{\frac{1-\sqrt{\frac{1}{1+tg^2\alpha}}}{1+\sqrt{\frac{1}{1+tg^2\alpha}}}}} - tg\alpha \right]^2 \sqrt{\frac{1}{1+tg^2\alpha}}$$

From the geometric meaning of the first derivative, it follows that

$$y' = \frac{dy}{dz} = tg\alpha\,, \qquad (1.7)$$

where $y=y(z)$ – the function, which describe the geometry of the back surface of the retaining wall.

In view of (1.7) we have:

$$l = \frac{tg\gamma + \sqrt{\dfrac{1-\sqrt{\dfrac{1}{1+y'^2}}}{1+\sqrt{\dfrac{1}{1+y'^2}}}}}{1-\gamma\times\sqrt{\dfrac{1-\sqrt{\dfrac{1}{1+y'^2}}}{1+\sqrt{\dfrac{1}{1+y'^2}}}}} - tg\alpha\Bigg]^2 \sqrt{\frac{1}{1+y'^2}}\,;$$

Substituting of variable.: $f = \sqrt{\dfrac{1}{1+y'^2}}$. We express out y':

$$f^2 = \frac{1}{1+y'^2}\;\;;\;\; \frac{1}{f^2} = 1+y'^2\;\;;\;\; y'^2 = \frac{1-f^2}{f^2}\;\;;\;\; y' = tg\alpha = \pm\sqrt{\frac{1-f^2}{f^2}}$$

$$l = \frac{tg\gamma + \sqrt{\dfrac{1-f}{1+f}}}{1-\gamma\times\sqrt{\dfrac{1-f}{1+f}}} - tg\alpha\Bigg]^2 f\,;$$

From (1.5): $l = \dfrac{s}{g(z_o+z_1)}$, *where*: $z=z_o+z_1$ – current depth (Figure 1.2); finally: $l = \dfrac{s(z)}{z\times g}$

Given that the values of γ, z_o, and φ are known, and the magnitude of the intensity of normal pressure can be represented as a known function of the depth $\sigma=\sigma(z)$, is permissible to write the following equation:

$$\frac{tg\gamma + \sqrt{\dfrac{1-f}{1+f}}}{1-\gamma\times\sqrt{\dfrac{1-f}{1+f}}} - \sqrt{\frac{1-f^2}{f^2}}\Bigg]^2 f = \frac{s(z)}{z\times g}\,; \qquad (1.8)$$

We make one more substitution of variable, $F(z) = \sqrt{\dfrac{s(z)}{z\times g}}$ Þ $F^2(z) = \dfrac{s(z)}{z\times g}$, then:

$$\frac{tg\gamma + \sqrt{\dfrac{1-f}{1+f}}}{1-\gamma\times\sqrt{\dfrac{1-f}{1+f}}} - \sqrt{\frac{1-f^2}{f^2}}\Bigg]^2 f = F^2(z)$$. Further, let that: $k^2 = \dfrac{1-f}{1+f}$

We express $f = f(k)$: $1-f = (1+f)k^2$; $1-f = k^2 + f\times k^2$; $f\times k^2 + f = 1-k^2$;

$f(k^2+1) = 1-k^2$; $f = \dfrac{1-k^2}{1+k^2}$,

$$\frac{1-f^2}{f^2}=\frac{1}{f^2}-1=\frac{1}{\left(\frac{1-k^2}{1+k^2}\right)^2}-1=\frac{\left(1+k^2\right)^2}{\left(1-k^2\right)^2}-1=\frac{1+2k^2+k^4}{1-2k^2+k^4}-1=$$

$$=\frac{1+2k^2+k^4-1+2k^2-k^4}{1-2k^2+k^4}=\frac{4k^2}{\left(1-k^2\right)^2}$$

In addition: $\sqrt{\frac{1-f^2}{f^2}}=\sqrt{\frac{4k^2}{\left(1-k^2\right)^2}}=\frac{2k}{1-k^2}$;

As a result, we have:

$$\left(\frac{tg\gamma+k}{1-g\gamma\times k}-\frac{2k}{1-k^2}\right)^2\frac{1-k^2}{1+k^2}=F^2(z);\quad\left(\frac{(tg\gamma+k)(1-k^2)-2k(1-g\gamma\times k)}{(1-g\gamma\times k)(1-k^2)}\right)^2\frac{1-k^2}{1+k^2}=F^2(z);$$

$$\left(\frac{tg\gamma-k^2tg\gamma+k-k^3-2k+2k^2tg\gamma}{(1-g\gamma\times k)(1-k^2)}\right)^2\frac{1-k^2}{1+k^2}=F^2(z);\quad\left(\frac{tg\gamma-k^3+k^2tg\gamma-k}{(1-g\gamma\times k)(1-k^2)}\right)^2\frac{1-k^2}{1+k^2}=F^2(z);$$

$$\left(\frac{tg\gamma(1+k^2)-k(1+k^2)}{(1-g\gamma\times k)(1-k^2)}\right)^2\frac{1-k^2}{1+k^2}=F^2(z);\quad\left(\frac{(1+k^2)(tg\gamma-k)}{(1-g\gamma\times k)(1-k^2)}\right)^2\frac{1-k^2}{1+k^2}=F^2(z);$$

$$\frac{(1+k^2)^2(tg\gamma-k)^2}{(1-g\gamma\times k)^2(1-k^2)^2}\frac{(1-k^2)}{(1+k^2)}=F^2(z);\quad\frac{(1+k^2)(tg\gamma-k)^2}{(1-g\gamma\times k)^2(1-k^2)}=F^2(z);$$

$$\frac{(1+k^2)(tg\gamma-2k\times tg\gamma+k^2)}{(1-k^2)(1-2tg\gamma\times k+tg^2\gamma\times k^2)}-F^2(z)=0;$$

$$\frac{tg^2\gamma-2k\times tg\gamma+k^2+k^2tg^2\gamma-2k^3tg\gamma+k^4}{1-2k\times tg\gamma+k^2tg^2\gamma-k^2+2k^3tg\gamma-k^4tg^2\gamma}-F^2(z)=0;$$

$$tg^2\gamma-2k\times tg\gamma+k^2+k^2tg^2\gamma-2k^3tg\gamma+k^4-\ldots$$
$$\ldots-F^2(z)\times\left(1-2k\times tg\gamma+k^2tg^2\gamma-k^2+2k^3tg\gamma-k^4tg^2\gamma\right)=0;$$

$$\left[1+F^2(z)\times tg^2\gamma\right]\times k^4+\left[-2tg\gamma-2F^2(z)\times tg\gamma\right]\times k^3+\left[1+tg^2\gamma-F^2(z)\times tg^2\gamma+F^2(z)\right]\times k^2+\ldots$$
$$\ldots+\left[2\times F^2(z)\times tg\gamma-2\times tg\gamma\right]\times k+\left[tg^2\gamma-F^2(z)\right]=0;$$

$$k^4+\frac{-2tg\gamma-2F^2(z)\times tg\gamma}{1+F^2(z)\times tg^2\gamma}\times k^3+\frac{1+tg^2\gamma-F^2(z)\times tg^2\gamma+F^2(z)}{1+F^2(z)\times tg^2\gamma}\times k^2+\ldots$$
$$\ldots+\frac{2\times F^2(z)\times tg\gamma-2\times tg\gamma}{1+F^2(z)\times tg^2\gamma}\times k+\frac{tg^2\gamma-F^2(z)}{1+F^2(z)\times tg^2\gamma}=0;$$

Finally, we have: $k^4+d_2\times k^3+d_3\times k^2+d_4\times k+d_5=0$

(1.9)

where: $d_2=\frac{-2tg\gamma-2F^2(z)\times tg\gamma}{1+F^2(z)\times tg^2\gamma}$; $d_3=\frac{1+tg^2\gamma-F^2(z)\times tg^2\gamma+F^2(z)}{1+F^2(z)\times tg^2\gamma}$;

$$d_4=\frac{2\times F^2(z)\times tg\gamma-2\times tg\gamma}{1+F^2(z)\times tg^2\gamma};\quad d_5=\frac{tg^2\gamma-F^2(z)}{1+F^2(z)\times tg^2\gamma};\quad F(z)=\sqrt{\frac{\sigma(z)}{z\times g}}$$

z_o – depth, within which the pressure increases linearly up to the required value $\sigma(z_0)$, (Figure 1.2);

z – the variable depth (Figure 1.2);

$\sigma(z)$ - - *the pressure at* z;

For the particular case $\sigma(z)=\sigma=const$, $\sigma(z)=\sigma=const$, the ordinate of the curve does not depend on the specific weight of soil - g. Considering the pressure σ on the vertical wall at the level $z=z_0$ equals to

$s = l \times g \times z_o$, *we note that the coefficients of equation (1.9)* g enters only through $F(z)$. Substituting the above expressions we have $F(z) = \sqrt{l \times g \times z_o \times (z \times g)^{-1}}$, and finally: $F(z) = \sqrt{l \times z_o \times (z)^{-1}}$. Q.E.D.
Note also, that it is advisable using numerical methods for solution of (1.9).

1.3. Analytical Solution

For formation an analytical solution of (1.9) (which simplifies the analysis), we introduce the following hypothesis

$$\cos a = \cos^2 a \qquad (1.10)$$

The inclination angle of the wall depends on the angle of internal friction j. Increasing of j leads to decrease a. From the physical meaning of the problem, that the angle is in range: $-j < a \le 0$. It is known (Sorochan and Trofimenkov., 1985) that for a variety types of soils j lies in the range $7^0 < j \le 43^0$.
Equality (1.10) with an error not exceeding 20% is valid for $a \in \{0^0, 36^0\}$, that is 83% of the range of the angle of internal friction j. In other cases, the error may reach 37%.
We give below a table showing the acceptability of introduced hypotheses:

Table 1

α	cosα	$\cos^2\alpha$	%
0	1.000000	1.000000	0.00
1	0.999848	0.999695	0.02
2	0.999391	0.998782	0.06
3	0.998630	0.997261	0.14
4	0.997564	0.995134	0.24
5	0.996195	0.992404	0.38
6	0.994522	0.989074	0.55
7	0.992546	0.985148	0.75
8	0.990268	0.980631	0.98
9	0.987688	0.975528	1.25
10	0.984808	0.969846	1.54
11	0.981627	0.963592	1.87
12	0.978148	0.956773	2.23
13	0.974370	0.949397	2.63
14	0.970296	0.941474	3.06
15	0.965926	0.933013	3.53
16	0.961262	0.924024	4.03
17	0.956305	0.914519	4.57
18	0.951057	0.904508	5.15
19	0.945519	0.894005	5.76
20	0.939693	0.883022	6.42
21	0.933580	0.871572	7.11
22	0.927184	0.859670	7.85
23	0.920505	0.847329	8.64
24	0.913545	0.834565	9.46
25	0.906308	0.821394	10.34
26	0.898794	0.807831	11.26
27	0.891007	0.793893	12.23
28	0.882948	0.779596	13.26
29	0.874620	0.764960	14.34
30	0.866025	0.750000	15.47
31	0.857167	0.734736	16.66
32	0.848048	0.719186	17.92
33	0.838671	0.703368	19.24
34	0.829038	0.687303	20.62
35	0.819152	0.671010	22.08
36	0.809017	0.654508	23.61
37	0.798636	0.637819	25.21
38	0.788011	0.620961	26.90
39	0.777146	0.603956	28.68
40	0.766044	0.586824	30.54
41	0.754710	0.569587	32.50
42	0.743145	0.552264	34.56
43	0.731354	0.534878	36.73

Table 2a: The angle of internal friction j n, deg. of sandy soils.

Sandy soil	Annotation of soil characteristics	Characteristic of soil with void ratio *e*			
		0,45	0,55	0,65	0,75
Gravelly and larger		43	40	38	-
Medium-grained		40	38	35	-
Fine	j_n	38	36	32	28
Silt	j_n	36	34	30	26

Table 2b: Normative values of the angle of internal friction j n, of deg. silty-clay soils.

Soil Type and its liquid limit		Annotation of soil characteristics	Characteristic of soil with void ratio *e*						
			0,45	0,55	0,65	0,75	0,85	0,95	1,05
Sandy loam	$0 \le I_L \le 0{,}25$	φ_n	30	29	27	24	-	-	-
	$0{,}25 < I_L \le 0{,}75$	φ_n	*28*	26	24	21	18	-	-
Loam	$0 < I_L \le 0{,}25$	φ_n	26	25	24	23	22	20	-
	$0{,}25 < I_L \le 0{,}5$	φ_n	*24*	23	22	21	19	17	-
	$0{,}5 < I_L \le 0{,}75$	φ_n	-	-	19	18	16	14	12
clay	$0 < I_L \le 0{,}25$	φ_n	-	21	20	19	18	16	14
	$0{,}25 < I_L \le 0{,}5$	φ_n	-	-	18	17	16	14	11
	$0{,}5 < I_L \le 0{,}75$	φ_n	-	-	15	14	12	10	7

After introduction of (1.10) The resolution equation becomes:

$$I = \left[tg\left(45 - \frac{\varphi + \alpha}{2}\right) + tg\alpha\right]^2 \cos^2\alpha ;$$

Substituting $\gamma = 45 - \frac{\varphi}{2}$, then: $I = \left[tg\left(\gamma + \frac{\alpha}{2}\right) + tg\alpha\right]^2 \cos^2\alpha$.

Assuming, as before, $\cos\alpha = \pm\sqrt{\frac{1}{1+tg^2\alpha}}$: and choosing the sign according to the physical meaning of the problem we have: $\cos\alpha = \sqrt{\frac{1}{1+tg^2\alpha}}$. Thus:

$$I = \left[\frac{tg\gamma - tg\left(\frac{\alpha}{2}\right)}{1 + g\gamma \times tg\left(\frac{\alpha}{2}\right)} + tg\alpha\right]^2 \frac{1}{1+tg^2\alpha}$$

Considering: $\left(-\varphi < \alpha \le 0\right)$ (1.6)

Setting: $tg\frac{\alpha}{2} = -\sqrt{\frac{1-\cos\alpha}{1+\cos\alpha}}$, we have:

$$I = \left[\frac{tg\gamma + \sqrt{\frac{1-\cos\alpha}{1+\cos\alpha}}}{1 - g\gamma \times \sqrt{\frac{1-\cos\alpha}{1+\cos\alpha}}} - tg\alpha\right]^2 \frac{1}{1+tg^2\alpha} = \left[\frac{tg\gamma + \sqrt{\frac{1-\sqrt{\frac{1}{1+tg^2\alpha}}}{1+\sqrt{\frac{1}{1+tg^2\alpha}}}}}{1 - g\gamma \times \sqrt{\frac{1-\sqrt{\frac{1}{1+tg^2\alpha}}}{1+\sqrt{\frac{1}{1+tg^2\alpha}}}}} - tg\alpha\right]^2 \frac{1}{1+tg^2\alpha}$$

Assuming, as before, $y' = \frac{dy}{dz} = tg\alpha$, we get

$$I = \left[\frac{tg\gamma + \sqrt{\dfrac{1-\sqrt{\dfrac{1}{1+y'^2}}}{1+\sqrt{\dfrac{1}{1+y'^2}}}}}{1-g\gamma\times\sqrt{\dfrac{1-\sqrt{\dfrac{1}{1+y'^2}}}{1+\sqrt{\dfrac{1}{1+y'^2}}}}} - tg\alpha \right]^2 \frac{1}{1+y'^2}$$

substituting $f = \sqrt{\dfrac{1}{1+y'^2}}$

we have: $f^2 = \dfrac{1}{1+y'^2}$; $\dfrac{1}{f^2} = 1+y'^2$;

$$y'^2 = \frac{1-f^2}{f^2} \quad ; \quad y' = tg\alpha = \pm\sqrt{\frac{1-f^2}{f^2}} ;$$

Then: $I = \left[\dfrac{tg\gamma + \sqrt{\dfrac{1-f}{1+f}}}{1-g\gamma\times\sqrt{\dfrac{1-f}{1+f}}} - tg\alpha \right]^2 f^2$; From (1.5): $I = \dfrac{s}{g(z_o+z_1)}$;

Finally:

$$\left[\frac{tg\gamma + \sqrt{\dfrac{1-f}{1+f}}}{1-g\gamma\times\sqrt{\dfrac{1-f}{1+f}}} - \sqrt{\frac{1-f^2}{f^2}} \right]^2 f^2 = \frac{s(z)}{z\times g}$$; substituting: $F(z) = \sqrt{\dfrac{s(z)}{z\times g}}$ Þ $F^2(z) = \dfrac{s(z)}{z\times g}$;

$$\left[\frac{tg\gamma + \sqrt{\dfrac{1-f}{1+f}}}{1-g\gamma\times\sqrt{\dfrac{1-f}{1+f}}} - \sqrt{\frac{1-f^2}{f^2}} \right]^2 f^2 = F^2(z)$$; substituting: $k^2 = \dfrac{1-f}{1+f}$;

We express $f = f(k)$:

$$1-f = (1+f)k^2 ; \; 1-f = k^2 + f\times k^2 ; \; f\times k^2 + f = 1-k^2 ; \; f(k^2+1) = 1-k^2 ; \; f = \frac{1-k^2}{1+k^2} ;$$

$$\frac{1-f^2}{f^2} = \frac{1}{f^2} - 1 = \frac{1}{\left(\dfrac{1-k^2}{1+k^2}\right)^2} - 1 = \frac{(1+k^2)^2}{(1-k^2)^2} - 1 = \frac{1+2k^2+k^4}{1-2k^2+k^4} - 1 =$$

$$= \frac{1+2k^2+k^4-1+2k^2-k^4}{1-2k^2+k^4} = \frac{4k^2}{(1-k^2)^2} ;$$

So:

$$\sqrt{\frac{1-f^2}{f^2}} = \sqrt{\frac{4k^2}{(1-k^2)^2}} = \frac{2k}{1-k^2} ;$$

Finally, we obtain: $\left[\dfrac{tg\gamma + k}{1-g\gamma\times k} - \dfrac{2k}{1-k^2} \right]^2 \left(\dfrac{1-k^2}{1+k^2}\right)^2 = F^2(z)$;

Taking the square root of the left and right part of equation we have:

$$\left[\frac{tg\gamma + k}{1-g\gamma\times k} - \frac{2k}{1-k^2} \right] \left(\frac{1-k^2}{1+k^2}\right) = F(z) ; \; \left[\frac{(tg\gamma + k)(1-k^2) - 2k(1-g\gamma\times k)}{(1-g\gamma\times k)(1-k^2)} \right] \left(\frac{1-k^2}{1+k^2}\right) = F(z) ;$$

$$\left[\frac{tg\gamma - k^2 tg\gamma + k - k^3 - 2k + 2k^2 tg\gamma}{(1-g\gamma\times k)(1-k^2)} \right] \left(\frac{1-k^2}{1+k^2}\right) = F(z) ; \; \left[\frac{tg\gamma - k^3 + k^2 tg\gamma - k}{(1-g\gamma\times k)(1-k^2)} \right] \left(\frac{1-k^2}{1+k^2}\right) = F(z) ;$$

$$\left[\frac{tg\gamma\left(1+k^2\right)-k\left(1+k^2\right)}{\left(1-g\gamma\times k\right)\left(1-k^2\right)}\right]\left(\frac{1-k^2}{1+k^2}\right)=F(z);\ \frac{\left(1+k^2\right)\left(tg\gamma-k\right)}{\left(1-g\gamma\times k\right)\left(1-k^2\right)}\frac{\left(1-k^2\right)}{\left(1+k^2\right)}=F(z);\ \frac{\left(tg\gamma-k\right)}{\left(1-g\gamma\times k\right)}=F(z);$$

$$tg\gamma-k=F(z)\times\left(1-g\gamma\times k\right);\ tg\gamma-k=F(z)-F(z)\times tg\gamma\times k;\ F(z)\times tg\gamma\times k-k=F(z)-tg\gamma;$$

$$k\times\left(F(z)\times tg\gamma-1\right)=F(z)-tg\gamma;$$

$$k=\frac{F(z)-tg\gamma}{F(z)\times tg\gamma-1};$$

$$\gamma=\pm\sqrt{\frac{1-f^2}{f^2}}=\pm\frac{2k}{1-k^2};$$

$$y=\pm\int\frac{2k}{1-k^2}dz;$$

Where: $k^2=\left[\frac{F(z)-tg\gamma}{F(z)\times tg\gamma-1}\right]^2$;

$$1-k^2=1-\frac{\left[F(z)-tg\gamma\right]^2}{\left[F(z)\times tg\gamma-1\right]^2}=\frac{\left[F(z)\times tg\gamma-1\right]^2-\left[F(z)-tg\gamma\right]^2}{\left[F(z)\times tg\gamma-1\right]^2}=$$

$$=\frac{F^2(z)\times tg^2\gamma-2F(z)\times tg\gamma+1-F^2(z)+2F(z)\times tg\gamma-tg^2\gamma}{\left(F(z)\times tg\gamma-1\right)^2}=$$

$$=\frac{tg^2\gamma\times\left(F^2(z)-1\right)-\left(F^2(z)-1\right)}{\left(F(z)\times tg\gamma-1\right)^2}=\frac{\left(F^2(z)-1\right)\left(tg^2\gamma-1\right)}{\left(F(z)\times tg\gamma-1\right)^2};$$

$$\frac{2k}{1-k^2}=\frac{2\left(F(z)-tg\gamma\right)\left(F(z)\times tg\gamma-1\right)^2}{\left(F(z)\times tg\gamma-1\right)\left(F^2(z)-1\right)\left(tg^2\gamma-1\right)};$$

Finally:

$$\frac{2k}{1-k^2}=\frac{2\left(F(z)-tg\gamma\right)\left(F(z)\times tg\gamma-1\right)}{\left(F^2(z)-1\right)\left(tg^2\gamma-1\right)};$$

Given that: $F^2(z)=\frac{s(z)}{z\times g}$ (1.11)

and differentiating the left and right side of equation (1.11), we define dz:

$$2F(z)dF(z)=\frac{1}{g}\times\frac{ds(z)\times z-s(z)\times dz}{z^2}=\frac{1}{g}\times\frac{dz\left(\frac{ds(z)}{dz}\times z-s(z)\right)}{z^2};$$

$$dz=\frac{2F(z)z^2\times g\times dF(z)}{\left(\frac{ds(z)}{dz}\times z-s(z)\right)};$$

$$y=\pm\int\frac{2\left(F(z)-tg\gamma\right)\left(F(z)\times tg\gamma-1\right)}{\left(F^2(z)-1\right)\left(tg^2\gamma-1\right)}\frac{2F(z)z^2\times g}{\left(\frac{ds(z)}{dz}\times z-s(z)\right)}dF(z)$$ (1.12)

Consider the special case $s(z)=const=s$, Then $F(z)=\sqrt{\frac{s}{z\times g}}$:

$$dz=-\frac{2F(z)z^2\times g\times dF(z)}{s}\times\frac{g\times s}{g\times s}=-\frac{2F(z)z^2\times g\times dF(z)}{s}\times\frac{g\times s}{g\times s}=-\frac{2\times F(z)\times s}{F^4(z)\times g}dF(z)=-\frac{2\times s}{F^3(z)\times g}dF(z)$$

$$y=m\int\frac{2\left(F(z)-tg\gamma\right)\left(F(z)\times tg\gamma-1\right)}{\left(F^2(z)-1\right)\left(tg^2\gamma-1\right)}\frac{2\times s}{F^3(z)\times g}dF(z).$$ We give: $tg^2\gamma=m$, we obtain:

$$y = \mu\frac{4\times\sigma}{g}\int\frac{(F(z)-m)(F(z)\times m-1)}{(F^2(z)-1)(m^2-1)\times F^3(z)}dF(z) = \mu\frac{4\times\sigma}{g}\int\frac{(F(z)-m)(F(z)\times m-1)}{(F^2(z)-1)(m^2-1)\times F^3(z)}dF(z) =$$

$$= \mu\frac{4\times\sigma}{g}\int\frac{F^2(z)\times m - F(z)\times m^2 - F(z)+m}{(F^2(z)-1)(m^2-1)\times F^3(z)}dF(z) = \mu\frac{4\times\sigma}{g}\int\frac{F^2(z)\times m - F(z)\times(m^2+1)+m}{(F^2(z)-1)(m^2-1)\times F^3(z)}dF(z)$$

$$y = \mu\frac{4\times\sigma\times m}{g(m^2-1)}\left[\int\frac{1}{(F^2(z)-1)\times F(z)}dF(z) - \frac{(m^2+1)}{m}\int\frac{1}{(F^2(z)-1)\times F^2(z)}dF(z)+\ldots\right.$$

$$\left.\ldots+\int\frac{1}{(F^2(z)-1)\times F^3(z)}dF(z)\right]; \quad (1.13)$$

The integrals in (1.13), taken closed. We obtain:

$$y = \mu\frac{4\times\sigma\times m}{g(m^2-1)}\left[\frac{1}{2\times F^2(z)} - \ln\left(\frac{F^2(z)}{1-F^2(z)}\right)+\frac{(m^2+1)}{m}\left(-\frac{1}{F(z)}+\frac{1}{2}\ln\left(\frac{1+F(z)}{1-F(z)}\right)\right)\right] \quad (1.14)$$

We introduce the notation:

$$W(F(z)) = \left[\frac{1}{2\times F^2(z)} - \ln\left(\frac{F^2(z)}{1-F^2(z)}\right)+\frac{(m^2+1)}{m}\left(-\frac{1}{F(z)}+\frac{1}{2}\ln\left(\frac{1+F(z)}{1-F(z)}\right)\right)\right]; \quad (1.15)$$

And finally:

$$y = \mu\frac{4\times\sigma\times m}{g(m^2-1)}W(F(z)) \quad (1.16)$$

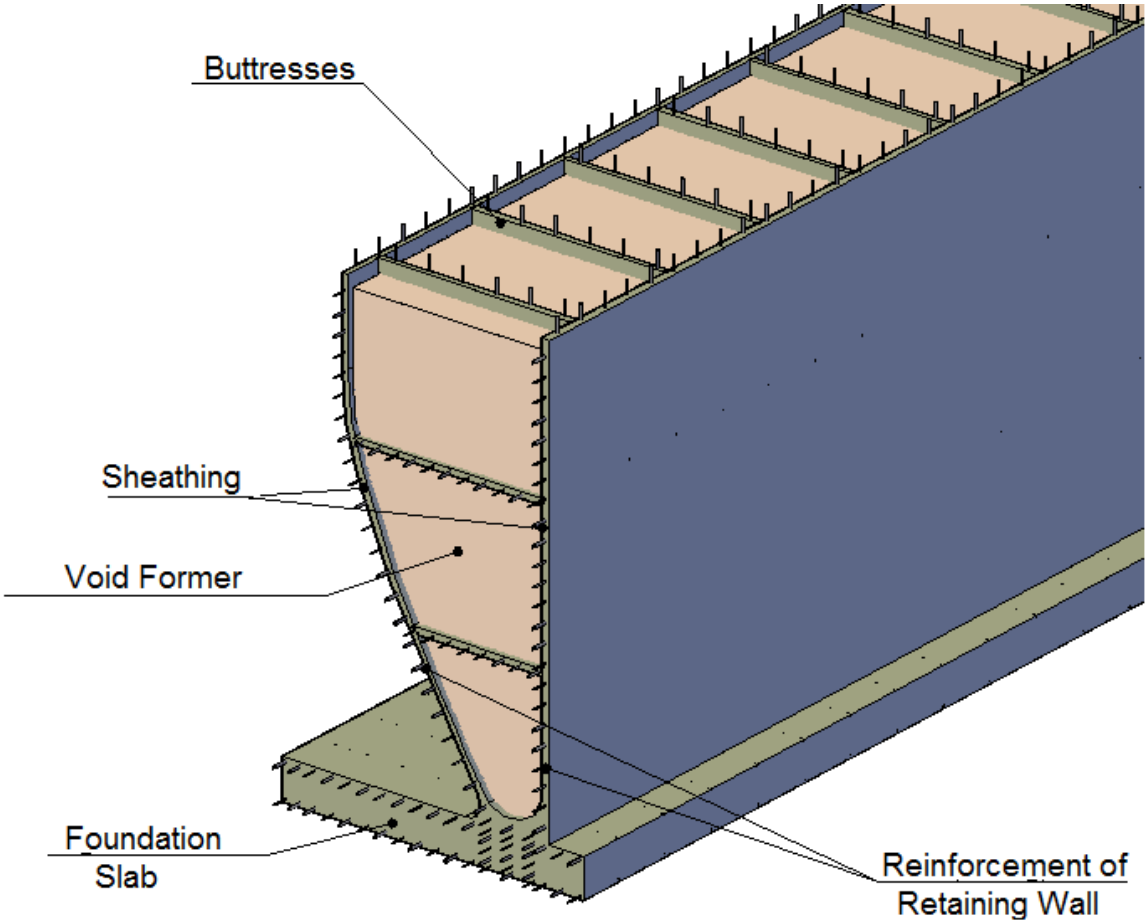

Figure 1.3. The effective retaining wall

To visual demonstration of solutions we consider some examples.

Пример 1

Data:

Angle of internal friction $\varphi = 40^0$ Total depth z_{max}=18m

Iinitial depth z_0=3m ratio $\frac{z_{max}}{z_0}=6$

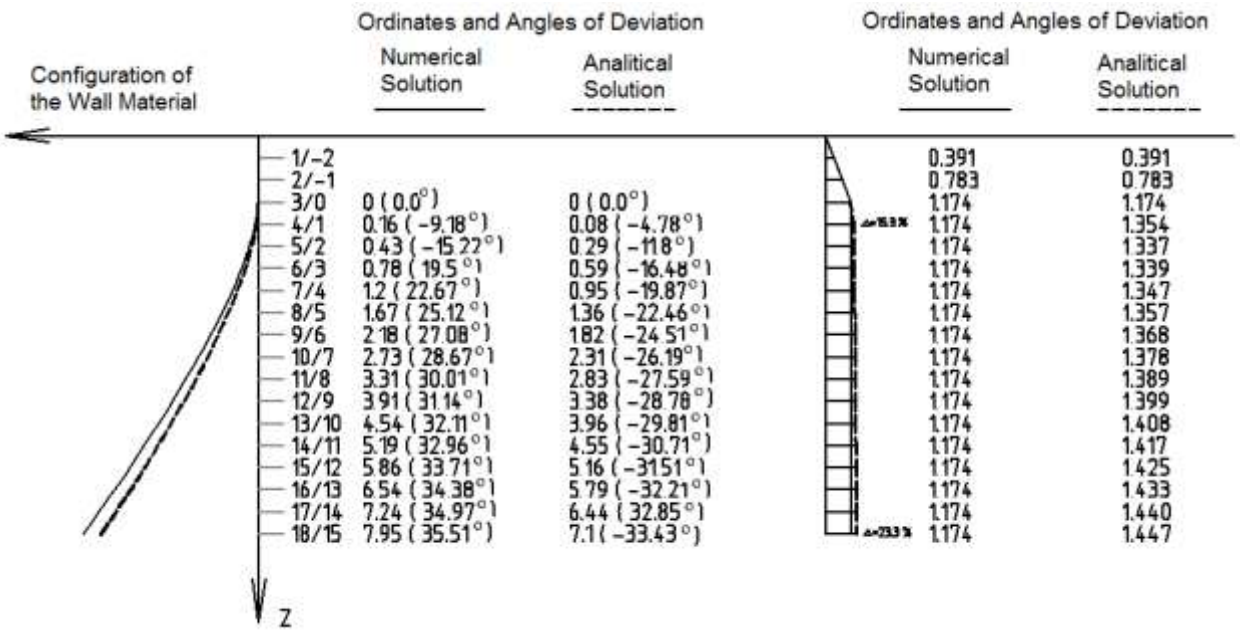

The integral error is 16.0%.

Example 2

Data:

Angle of internal friction $j = 30^0$ Total depth z_{max}=18m

Initial depth z_0=m ratio $\frac{z_{max}}{z_0}=6$

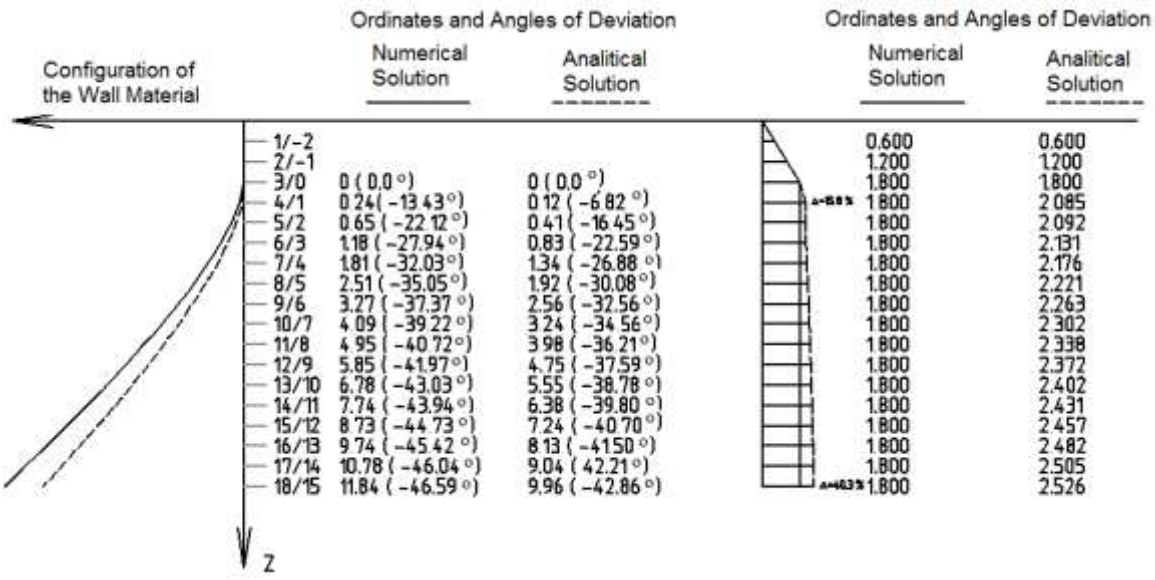

The integral error is Δ =25.0 %.

Example 3

Data: Angle of internal friction $j = 20^0$ Total depth z_{max}=18m

Initial depth z_0=3m ratio $\frac{z_{max}}{z_0}=6$

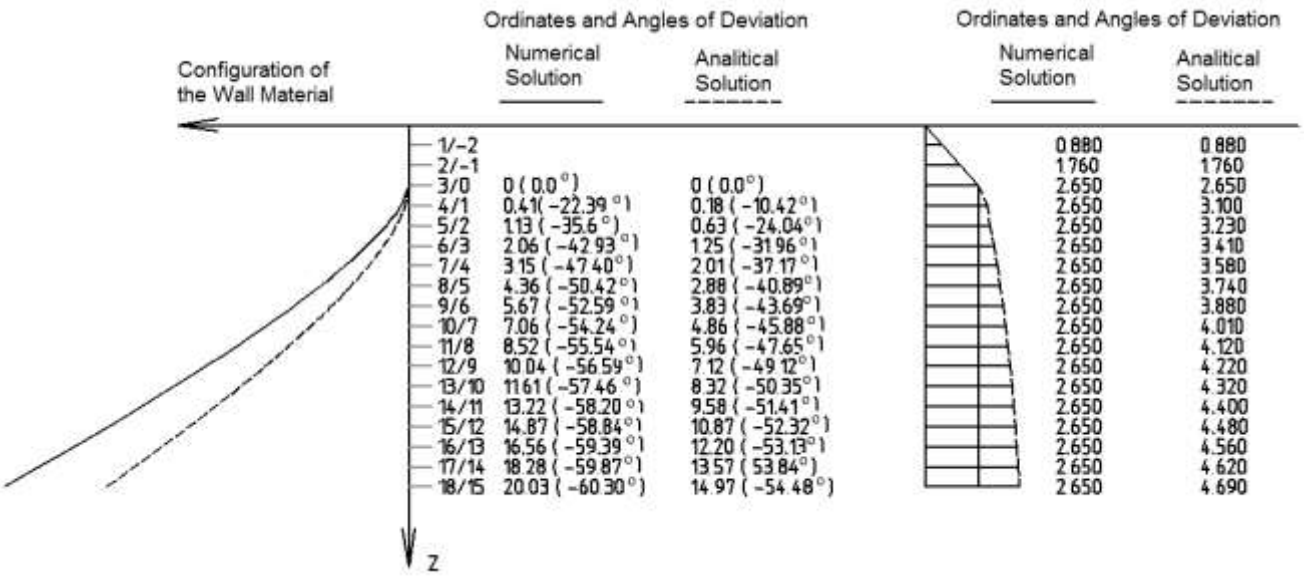

integral error is Δ =44.8 %.

Example 4

Data: Angle of internal friction $\varphi = 40^0$ Total depth z_{max}=18m

Initial depth z_0=5m ratio $\frac{z_{max}}{z_0} = 3.6$

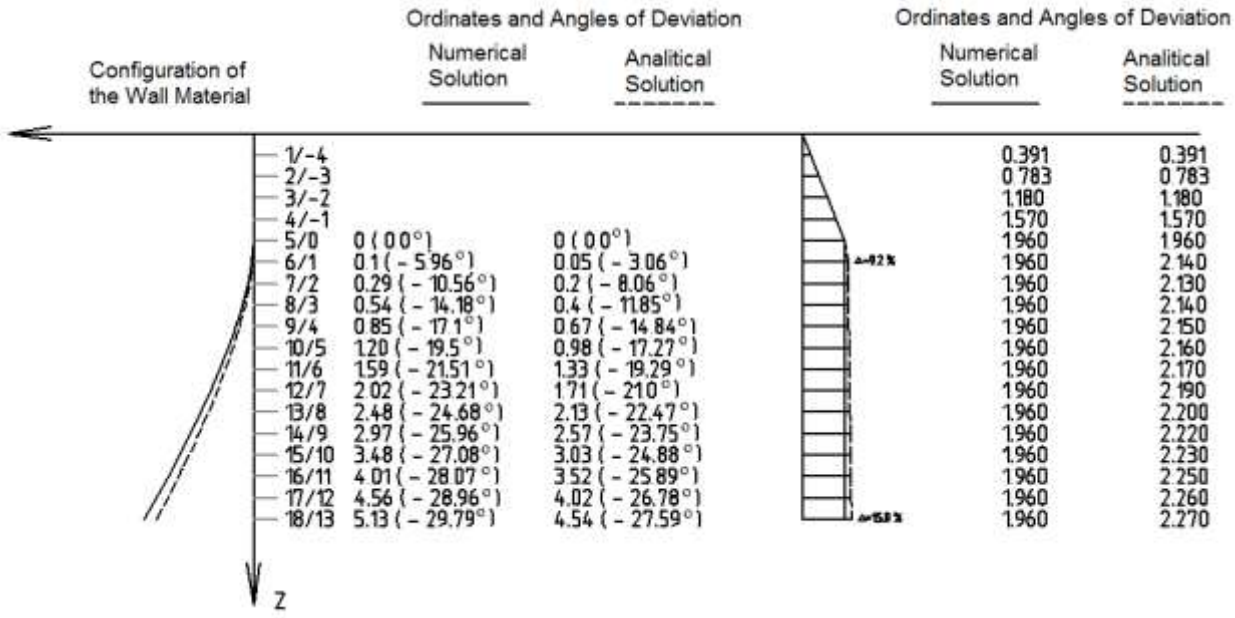

Integral error is Δ =9.5 %.

Example 5

Data: Angle of internal friction $\varphi = 30^0$ Total depth z_{max}=18m

Initial depth z_0=5m ratio $\frac{z_{max}}{z_0} = 3.6$

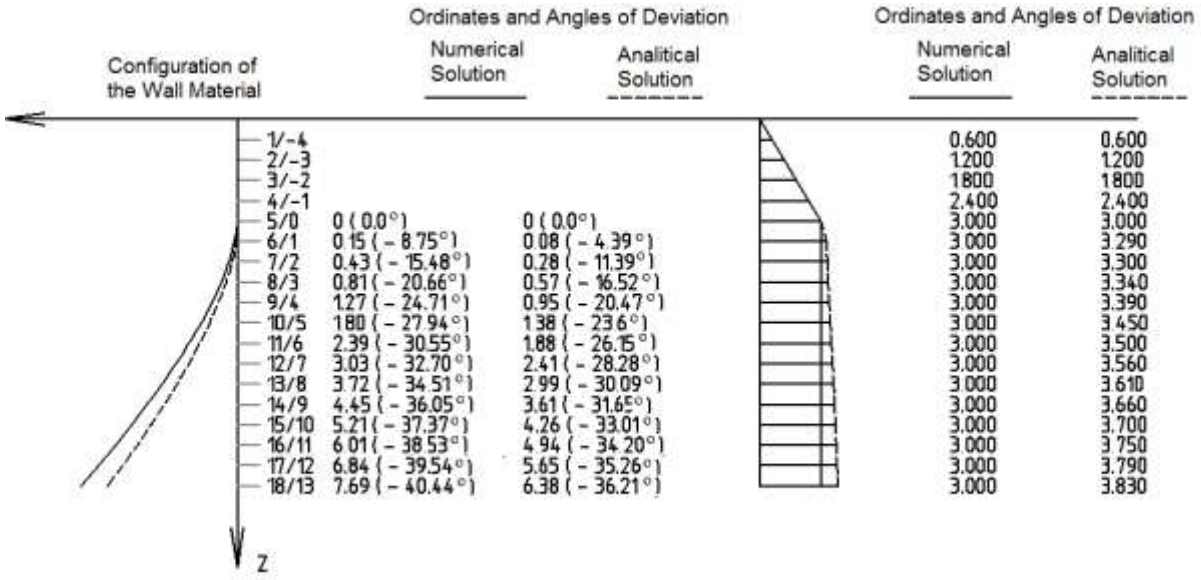

Integral error is $\Delta = 14.5$ %.

Example 6

Data: Angle of internal friction $\varphi = 20^0$ Total depth z_{max}=18m

Initial depth z_0=5m ratio $\frac{z_{max}}{z_0} = 3.6$

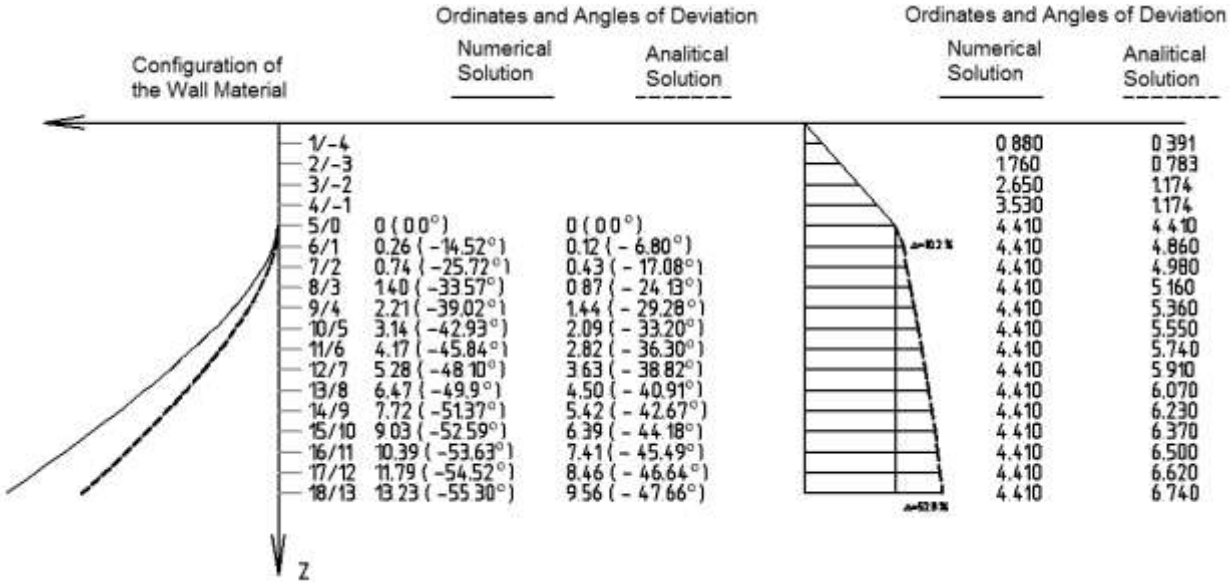

Integral error is $\Delta = 25.7$ %.

Example7

Data: Angle of internal friction $\varphi = 40^0$ Total depth z_{max}=18m

Initial depth z_0=7m ratio $\frac{z_{max}}{z_0} = 2.57$

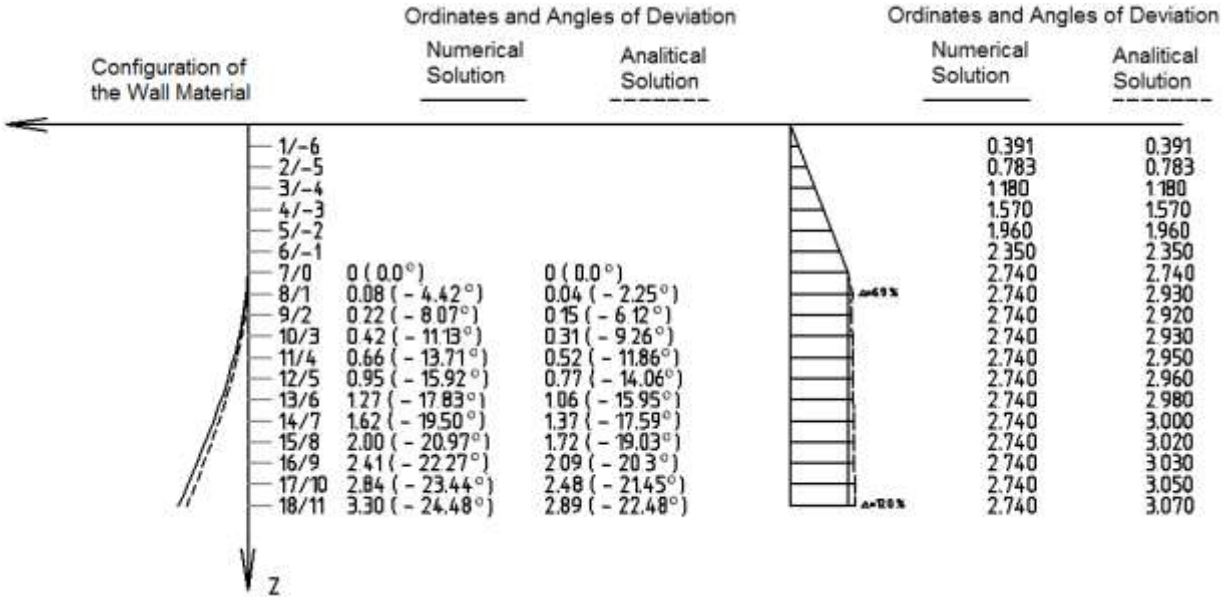

Integral error is Δ =6.4 %.

Example8

Data: Angle of internal friction $\varphi = 30^0$ Total depth z_{max}=18m

Initial depth z_0=7m ratio $\frac{z_{max}}{z_0} = 2.57$

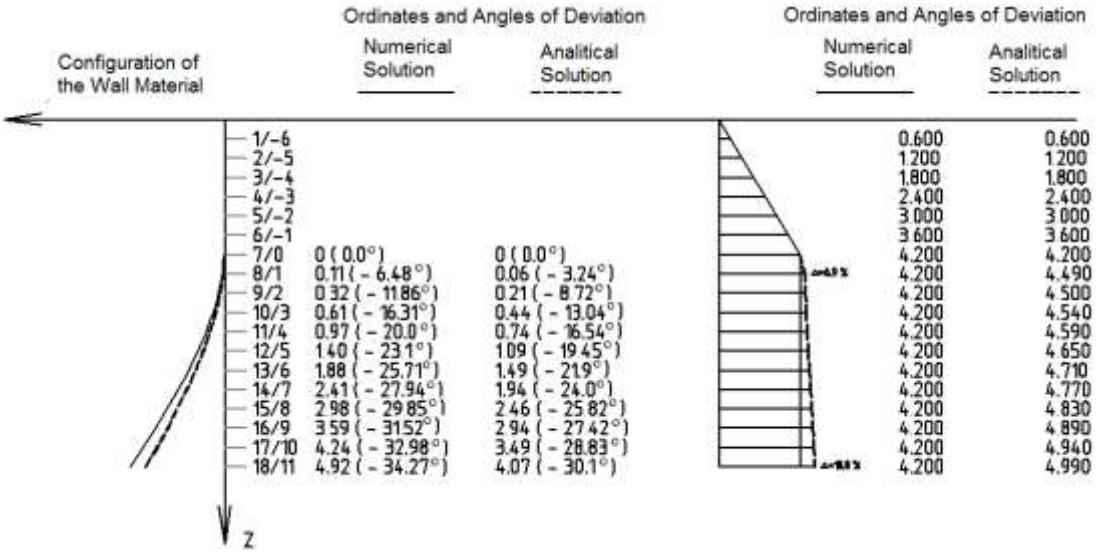

Integral error is Δ =8.7 %.

Example9

Data: Angle of internal friction $\varphi = 20^0$ Total depth z_{max}=18m

Initial depth z_0=7m ratio $\frac{z_{max}}{z_0} = 2.57$

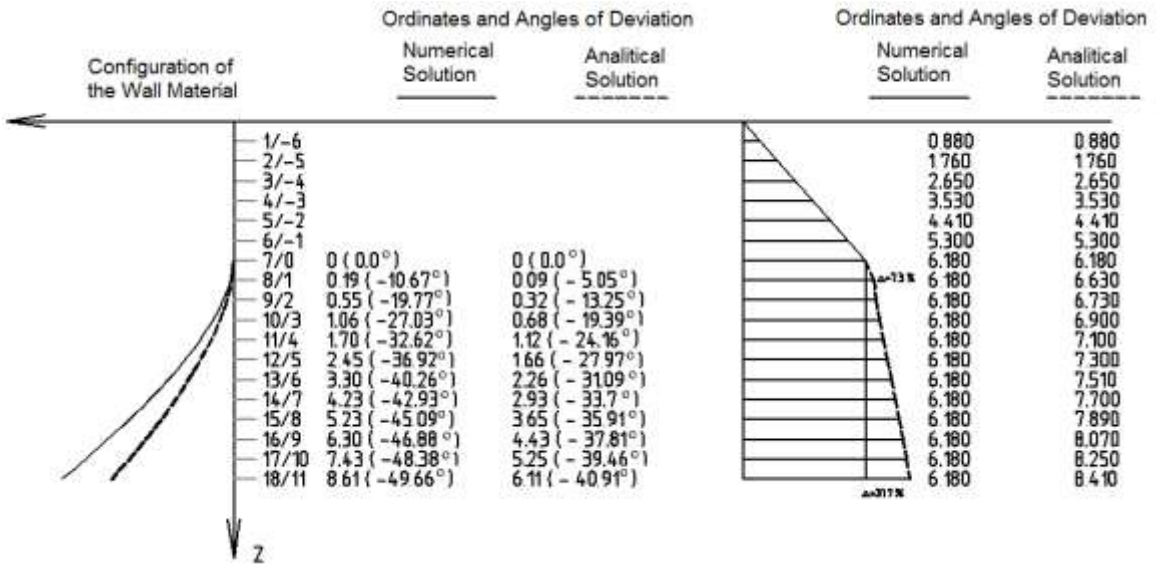

Integral error is $\Delta = 14.9\%$.

The error of approximation analytical solution was estimated by comparing the areas of pressure diagrams. As shown in Figure 1.3 for the majority of cases, the error does not exceed 25%.

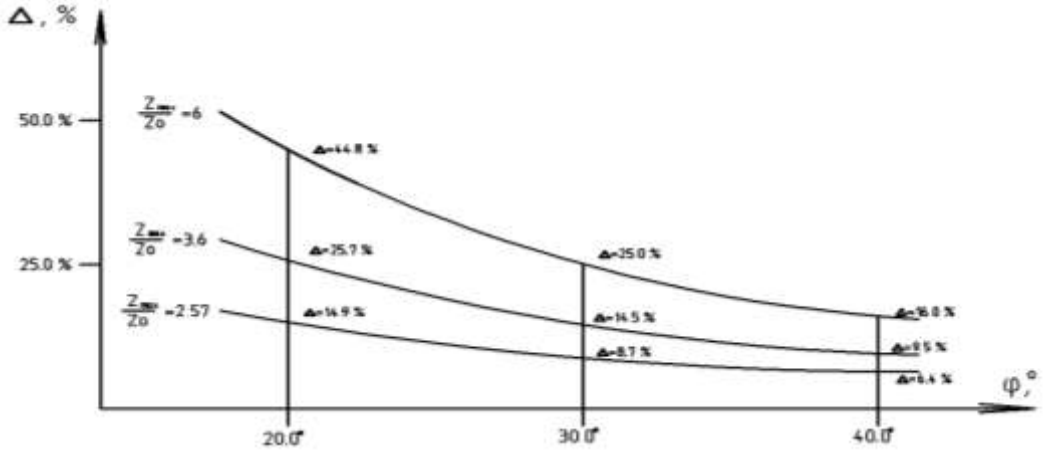

Figure1.3. Error (%) of the analytical solution depending on the angle of internal friction.

2. Formation of Energetically Equi-Strength Element of Retaining Wall.

2.1 Basic Assumptions

For simplifying, the following conditions are assumed:

Retaining wall is infinitely long caisson-type structure (Fig. 2.1). In this regard, we consider it as the plane problem;

As The I-shape element is taken as design element (Fig. 2.2), and the width of the flanges is equal to the distance between the buttresses (ribs), and the height of the cross section is equal to the total thickness of the wall (regulating parameter), the thickness of the flanges and ribs are assigned based on the technological possibility (quality requirements of vertical concreting);- During the forming of algorithm for determining the height of the section of wall element its self weight is neglected. (to reserve);

Ultimate tensile strength of reinforced concrete generated by conditional reduction value

$$R_{red}^{+} = \frac{R_{bt} + mR_s}{1 + mn} \le R_B, \qquad (2.1)$$

where $m = \frac{A_s}{A_B}$ - reinforcement ratio,

A_s; A_b – cross sectional area of reinforcement and concrete I-beam, respectively.

R_s; R_{bt} – ultimate tensile strength of reinforcement and concrete;

R_b – ultimate compressive strength of concrete (prism strength);

$$n = \frac{E_s}{E_b};$$

E_s; E_b – modules of deformations of the first kind of reinforcement and concrete, respectively;

considered that the «σ-ε» diagram of concrete in tension, compression and shear are known;

Lateral (active) soil pressure $\sigma = \sigma(z)$ is represented by a trapezoid with ordinates q_1 (top), q_2 (bottom);

In the final form retaining wall is a set of composed of I-shape (box-like) elements of constant cross section with the internal cavity of variable cross section.

The sign of strain in the appointment of the ultimate strength determined on the basis of sign of parameter Lode-Nadai $-1 \le c_e \le +1$.

2.2. Geometrical Characteristics of Element of Wall.

Needed characteristic of cross-section, for further calculations (Fig. 2.2) are:

$$I_x = \frac{BH^3}{12}\psi \text{ - moment of inertia;} \qquad W_x = \frac{BH^2}{6}\psi \text{ - section modulus;} \qquad (2.2)$$

$$S_x = \frac{BH^2}{8}\eta \text{ - static moment, where: } \psi = \alpha + 6(1-\alpha)(1-\beta)^2\beta, \qquad (2.3)$$

$$\eta = \alpha + 4(1-\alpha)(1-\beta)\beta \qquad (2.4)$$

$\alpha = \frac{d}{B}$; $\beta = \frac{D}{H}$, δ, Δ – known quantities, $\alpha \in [0,1]$, $\beta \in [0,0.5]$.

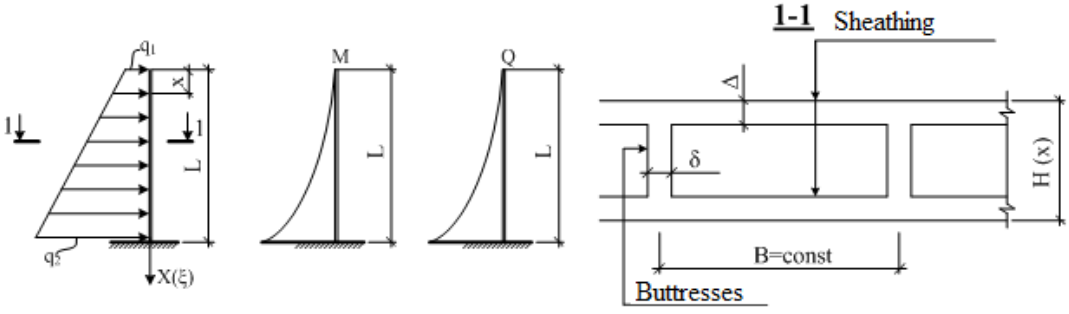

Figure 2.1. Design scheme of retaining wall

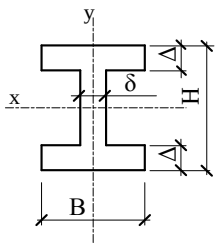

Fig.2.2. the current cross section of wall.

2.3. Internal Forces

Since, considered the plane bending, there are bending moment and shear force at sections of element (Fig. 2.1):

$$M(x)=\frac{q_2L^2}{6}x^2\left[3g+(1-g)x\right], \tag{2.5}$$

$$Q(x)=\frac{q_2L}{2}\times x\left[2g+(1-g)x\right], \tag{2.6}$$

$g=\frac{q_1}{q_2}$, $x=\frac{x}{L}$, γ, $x\hat{\imath}\ [0;1]$, L – height of wall;

M(ξ); Q(ξ) – bending moment and shear force.

2.4. Terms of Rationalization.

The height of section of wall *H(ξ)* will be searched from condition [3]:

$$\frac{1-n}{2}|s|+\frac{1+n}{2}\sqrt{s^2+mt^2}=R^+_{red}, \tag{2.7}$$

where the parameters *v* and *m* correspond to different criteria, and limit states are defined by the following table:

Table 2.1

№	criterion	ν	m
1	Galileo-Rankine	0	4
2	Saint-Venant	$\bar{m}$*	4
3	Coulomb	1	4
4	Mohr $D=\frac{R_{bt}}{R_b}$	Δ	4
5	Mises-Genk	1	3
*)	$\bar{m}$– Poisson's ratio		

Considering (2.2) (2.3) (2.4) (2.5) (2.6), normal and shear stresses are represented by the following dependencies:

$$s=\frac{6M(x)}{B\times j\times H^2(x)}, \tag{2.8}$$

$$t=\frac{3Q(x)\times h}{2a\times B\times j\times H(x)}, \text{ and } \quad B(x)=w\times H(x)=const. \tag{2.9}$$

In addition to five criteria, presented in Table 2.1, criterion introduced in [2] is considered:

$$e(x)=e_u, \tag{2.10}$$

where *e(ξ)* –- the yield value of the potential strain energy density per unit length;

$$e_u=0{,}5c_e^2\left[(c_e+1)e_{cu}-(c_e-1)e_{tu}\right]+(1-c_e^2)e_{shu}, \tag{2.11}$$

e_u – the ultimate value of the potential strai energy density per unit length,

$c_e=\frac{2e_2-e_1-e_3}{e_1-e_3}$ - Lode-Nadai parameter,

$e_1 \geq e_2 \geq e_3$ - *principal linear strain*

$$e_{cu} = \int_0^{e_{uc}} s_c(e)de, \tag{2.12}$$

$$e_{tu} = \int_0^{e_{ut}} s_t(e)de, \tag{2.13}$$

$$e_{shu} = \int_0^{g_u} t(g)dg, \tag{2.14}$$

$s_c = s_c(e)$; $s_t = s_t(e)$; $t = t(g)$ - *known functions* that describe the "stress - strain" diagram for compression, tension, and shear, respectively, mainly obtained by experiment;

$e_{uc}; e_{ut}; g_u$ - *The ultimate compression, tension, and shear strain of concrete, respectively.*

Equation (2.10) determines the conditional energetically equi-strength element, as it is performed only in some points of the cross section.

Substituting (2.8) and (2.9) into (2.7), and after some transformations we obtain:

$$H^4(x) - a_2 H^2(x) - a_3 = 0, \tag{2.15}$$

where the coefficients $a_i (i=2, 3)$ are given by:

$$a_2 = \frac{6(1-n)M(x)}{B \times j \times R_{red}} + \frac{9(1+n)^2 m \times h^2 Q^2(x)}{16B^2 \times j^2 \times a^2 \times R_{red}^{+2}}, \tag{2.16}$$

$$a_3 = \frac{36M^2(x)n}{B^2 R_{red}^{+2} j^2}, \tag{2.17}$$

Ignoring the negative values of H(ξ), as inconsistent with the physical meaning of the problem, in view of (1.16, 1.17), we obtain

$$H(x) = \sqrt{\frac{a_2}{2} + \sqrt{\frac{a_2^2}{4} + a_3}} \tag{2.18}$$

In turn, for criterion (3.10), current height of the cross section of the wall is formed on the basis of the iterative procedure [2]:

$$H_{ij}(x) = H_{i(j-1)}(e_t)\left(\frac{e_i}{e_u}\right)^P, \tag{2.19}$$

where j – number of iteration,

i – number of section,

$P \in [0;1]$ - the parameter which describes rate of convergence of the iterative process.

Refinement of the heights of section will be continued until performance of limitations:

$$\left|H_{ij} - H_{i(j-1)}\right| \leq d, \tag{2.20}$$

where δ – given accuracy.

Determination of components of the stress-strain state (SSS) is performed by using Program Complex (PC), "LIRA" (Gorodtsly et al., 2003). Gorodtsly et al

The numerical solution is illustrated by the graphs shown in Figures 2.3-2.8.

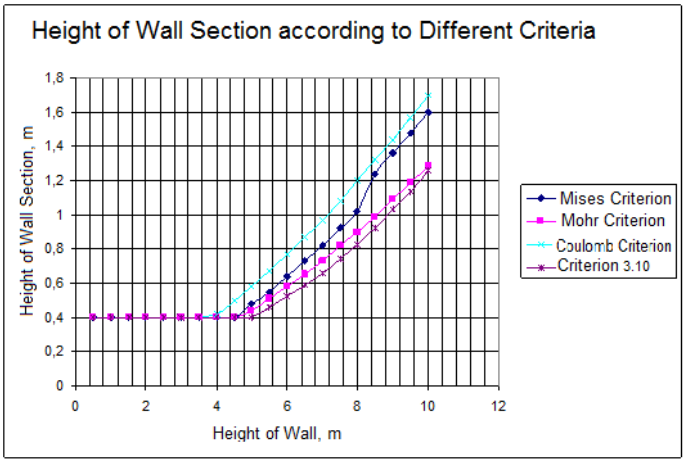

Fig.2.3 Dependence "height of wall section - height of wall," determined by various criteria.

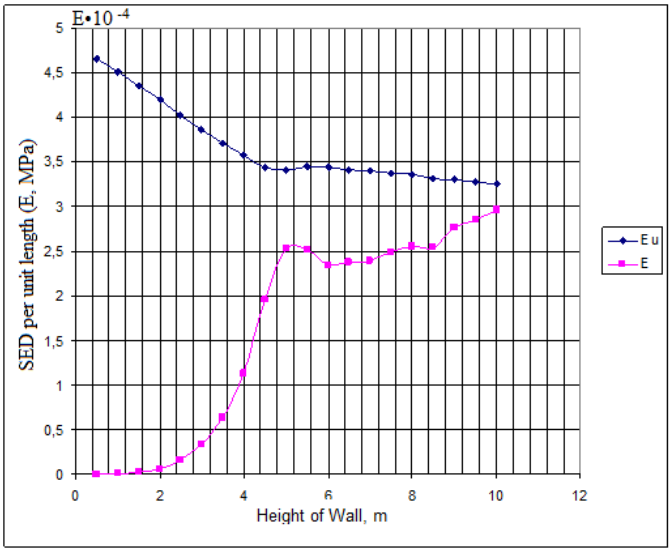

Fig.2.5. Dependence of the "SED per unit length - height of wall," as defined by Mohr: e_u- ultimate SED at a point, e- actual SED at the same point.

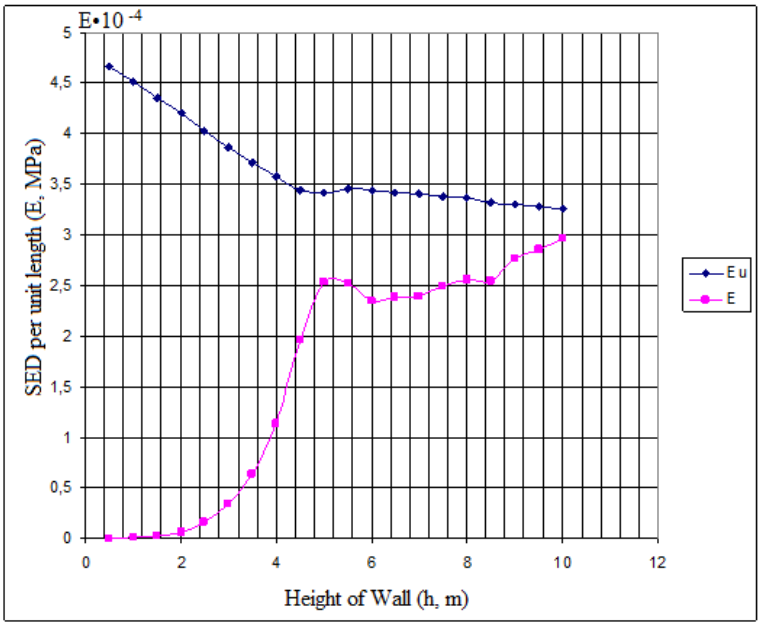

Fig.2.6. Dependence of the "SED per unit length - height of wall," as defined by energy criterion: e_u- ultimate SED at a point, e- actual SED at same point.

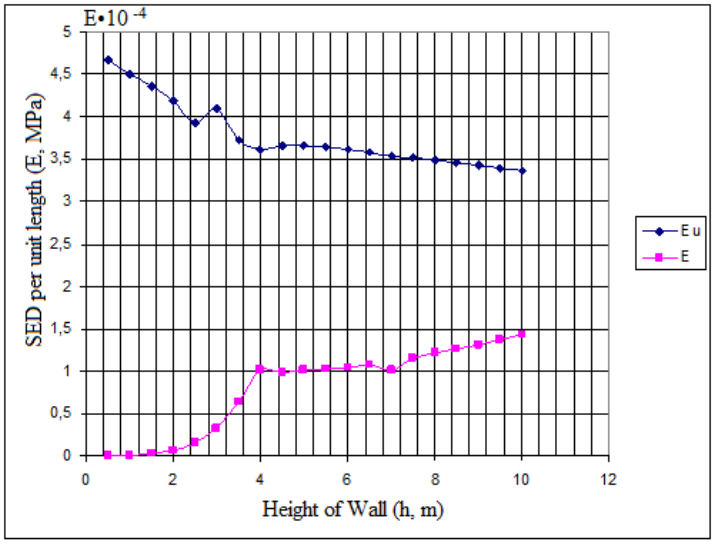

Fig.2.7. Dependence of the "SED per unit length - height of the wall," as defined by Coulomb's law: e_u- ultimate SED at a point, *e*- actual SED at same point.

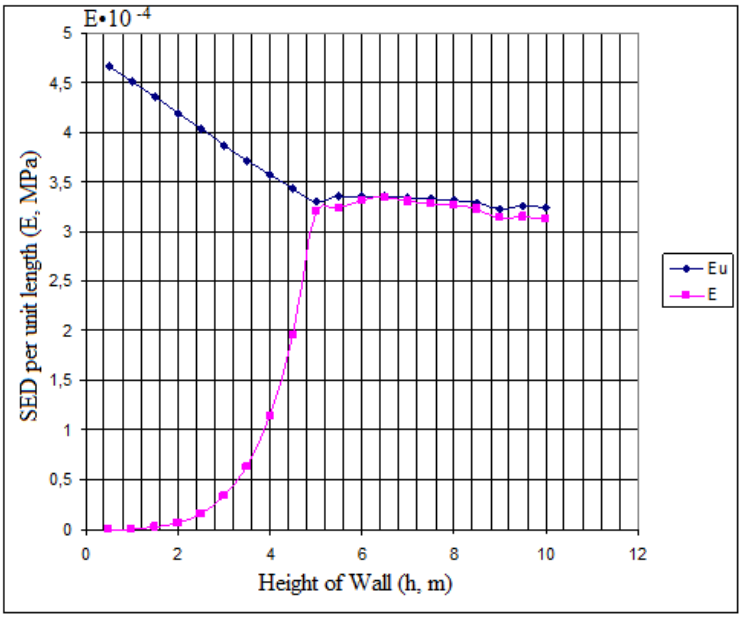

Fig.2.8. Dependence of the "SED per unit length - height of wall," as defined by (3.10): e_u- ultimate SED at a point, *e*- actual SED at same point.

Analysis of the achieved results allows the following conclusions:
Criteria (2.7) approximately define the same height of wall section (the difference does not exceed 23.5%). The SED is distributed along element ununiformly;

- The criterion (2.10) defines an energetically equi-strength element, but due to this, material saving is about 20% in relation to the criteria (2.7);
- Criteria Galileo-Rankine and Saint-Venant determine the height of wall section does not performance conditions of $e_u > e$, which is unacceptable.

Thus, isoenergetic SSS of structure causes the most acceptable distribution of material and it's effective service in structure.

3. Features of the direct design anchor retaining wall.

We will consider the anchor retaining wall (Fig. 3.1). Leaving unchanged its earlier hypothesis and the composition of the internal parameters (Fig. 2.2), we introduce a new external parameter, ie, the force in pre-tensioning (prestressed) anchor. In the case of inclined anchor the vertical loading of wall is neglected. Tensile force in which is equal to $P_{opt}^{tot} = P_{opt} / \cos \overline{\overline{b}}$

where $\overline{\overline{b}}$ - angle between anchor and horizontal axis.

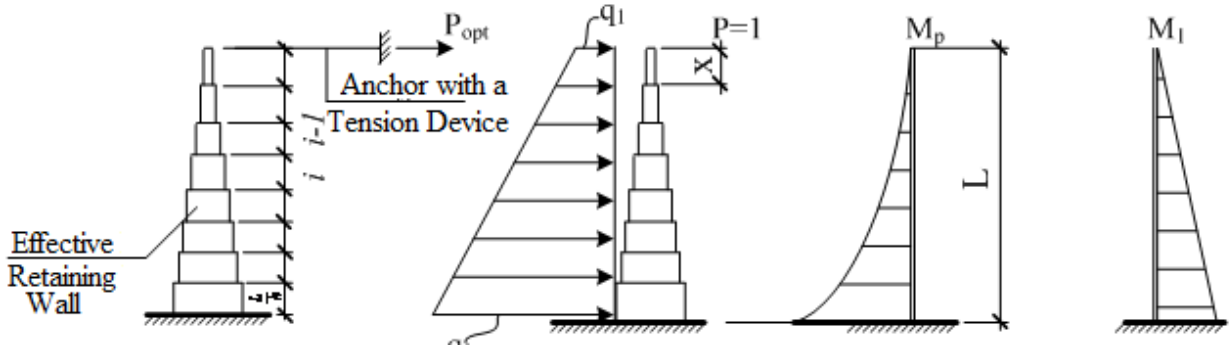

Figure 3.1. Design scheme of anchor retaining wall

Solution of problem tends to construction of energetically equi-strength wall with additional support in form of horizontal prestressed anchor. Technologically, making the advanced anchoring does not cause major difficulties
Based on the ideology of formation of rational structures, presented in (Shmukler and Klimov, 2008, Vasilkov 2008)) we assume, that the external parameter, approximately, can be determined from the condition:

$$U = \inf U(a^n) \quad n = 1,2,..., \tag{3.1}$$

where n - number of variants of comparison,
$a \in M$, M – *set of permissible values* of the pretensioning force of anchor,
U – potential strain energy (PSE).
At the same time, we introduce the assumption of unimodality of the function U.
Given, that we considered strain of plane bending for the PSE, we have:

$$U = \frac{1}{2}\int \frac{M^2(x)dx}{EI} \tag{3.2}$$

Since, rationalized wall is an element of variable cross section, equation (3.2) takes the form:

$$U = \frac{1}{2}\sum_{i=1}^{N} \int_{\frac{(i-1)L}{N}}^{\frac{iL}{N}} \frac{M^2(x)dx}{(EI)_i}, \tag{3.3}$$

where N – number of segments (sectors) of wall along it's height,
i – текущий номер участка,

$\frac{L}{N}$ - length of segment (uniform partition), L – height of wall,

$[EI]_i$ – bending stiffness of the i-th segment, $M(x)$ – bending moment.
In this case,

$$M(x) = M_g(x) + P_{opt} \times x, \tag{3.4}$$

where $M_g(x) = -ax^3 - bx^2$, $a = \frac{q_2 - q_1}{6L}$; $b = \frac{q_1}{2}$;

P_{opt} – rational value of force in anchor.
Substituting (3.4) into (3.3), after integration we obtain:

$$U = \frac{L^7}{2N^7}\sum_{i=1}^{N} \frac{1}{(EI)_i}\left\{\frac{a^2}{7}\left[i^7 - (i-1)^7\right] + \frac{abN}{3L}\left[i^6 - (i-1)^6\right] + \right.$$
$$+ \frac{N^2(b^2 - 2aP_{opt})}{5L^2}\left[i^5 - (i-1)^5\right] - \frac{bP_{opt}N^3}{2L^3}\left[i^4 - (i-1)^4\right] + \tag{3.5}$$
$$\left. + \frac{P_{opt}^2 N^4}{3L^4}\left[i^3 - (i-1)^3\right]\right\}$$

we find force P_{opt} from the condition $\frac{\partial U}{\partial P_{opt}} = 0$, and then differentiating (2.5). by P_{opt} to define:

$$P_{opt} = \frac{3L^4 \sum_{i=1}^{N} \frac{1}{(EI)_i} \left\{ \frac{2aN^2}{5L^2} \left[i^5 - (i-1)^5 \right] + \frac{bN^3}{2L^3} \left[i^4 - (i-1)^4 \right] \right\}}{2N^4 \sum_{i=1}^{N} \frac{1}{(EI)_i} \left[i^3 - (i-1)^3 \right]} \qquad (3.6)$$

In the particular case $q_1=q_2=q$, a $N=1$. $P_{opt} = 0{,}375qL$, (3.7)

which coincides with the result, obtained in [5]. Since the system is statically indeterminate to the first degree

$$P_{opt} = P_f + P_{ps}, \qquad (3.8)$$

Where P_f – selftensile force, P_{ps} – pre-tensioning force.

Hence, the required value of pre-tensioning force of anchor is equal to $P_{ps} = P_{opt} - P_f$, (3.9)

selftensile force defined by force method

$$P_f = -\frac{\Delta_{1p}}{\delta_{11}}, \qquad (3.10)$$

$$\delta_{11} = \frac{L^3}{3N^3} \sum_{i=1}^{N} \frac{1}{(EI)_i} (3i^2 - 3i + 1)$$

$$\Delta_{1p} = -\frac{L^5}{N^5} \sum_{i=1}^{N} \frac{1}{(EI)i} \left\{ \frac{a}{5} \left[i^5 - (i-1)^5 \right] + \frac{Nb}{4L} \left[i^4 - (i-1)^4 \right] \right\}.$$

The primary structure of force method and moment diagrams are shown in Figure 3.1. Finally

$$P_f = \frac{3L^2}{N^2} \times \frac{\sum_{i=1}^{N} \frac{1}{(EI)_i} \left\{ \frac{a}{5} \left[i^5 - (i-1)^5 \right] + \frac{bN}{4L} \left[i^4 - (i-1)^4 \right] \right\}}{\sum_{i=1}^{N} \frac{1}{(EI)_i} (3i^2 - 3i + 1)} \qquad (3.11)$$

Comparing the expressions (3.6) and (3.11) can be noted that $P_{opt} = P_f$, (3.12)

and as result $P_{ps} = 0$;

This result is very interesting and shows that in the case of condition (3.1) pre-tension of anchor is not required. The general solution is an iterative procedure consisting of two cycles. The external cycle implements a consistent change in the force of pre-tensioning of anchor until performance of condition:

$$P_{ps}^m - P_{ps}^{m-1} \le e, \qquad (3.13)$$

where m - number of external iteration, ε - given accuracy.

As initial approximation, is taken distribution of heights of wall sections, which found for cantilever system by (1.19) (1.20). Further, the internal iteration cycle is executed, generated by (1.10) (1.19) (1.20). The analysis of system was done by using PC "LIRA". The results of formation of geometry of wall by (1.10) are shown in Fig. 3.2

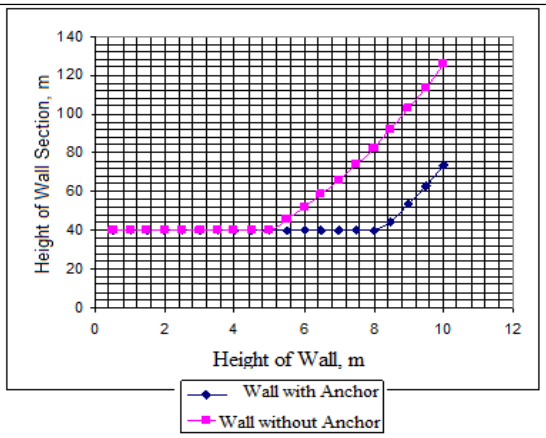

3.2. Dependence "height wall of section - height of wall," as defined by (3.10) in the wall with anchor: *eu* - ultimate SED, *e* - actual SED.

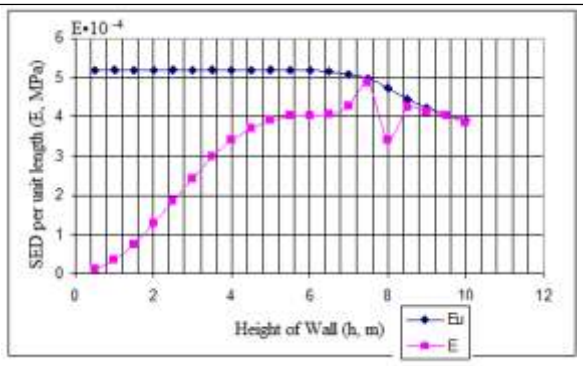

3.3. Dependence "SED per unit length - height of wall," as defined by (3.10) in the wall with anchor: e_u - ultimate SED, *e* - actual SED.

As seen from the graphs, the anchor reduces the height of section of equally strength wall by 41.5%, and changes, the qualitative nature of its height.

4. Numerical Verification and Analysis of SSS of the Proposed Structure.

Investigation of SSS of the proposed structure of retaining wall was realized using finite element (FE) modeling. Actually the calculations were carried out in LIRA environment, version 9.6R8.

Characteristics of the model are as follows:

- Type of a FE - zero Gaussian curvature shell element;
- size of FE - 25 × 25 cm;

load is uniform distributed, at depth $z_o=3m$, is equal to $11.74\ kN/m^2$ and is applied to the back surface of the wall;

- design scheme of cross-section of wall shown in Figure 4.1.

The results of analysis are illustrated by fields of displacements and internal forces (Fig. 4.2-4.6)

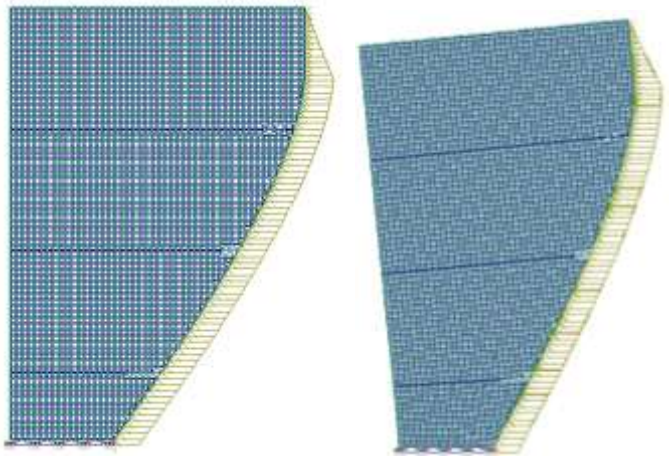

Fig. 4.2. Deformed scheme of buttress, combined with transformed pressure diagram.

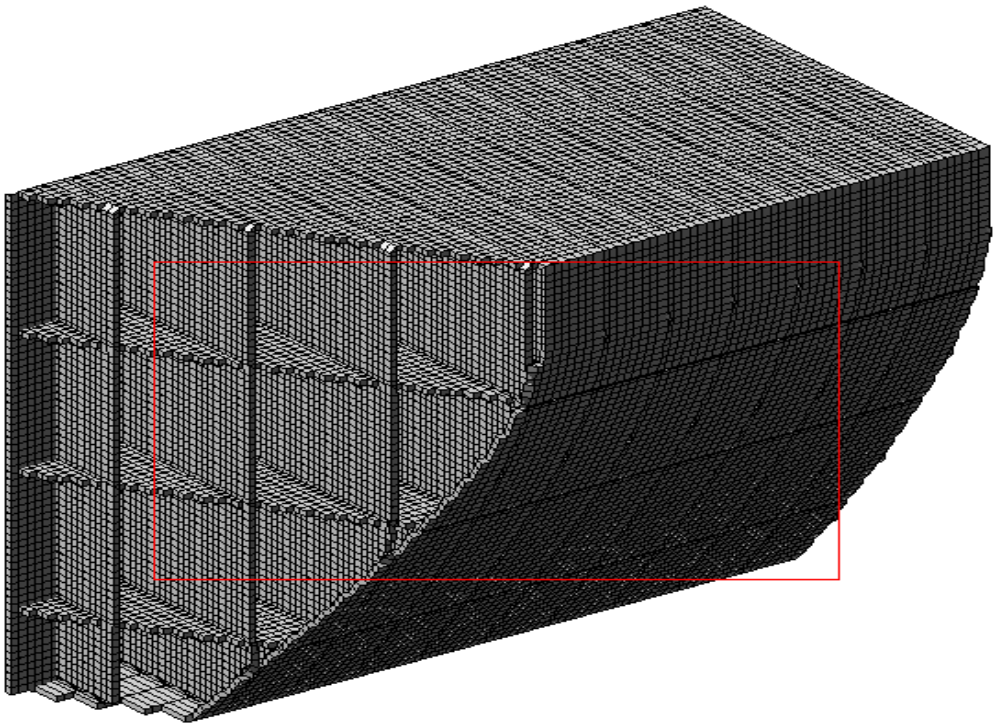

Fig. 4.1. Finite-element model of retaining wall

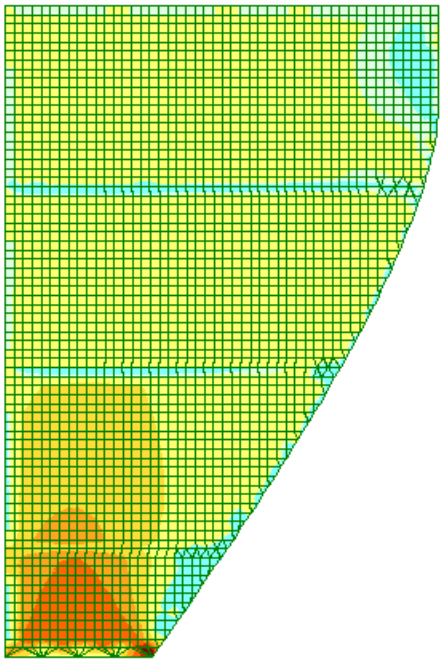

Fig. 4.2. Distribution of shear stresses in walls-diaphragms.

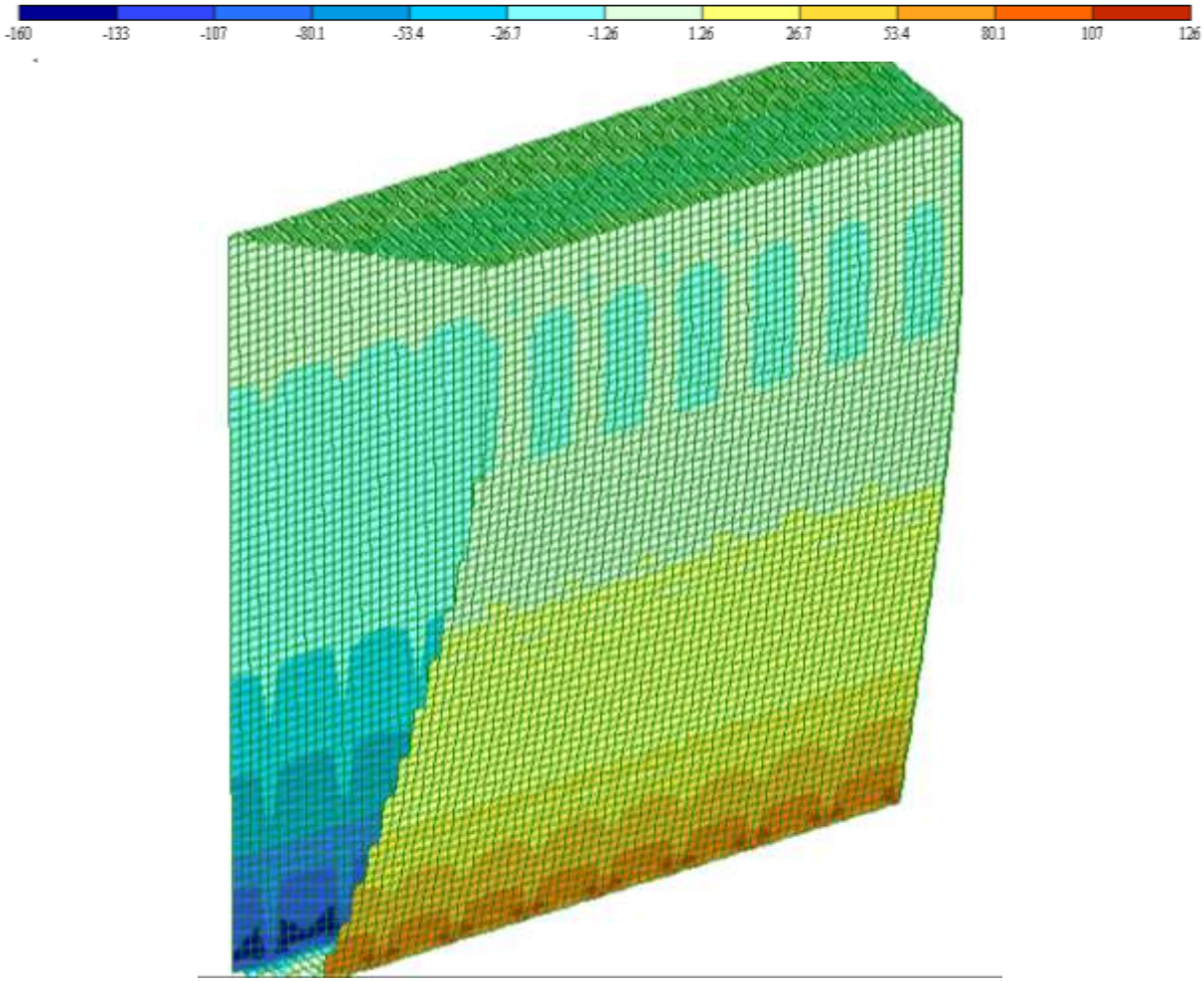

Fig.4.3. Distribution of Nx

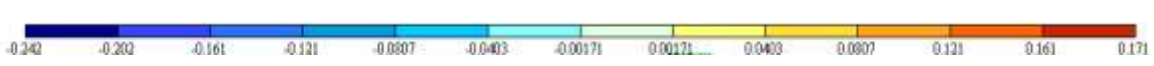

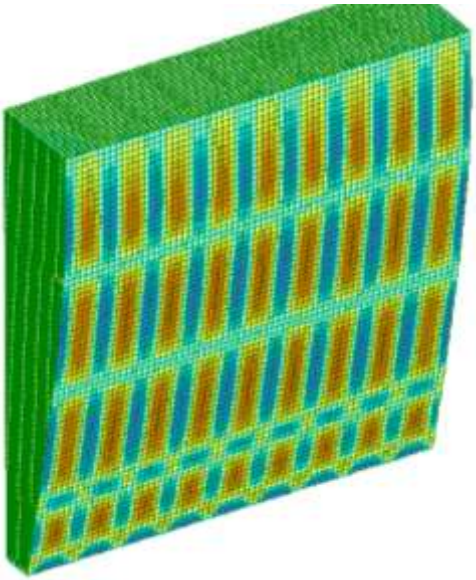

Fig.4.4. Distribution of moments My

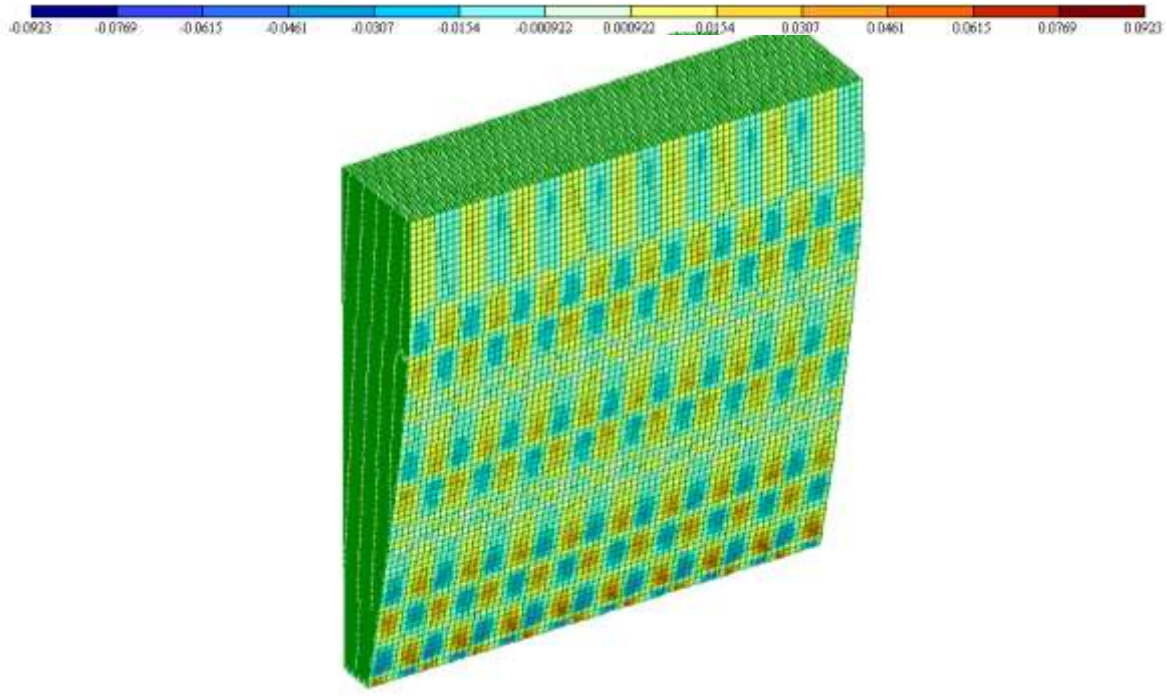

Fig.4.5. Distribution of torque Mxy

Analysis of displacement and distribution of internal forces (Fig.4.2-4.6) allows confirming representativeness of assumed hypotheses and assumptions, and appropriateness of performance management of characteristics of system, realizing the given distribution of components of SSS in the considered structure.

5. Technological Features of the Construction of Considered structures.

In this paper we consider a way to reduce weight (material consumption) of retaining walls, by means of creation of internal voids, which are performed using the removable void formers (RVF) or expendable void formers (EVF). Void formers can be made of plywood, chipboard, plastic, foam, lightweight concrete, and etc.
The main advantage of RVF is their re-use, and disadvantage - the possibility of the collapse of walls of freshly molded structure in low strength stage of concrete, or the complexity of removing. For the case of EVF, on the contrary, the disadvantages are their one-time use, and advantage - the absence of extraction operation.
It should be noted, that with the increment of degree of rationality of structures (within the accepted criteria), the use of RVF from hard materials (plywood, metal, etc.) is practically, impossible by reason of complexity of disassembly.

If there is thermal insulation requirement for retaining wall, while the effectiveness of EVF can be increased, which made of materials with low thermal conductivity, such as polystyrene.
In addition, for compaction of concrete mix should be used vibroformwork or self compacted concrete with high workobility.
Testing of technology solutions implementing the ideas of RVF and EVF was carried out during the construction of retaining walls of recreation hotel complex in Kharkiv.
The management of construction of retaining wall was carried out on flow diagram in which the process of construction was divided into streams (reinforcing, void formers and formwork instalation, concreting, formwork dismantling). For the increasing concreting process, wall was subdivided into the segments about 50m^3 per shift (8 hours) and, respectively, the minimum wall area=50x0.52=26m^2 (0.52- used concrete (m^3) in 1m^2 of wall). If height of story was 3.4m, the length of the segment was 26/3.4≈7-8 meters. The individual steps of the construction of an effective retaining wall of height about 15m are shown in Fig. 5.1. Worth noting that, an office center (eight-story building) is located at a distance of four meters from this retaining wall. Patterns of retaining wall construction (on floor, work carried out in one shift) with RVF and non-EVF are shown in Fig. 5.2 and 5.3, respectively.

Fig. 5.1. Stages of construction of effective retaining wall.

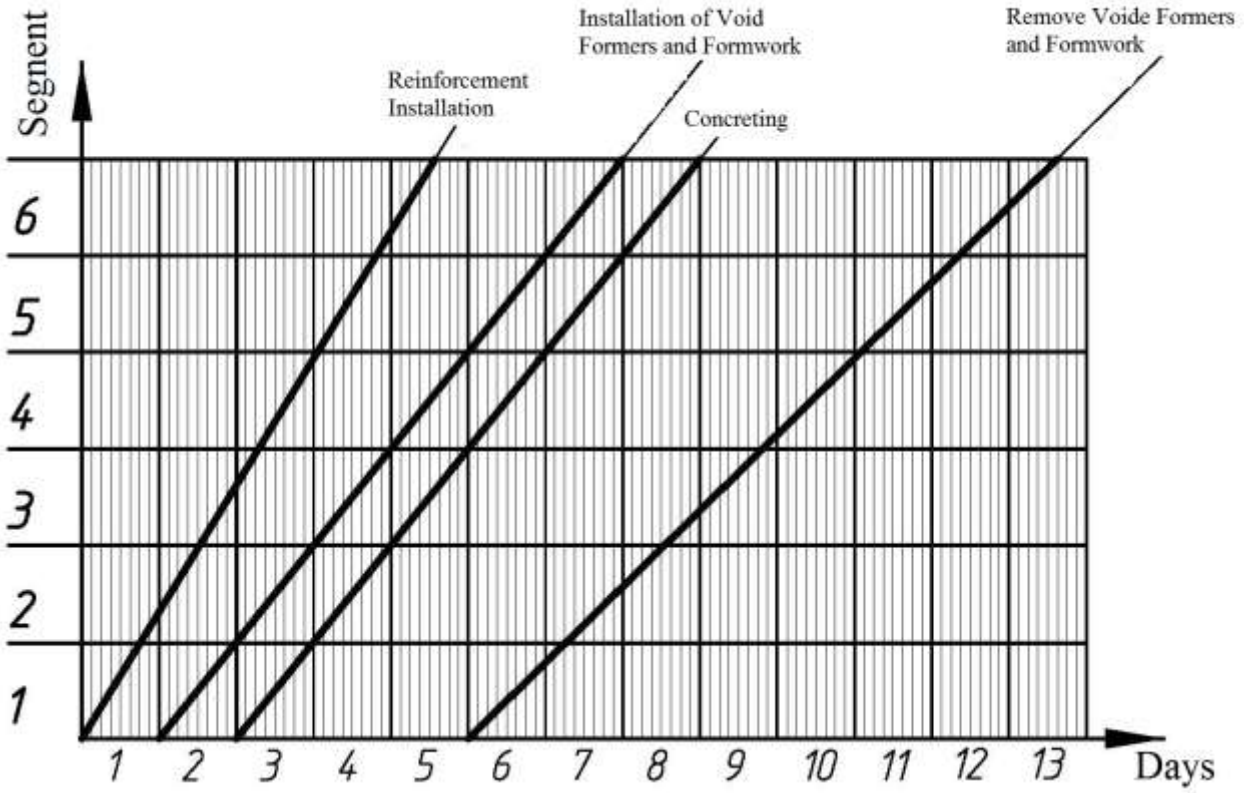

Fig. 5.2. Cyclogram for wall with RVF

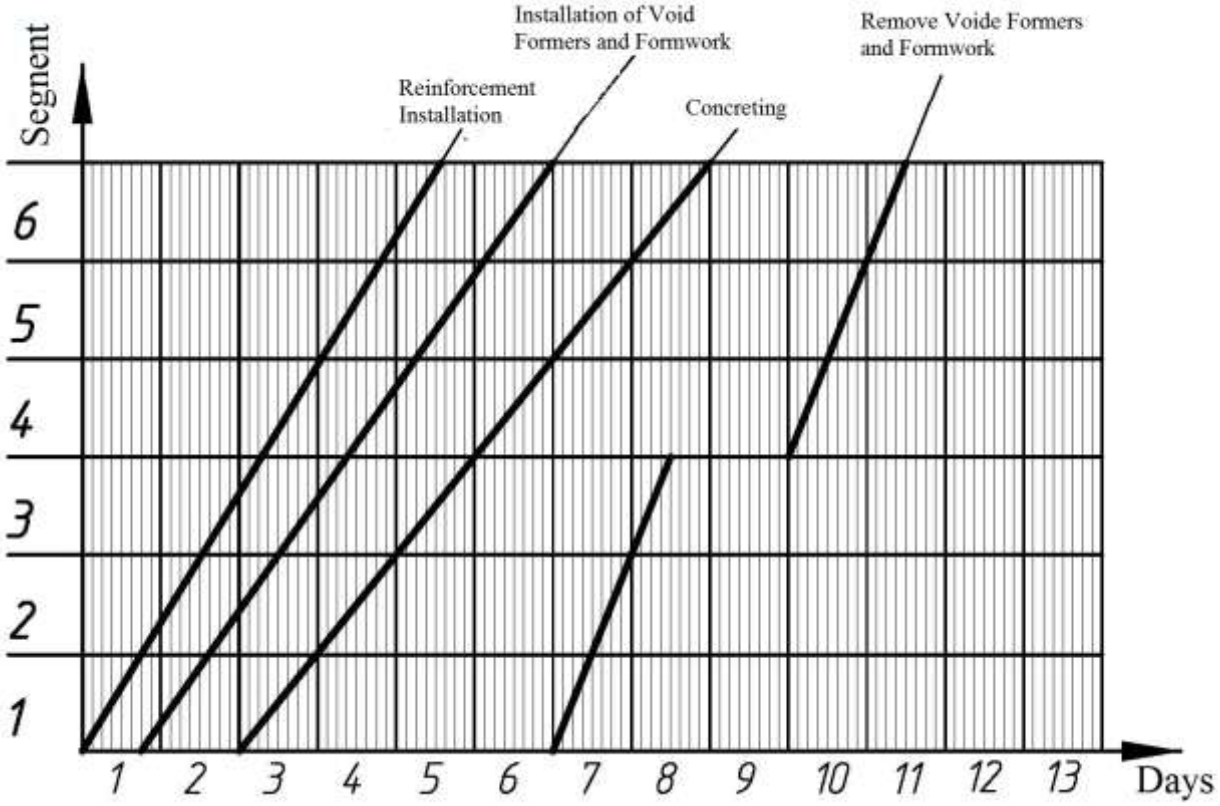

Fig. 5.3. Cyclogram for wall with EVF

Indicators of construction of retaining walls with RVF and EVF are shown in Table. 5.1.

Table 5.1 The laboriousness of the construction of retaining walls in the man-hours per 1m^2 of wall

work	RVF from inventory formwork	Styrofoam EVF
Reinforcement Installation	0,95	
Void Former Installation	0,75	0,34
Formwork Installation	0,5	
Concreting	2,3	
Void Former Removing	0,5	–
Dismantling of formwork	0,32	
Total	5,32	4,41

Approximate cost of construction of retaining walls are shown in Table 5.2. To compare the cost characteristics of technology of RVF and EVF we assumed that the cost of concrete delivery=106UAH/m^3, reinforcement=1000UAH/t, polystyrene =400UAH/m^3, 1 man-hour = 12UAH, crane rent=63UAH/hr, formwork rentals 0.5=UAH/m^{2}day.

Table 5.2 Approximate cost of construction of retaining walls UAH per 1m^2 of wall (not including consignment expenses and value-added tax)

Work	RVF from inventory formwork	Styrofoam EVF
Concret	0,52x106=55	
Reinforcement	0,049x1000=49	
Styrofoam	–	0,6x40=24
Construction of wall according to table 5.1	5,32x12=64	4,41x12=53
Crane Rental	0,16x63=10	
Formwork Rental	4,9x5x0,5=12	2x5x0,5=5
Total	190	196

Analysis of data in Table 5.2 shows that walls with EVF are costly compared with wall with RVF about $\frac{194 - 190}{190}, 100\% = 2.1\%$, however, the laboriousness of construction of second wall exceeds the laboriousness of construction of first. Just heat and sound insulating characteristics of the first several times higher than second, due to the presence of polystyrene void formers. The economic feasibility of EVF increases with decrease in volume of internal voids, and consequently, the consumption of polystyrene.

Thus, for optimal (complex geometry) structures of retaining walls, for the vast majority of cases it is advisable to use EVF made from effective materials such as styrofoam.

CONCLUSION

Consideration of strain of "retaining wall - soil" together, increases the correctness of the models, by providing the features of resistance this biagregata. Representation of similar structure (retaining wall) in the form of finite element determines the possibility of direct and indirect problems of design. In turn, the dirct (optimization) approach allows us to create a structure with rational and high competitive characteristics.

REFERENCES

- Klein, G. K. (1964). Analysis of Retaining Walls. Publ. High School, Moscow, p1964 to p1969.
- Shmukler V. S., Klimov U. A., Burak N. P., Lightweight Frame System. Kharkov, Golden Pages, 2008, 336p.
- Vasilkov G. V., Evolutionary Theory of Life Cycle of Mechanical Systems: Theory of structures, publ. LKI, Moscow: 2008, 320.
- Sorochan E. A., Trofimenkov U.G., Soil, Foundation and Underground Structures. Stroiizdat, Moscow, 1985, 408p.
- Shmukler V. S., About One Possibility of Compromise-Criterion Construction in Structure Parameter Rationalization Task Dundee, Scotland, 2008
- Shmukler V. S., Evolutionist approach in rationalization of building structures. /ISEC-03 Third Internetional structural Engineering and construction Conference, Shunan, Japan, 2005.

www.buitms.edu.pk

UAN: (081) 111-717-111